JOURNAL OF ATMOSPHERIC AND TERRESTRIAL PHYSICS

EDITORIAL ADVISORY BOARD

H. O. G. ALFVEN–STOCKHOLM · **J. BARTELS**–GÖTTINGEN · **W. J. G. BEYNON**–SWANSEA · **P. M. S. BLACKETT**–LONDON · **E. G. BOWEN**–SYDNEY · **SIR DAVID BRUNT**–LONDON · **R. BUREAU**–BAGNEUX · **S. CHAPMAN**–ALASKA · **J. EGEDAL**–COPENHAGEN · **H. FICKER**–VIENNA · **V. F. HESS**–NEW YORK · **E. O. HULBURT**–WASHINGTON, D.C. · **H. ISRAEL**–AACHEN · **D. K. MENZEL**–CAMBRIDGE, MASS. **S. K. MITRA**–CALCUTTA · **M. NICOLET**–UCCLE · **E. H. NORINDER**–UPSALA **B. van der POL**–GENEVA · **N. V. PUSHKOV**–MOSCOW · **J. A. RATCLIFFE**–CAMBRIDGE **O. E. H. RYDBECK**–GOTHENBURG · **SIR GEORGE SIMPSON**–LONDON **H. SOLBERG**–OSLO · **J. VELDKAMP**–DE BILT · **M. WALDMEIER**–ZÜRICH **J. ZENNECK**–ALTHEGNENBERG

VOL. 11 1957

EDITOR IN CHIEF

SIR EDWARD APPLETON, F.R.S.
EDINBURGH

VOLUME 11
1957

PERGAMON PRESS
NEW YORK · LONDON · PARIS · LOS ANGELES

J. Atmosph. Terr. Phys.

VOL
11
195

CONTENTS

No. 1

H. Volland: Zur Feinstruktur des erdmagnetischen Sonnenfinsterniseffektes 1
J. Taubenheim: Über den Einfluss von Sonneneruptionen auf die ionosphärische *E*-Schicht . 14
J. A. Lockwood and A. R. Calawa: On the barometric pressure coefficient for cosmic-ray neutrons 23
C. Lakshmi Bai: Application of the generalized magneto-ionic theory to the propagation of radio waves at the magnetic dip-poles of the earth 31
C. O. Hines: Heavy-ion effects in audio-frequency radio propagation 36
R. Montalbetti and A. Vallance Jones: H_α emissions during aurorae over west-central Canada 43
G. L. Rogers: An experimental verification of diffraction microscopy, using radio waves . 51
G. R. Ellis: Measurement of the gyro-frequency in the *F* region 54
R. A. Watson: Magnetic activity following a solar flare 59
K. R. R. Bowden and J. G. Davies: The time distribution of meteors 62
Research Notes:
D. M. Hunten: Correction for Rayleigh-scattered light of sodium observations in twilight . 67
D. R. Bates and B. L. Moiseiwitsch: On the remarks of V. I. Krassovsky regarding the O_3 and O_2* hypotheses of the OH airglow 68
E. T. Pierce: Nuclear explosions and a possible secular variation of the potential gradient in the atmosphere 70
W. N. Abbott: Quelques intéressantes variations du souffle de fond observées sur les fréquences de 17·6 Mc/s 72
K-indices of geomagnetic activity of the observatories at Eskdalemuir, Lerwick and Hartland for April and May 1957 75

VOL. 11 1957

No. 2

C. G. Stergis, G. C. Rein and T. Kangas: Electric field measurements in the stratosphere . 77
C. G. Stergis, G. C. Rein and T. Kangas: Electric field measurements above thunderstorms . 83
S. A. Bowhill: Ionospheric irregularities causing random fading of very low frequencies . . 91
F. H. Hibberd: Self-distortion of radio waves in the ionosphere, near the gyro frequency . 102
R. L. Dowden: Short-range echoes observed on ionospheric recorders 111
M. Dagg: Radio-star ridges 118
Research note:
W. J. G. Beynon and G. M. Brown: Ionospheric indices of solar activity 128
Announcement 131
K-indices of geomagnetic activity of the observatories at Hartland, Eskdalemuir and Lerwick, June 1957 132

Nos. 3/4

M. Dagg: The origin of the ionospheric irregularities responsible for radio-star scintillations and spread-*F*—I. Review of existing theories 133
M. Dagg: The origin of the ionospheric irregularities responsible for radio-star scintillations and spread-*F*—II. Turbulent motion in the dynamo region 139
J. J. Gibbons and B. Ramachandra Rao: Calculation of group indices and group heights at low frequencies 151
Rudolph Eyfrig: A critical discussion about special ionospheric characteristics 163
G. L. Goodwin: The movements of sporadic-*E* layer clouds 177
J. W. Warwick and H. Zirin: Diurnal absorption in the *D*-region 187
A. W. Harrison and A. Vallance Jones: Measurements of the absolute intensity of the aurora and night airglow in the 0·9–2·0 μ region 192
D. R. Bates and M. R. C. McDowell: Atmospheric helium 200
G. A. M. King: Relation between virtual and actual heights in the ionosphere 209
J. Chapman: The waveforms of atmospherics and the propagation of very low frequency radio waves 223
K. Bullough, T. W. Davidson, T. R. Kaiser and C. D. Watkins: Radio reflections from aurorae—III. The association with geomagnetic phenomena 237
N. J. Rumsey: Curvature-induced error in the analysis of fading records 255
J. V. Evans: The electron content of the ionosphere 259
H. A. Miranda, Jr.: The radon content of the atmosphere in the New York area as measured with an improved technique 272
G. V. Groves: Determination of impact point of a vertically-falling body by acoustical observations 284

J. L. Pawsey: Radar observations of lightning on 1·5 metres 289
Research Notes:
N. G. Chapman and N. V. Ryder: Time variations of cosmic rays at Wellington, New Zealand 291
Benjamin Nichols: Drift motions of auroral ionization 292
G. Lange-Hesse: Einfluss der erdmagnetischen Unruhe auf die Durchschnittsabweichungen der *F1*-Schicht-Tagesgrenzfrequenzen 293
A. H. Jarrett and P. L. Byard: On the possibility of observing aurorae in the daytime . 295
V. C. A. Ferraro: The coefficient of diffusion of ions in the *F2*-regions 296
N. Barber: Timing errors in an equilateral array of receivers 298
Letter to the Editor:
J. Alan Chalmers: Point-discharge current, potential gradient and wind-speed 301
K-indices of geomagnetic activity of the observatories at Hartland, Eskdalemuir and Lerwick for July and August 1957 303

AUTHOR INDEX TO VOLUME 11

Abbott, W. N. p. 72
Bai C. Lakshmi p. 31
Barber, N. p. 298
Bates, D. R. pp. 68, 209
Beynon, W. J. G. p. 128
Bowden, K. R. R. p. 62
Bowhill, S. A. p. 91
Brown, G. M. p. 128
Bullough, K. p. 237
Byard, P. L. p. 295
Calawa, A. R. p. 23
Chalmers, J. Alan p. 301
Chapman, J. p. 223
Chapman, N. G. p. 291
Dagg, M. pp. 118, 133, 139
Davidson, T. W. p. 237
Davies, J. G. p. 62
Dowden, R. L. p. 111
Ellis, G. R. p. 54
Evans, J. V. p. 259
Eyfrig, Rudolph p. 163
Ferraro, V. C. A. p. 296
Gibbons, J. J. p. 151
Goodwin, G. L. p. 177
Groves, G. V. p. 284
Harrison, A. W. p. 192
Hibberd, F. H. p. 102
Hines, C. O. p. 36
Hunten, D. M. p. 67
Jarrett, A. H. p. 295
Jones, A. Vallance pp. 43, 192
Kaiser, T. R. p. 237
Kangas, T. pp. 77, 83
King, G. A. M. p. 209
Lange-Hesse G. p. 293
Lockwood, J. A. p. 23
McDowell, M. R. C. p. 200
Miranda, H. A. p. 272
Moiseiwitsch, B. L. p. 68
Montalbetti, R. p. 43
Nichols, Benjamin p. 292
Pawsey, J. L. p. 289
Pierce, E. T. p. 70
Rao, B. Ramachandra p. 151
Rein, G. C. pp. 77, 83
Rogers, G. L. p. 51
Rumsey, N. J. p. 255
Ryder, N. V. p. 291
Stergis, C. G. pp. 77, 83
Taubenheim, J. p. 14
Volland, H. p. 1
Warwick, J. W. p. 187
Watkins, C. D. p. 237
Watson, R. A. p. 59
Zirin, H. p. 187

Journal of Atmospheric and Terrestrial Physics, 1957, Vol. 11, pp. 1 to 13. Pergamon Press Ltd., London

Zur Feinstruktur des erdmagnetischen Sonnenfinsterniseffektes

The fine structure of the geomagnetic solar eclipse effect

H. VOLLAND
Heinrich-Hertz-Institut, Berlin-Adlershof

(*Received* 25 *March* 1957)

Zusammenfassung—Die Theorie des erdmagnetischen Sonnenfinsterniseffektes wird durch Einführung empirischer Funktionen sowie durch eine eingehende Diskussion der Induktionswirkung im Erdinneren und anderer Einflüsse derart erweitert, dass eine quantitativ richtige Beschreibung des Effektes möglich wird. Es wird sodann gezeigt, dass infolge der Höhenabhängigkeit des geographischen Ortes des Kernschattens eine Entscheidung darüber herbeigeführt werden kann, in welcher Höhe der Schwerpunkt der stromführenden Schicht liegt. Eine Methode zur Richtungsbestimmung des S_q-Stromes bei Finsternissen wird am Schluss erwähnt.

Abstract—The extension of the theory of the solar eclipse effect in the geomagnetic field by the introduction of empirical functions and the detailed discussion of the induction in the earth's interior and other influences makes possible a quantitative interpretation of the effect. The dependence of the shadow centre with the height is opportune for the decision in what height the S_q-current flows. A method to determine the direction of the S_q-current during an eclipse is mentioned.

VOL.
11
1957

1. EINLEITUNG

AN EINER anderen Stelle ist gezeigt worden (VOLLAND, 1956a), dass die Abnahme der Leitfähigkeit der Ionosphäre in der Umgebung des Kernschattens einer Sonnenfinsternis zu einer Deformation des S_q-Stromes und damit zu einer Abweichung der erdmagnetischen Variationen vom normalen Tagesgang führt. Diese Abweichung konnte als das Magnetfeld eines nur von der Sonnenfinsternis herrührenden Stromsystems D_e* bestimmt werden, das in entgegengesetzter Richtung wie S_q fliesst und sich mit dem Kernschatten auf der Zentrallinie der Finsternis bewegt. Die Magnetfeldkomponenten von D_e an der Erdoberfläche haben die Gestalt

$$\vec{\Delta H}_e = \begin{cases} H_\theta &= \varepsilon H_q \bar{X}(\theta) \sin \Lambda \\ H_\Lambda &= \varepsilon H_q \bar{Y}(\theta) \cos \Lambda \\ H_r &= \tfrac{1}{2} \varepsilon H_q \bar{Z}(\theta) \sin \Lambda \,, \end{cases} \tag{1}$$

wenn der D_e-Strom im Koordinatensystem (r, θ, Λ) mit dem Zentrum des Kernschattens als Pol parallel zum Nullmeridian von Nord nach Süd fliesst. ε ist ein Mass für den Rückgang der Elektronenkonzentration im Schattenzentrum, H_q ist der Betrag der Horizontalkomponente der ungestörten S_q-Variation in der Umgebung des Kernschattens, und die $\bar{X}$, $\bar{Y}$, $\bar{Z}$ sind theoretisch bestimmte Funktionen von θ. In (VOLLAND, 1956b) sind magnetische Messungen bei Sonnenfinsternissen mit Hilfe der Gleichung 1 ausgewertet worden. Die Induktionswirkung von D_e im Erdinneren war dadurch berücksichtigt worden, dass der Innenanteil dem Aussenanteil proportional gesetzt wurde. Der Vergleich von Messung und Rechnung zeigte, dass alle wesentlichen Zügeydes Sonnenfinsterniseffektes durch die Theorie richtig gedeutet werden konnten.

* D_e ist an Stelle des Symbols S_e in (VOLLAND, 1956a) gewählt worden, da es sich konsequenter der international gebräuchlichen Terminologie anschiesst (D = disturbance; e = eclipse).

Im Folgenden soll durch eine Modifikation der Gleichung 1 sowie durch eine genaue Diskussion des im Erdinneren induzierten Anteils und die Berücksichtigung einiger kleinerer Einflüsse auch eine qualitativ richtige Beschreibung der Messung durch die Rechnung erzielt werden.

2. Modifikation der $\bar{X}(\theta)$, $\bar{Y}(\theta)$, und $\bar{Z}(\theta)$

Die Abb. 1 stellt die $\bar{X}$, $\bar{Y}$, und $\bar{Z}$ dar. Ausserdem sind noch die auf Eins normierte Leitfähigkeit der D_e-Stromfunktion $\Gamma_{\text{theor.}}$ sowie das Mittel der aus

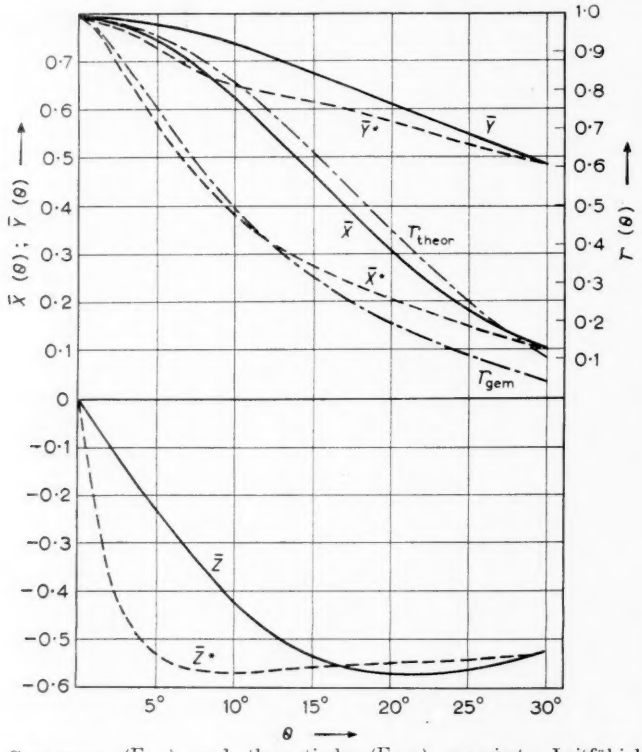

Abb. 1. Gemessene (Γ_{gem}) und theoretische (Γ_{theor}) normierte Leitfähigkeiten des D_e-Stromsystems sowie theoretisch und empirisch bestimmte (*) Funktionen $\bar{X}(\theta)$, $\bar{Y}(\theta)$, $\bar{Z}(\theta)$.

Grenzfrequenzmessungen der E- und F_1-Schicht bestimmten normierten Leitfähigkeit $\Gamma_{\text{gem.}}$ eingezeichnet. Während der Unterschied der beiden Γ zu grösseren Werten von θ hin sich günstig auswirkt (dadurch wird die Divergenz der Stromlinien des D_e-Stromsystems im Falle konstanter Leitfähigkeit kompensiert), macht sich bei kleinerem θ die Differenz beider Γ beim Vergleich von Messung und Rechnung bemerkbar. Der parallele Gang von $\Gamma_{\text{theor.}}$ und $\bar{X}$ verführt nun zu dem Versuch, ein empirisches $\bar{X}^*$ parallel zu $\Gamma_{\text{gem.}}$ einzuführen, das jedoch bei $\theta = 30°$ in $\bar{X}$ einmünden soll. Für $\bar{Z}$ folgt daraus sofort eine Verschiebung des Extremwertes zu kleineren θ hin, da der Wendepunkt von $\bar{X}^*$ etwa bei gleichem θ wie der Extremwert von $\bar{Z}^*$ liegen muss, und eine Erhöhung der

Amplitude. (Diese Tatsachen kann man sich an Hand von Beispielen ebener Flächenstrommodelle klarmachen.) Der weitere Verlauf von $\bar{Z}^*$ ist unbestimmt. $\bar{Z}^*$ soll deshalb wie $\bar{X}^*$ bei $\theta = 30°$ in $\bar{Z}$ einmünden. Der Verlauf von $\bar{Y}^*$ wird durch die Forderung festgesetzt, dass die Messergebnisse möglichst gut durch $\bar{Y}^*$ wiedergegeben werden sollen. Die Gleichung 1 werden also jetzt durch die Formeln

$$\overrightarrow{\Delta H_e} = \begin{cases} H_\theta^* = & \varepsilon H_q \bar{X}^*(\theta) \sin \Lambda \\ H_\Lambda^* = & \varepsilon H_q \bar{Y}^*(\theta) \cos \Lambda \\ H_r^* = & \tfrac{1}{2}\gamma \varepsilon H_q \bar{Z}^*(\theta) \sin \Lambda \end{cases} \tag{2}$$

ersetzt, wo die $\bar{X}^*(\theta)$ usw. die empirischen Funktionen der Abb. 1 sind und der zunächst unbestimmte Faktor γ die Überhöhung der Amplitude von $\bar{Z}^*(\theta)$ gegenüber $\bar{Z}(\theta)$ angibt.

3. Bestimmung des im erdinneren induzierten anteils

Zur Bestimmung der Induktionswirkung werden folgende Annahmen gemacht:

(a) Der Schatten bewege sich periodisch auf einem Grosskreis mit der konstanten mittleren Umlaufgeschwindigkeit von 3000 km/h. (Das entspricht einer Kreisfrequenz von $\omega = 1{,}3 \cdot 10^{-4}\, s_y^{-1}$.)

(b) Die Richtung von D_e relativ zur Bewegungsrichtung des Schattens sei während des ganzen Umlaufes konstant.

Die erste Vereinfachung ergibt sich aus der Tatsache, dass der halbe Umlauf des Schattenzentrums etwa 6,7 Stunden dauert, während die D_e-Störung nur 2,5 Stunden in Anspruch nimmt. Die Störung der ersten halben Periode ist also völlig abgeklungen, wenn die Störung der nächsten halben Periode beginnt. Die zweite Vereinfachung ist möglich, weil während der 2,5 stündigen D_e-Störung die Richtung des S_q-Stromes sich nur um wenige Grade ändert.

Es soll nun der Grosskreis, auf dem sich das Schattenzentrum bewegt, zum Äquator eines neuen Koordinatensystems (r, ϑ, λ) gemacht werden. Das äussere magnetische Potential von D_e, welches im Koordinatensystem (r, θ, Λ) lautet:

$$V_e^{(a)} = -\varepsilon H_q^{(a)} a \sum_n \frac{n+1}{2n+1} \left(\frac{r}{a'}\right)^n s_n{}^1 P_n{}^1 (\cos\theta) \sin \Lambda \qquad (r \leqq a') \tag{3}$$

hat dann nach einer Koordinatentransformation (siehe (Schmidt, (1899)) die Gestalt

$$V_e^{(a)} = \varepsilon H_q^{(a)} a \sum_n \sum_m \left(\frac{r}{a}\right)^n E_n{}^m P_n{}^m (\cos\vartheta) e^{im(\lambda - \omega t)} \tag{4}$$

mit

$$E_n{}^m = \frac{c_n{}^1}{n} (\cos \Lambda_p A_n^{m,1} + i \sin \Lambda_p B_n^{m,1})$$

$$c_n{}^1 = \frac{n(n+1)}{2n+1} \left(\frac{a}{a'}\right)^n s_n{}^1; \quad \begin{matrix} A_n^{m,1} \\ B_n^{m,1} \end{matrix} \Big\} = n \sqrt{\frac{2(n-1)!}{(n+1)!}} \begin{matrix} X_n{}^m (\cos 90°) \\ Y_n{}^m (\cos 90°) \end{matrix}$$

$$X_n{}^m (\cos\vartheta) = \frac{dP_n{}^m (\cos\vartheta)}{n\, d\vartheta}\,; \quad Y_n{}^m (\cos\vartheta) = \frac{m P_n{}^m (\cos\vartheta)}{n \sin\vartheta}$$

VOL. 11 1957

a = Erdradius,
a' = Radius der stromführenden Ionosphärenschicht,
Λ_p = Winkel zwischen Richtung des S_q-Stromes und der Bewegungsrichtung des Schattenzentruns
$H_q^{(a)}$ = Aussenanteil der magnetischen Horizontalkomponente des ungestörten S_q-Stromes

Der Faktor $e^{-im\omega t}$ bewirkt die periodische Bewegung des Schattens auf dem Äquator. In der Darstellung der Gleichung 4 ist von der bequemen komplexen Schreibweise Gebrauch gemacht worden. Davon wird nur der Realteil betrachtet.

Der Innenanteil des magnetischen Potentials von D_e sei

$$V_e^{(i)} = \varepsilon H_q^{(a)} a \sum_n \sum_m \left(\frac{a}{r}\right)^{n+1} I_n^m P_n^m (\cos\vartheta)\, e^{im(\lambda - \omega t)} \qquad (r \geqq a) \tag{5}$$

Bei einfachen Leitfähigkeitsverhältnissen (Erdkern mit konstanter Leitfähigkeit κ, umgeben von nichtleitender Hülle) wird, wie Chapman gezeigt hat (CHAPMAN und BARTELS, 1940)

$$I_n^m = E_n^m \frac{n}{n+1} q^{2n+1} (\gamma_n^m + i\delta_n^m) \tag{6}$$

mit

$$\gamma_n^m = 1 - \frac{2n+1}{2\beta} + \frac{n(2n^2 - n - 1)}{8\beta^3} + \ldots$$

$$\delta_n^m = \frac{2n+1}{2\beta}\left(1 - \frac{n}{\beta} + \frac{n(n-1)}{4\beta^2} - \ldots\right)$$

$a'' = qa$ = Radius des leitenden Erdkerns,
$\beta^2 = 2\pi\omega a''^2 \kappa m$.
Der Realteil von $V_e^{(i)}$ ist ($\lambda - \omega t = \lambda'$)

$$V_e^{(i)} = \varepsilon H_q^{(a)} a \sum_n \sum_m \frac{c_n^1}{n+1} q^{2n+1} \left(\frac{a}{r}\right)^{n+1} P_n^m (\cos\vartheta)\, [a_n^m \cos m\lambda' + b_n^m \sin m\lambda'] \tag{7}$$

mit

$$a_n^m = \gamma_n^m A_n^{m,1} \cos\Lambda_p - \delta_n^m B_n^{m,1} \sin\Lambda_p,$$

$$b_n^m = \gamma_n^m B_n^{m,1} \sin\Lambda_p + \delta_n^m A_n^{m,1} \cos\Lambda_p.$$

Für unsere Zwecke genügt es, das Magnetfeld von V_e für zwei Spezialfälle zu betrachten:

(a) $\Lambda_p = 90°$ entspricht einer Sonnenfinsternis in mittleren Breiten in den frühen Nachmittagsstunden ($\bar{X}$-Typ). In der Abb. 2a sind die Magnetfeldkomponenten des Innen—und Aussenanteils von V_e auf dem Äquator ($\vartheta = 90°$; $r = a$)

$$\overrightarrow{\Delta H_e^{(i)}} = \begin{cases} H_\vartheta^{(i)} = \Delta X_i = 0 \\ H_\lambda^{(i)} = \Delta Y_i \\ H_r^{(i)} = \Delta Z_i \end{cases} ; \qquad \overrightarrow{\Delta H_e^{(a)}} = \begin{cases} H_\vartheta^{(a)} = \Delta X_a = 0 \\ H_\lambda^{(a)} = \Delta Y_a = \bar{X}(\lambda') \\ H_r^{(a)} = \Delta Z_a = \bar{Z}(\lambda') \end{cases}$$

sowie die Summe beider eingezeichnet. Die gestrichelten Linien gelten für den Fall, dass der Innenanteil dem Aussenanteil proportional gesetzt ist.

(b) $\Lambda_p = 180°$ entspricht einer Finsternis in niederen Breiten um die Mittagszeit ($\overline{Y}$-Typ). Auf dem Äquator sind jetzt nur die Komponenten

$$H_\vartheta^{(i)} = -\Delta X_i; \qquad H_\vartheta^{(i)} = -\Delta X_a = -\overline{Y}(\lambda')$$

von Null verschieden. Diese sowie die Summe beider sind in der Abb. 2b dargestellt.

Dieser Rechnung wurden die von Chapman gefundenen Werte

$$\kappa = 3{,}6 \cdot 10^{-13}; \qquad q = 0{,}96$$

zugrunde gelegt. Die gleiche Rechnung wurde mit den von Benkova (Benkova, 1940) ermittelten Werten ($\kappa = 5 \cdot 10^{-12}$; $q = 0{,}94$) wiederholt. In den nun folgenden Ergebnissen entsprechen die eingeklammerten Daten dem Benkova-Modell. Da Benkova's Analyse später und vollständiger erfolgte als Chapman's Untersuchung, dürften diese Daten zuverlässiger sein.

Der Abb. 2 entnimmt man folgendes:

(1) Der Innenanteil erlebt eine Phasendifferenz gegenüber dem Aussenanteil von etwa 4° (1°).

(2) Die Phasenverzögerung der Extremwerte von ΔX und ΔY gegenüber ΔX_a und ΔY_a beträgt etwa 1° (0°,25) (das entspricht einer Zeit von 2,2 (0,5) Minuten). ΔZ zeigt gegenüber ΔZ_a eine Niveauerhöhung und einen Vorlauf des Nulldurchganges von etwa 2° (0°,5).

(3) Durch die Innenanteile wird zu Beginn der Finsternis das Niveau von ΔX und ΔY gegenüber dem mittleren Niveau erniedrigt, am Ende der Finsternis erhöht. (Beim Benkova-Modell ist die Abweichung vom mittleren Niveau geringer.)

In diese Rechnung ging die nicht modifizierte Vertikalkomponente $H_r^{(a)}$ von D_e ein. Das modifizierte $H_r^{(a)}*$ würde sich durch Überwiegen der Glieder mit hohem m in der Kugelfunktionsentwicklung auszeichnen. Nun liegt aber der Extremwert eines Gliedes der Horizontalkomponente des Innenanteiles bei

$$\lambda_0 = -\frac{1}{m} \operatorname{arctg} \frac{\delta_n^m}{\gamma_n^m} \approx -\frac{2n+1}{2m\beta}. \tag{8}$$

Mit wachsendem m wird demnach die Phasendifferenz eines Gliedes kleiner. Damit wird die gesamte Phasenverzögerung des Innenanteils kleiner, also auch die der Extremwerte von ΔX und ΔY. In gleicher Richtung wirken die steileren Maxima von $H_\vartheta^{(a)}*$ und $H_\Lambda^{(a)}*$, sodass die gesamte Phasenverzögerung sicherlich kleiner als 1 Minute sein wird.

Dieses Ergebnis rechtfertigt die Gleichung 1, wo der Innenanteil dem Aussenanteil proportional gesetzt worden war. Auf dieser Grundlage sollen jetzt die Beiträge der einzelnen Anteile abgeschätzt werden. Es sei

$$\begin{matrix} \Delta X_a \\ \Delta Y_a \end{matrix} \Big\} = \rho \begin{Bmatrix} \Delta X \\ \Delta Y \end{Bmatrix}; \qquad \begin{matrix} \Delta X_i \\ \Delta Y_i \end{matrix} \Big\} = \xi \begin{Bmatrix} \Delta X \\ \Delta Y \end{Bmatrix}$$
$$\Delta Z_a = \rho\gamma Z; \qquad \Delta Z_i = -\eta\gamma Z \tag{9}$$

Der Abb. 2 entnimmt man die Werte:

$$\frac{\rho}{\xi} = 2{,}4\ (2{,}6); \qquad \left|\frac{\rho}{\eta}\right| = 1{,}7\ (1{,}8) \tag{10}$$

VOL. 11 1957

Aus den Messungen war gefunden worden

$$\rho + \xi \approx 1; \qquad (\rho - \eta)\gamma \approx 0{,}5 \tag{11}$$

Daraus folgt:

$$\rho = 0{,}71\ (0{,}72); \qquad \eta = 0{,}42\ (0{,}40)$$

$$\xi = 0{,}29\ (0{,}28); \qquad \gamma = 1{,}7\ (1{,}6)$$

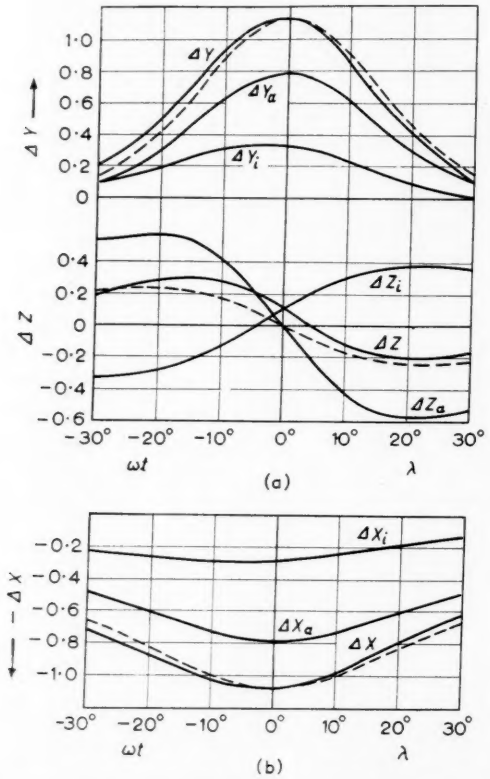

Abb. 2. Magnetfeldkomponenten des äusseren (a) und inneren (i) Anteils des D_q-Stromsystems sowie die Summe beider Anteile am Äquator ($\theta = 90°$). Die gestrichelten Linien gelten für den Fall, dass der innere Anteil dem äusseren proportional ist. (Zeitachse nach links positiv!)

(a) S_q-Strom senkrecht zur Bewegungsrichtung des Schattens ($\overline{X}$-Typ).

(b) S_q-Strom parallel zur Bewegungsrichtung des Schattens ($\overline{Y}$-Typ).

Die in (VOLLAND, 1956a) erfolgte Tiefenabschätzung des induzierten Stromes wird allerdings jetzt problematisch, denn aus Gleichung 10 folgt:

$$\left|\frac{\xi}{\eta}\right| = \alpha < 1 \tag{12}$$

Das würde bedeuten, dass der Schwerpunkt des induzierten Stromes in der Tiefe $|\alpha H| < H$ (H = Höhe der stromführenden Ionosphärenschicht) fliessen müsste.

Die Annäherung des induzierten Stromes durch einen Linienstrom führt also zu falschen Ergebnissen und ist deshalb nicht gerechtfertigt.

4. Der Einfluss der Selbstinduktivität auf D_e

Der Einfluss des Eigenmagnetfeldes von D_e auf den mit der Geschwindigkeit u wandernden Stromwirbel D_e selbst war in den bisherigen Rechnungen vernachlässigt worden. Die Wirkung dieses Magnetfeldes ist eine Verzögerung von D_e gegenüber der zeitlich variablen Leitfähigkeit $\sigma_e(t)$ der Ionosphäre infolge Selbstinduktion.

Das vollständige Gleichungs-System für die Bestimmung der Bewegung eines Plasmas im Magnetfeld (unter Vernachlässigung der eingeprägten Feldstärken) lautet

$$\frac{\partial \vec{H}}{\partial t} - \operatorname{rot}[\vec{v},\vec{H}] = -\operatorname{rot}\frac{\vec{j}}{\sigma} \tag{18}$$

$$\vec{j} = \operatorname{rot}\vec{H}$$

Für eine Abschätzung wird folgende Vereinfachung gemacht: Die Ionosphäre sei eine unendlich ausgedehnte Fläche in der Ebene $z = 0$ mit der Leitfähigkeit

$$\sigma_e = \frac{1}{\rho} = \sigma_e(y - ut).$$

Es sei weiter

$$\vec{v} = v_x = \text{const.}$$

$$\vec{H} = H_{z0} - \nabla V_e^{(a)} - \nabla V_e^{(i)} \qquad (H_{z0} = \text{const.})$$

$$\sigma_e = \varepsilon\sigma_0 \frac{a^2}{a^2 + (y - ut)^2} = \varepsilon\sigma_0\Gamma(y - ut) \qquad (a = \text{const.})$$

$$\left.\frac{\partial V_e^{(i)}}{\partial z}\right|_{z=0} \approx -\alpha \left.\frac{\partial V_e^{(a)}}{\partial z}\right|_{z=0} \quad (\alpha = \text{const.})$$

Durch diesen Ansatz werden die Verhältnisse in mittleren Breiten angenähert ($\bar{X}$-Typ), wo die Stromrichtung senkrecht zur Ausbreitungsrichtung des Schattens ist.

Das Gleichungssystem (18) vereinfacht sich dann (siehe (Price, 1949)) zu der Potentialgleichung

$$\Delta V_e^{(a)} = 0 \tag{19}$$

mit den Randbedingungen

$$V_e^{(a)} \to 0 \qquad \text{für } z \to \infty$$

und

$$\rho \left.\frac{\partial^2 V_e^{(a)}}{\partial y^2}\right|_{z=0} + \left.\frac{\partial \rho}{\partial y}\frac{\partial V_e^{(a)}}{\partial y}\right|_{z=0} + (1 - \alpha)2\pi \frac{\partial}{\partial t}\left[\frac{\partial V_e^{(a)}}{\partial z}\right]_{z=0} = 0$$

VOL. 11 1957

Die Lösung von (19) lautet

$$V_e^{(a)} = -2\pi j_0 a' \operatorname{arctg} \frac{y - ut + b'}{z + a'} \quad (z \geqq 0) \tag{20}$$

mit $\left.\begin{matrix} a' \\ b \end{matrix}\right\} = \frac{a}{\sqrt{2}}\sqrt{\sqrt{1+\gamma^2} \pm 1} \approx \begin{cases} a \\ a\gamma/2 \end{cases}$; $\gamma = 2\pi u(1-\alpha)\sigma_0\varepsilon$.

Die Stromfunktion D_e ergibt sich zu

$$D_e = \frac{V_e^{(a)}}{2\pi}\bigg|_{z=0} = -j_0 a' \operatorname{arctg} \frac{y - ut + b'}{a'} \,. \tag{21}$$

Für kleine γ bedeutet dies lediglich eine zeitliche Verschiebung von D_e gegenüber σ_e um der Wert

$$t = \frac{b'}{u} = a\pi(1-\alpha)\sigma_0\varepsilon. \tag{22}$$

Nun ist $\sigma_0 < 5 \cdot 10^{-8}\ \mathrm{s}^{-1}$; $a < 10^8$ c
$u < 10^5\ \mathrm{cs}^{-1}$; $\varepsilon < 1$
$\alpha > 0{,}3$
also: $t < 10$ sec.

5. Berücksichtigung des Elliptischen Schattens

Bei der ursprünglichen Berechnung von D_e war ein kreissymmetrischer Mondschatten auf der Erdoberfläche vorausgesetzt worden. Dies gilt streng nur dann, wenn die Sonne in Zenit steht. Im allgemeinen ist der Schatten mehr oder weniger elliptisch verzerrt. Zu merkbaren Abweichungen kommt es jedoch nur in den Morgen—oder Abendstunden.

Der Einfluss der Elliptizität kann folgendermassen berücksichtigt werden:

Es wird ein Koordinatensystem, mit der Ekliptik als x-y-Ebene und der Richtung zur Sonne als x-Achse gewählt. In der Projektion auf die Ekliptikebene erscheint der Abstand eines Beobachtungsortes vom Schattenzentrum in erster Näherung wie

$$\theta' = \frac{\theta}{\cos\tau'} \tag{23}$$

vergrössert.

Hier ist

$$\operatorname{cotg}\tau' = \frac{\cos\delta\cos\tau_m + \sin\delta\operatorname{tg}\varphi_m}{\sin\tau_m}$$

mit $\tau_m = \frac{\tau_0 + \tau}{2}$; (φ_0, τ_0) = Koordinaten des Schattenzentrums,

$\varphi_m = \frac{\varphi_0 + \varphi}{2}$; (φ,τ) = Koordinaten des Beobachtungsortes,

δ = scheinbare Deklination der Sonne,
τ = Stundenwinkel,
φ = geographische Breite.

Da der Schatten sich vorzugsweise in westöstlicher Richtung bewegt, kann die Verzerrung in Nord-Süd-Richtung vernachlässigt werden. θ' wird an Stelle von θ in Gleichung 2 eingesetzt.

6. Berücksichtigung der Schrägeinstrahlung der Sonne in die Ionosphäre

Für die Berechnung des magnetischen Sonnenfinsterniseffektes ist die geographische Lage des Schattenzentrums in der Höhe des Schwerpunktes des S_q-Stromsystems massgebend. Nun strahlt die Sonne im allgemeinen schräg in die Ionosphäre ein. Aus den Astronomischen Jahrbüchern ist aber nur der Ort des Kernschattenzentrums am Erboden bekannt. Mit Hilfe einer einfachen geometrischen Uberlegung lässt sich aus diesen Daten die geographische Lage des Schattenzentrums in der Höhe bestimmen.

Es seien (r_1, φ_1, τ_1) die Koordinaten des Schattenzentrums in der Höhe $\Delta r = r_1 - r_0$ über dem Erdboden. Dann ist $(\rho = r_0/r_1)$

$$\sin \varphi_1 = \rho \cos^2\delta \,(\sin \varphi_0 - \cos \varphi_0 \cos \tau_0 \operatorname{tg} \delta) + \sin \delta \sqrt{1 - \rho^2[\sin^2 \phi_0 \cdot \sin^2 \tau_0 + \cos^2 \delta(\sin \varphi_0 - \cos \varphi_0 \cos \tau_0 \operatorname{tg} \delta)^2]} \tag{24}$$

und

$$\sin \tau_1 = \frac{\cos \varphi_0}{\cos \varphi_1} \sin \tau_0 \tag{25}$$

VOL. 11 1957

7. Diskussion weiterer Einflüsse

Ausser den besprochenen Einflüssen ist noch die Wirkung der endlichen Rekombinationskoeffizienten der einzelnen Ionosphärenschichten von Bedeutung. Durch die Rekombinationskoeffizienten wird das Minimum der Leitfähigkeit der Ionosphäre gegenüber der Hauptphase der Finsternis um etwa 2 Minuten verzögert. Diese Verzögerung kann mit Hilfe von Grenzfrequenzaufnahmen exakt bestimmt werden.

Die bisher vernachlässigte endliche Ausdehnung des Kernschattengebietes führt lediglich zu einer geringen Verbreiterung des Extremwertes der Horizontalkomponenten von D_e und braucht nicht besonders diskutiert zu werden.

Ebenfalls vernachlässigt werden kann die Richtungs—und Amplitudenänderung des S_s—Stromes während der Finsternis. Denn dieser Einfluss ist nur bemerkbar, wenn sich das Schattenzentrum in grösseren Entfernungen vom Beobachtungsort befindet. Dort ist aber bereits die vorausgesetzte Homogenität des S_q-Stromes nicht mehr gut erfüllt, sodass sich die Feinstrukturuntersuchungen in der Hauptsache auf die nähere Umgebung des Kernschattens beschränken müssen.

8. Neuauswertung Magnetischer Messungen bei Sonnenfinsternismessungen

Unter den oben angeführten Gesichtspunkten sind nun die folgenden Messergebnisse von magnetischen Sonnenfinsternisbeobachtungen neu ausgewertet worden.

Die Abb. 3 zeigt

$$\Delta Y_e = \Delta Y - \Delta Y_q$$
$$\Delta Z_e = \Delta Z - \Delta Z_q$$

von Niemegk am 30 Juni 54.

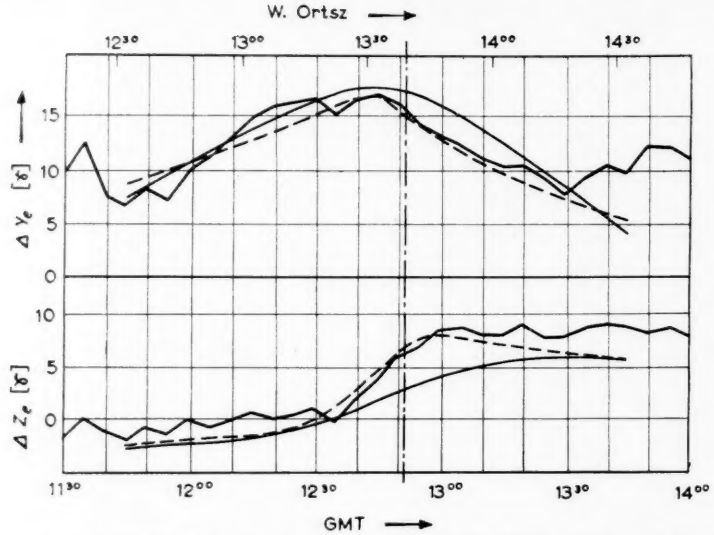

Abb. 3. ΔY_e und ΔZ_e von Niemegk am 30 Juni 1954. Gestrichelt: berechnete Werte von ΔY_e und ΔZ_e. Dünn ausgezogen: die alten theoretischen Kurven.

Gestrichelt sind die neuberechneten Werte eingetragen. Die dünn ausgezogenen Linien geben die alten nicht korrigierten berechneten Daten an. Abb. 4 stellt die Differenzkurven

$$\Delta Y_{e_{\text{Burgos}}} - \Delta Y_{e_{\text{Phillippeville}}}$$

$$\Delta Y_{e_{\text{Tortosa}}} - \Delta Y_{e_{\text{Phillippeville}}}$$

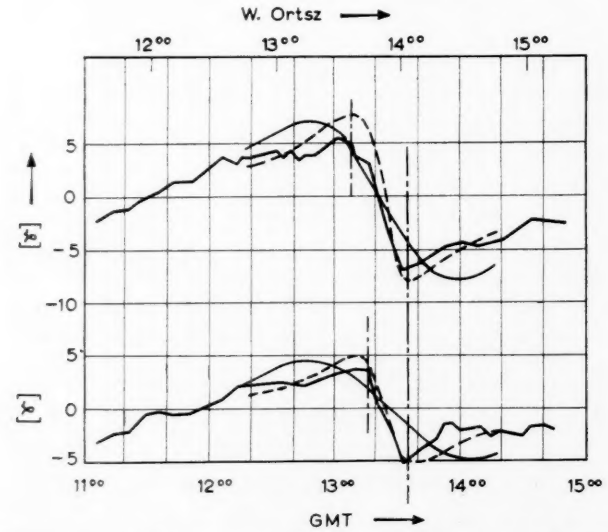

Abb. 4. Differenzkurven $\Delta Y_{e_{\text{Burgos}}} - \Delta Y_{e_{\text{Phillippeville}}}$ (oben) und $\Delta Y_{e_{\text{Tortosa}}} - \Delta Y_{e_{\text{Phillippeville}}}$ (unten) am 30 August 1905. Gestrichelt: neu berechnete Differenzkurven. Dünn ausgezogen: alte theoretische Kurven.

der Sonnenfinsternis vom 30 August 1905 dar. Abb. 5 zeigt ein Messergebnis der Sonnenfinsternis vom 18 Mai 1901 in Karang Sago am Äquator. Durch die Einführung der modifizierten $\bar{X}^*$ usw. ist jetzt in der Umgebung der Hauptphase eine quantitativ richtige Wiedergabe der Messung durch die Rechnung möglich,

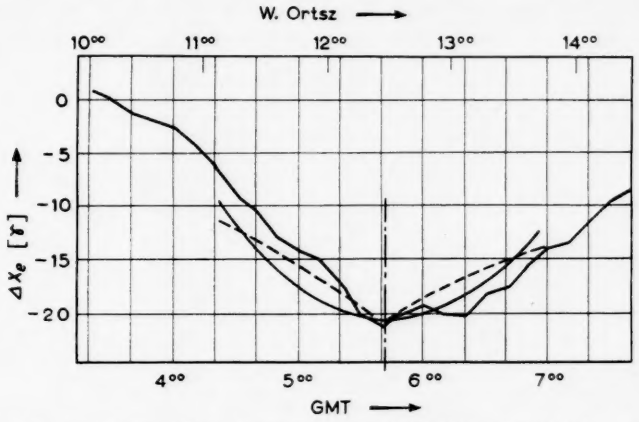

Abb. 5. ΔX_e von Karang Sago (Sumatra) am 18 Mai 1901. Gestrichelt: neuberechnete Werte von ΔX_e. Dünn ausgezogen: alte theoretische Kurve.

VOL. 11 1957

wie dies deutlich die steilen Anstiege von ΔZ_e (1954) und der Differenzkurven (1905) sowie die scharfen Extremwerte von ΔY_e (1954) und ΔX_e (1901) zeigen. Die Wirkung des induzierten Anteils-nämlich Senkung des Niveaus vor der Hauptphase, Hebung des Niveaus darnach—kommt bei ΔY_e (1954) und bei ΔX_e (1901) zum Ausdruck. Da bei grösseren Entfernungen vom Kernschatten die $\bar{X}^*$ und $\bar{X}$ usw. identisch werden, kann man am Unterschied der alten und neu berechneten Kurven zu Beginn und am Ende der Finsternis den Einfluss der Elliptizität erkennen, der in diesen Fällen offenbar gering ist.

Der Einfluss der Elliptizität macht sich wesentlich stärker in den frühen Morgenstunden der Finsternis vom 28 Mai 1900 bemerkbar (siehe Abb. 6). Hier ist ausserdem eine wirksame Schichthöhe von 0, 200 und 400 km der Rechnung zugrundegelegt worden. (Der Kernschattenverlauf in den verschiedenen Höhen ist in der Abb. 7 dargestellt.) Die oben diskutierten Verzögerungsfaktoren sind durch eine Zeitverschiebung im Verlauf des Schattenzentrums von 3 Minuten berücksichtigt worden. Der Fehler dieser Zeitgrösse dürfte nicht grösser als 1 Minute sein. Eine Höhendifferenz von 200 km verschiebt das Minimum von ΔY_e um 4,5 Minuten. Man erkennt, dass die gemessenen Extremwerte von ΔY_e einer Höhe des S_q-Stromes von weniger als 200 km entsprechem. Die Genauigkeit dieser Angabe wird allerdings dadurch eingeschränkt, dass von den hier verwendeten Messergebnissen nur die 5 Minuten-Mittelwerte der Deklination veröffentlicht worden sind. Es wird jedoch aus dieser Darstellung ersichtlich, dass sowohl die Schärfe der Extremwerte als auch deren Zeitdifferenz gross genug sind, um eine Entscheidung darüber herbeizuführen, in welcher Höhe der Schwerpunkt der stromführenden Schicht liegt; vorausgesetzt natürlich, dass es sich wie in diesem Falle um einen erdmagnetisch ruhigen Tag handelt.

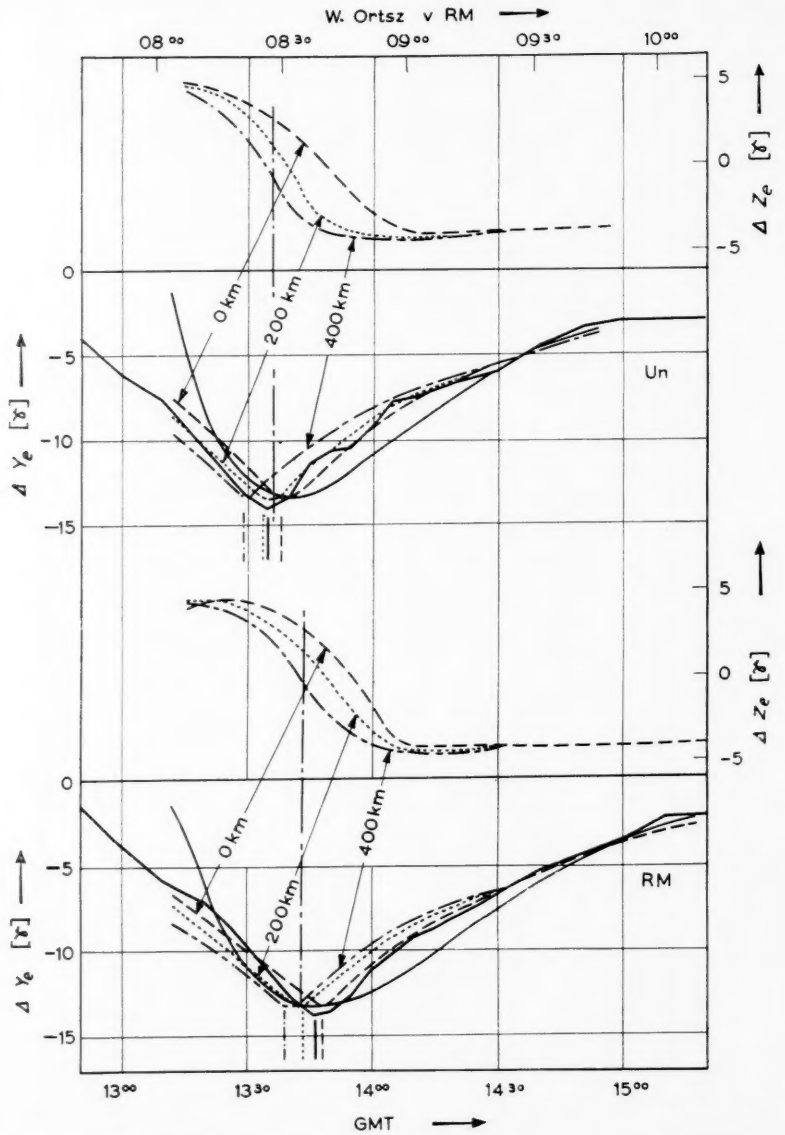

Abb. 6. ΔY_e von Union Spring (oben) und Rocky Mount (unten) am 28 Mai 1900 und neu berechnete Werte von ΔY_e und ΔZ_e bei Zugrundelegung einer Höhe der stromführenden Ionosphärenschicht von 0, 200, und 400 km. Die vertikalen Striche geben die Zeiten der Minima der einzelnen ΔY_e Kurven an. Dünn ausgezogen: die alten theoretischen Kurven.

In Abb. 6 ist auch der theoretische Verlauf von ΔZ_e für die verschiedenen Höhen des S_q-Stroms eingezeichnet. Man erkennt, dass die Registrierung von ΔZ ebenfalls für eine Höhenbestimmung günstig ist.

Dass prinzipiell auch eine Richtungsbestimmung des S_q-Stromes möglich ist,

soll hier nur angedeutet werden. Wenn etwa im Punkte A (Abb. 7) eine weitere Station aufgestellt worden wäre, dann hätten bei Übereinstimmung der angenommenen mit der tatsächlichen Richtung des ungestörten S_q-Stromes die Zeiten der Minima von ΔY_e an beiden Stationen unabhängig von der Höhe der

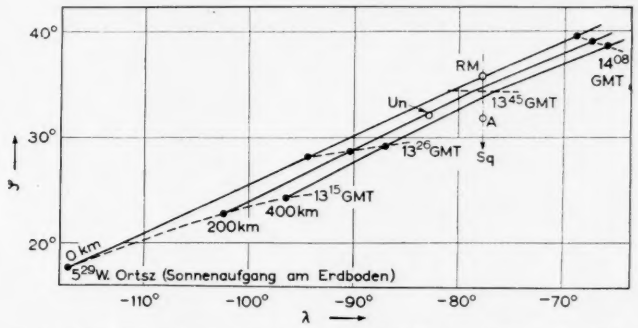

Abb. 7. Verlauf des Schattenzentrums am 28 Mai 1900 in 0, 200, und 400 km Höhe. Die gestrichelten Linien verbinden die Orte gleicher Zeiten. Die Kreise bezeichnen die Lage der Beobachtungsorte Union Spring (Un), Rocky Mount (RM), und eines fiktiven Ortes A. Die strichpunktierte Gerade gibt die Richtung des ungestören S_q-Stromes zur Zeit des Kernschattendurchganges in RM an.

VOL. 11 1957

stromführenden Schicht gleich sein müssen. Eine Abweichung der Richtung vom angenommenen Wert macht sich in einem Zeitunterschied der Minima von ΔY_e bemerkbar, und zwar hätte in diesem Falle bei einer Zeitdifferenz von 1 Minute die Winkelabweichung etwa 6° betragen.

Literatur

Benkova N. P.	1940	*Terr. Magn. Atmos. Elect.* **45,** 425.
Chapman S. and Bartels J.	1940	*Geomagnetism* p. 743. Oxford.
Price A. T.	1949	*Quarterly J. Mech. Appl. Math.* **2,** 283.
Schmidt A.	1899	*Z. Math. Phys.* **44,** 327.
Volland H.	1956a	*J. Atmosph. Terr. Phys.* **9,** 131.
Volland H.	1956b	*Gerland's Beitr. Geophys.* **65,** 331.

Journal of Atmospheric and Terrestrial Physics, 1957, Vol. 11, pp. 14 to 22. Pergamon Press Ltd., London

Über den Einfluss von Sonneneruptionen auf die ionosphärische *E*-Schicht

The influence of solar flares on the ionospheric *E* layer

J. Taubenheim
Heinrich-Hertz-Institut der Deutschen Akademie der Wissenschaften, Berlin-Adlershof

(*Received* 25 *March* 1957)

Zusammenfassung—Die gleichzeitig mit Mögel-Dellinger-Effekten auftretenden Erhöhungen der *E*-Schicht-Grenzfrequenz werden an einigen ausgewählten Tagen quantitativ untersucht, wobei sich zeigt, dass die Elektronendichtestörung wesentlich länger anhält, als es der Mögel-Dellinger-Effekt erkennen lässt. Eine Lösung der ionosphärischen Kontinuitätsgleichung für einen sehr einfachen Fall gestattet eine brauchbare Abschätzung des Einflusses einer Verstärkung der ionisierenden Strahlung auf die *E*-Schicht, aus der hervorgeht, dass der beobachtete Verlauf der Elektronendichtestörung entscheidend durch das langsame Abklingen der ionisierenden Strahlung und weniger durch die Rekombination bestimmt ist. Der Betrag der Strahlungserhöhung kann näherungsweise berechnet werden.

Abstract—The enhancements of *E*-layer critical frequency connected with sudden ionospheric disturbances are quantitatively discussed for a number of selected days. The increase of electron density lasts considerably longer than is deduced from the radio fadeout. A satisfactory estimate of the response of *E*-layer electron density to enhancements of the ionizing radiation is given by a solution of the ionospheric continuity equation for a very simple case. It follows that the observed variation of electron density is controlled decisively by the slow decrease of the radiation excess rather than by recombination. The magnitude of the enhancement of ionizing radiation can be calculated approximately.

1. Sonneneruptionseffekte in der *E*-Schicht

Bis vor wenigen Jahren war man der Ansicht, dass chromosphärische Eruptionen (solar flares) nur in der *D*-Schicht die Erscheinungen des Mögel-Dellinger-Effektes (S.I.D.) erzeugen. Gelegentlich beobachtete Einflüsse auf die oberen Schichten der Ionosphäre (Berkner und Wells, 1937; Becker und Dieminger, 1950) wurden als Ausnahmefälle betrachtet.

Dagegen hat Bibl (1951) statistisch nachgewiesen, dass alle grösseren Abweichungen der normalen *E*-Grenzfrequenz (f_E^0) vom mittleren Tagesgang mit Mögel-Dellinger-Effekten zusammenfallen. Umgekehrt lässt sich aus den halbstündlichen Grenzfrequenzmessungen in Lindau/Harz 1951 bis 1956 der Nachweis führen, dass auch nach Eliminierung des ungestörten Tagesganges die Mehrzahl aller Mögel-Dellinger-Effekte eine Erhöhung der Grenzfrequenz der normalen *E*-Schicht gegenüber dem Wert vor Beginn des Effektes mit sich bringt (Taubenheim, 1957a). Berücksichtigt man dabei, dass eine grosse Anzahl dieser Effekte in die Zwischenzeit zwischen zwei Grenzfrequenzmessungen fiel und beim Beginn der nächstfolgenden Messung bereits beendet war, so erscheint die Vermutung gerechtfertigt, dass wahrscheinlich jeder Sonneneruptionseffekt in der *D*-Schicht auch von einem Effekt in der *E*-Schicht begleitet ist.

Die sehr grosse Stetigkeit des Tagesganges und die geringe Streuung der Grenzfrequenzen der normalen *E*-Schicht legen es nun nahe, den Sonnenerup tionseffekt in der *E*-Schicht auch quantitativ zu untersuchen. In Abb. 1 sind einige ausgewählte Fälle auf Grund der Messungen der Ionosphärenstation Lindau/Harz aus den Jahren 1951 bis 1956 dargestellt. Die Diagramme zeigen den

Tagesverlauf des Verhältnisses der halbstündlich gemessenen f_E^0 zum Mittelwert $\overline{f_E^0}$ der Nachbartage (im allgemeinen je drei Tage vor und nach dem Effekt). Der schwarze Balken entlang der Zeitachse gibt jeweils die Dauer eines Mögel-Dellinger-Effektes an. Die damit verbundenen Ionisationserhöhungen und deren langsames Abklingen sind auch dann deutlich zu erkennen, wenn die Abweichungen vom Mittel bereits in die Grössenordnung der zufälligen Schwankungen fallen. Dass Sonneneruptionen auch kurz vor Sonnenuntergang noch merkliche Auswirkungen haben können, ist am 15 März 1956 zu ersehen.

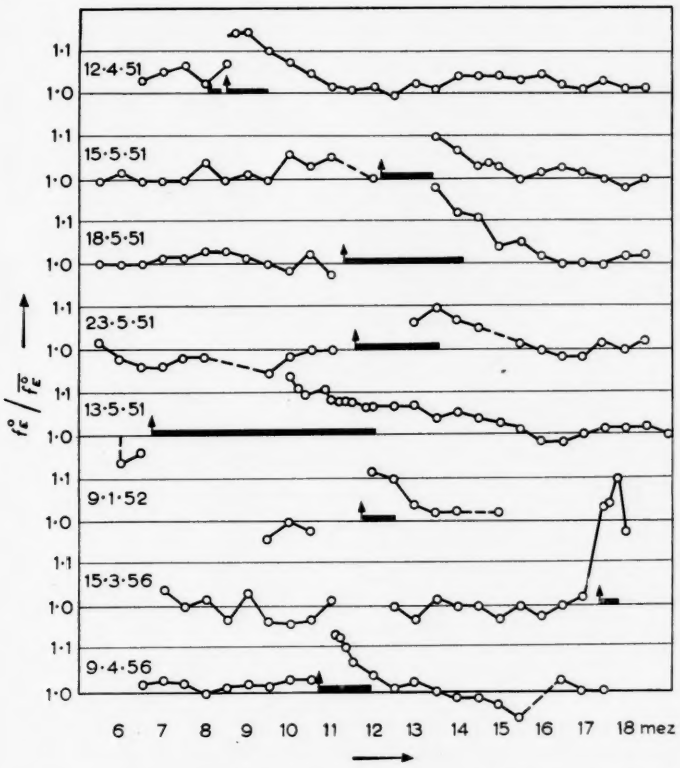

Abb. 1. Abweichungen der E-Grenzfrequenzen vom Mittelwert der Nachbartage bei Mögel-Dellinger-Effekten (Lindau/Harz). Berichtigung: Statt 13.5.51. lies: 13.6.51.

Bei der Betrachtung der Abb. 1 fällt auf, dass die Sonneneruptionseffekte in der E-Schicht sehr langsam abklingen, so dass der ungestörte Wert ($f_E^0/\overline{f_E^0} = 1$) erst längere Zeit nach dem Ende des Mögel-Dellinger-Effektes erreicht wird. Es entsteht die Frage, ob dieser zeitliche Verlauf der Elektronendichte einer Abnahme der ionisierenden Strahlung der Eruption entspricht oder durch die Rekombination in der E-Schicht bestimmt wird. Dies ist von besonderem Interesse, um auf den Verlauf der ionisierenden Strahlung rückschliessen zu können. Eine Antwort hierauf ist bereits durch eine einfache theoretische Abschätzung möglich.

VOL. 11 1957

2. Theoretische Abschätzung des Einflusses einer Sonneneruption auf die E-Schicht

Durch eine Erhöhung der Ionenproduktion q um den Faktor p gegenüber dem Normalwert q_0

$$q = p \cdot q_0 \tag{1}$$

werde die maximale Elektronendichte N um den Faktor μ erhöht:

$$N = \mu \cdot N_0 \tag{2}$$

Für den ungestörten Tagesgang der E-Schicht können im allgemeinen quasistationäre Verhältnisse vorausgesetzt werden (siehe Anhang), so dass

$$\frac{dN_0}{dt} \ll \alpha N_0^2 \tag{3}$$

(α = effektiver Rekombinationskoeffizient).

Dann folgt aus der ionosphärischen Kontinuitätsgleichung im Schichtmaximum

$$\frac{dN}{dt} = q - \alpha N^2 \tag{4}$$

eine Differentialgleichung für die Störung μ der Elektronendichte:

$$\frac{d\mu}{dt} + \alpha N_0(t) \cdot \mu^2 = \alpha N_0(t) \cdot p \tag{5}$$

Diese nichtlineare Differentialgleichung ist für ein variables $p(t)$ nicht lösbar, jedoch ist eine allgemeine Lösung möglich für den Fall $p = \text{const}$. Stellen wir die Störung der ionisierenden Strahlung bei einer chromosphärischen Eruption durch ein einfaches Modell dar in der Form:

$$\left.\begin{aligned} &q = q_0 \quad \text{für } t \leqq t_0 \\ &q = p \cdot q_0 \quad \text{für } t_0 < t < t_1; \quad p = \text{const.} \\ &q = q_0 \quad \text{für } t \geqq t_1 \end{aligned}\right\} \tag{6}$$

(siehe Abb. 2), so ergeben sich die Lösungen von (5) zu

$$\mu = \sqrt{p} \cdot \tanh\left\{\alpha\sqrt{p}\int_{t_0}^{t} N_0\,dt' + \tfrac{1}{2}\ln\left(\frac{\sqrt{p}+\mu_0}{\sqrt{p}-\mu_0}\right)\right\} \qquad \text{für } t_0 \leqq t \leqq t_1 \tag{7}$$

$$\mu = \coth\left\{\alpha\int_{t_0}^{t} N_0\,dt' + \tfrac{1}{2}\ln\left(\frac{\mu_1+1}{\mu_1-1}\right)\right\} \qquad \text{für } t \geqq t_1 \tag{8}$$

wobei

$$\left.\begin{aligned} &\mu_0 = \mu \text{ bei } t = t_0 \\ &\mu_1 = \mu \text{ bei } t = t_1 \end{aligned}\right\} \tag{9}$$

ist. Für die praktische Auswertung lassen sich die Formeln (7) und (8) vereinfachen, wenn man den näherungsweisen Ansatz

$$N_0 = N_M \cdot f(t) \tag{10}$$

macht, worin N_M die maximale Elektronendichte um 1200 Uhr MEZ und $f(t)$ eine Funktion der Tageszeit ist, deren Form nur langsam mit der Jahreszeit variiert. Dann kann man eine " reduzierte Zeit"

$$\vartheta = \int f(t)\, dt \tag{11}$$

einführen, die sich in der Umgebung des Mittags nur geringfügig von der wahren Zeit unterscheidet. Nur in den je zwei Stunden vor Sonnenuntergang und nach

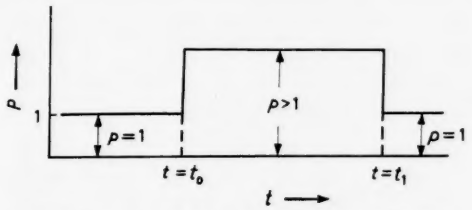

Abb. 2 Einfache Form einer Strahlungsstörung.

Sonnenaufgang überschreitet der Unterschied zwischen einer "reduzierten Minute" und einer wahren Minute den Faktor 2. In (7) und (8) ist nach (10) und (11) einzusetzen

$$\int_{t_0}^{t} N_0\, dt' = N_M(\vartheta - \vartheta_0) \quad ; \quad \int_{t_1}^{t} N_0\, dt' = N_M\,(\vartheta - \vartheta_1) \tag{12}$$

Bestimmt man aus (8) die "Abklingzeit" ϑ^*, nach der die Erhöhung der Elektronendichte bis auf einen bestimmten Wert μ^* abgenommen hat, so ergibt sich

$$\vartheta^* = \frac{1}{2\alpha N_M}\left\{\ln\left(\frac{\mu^*+1}{\mu^*-1}\right) - \ln\left(\frac{\mu_1+1}{\mu_1-1}\right)\right\} \tag{13}$$

Diese Abklingzeit kann nicht beliebig gross werden, sondern strebt, wie man bereits in (8) sieht, für $\mu_1 \to \infty$ einem Grenzwert $\vartheta^*_{\max}$ zu:

$$\vartheta^*_{\max} = \frac{1}{2\alpha N_M}\ln\left(\frac{\mu^*+1}{\mu^*-1}\right) \tag{14}$$

Berechnet man dies für $\mu^* = 1{,}02$ (Grenze der Beobachtungsgenauigkeit) und setzt $N_M = 1 \cdot 10^5\ \mathrm{cm^{-3}}$ und $\alpha_E = 1 \cdot 10^{-8}\ \mathrm{cm^3\ sec^{-1}}$, so ergibt sich

$$\vartheta_{\max}\,(2\%) = 38{,}5 \text{ (reduzierte) Minuten} \tag{15}$$

Die Abklingkurven $\mu(\vartheta)$ nach (8) bei einem effektiven Rekombinationskoeffizienten $\alpha_E = 1 \cdot 10^{-8}\ \mathrm{cm^3\ sec^{-1}}$ sind in Abb. 3 dargestellt. Die Zeitskala bezieht sich auf einen Wert $N_M = 1 \cdot 10^5\ \mathrm{cm^{-3}}$. Anstelle von μ_1 ist als Parameter der Wert p angeschrieben, wobei vorausgesetzt ist, dass bei Ende der Strahlungsstörung

VOL. 11 1957

bereits der aus (7) folgende asymptotische Wert $\mu = \sqrt{p}$ erreicht war, was nach (7) im allgemeinen bereits einige Minuten nach Beginn der Strahlungsstörung in hinreichender Annäherung erfüllt ist.

Das hier berechnete Modell liefert zweifellos den Grenzfall zur Abschätzung aller allgemeineren Formen der Strahlungsstörung. Erfolgt der Rückgang der Ionenproduktion auf den ungestörten Wert q_0 nicht unstetig, sondern stetig, so

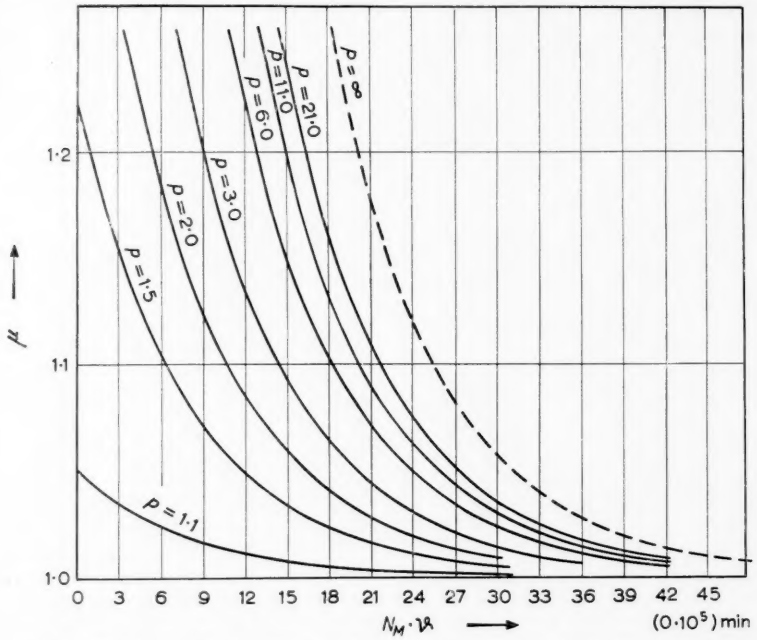

Abb. 3. Elektronendichteverlauf in der E-Schicht nach Ende der Strahlungsstörung ($N_M = 1 \cdot 10^5$ cm^{-3}; $\alpha_E = 1 \cdot 10^{-8}$ cm^3 sec^{-1}).

wird die Abklingzeit ϑ^* nach (13) von dem Zeitpunkt an gerechnet, wo $q = q_0$ wird. Dann aber ist ϑ^* auf jeden Fall kleiner als der für den gleichen maximalen Störungsfaktor p berechnete Wert aus Gleichung (14) bzw. der Grenzwert (15).

3. Diskussion der Beobachtungen

Setzt man voraus, dass das Abklingen der Elektronendichtestörung ausschliesslich eine Folge der Rekombination ist, d.h. dass am Ende des Mögel-Dellinger-Effektes (Ende des schwarzen Balkens in Abb. 1) wieder $q = q_0$ ist, so lässt sich mit Hilfe der Formel (13) aus den gemessenen Werten μ und N_M der Rekombinationskoeffizient α bestimmen. Solche Berechnungen ergeben jedoch bei den in Abb. 1 dargestellten und mehreren weiteren Fällen α—Werte in der Grössenordnung 10^{-9} und 10^{-10} cm^3 sec^{-1}. Das steht im Widerspruch zu allen bisherigen Ergebnissen (vgl. Mitra und Jones, 1954), insbesondere zu den neueren Bestimmungen von α_E aus Sonnenfinsternissen (z.B. Minnis, 1955). Die Möglichkeit, dass der Wert des effektiven Rekombinationskoeffizienten selbst durch die Strahlungserhöhung eine Änderung erleidet, ist nach einer eingehenden Diskussion an

anderer Stelle (TAUBENHEIM, 1957b) sehr unwahrscheinlich. Daher ist als wahrscheinlichster Wert von α_E auch während der Sonneneruption $\alpha_E = 1 \cdot 10^{-8}$ cm^3 sec^{-1} anzunehmen. Der Verlauf des Abklingens der Elektronendichtestörung kann hiernach nicht allein eine Folge der Rekombination sein, sondern muss einer reellen Abnahme der ionisierenden Strahlung entsprechen.

4. Der Verlauf der Ionisierenden Strahlung.

So lange die quasistationäre Bedingung (3) gilt (siehe Anhang), kann mit Hilfe der Gleichung (5) aus dem gemessenen Verlauf von μ und dem mittleren Tagesgang $N_0(t)$ der zeitliche Verlauf der Strahlungserhöhung $p(t)$ mit ausreichender Genauigkeit berechnet werden. Dabei wird $\alpha_E = 1 \cdot 10^{-8}$ cm^3 sec^{-1} angesetzt. Die so gewonnenen Kurven unterscheiden sich in ihrer Form nur geringfügig von den Kurven der Abb. 1, wenn man den Massstab in $p \sim (f_E^0/f_E^{\bar{0}})^4$ ändert, und brauchen daher hier nicht besonders wiedergegeben zu werden. Danach zeigt sich, dass tatsächlich die Erhöhung der ionisierenden Strahlung in fast allen Fällen länger anhält, als es aus den Angaben des Mögel-Dellinger-Effektes zu ersehen ist. Da aber bei der Registrierung von Empfangsfeldstärken die Zeitangabe der Erreichung des "normalen" Wertes ausserordentlich ungenau ist, dürfte dieser Diskrepanz keine zu grosse Bedeutung beizumessen sein. Vielmehr ist offensichtlich die Messung der E-Grenzfrequenz das genaueste Mittel zur Verfolgung der Schwankungen der ionisierenden Strahlung.

VOL. 11 1957

Im allgemeinen reicht aber der Exzess der ionisierenden Strahlung auch über das Ende der spektroheliographisch (H_α-Linie) beobachteten chromosphärischen Eruption hinaus. Dieses "Ende der Eruption" durfte bei visueller Beobachtung einem Helligkeitsunterschied zwischen Eruption und Sonnenoberfläche von wenigen prozent entsprechen (nach den von BLACKWELL (1946) angegebenen Kontrastschwellen). Zieht man dabei die Kleinheit der Eruptionsfläche gegenüber der ganzen Sonnenscheibe in Betracht, so unterscheidet sich dann die Gesamtemission der Sonne in der H_α-Linie nur um einen verschwindend geringen Bruchteil gegenüber der ungestörten Sonne, während zur gleichen Zeit die ionisierende Strahlung noch in der Grössenordnung von 10% über dem Mittelwert liegt. Allerdings braucht der zeitliche Verlauf von ionisierender Strahlung und H_α-Emission nicht notwendig übereinzustimmen, wenn die beiden Wellenlängenbereiche nicht im gleichen physikalischen Vorgang erzeugt werden. Die neueren Vorstellungen über die Ionisation der E-Schicht durch eine weiche Röntgenstrahlung (ELWERT, 1953; RAWER und ARGENCE, 1954) legen den Gedanken nahe, dass die Ursprungsgebiete der ionisierenden Strahlung (etwa die innere Korona) durch die chromosphärische Eruption erst sekundär zur Strahlungsemission angeregt werden.

5. Abschätzung des Maximums der Strahlungsstörung

Der mittels Gleichung (5) berechnete Verlauf der ionisierenden Strahlung $p(t)$ hat in mehreren Fällen deutlich eine exponentielle Form. Man kann schreiben

$$p = 1 + (p^* - 1)e^{-(t-t_0)/T} \qquad \text{für } t \geqq t_0 \tag{16}$$

wo t_0 den Beginn des Sonneneruptionseffektes bezeichnet, und p^* die maximale

Erhöhung der ionisierenden Strahlung ist. In Abb. 4 ist für zwei besonders ausgeprägte Fälle die Grösse $(p - 1)$ logarithmisch über $(t - t_0)$ aufgetragen, so dass bei Übereinstimmung mit (16) die Punkte auf einer Geraden liegen. Die Relaxationszeiten T ergeben sich dabei zu 67 bzw. 48 Minuten. Extrapoliert man die Geraden bis zum Punkte $t = t_0$, so gibt der Schnittpunkt mit der Ordinatenachse eine Abschätzung des Maximums p^* der Strahlungsstörung. Man findet $p^* = 2{,}1$ am 12. April 1951 und $p^* = 2{,}5$ am 9. April 1956, also eine Erhöhung der ionisierenden Strahlung auf etwas mehr als die doppelte Intensität. Dieses Ergebnis ist insofern bemerkenswert, als für die D-Schicht aus den Mögel-Dellinger-Effekten auf Strahlungserhöhungen um das Zehn- bis Hundertfache geschlossen

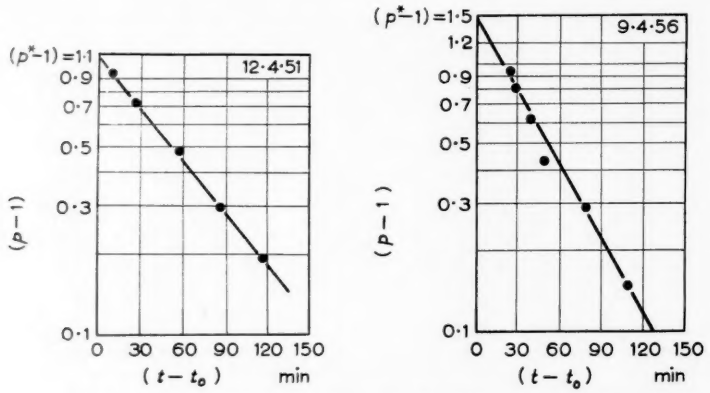

Abb. 4. Abklingen der ionisierenden Strahlung bei zwei ausgewählten Sonneneruptionseffekten.

werden muss. Das spricht gegen eine gemeinsame Ionisationsursache für E- und D-Schicht, bedarf jedoch noch der Bestätigung durch umfangreicheres Beobachtungsmaterial.

Anerkennung—Herrn Prof. Dr. O. HACHENBERG, Direktor des Heinrich-Hertz-Institutes, bin ich für sein förderndes Interesse an dieser Arbeit sehr zu Dank verpflichtet. Herrn Prof. Dr. W. DIEMINGER, Lindau/Harz, danke ich für die Erlaubnis, unveröffentlichte Beobachtungen seines Institutes verwerten zu dürfen.

ANHANG

Gültigkeit der quasistationären Näherung für die ungestörte E-Schicht

Um die Gültigkeit der quasistationären Bedingung (Gleichung 3) zu prüfen, wurde aus den Monats-Medianwerten der Ionosphärenstation Lindau/Harz für die Jahre 1951 bis 1955 die Grösse

$$x = \frac{1}{\alpha N_0^2} \cdot \frac{dN_0}{dt} \tag{17}$$

für die E-Schicht berechnet. Es zeigt sich, dass eine strenge Forderung $x < 10^{-2}$

nur während weniger Stunden um Mittag erfüllt ist. Für kleinere Strahlungsstörungen ist jedoch eine hinreichend genaue Beschreibung durch die Gleichung (5) auch bei $x < 10^{-1}$ möglich, was während des grössten Teiles des Tages gegeben ist.

Da die Messung der Elektronendichten N keinesfalls genauer als auf $\pm 2\%$ ist, beträgt der Fehler für μ etwa $\pm 0{,}02$ und daher der aus der Beobachtungsgenauigkeit folgende Fehler von p mindestens $\pm 0{,}04$. Solange der durch die quasistationäre Näherung entstehende Fehler unter diesem Wert bleibt, erscheint die Anwendung der Gleichung (5) zur Berechnung von p statthaft.

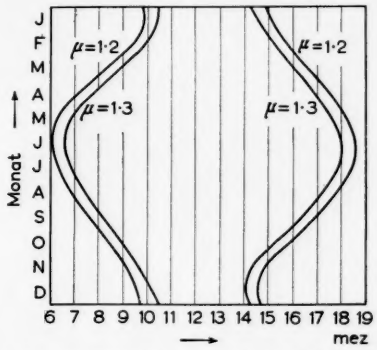

Abb. 5. Grenzen der Anwendbarkeit der quasistationären Näherung in der E-Schicht über Lindau/Harz.

Aus einer exakten Ableitung aus Gleichung (4) folgt mit (17)

$$p(1 + x) = \frac{1}{\alpha N_0} \frac{d\mu}{dt} + \mu^2 + x\mu \tag{18}$$

aus der Näherungsgleichung (5) dagegen

$$p' = \frac{1}{\alpha N_0} \frac{d\mu}{dt} + \mu^2 \tag{19}$$

Der entstehende Fehler $|\Delta p| = |p' - p|$ ist also

$$|\Delta p| = |x| \cdot |p - \mu| \tag{20}$$

oder, da während des Abklingens der Störung $\left(\frac{dp}{dt} < 0\right)$ auf jeden Fall $1 \leqq p \leqq \mu^2$ ist,

$$|\Delta p| \leqq \mu(\mu - 1) \cdot |x| \tag{21}$$

In Abb. 5 sind die Grenzen der Tageszeit angegeben, innerhalb derer für $\mu \leqq 1{,}2$ und für $\mu \leqq 1{,}3$ der Fehler $|\Delta p| \leqq 0{,}04$ bleibt. Man ersieht daraus, dass die untersuchten Sonneneruptionseffekte mit nur einer Ausnahme (15 März 1956) in den Bereich fallen, wo die Gleichung (5) zur Berechnung von p benutzt werden kann.

VOL. 11 1957

Literatur

Becker W. u. Dieminger W.	1950	*Z.Naturforsch.* **5a,** 308.
Berkner L. V. u. Wells H. W.	1937	*Terr. Magn. Atmos. Elect.* **42,** 183, 301.
Bibl K.	1951	*Ann. Géophys.* **7,** 208.
Blackwell H. R.	1946	*J. Opt. Soc. Amer.* **36,** 624.
Elwert G.	1953	*J. Atmosph. Terr. Phys.* **4,** 68.
Minnis C. M.	1955	*J. Atmosph. Terr. Phys.* **6,** 91; **7, 172.**
Mitra A. P. u. Jones R. E.	1954	*J. Geophys. Res.* **59,** 391.
Rawer E. u. Argence E.	1954	*Phys. Rev.* **94,** 253.
Taubenheim J.	1957a	*Diss. Math.-Nat. Fak. Humb.-Univ. Berlin.*
Taubenheim J.	1957b	*Tagungs-Ber. Probleme d. Plasmas* (Leipzig, Oktober 1956). Akademie-Verlag, Berlin. Im Druck.

Journal of Atmospheric and Terrestrial Physics, 1957, Vol. 11, pp. 23 to 30. Pergamon Press Ltd., London

On the barometric pressure coefficient for cosmic-ray neutrons*

J. A. Lockwood and A. R. Calawa†
University of New Hampshire, Durham, N.H.

(*Received* 8 *April* 1957)

Abstract—From the cosmic-ray neutron intensity recorded at Mount Washington, N.H., during 1954–1955, an accurate determination has been made of the barometric pressure which best measures the average air mass above this mountain, where high wind velocities are prevalent. The results indicate that the existing pitot tube system for compensating for the pressure deficiency produced by the airflow over the mountain is reliable to an estimated standard deviation of $\pm 0{\cdot}03$ in. Hg. It also appears that the barometric pressure correction for the neutron intensity at any location is one of the largest sources of error in studying primary cosmic-ray intensity-time variations from the time variations of the neutron intensity deep within the atmosphere.

VOL. 11 1957

1. Introduction

Simpson has shown that the intensity-time variations in the low-energy portion of the primary cosmic radiation can be studied by measuring the nucleonic component deep within the earth's atmosphere, after correcting for the effects of changes in meteorological conditions (Simpson *et al.*, 1953). It has been found recently that the only significant meteorological factor producing variations in the nucleonic component is the air mass effect (Simpson *et al.*, 1953; Lockwood and Yingst, 1956). Since the nucleonic component incident on a lead-paraffin pile is confined largely to the vertical direction for sea-level and mountain locations, the average air-mass effect may be evaluated by determining the dependence of the neutron counting rate of the pile upon the local barometric pressure.

Since high counting rates are necessary to determine small intensity-time variations, it is desirable to locate the monitoring stations at mountain elevations. It is difficult, however, to determine accurately the barometric pressure at mountain elevations where high wind-speeds are prevalent. Such conditions introduce an uncertainty in the conventional pressure measurements, the magnitude of which will depend upon the wind velocity, the contour of the mountain, and the location and type of structure housing the barometer. For example, at Mount Washington, gales of 60 m.p.h. are common. This wind-speed will reduce the barometric pressure reading at the summit by approximately 0·15 in. Hg. compared with the pressure at the same level in the free air away from the influence of the mountain (Falconer, 1947). At this location a statistical accuracy of 0·2 per cent may be obtained for the hourly neutron counting rate of a standard lead-paraffin pile (Simpson, 1955). For periods of approximately 24 hr, the stability of the circuits may be held to within $\pm 0{\cdot}1$ per cent. Since the pressure coefficient α for the nucleonic component as measured by a lead-paraffin pile is $-25{\cdot}0$ per cent /in. Hg. the above-mentioned pressure deficiency produces an apparent intensity variation of $\sim 3{\cdot}7$ per cent. It is estimated that at other mountain stations this pressure deficiency would be

* Supported by the Geophysical Research Directorate of the United States Air Force Cambridge Research Center, Air Research and Development Command.

† Now at Fansteel Metallurgical Corporation, North Chicago, Illinois.

smaller, and consequently the error in correcting the neutron counting rate would be less. To keep the uncertainty introduced by the barometric pressure correction approximately equal to a statistical accuracy of 0·2 per cent, it is necessary to determine the true barometric pressure to an accuracy of less than $\pm 0{\cdot}01$ in. Hg. Therefore, an accurate determination must be made for each station of the barometric pressure which best measures the average air mass above it.

At Mount Washington, Falconer has developed a method for partially correcting the observed barometric pressure (Falconer, 1947). The dynamic head of a pitot tube located on the top of the building and vaned into the wind is connected to a sealed fixed-cistern mercury barometer and a sealed microbarograph. The pressure readings for this system are greater than the observed pressure inside the building by approximately $1/2\rho V^2$, where ρ = air density and V = the wind-speed. Constrictions, in the form of small glass capillary tubes, have been placed in the pressure leads to dampen the violent pressure changes due to gusts of wind. In its particular location, this device seems to provide adequate compensation for the pressure deficiency. The barometric pressure recorded hourly by this system will be designated as B_p and that recorded hourly by a microbarograph open to the inside building pressure as B_u. Since the air-mass effect for the nucleonic component is large, it seemed feasible to use the neutron counting rate to determine the effects of wind velocity on the barometric pressure corrections for this station. Further, it was definitely established that the neutron intensity-time variations were at a minimum in 1954, corresponding to the minimum in solar activity (Meyer and Simpson, 1954; Lockwood and Yingst, 1956). Therefore, the neutron data recorded during 1954 were used in this analysis.

2. Experimental Results

To determine whether the hourly neutron counting rate follows the pressurized (B_p) or unpressurized (B_u) barometer on Mount Washington, we shall plot the barometric pressure derived from the neutron counting rate of a lead-paraffin pile (for the design, see Lockwood, and Yingst, 1956) as a function of the B_p and B_u for the summer of 1954. The absence then of any intensity-time variations greater than 2·0 per cent allows a reliable determination of the barometric pressure. The results of this analysis are shown in Fig. 1. To determine the barometric-pressure reading P_N from the neutron intensity, the mean hourly neutron intensity was normalized to the mean B_p for the period. The known dependence of neutron intensity upon air mass

$$N = N_0 e^{+\alpha(p-p_0)}, \tag{1}$$

where N = observed neutron intensity at pressure p, N_0 = neutron intensity at some standard pressure p_0, and $\alpha = (-9{\cdot}7 \pm 0{\cdot}2)$ per cent/cm Hg, was used to convert the observed neutron counting rate into a pressure. For example, $\bar{N} = 3783$ hr^{-1} for 196 hourly readings and $\bar{B}_p = 23{\cdot}800$. Thus, for an observed counting rate 3900 hr^{-1}, $N/N_0 = 1{\cdot}030$, and the pressure P_N given by (1) is 23·680 in. Hg. The results of a linear correlation of P_N and B_p, curve B, Fig. 1, indicate that B_p measures the true air mass over the detector to within $\pm 0{\cdot}05$ in. Hg. The dashed curve shown in Fig. 1 has a unit slope and represents the curve of a barometer

reading of the actual air mass overhead. It is evident from Fig. 1 that B_u does not measure the air mass above the detector for barometric pressures less than 23·500 in. Hg. For $P_N \geqslant 23{\cdot}500$, the difference between B_p and B_u is less than the standard error of estimate. This is to be expected, since, in general, the higher wind velocities occur at lower barometric pressures. Therefore, the neutron intensity at this location must be corrected for air-mass variations by use of the pressurized barometer readings.

During 1953–1954 several analyses (Lockwood and Yingst, 1956) were made to determine accurately the barometric-pressure coefficient α for the neutron intensity. The value as determined for a lead-paraffin pile operating at sea-level

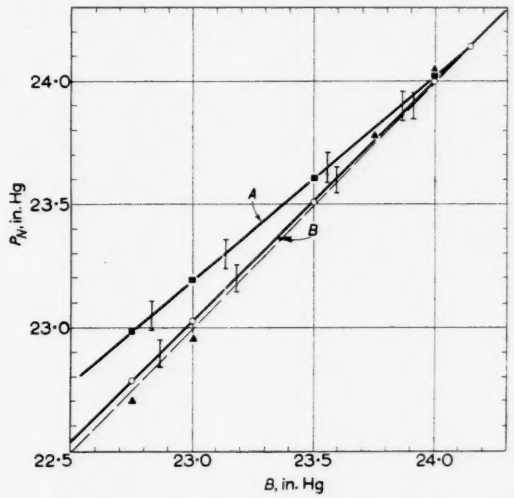

Fig. 1. The barometric pressure P_N derived from the neutron intensity as a function of B_p (curve B) and of B_u (curve A). The dashed curve is a line of unit slope. The standard errors of estimate are shown for each figure.
▲ 1955–1956; ■ 1954; ○ 1954.

(Durham, N. H.) is $\alpha = (-9{\cdot}70 \pm 0{\cdot}15)$ per cent/cm Hg. For the detector at Mount Washington, $\alpha = (-9{\cdot}7 \pm 0{\cdot}2)$ per cent/cm Hg, using the pressurized barometer readings. If the unpressurized barometer readings B_u are correlated with the neutron intensities, $\alpha = (-8{\cdot}1 \pm 0{\cdot}3)$ per cent/cm Hg, which is not in agreement with α for the detector at sea-level or with previously reported values (Simpson *et al.*, 1953; Lockwood and Yingst, 1956; Rose, Fenton, and Katzman, 1956).

Further, the neutron intensity recorded at Mount Washington when corrected for barometric pressure should obviously not depend upon the wind-speed. It is found that there is no significant correlation of the corrected neutron intensity with wind-speed if the pressurized barometric pressure is used, i.e. the correlation coefficient $r < -0{\cdot}05$. However, if the neutron intensity is corrected for pressure variations by the unpressurized barometer, a significant correlation with wind-speed, $r = -0{\cdot}65$, is found. It is thus apparent that some type of correction must be made at this location to the usual microbarograph or aneroid readings made inside the building.

VOL. 11 1957

In the event of the failure of the pitot tube, which occurs occasionally during periods of high winds and icing conditions, the correct barometric pressure could be obtained from the unpressurized barometer, provided the difference $\Delta B = B_p - B_u$ had been determined as a function of wind-speed. The results of a correlation of

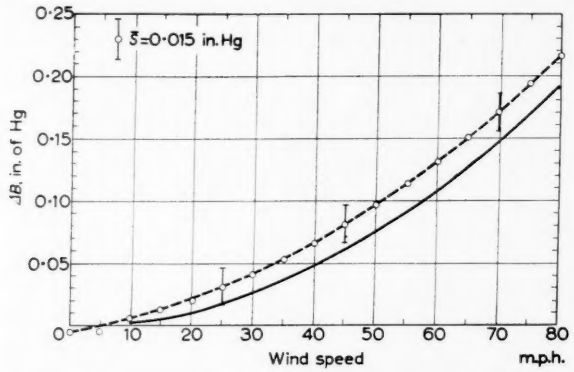

Fig. 2. The difference in barometric pressures ΔB on Mount Washington as a function of wind-speed is given by the dotted curve with a standard error of estimate, $\bar{S} = \pm 0{\cdot}015$ in. Hg. $\Delta B = B_p - B_u$, where B_p is the pressurized barometric pressure and B_u the barometric pressure recorded on a conventional microbarograph, both having a precision of $\pm 0{\cdot}005$ in. Hg. The smooth curve is $\Delta_p = \frac{1}{2}\bar{\rho}V^2$, where $\bar{\rho} = 1{\cdot}010 \times 10^{-3}$ g cm^{-3}, the mean air density at the station, V the wind-speed (m.p.h.), and Δp the pressure difference (in. Hg).

ΔB with the wind-speed on Mount Washington during the period July to September 1954 are shown in Fig. 2. The dotted curve is a plot of

$$\Delta B = -0{\cdot}005 + 7{\cdot}88 \times 10^{-4}V + 2{\cdot}49 \times 10^{-5}V^2 \quad \text{in. Hg} \qquad (2)$$

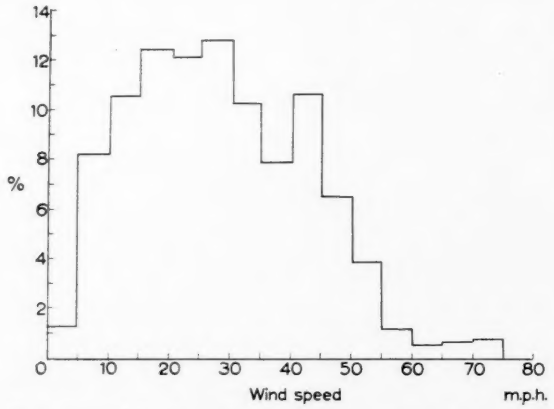

Fig. 3. Histogram of the frequency distribution of wind-speeds expressed as a per cent/5 m.p.h. interval for the summer 1954.

where V = wind-speed in m.p.h. The standard error of estimate $\bar{S} = \pm 0{\cdot}015$ in. Hg is slightly less for this curvilinear correlation than for a linear correlation of ΔB with V^2. If one assumes a simple Bernoulli effect for the air-flow over the mountain, the smooth curve in Fig. 2 results. For wind-speeds greater than 40

m.p.h. it appears that the barometric correction is simply KV^2, where K is some constant. The frequency distribution of winds for this period, expressed as a per cent/5 m.p.h. interval is shown in Fig. 3.

Fig. 4 is a similar plot of ΔB against V for a sample of readings in November and December of 1955 and January 1956, using both linear and curvilinear correlations. It appears that the observed pressure difference is smaller in 1955–1956 than 1954, which is probably due to the erection of an additional structure at the summit, changing the wind-flow near the building housing the pitot tube and the nucleonic detector. Further, comparison with a sample of ΔB and corresponding wind-speeds

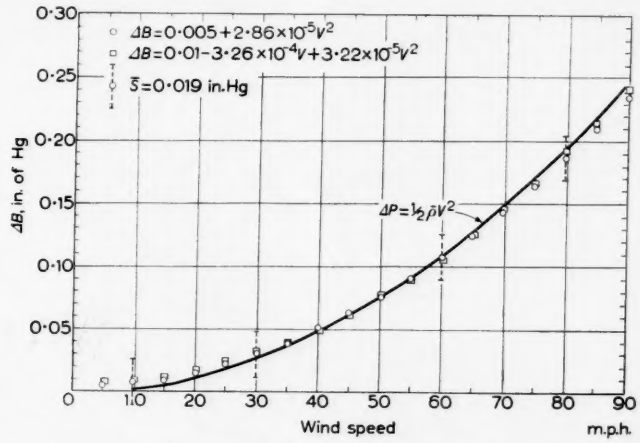

Fig. 4. The barometric pressure difference ΔB on Mount Washington in 1955–1956 as a function of wind-speed. The smooth curve represents $\Delta_c = \frac{1}{2}\bar{\rho}V^2$, (see Fig. 1). The results of a curvilinear correlation of ΔB with V and V^2 and a linear correlation of ΔB with V^2 are shown, the standard error of estimate $\overline{S} = \pm 0{\cdot}019$ in. Hg.

for December 1956 shows a dependence of ΔB upon V agreeing within the standard error of estimate with the 1955 data.

The regression equations plotted in 1954 and 1955–1956 were obtained from the hourly average wind-speed and hourly average barometric pressures. A total of 1533 corresponding readings were analysed for the 1954 period and 408 for the 1955–1956 periods. The correlation coefficient r was 0·921 for the 1954 period and 0·931 for 1955–1956. When the wind-speeds are high and variable, considerable fluctuation in ΔB occurs over the period of 1 hr. These fluctuations contribute significantly to the spread in the values of ΔB for a given wind-speed. Some indication of the fluctuations in ΔB within a 1 hr period may be obtained from Fig. 5. Here the barometric pressure difference $\Delta B'$ at 15-min intervals is plotted against the hourly average wind-speed. $\Delta B'$ is the difference between the 1-hr average B_p and the readings at 15 min intervals of an aneroid barometer (precision of $\pm 0{\cdot}005$ in. Hg) exposed to the inside building pressure. It is seen that variations considerably greater than 0·01 in. Hg occur within 15-min intervals. On occasions when either the direction or magnitude of the wind velocity is changing rapidly, larger variations than shown in Fig. 5 occur, particularly at high wind-speeds.

For the period in 1954, the data were divided into three classes according to

VOL. 11 1957

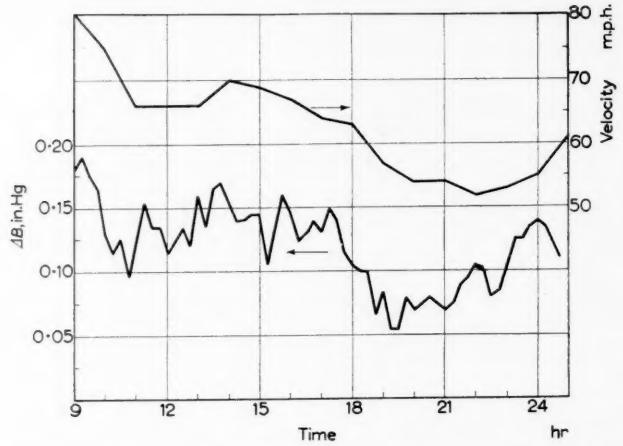

Fig. 5. The barometric pressure difference $\Delta B'$ at 15 min intervals and the hourly average wind-speed on 20 December 1956. $\Delta B' = B_p - B_A$, where B_A = barometric pressure recorded at 15-min intervals on an aneroid barometer (precision of $\pm 0{\cdot}005$ in. Hg).

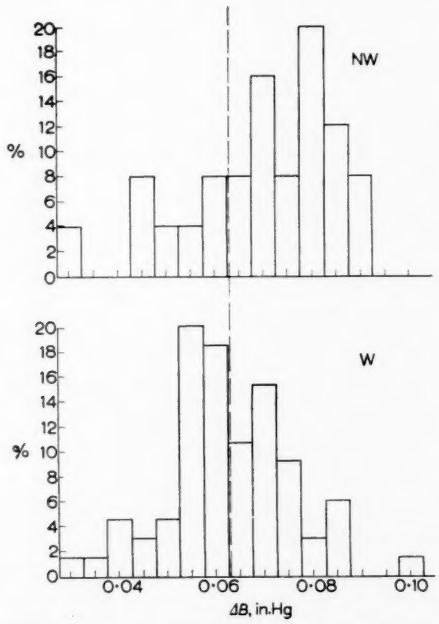

Fig. 6. The frequency distribution ΔB as a function of wind direction for a wind-speed of 40 ± 1 m.p.h.

wind-speed: $\bar{V} \leqslant 20$, $20 \leqslant \bar{V} \leqslant 40$, $\bar{V} \geqslant 40$ m.p.h. where $\bar{V}$ indicates the average speed over at least a 10-hr period. From this grouping, it is found that the data are best represented over the entire range of wind-speeds shown in Fig. 2 by equation (2). It would appear that the correction over the entire range of wind-speeds is given approximately as a function of V^2, the deviation being significant only at low wind-speeds.

In these same data the variation of ΔB for a particular wind-speed was analysed. A χ-square test of the frequency distribution of ΔB for wind-speeds of 25 ± 1, 40 ± 1, and 50 ± 1 m.p.h. showed that the distribution was normal considering $Px_2 = 0{\cdot}05$ as the limiting probability (WORTHING and GEFFNER, 1954). However, if the dependence of ΔB upon wind direction for a wind-speed of 40 m.p.h. is considered, a frequency distribution as shown in Fig. 6 results. Only two wind directions, north-west and west, are plotted, since more than 80 per cent of the readings in the sample selected were for these two directions. There appears to be a small directional effect in the correction ΔB. In this case, the most probable value of ΔB is greater by $\sim 0{\cdot}015$ in. Hg for north-west winds. This effect is due most likely to a change in the building effect for different wind directions.

Therefore, from the curve shown in Fig. 4, the necessary corrections may be made to the barometer readings recorded inside the building in the event of failure of the pitot tube.

3. DISCUSSION

First, from these results it is evident that the pressurized barometer reading B_p is a measure of the average air mass over the nucleonic detector at Mount Washington. It is clear that this system partly compensates for the pressure deficiency produced there by the air-flow over the summit. Of course, a plot such as given in Fig. 2 or Fig. 4 represents the pressure deficiency due to air-flow both over the mountain and around the building. The latter effect is rather uncertain to evaluate, and probably accounts for some of the difference in ΔB with wind direction at a constant wind-speed.

VOL. 11 1957

To evaluate the accuracy with which B_p measures the air mass above the detector, a sample of the hourly average neutron counting rates corrected for barometer using the values of B_p as a first-order approximation showed a standard deviation of $\pm 1{\cdot}4$ per cent. A pressure variation of $\sim 0{\cdot}05$ in. Hg would introduce approximately as large a variation in the neutron counting rate. Therefore, the small cosmic-ray intensity-time variations present in 1954, and any electronic circuit fluctuations ($\sim 0{\cdot}5$ per cent), were probably the largest source of error in this analysis. On this basis, the pressurized barometer reading B_p is a measure of the air mass above the detector at Mount Washington to an estimated standard deviation of $\pm 0{\cdot}03$ in. Hg. This corresponds to a variation of $\sim \pm 0{\cdot}5$ per cent in the neutron counting rate.

Second, the barometric pressure correction appears to be one of the largest sources of error in studying primary cosmic-ray intensity-time variations by measuring the nucleonic component deep within the earth's atmosphere, especially for hourly variations. Even at sea-level it is doubtful that an ordinary microbarograph or aneroid barometer would reliably indicate the true air mass above it with an error $< \pm 0{\cdot}02$ in. Hg. This uncertainty would arise due to turbulence in the atmosphere, air-flow around the building, and a small instrument error. Therefore, a very definite limitation is placed upon the reliability of small hourly variations in the neutron intensity even for a large lead-paraffin pile with a low statistical error. If, for example, the hourly counting is $4{\cdot}2 \times 10^5$ hr^{-1}, then the statistical uncertainty $\sigma_s = \pm 0{\cdot}15$ per cent. To keep the uncertainty in N from other sources to $\sim 0{\cdot}15$ per cent is extremely difficult. The standard deviation in α

determined from a correlational analysis is $\sim 0{\cdot}2$ per cent, which introduces a $\sim 0{\cdot}2$ per cent uncertainty in the factor to correct the neutron intensity for barometric pressure changes, provided the true pressure is known. To keep the uncertainty in N due to the barometric correction $< 0{\cdot}2$ per cent, the barometric pressure measuring the air mass above the detector must be determined to $< \pm 0{\cdot}01$ in. Hg, which from the above analysis does not seem possible to attain.

Acknowledgements—We want to thank the Mount Washington Observatory staff for their assistance, Miss Margaret Shea and Mr. Thomas Eichelberger for computional assistance, and Dr. Frank Woods and Dr. John Mulhern for several stimulating discussions.

References

Falconer R. E.	1947	*Trans. Amer. Geophys. Union* **28,** 385.
Lockwood J. A. and Yingst H. E.	1956	*Phys. Rev.* **104,** 1718.
Meyer P. and Simpson J. A.	1954	*Phys. Rev.* **96,** 1085.
Rose D. C., Fenton K. B., and Katzman J.	1956	*Canad. J. Phys.* **34,** 968.
Simpson J. A., Fonger W., and Treiman S. B.	1953	*Phys. Rev.* **90,** 935.
Simpson J. A.	1955	*Cosmic Radiation Neutron Intensity Monitor* p. 1. University of Chicago.
Worthing J. A. and Geffner J.	1943	*Treatment of Experimental Data* p. 177. John Wiley, New York.

Journal of Atmospheric and Terrestrial Physics, 1957, Vol. 11, pp. 31 to 35. Pergamon Press Ltd., London

Application of the generalized magneto-ionic theory to the propagation of radio waves at the magnetic dip-poles of the earth

C. Lakshmi Bai
Radio Communication Laboratory, Engineering College, Banaras Hindu University
Banaras, India

(*Received* 11 *February* 1957)

Abstract—The generalized magneto-ionic theory of Booker is applied to the propagation of radio waves at the magnetic dip-poles of the earth, to obtain rigorous values for the levels of reflection in the ionosphere, of the magneto-ionic components. The propagation is discussed for various angles of incidence and for operating frequencies greater and less than the magneto-ionic frequency. The application of these results for finding out the maximum usable frequency for a given transmission distance at the magnetic dip-poles is indicated.

VOL. 11 1957

1. Introduction

The magneto-ionic theory for the propagation of radio waves through the ionosphere as given by Appleton (1925, 1932), Goldstein (1928), and Hartree (1929), is suitable for investigating vertical propagation in the ionosphere. Schekulin (1930) has attempted to explain the propagation for the case of oblique incidence in the presence of the magnetic field. Booker (1938a), however, has developed a generalization of Appleton's magneto-ionic theory capable of dealing with waves incident obliquely at the ionosphere. In this method Booker has avoided the use of the refractive index, which depends on the angle of refraction in a rather complicated manner, and also on the angle between the direction of propagation and the earth's magnetic field. His explanation of the result depends on the fact that, in a doubly refracting medium, the velocity of group propagation in general differs from that of phase propagation not only in magnitude but also in direction. These two directions for phase and group propagation are coincident in all the special cases where the earth's magnetic field has a symmetrical influence upon the propagation of the upgoing and downcoming waves. Booker has given the solution for propagation in the magnetic equatorial regions and also for east–west propagation in any magnetic latitude. Making use of this generalized theory, the present communication gives a rigorous analytical solution for the propagation of radio waves at the magnetic dip-poles of the earth, which can be applied for finding the MUF for a given transmission distance.

2. Notations

e = Charge on an electron (e.s.u.).
m = mass of an electron.
c = velocity of electromagnetic waves in free space.
N = electron density.
H = earth's magnetic field (e.m.u.).
ν = mean collisional frequency.
p = 2π times the wave frequency f.
K = absorption per unit length.

$p_H = \left|\frac{eH}{mc}\right| = 2\pi$ times the magneto-ionic frequency.

$Y = \left(\frac{e}{mcp}\right) . H.$

$y = |Y| = \frac{p_H}{p}.$

$X = \left(\frac{4\pi e^2}{mp^2}\right) N.$

$Z = \nu/p =$ damping factor.

$U = 1 - iZ.$

$\rho_0 = \frac{-U}{X} =$ reciprocal of the scattering index of the free electrons in an ionized gas when no magnetic field is imposed.

$\rho = \frac{-Y}{X}.$

$\mu =$ refractive index of the medium.

$\psi =$ angle of refraction.

$\theta =$ angle of incidence.

$q = \mu(\psi) \cos \psi =$ vertical component of phase propagation vector.

3. Propagation at the Magnetic Dip-pole

Before proceeding with the subject of the present communication we shall briefly state for convenience the generalized magneto-ionic theory of Booker, with the necessary equations.

Let ox_1, ox_2, ox_3 be the three mutually perpendicular co-ordinate axes, where ox_3 is vertical and x_2ox_3 is the plane of phase propagation. Similarly, the suffixes for any quantity will represent the components along the above co-ordinate axes. The fundamental quartic equation of the generalized magneto-ionic theory in case of a plane harmonic wave of frequency $f = KC/2\pi$ incident upon the ionosphere at an angle θ to the vertical in the plane x_2ox_3 is given by

$$\alpha q^4 + \beta q^3 + \gamma q^2 + \delta q + \epsilon = 0 \tag{1}$$

where α, β, γ, δ, and ϵ contain N as a variable together with H, f and θ as parameters, and their values are given below.

$$\alpha = U(U^2 - y^2) - X(U^2 - y_3^2) \tag{2}$$

$$\beta = 2(\sin \theta) . Xy_2y_3, \tag{3}$$

$$\gamma = 2U\{(\cos^2 \theta)y^2 - (U - X)(U \cos^2 \theta - X)\} - X\{y_1^2 + y_2^2 . \cos^2 \theta + (1 + \cos^2 \theta)y_3^2\}, \tag{4}$$

$$\delta = -2(\cos^2 \theta . \sin \theta)Xy_2y_3, \tag{5}$$

$$\epsilon = (U - X)\{(U \cos^2 \theta - X)^2 - y_2^2 \cos^4 \theta\} - \cos^2 \theta(U \cos^2 \theta - X)(y_1^2 + y_3^2) \tag{6}$$

It will be noted that in the above equations $U \to 1$, when damping is neglected. Though in the present communication the direct effect of damping has not been

considered, the graphs are drawn between X and $\lim_{N\to 1} q^2$, so that the effect of transition from the ordinary to the extraordinary component, during the course of the propagation through the ionosphere, may be included as shown below.

While applying the generalized magneto-ionic theory of BOOKER to the propagation of radio waves at the magnetic dip-poles of the earth, it is to be noted that these magnetic dip-poles are different from the regular magnetic poles of the earth (VESTINE *et al.*, 1947). At these magnetic dip-poles, the angle of dip $= \pi/2$, as the earth's magnetic field is vertical and therefore it has no components in the horizontal plane. Thus the analytical conditions are $H_1 = H_2 = 0$ and $H_3 = H$. It may be observed that these conditions hold good for propagation in any plane of phase propagation and for any angle of incidence. For the above conditions the original explicit expression for q^2 in terms of X, y, y_1, y_2, y_3, Z, $\sin\theta$, and $\cos\theta$ can be expressed in the simplified form as,

$$q^2 = \cos^2\theta - \frac{X(U-X)}{U(U-X) - \frac{1}{2}y^2\sin^2\theta \pm \sqrt{\frac{1}{4}y^4\sin^4\theta + y^2(U\cos^2\theta - X)(U-X)}} \tag{7}$$

and the zeros of q^2 corresponding to the different levels of reflection of the magneto-ionic components are given by the roots of the equation

$$\epsilon \equiv (1-X)\{(\cos^2\theta - X)^2\} - (\cos^2\theta)(y^2)(\cos^2\theta - X) = 0 \tag{8}$$

when the effect of damping is neglected. The positive sign before the radical sign in the denominator of equation (7) corresponds to the ordinary wave and the negative sign corresponds to the extraordinary wave.

The four roots of the quartic equation (1) for q correspond to the upgoing and downcoming ordinary and extraordinary waves. The level of reflection of either of the magneto-ionic components is given by the condition that a root of the quartic equation (1) for q corresponding to the *upgoing* magneto-ionic component should be equal to a root corresponding to a *downcoming* magneto-ionic component. The solution of the problem of oblique propagation therefore depends on the solutions of the fundamental quartic equation (1). In general, β and δ in equation (1) are different from zero; but when either $H_2 = 0$, $H_3 = 0$, or $\sin\theta = 0$, we have $\beta = \delta = 0$, and the path of phase propagation coincides with that of group propagation. In such special cases, the quartic equation (1) becomes a quadratic in q^2, leading to a rigorous analytical solution of equation (1) which is sufficiently simple for practical use.

4. Discussion of Results

In Figs. 1 and 2, graphs are drawn between X and $\lim_{U\to 1} q^2$ as mentioned earlier, for the propagation at the magnetic dip-poles. The curves in Figs. 1 and 2 are drawn for the operating frequencies half and double the magneto-ionic frequency given by the condition $y = 2$ and $y = 1/2$ respectively. The continuous curves in the above figures, are for the ordinary wave and the dotted-line ones for the extraordinary wave.

The linear variation of q^2 with x in Figs. 1(a) and 2(a) for the case of vertical incidence, shows that both the magneto-ionic components are unaffected by the

VOL. 11 1957

presence of the earth's magnetic field as they should be, since the direction of propagation is parallel to the direction of the earth's magnetic field. In Fig. 1(a) ($y = 2, \theta = 0$) the level of reflection of the ordinary wave is given by $X = \cos^2\theta = 1$; but the ordinary wave does not reflect from this level because it happens to be

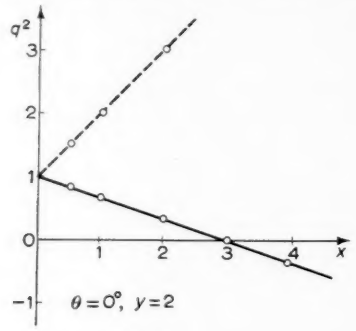

Fig. 1a.

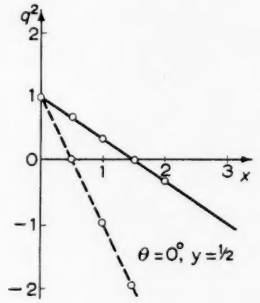

Fig. 2a.

the same as the level given by $X = \dfrac{2\cos^2\theta}{1 + \cos^2\theta} = 1$, where the independence of propagation of magneto-ionic components breaks down. Therefore the ordinary wave will penetrate this level and will be wholly reflected from the level, $X = \frac{1}{2}\{1 + \cos^2\theta + \sqrt{\sin^4\theta + 4y^2\cos^2\theta}\}$, which in this case takes the simplified form $x = 1 + y = 3$. For the above conditions, the extraordinary wave is not reflected

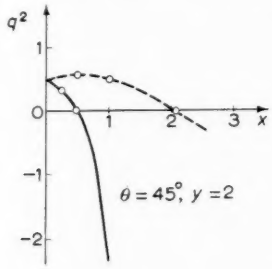

Fig. 1b.

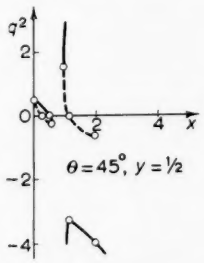

Fig. 2b.

and is wholly absorbed by the medium, as shown by the dotted line. In Fig. 2(a) ($\theta = 0,\ y = 1/2$) the ordinary wave is reflected from the level given by $X = \frac{1}{2}\{1 + \cos^2\theta + \sqrt{\sin^4\theta + 4y^2\cos^2\theta}\}$ and the extraordinary wave is reflected from the level, $X = \frac{1}{2}\{1 + \cos^2\theta - \sqrt{\sin^4\theta + 4y^2\cos^2\theta}\}$.

In Fig. 1(b), ($y = 2, \theta = 45°$), the ordinary wave is reflected from $X = \cos^2\theta$, and the extraordinary from $X = \frac{1}{2}\{1 + \cos^2\theta + \sqrt{\sin^4\theta + 4y^2\cos^2\theta}\}$. The infinity of the curve is at $X = 1$, and is independent of the angle of incidence as well as of the ratio of the operating frequency to the magneto-ionic frequency. In Fig. 2(b) ($y = 1/2, \theta = 45°$) we see that the infinity of q^2 is at $X = 1$, just as in Figs. 1(b), 1(c), and 2(c). The ordinary wave is reflected from $X = \cos^2\theta$ and the extraordinary from the two levels given by $X = \frac{1}{2}\{1 + \cos^2\theta \pm \sqrt{\sin^4\theta + 4y^2\cos^2\theta}\}$,

the reflection at the lower level (— sign for the radical) being only partial. It may be further added that in case of Fig. 2(b), the quantity under the radical sign in equation (7) has real and positive roots and therefore the two magneto-ionic components meet for values of X given by the roots of the equation $64X^2 - 96X + 33 = 0$ obtained by substituting the values of y and θ in the expression under the radical sign in equation (7). It is to be noted that Figs. 1(b) and 2(b) are representative of the behaviour of the magneto-ionic components for the angle of incidence $\theta < \pi/2$, but > 0.

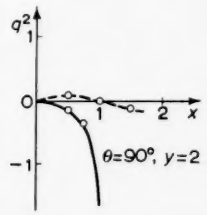

Fig. 1c.

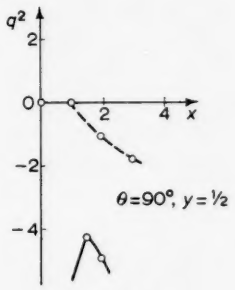

Fig. 2c.

VOL. 11 1957

In Figs. 1(c) and 2(c) ($\theta = \pi/2$), the case of glancing incidence, the ordinary wave is not reflected at all, it is wholly absorbed by the medium; but the extraordinary wave is reflected from the level corresponding to $X = \frac{1}{2}\{1 + \cos^2\theta + \sqrt{\sin^4\theta + 4y^2\cos^2\theta}\}$. In Fig. 2(c) ($\theta = \pi/2$, $y = 1/2$) q^2 has imaginary values between $X = 0$ and $X = 1$ both for the ordinary and extraordinary waves, presumably due to the effect of damping. In all these cases it is to be noted that the level of reflection of the ordinary wave is independent of the earth's magnetic field, as it should be by the definition of the split components. It may be added that in Figs. 1 and 2 the negative values of X have been omitted, as they do not have any physical significance, since the ionization density does not exist for these values of X.

The above results can be applied to actual radio transmission for calculating rigorous values for the maximum usable frequency for any given value of the transmission distance.

Acknowledgement—In conclusion, I express my grateful thanks to Dr. S. S. Banerjee for his valuable guidance in the preparation of this communication.

References

Appleton E. V.	1925	*Proc. Phys. Soc.* **37,** 16D.
Appleton E. V.	1932	*J. Inst. Elec. Engrs.* **71,** 642.
Booker H. G.	1938a	*Phil. Trans. Roy. Soc.* **A237,** 411.
Booker H. G.	1938b	*Phil. Trans. Roy. Soc.* **A237,** 434.
Goldstein S.	1928	*Proc. Roy. Soc.* **A121,** 260.
Hartree D. R.	1929	*Proc. Camb. Phil. Soc.* **25,** 47.
Schekulin W.	1930	*Hochfrequenztech. U. Elektroakust* **36,** 172.
Vestine E. H., Laporte L., Lance I., and Scott W. E.	1947	*The geomagnetic field, its description and analysis* Publication No. 582, Carnegie Institution, Washington D.C.

Journal of Atmospheric and Terrestrial Physics, 1957, Vol. 11, pp. 36 to 42. Pergamon Press Ltd., London

Heavy-ion effects in audio-frequency radio propagation

C. O. Hines
Radio Physics Laboratory, Ottawa

(*Received* 29 *April* 1957)

Abstract—The usual theory of whistler propagation, in which the effects of electrons alone are considered, leads to the conclusion that whistler ray directions cannot differ markedly from the direction of the geomagnetic field. When the effects of heavy ions are considered, however, it is found that all directions of propagation are possible at audio frequencies, and that the dispersion of frequencies takes place in opposite senses for longitudinal and transverse propagation. These theoretical results may suggest new possibilities for the detection of heavy ions and for the interpretation of some types of audio-frequency observations.

Introduction

The investigation reported in this paper arose from an earlier inquiry by Storey (1956), into the possibility of detecting ions in the outer atmosphere by an appropriate analysis of whistler dispersion curves. Storey's results indicated that such effects might be perceptible, but only at the lower end of the whistler spectrum and only if the ions involved were relatively light. In fact, even with an ionized hydrogen gas as his model of the outer atmosphere, he found that no distinct effects could be expected unless the dispersion curves were measured down to 2 kc/s or even below.

The theory of whistlers has been concerned largely with propagation along geomagnetic lines of force, and this was the case treated by Storey. In the search for possible ion effects, it seemed advisable to consider propagation in other directions as well, with the hope that more distinctive features might appear and that they might begin at higher frequencies. As it turns out, both of these hopes are justified by the theory, though the means of realizing them in practice are not yet determined.

Outline of the Theory

It is not necessary to go into the background analysis—the incorporation of heavy-ion terms in the magnetic-ionic equations—since the essentials are well understood and the formalism has been presented before in a number of investigations. (See Astrom, 1950, or Scott, 1951, for example; a brief outline of the necessary development is given in an appendix.) Instead, attention will be focused on the specific points which seem most pertinent to the study of whistlers and allied phenomena.

The discussion may begin with the appropriate magneto-ionic dispersion equation, which takes the usual form

$$\alpha_4 n^4 + \alpha_2 n^2 + \alpha_0 = 0$$

or

$$n^2 = [-\alpha_2 \pm (\alpha_2{}^2 - 4\alpha_0\alpha_4)^{1/2}]/2\alpha_4 \qquad (1)$$

in which n is the refractive index and the α's are known functions of the (circular) wave

frequency, ω, of the plasma frequencies and gyrofrequencies of the charge complexes, $\omega_r's$ and $G_r's$, and of the angle θ between the wave normal and the magnetic field:

$$\alpha_p = \alpha_p(\omega, \omega_r's, G_r's, \theta).$$

Qualitatively, α_2 and α_0 are of no particular interest to the present study, since they undergo little or no change as the direction of propagation is altered.

Such is not the case with α_4, however. This coefficient has the form

$$\alpha_4 = \kappa_1 \cos^2\theta + \kappa_2 \sin^2\theta\,, \tag{2}$$

where κ_1 and κ_2 are the "longitudinal" and "transverse direct" components of the dielectric matrix, as measured with respect to the magnetic field direction. It is quite apparent that, if κ_1 and κ_2 are different in sign, then there is some direction of propagation for which α_4 vanishes and one root of n^2 becomes infinite. In the usual theory of whistlers, where electrons alone are considered, κ_1 and κ_2 do differ in sign, α_4 does pass through a zero, and the refractive index appropriate to whistlers does become infinite. At angles θ exceeding the "cut-off" angle, the usual whistler mode cannot propagate.

At the high frequency end of the whistler spectrum, ion effects do not alter the situation appreciably. But at lower frequencies the presence of ions results in κ_2 changing sign, and the foregoing conditions no longer prevail. There is no longer a cut-off angle; the whistler mode now propagates in all directions.

VOL. 11 1957

This is a qualitative difference which is worthy of note. Of further interest is the frequency at which it comes into effect. In the simplest case, where only one type of heavy ion is considered, it is not difficult to show (see appendix) that the transition frequency normally occurs near the geometric mean of the ion and electron gyrofrequencies: $\omega_T \sim |G_i G_e|^{1/2}$. Typical values range up to 20 kc/s or so, well above those indicated for ion detection in the case of purely longitudinal propagation. It will be noted that the transition frequency is inversely proportional to the square root of the ion mass, whereas the frequency required for STOREY's effects is inversely dependent on the ion mass itself.

At first, the change in the propagation characteristics may not appear to be very significant, for the cut-off angles normally predicted are close to 90° for the lower frequencies. The matter is clarified by considering ray direction, and this may be done with the aid of Fig. 1. Here are plotted curves of the refractive index, n, measured radially from the origin, as a function of θ; θ is measured directly as an angle from the horizontal axis, which represents the magnetic field direction. A single set of representative values was adopted for the gyro and plasma frequencies, and the various curves were drawn for various wave frequencies. The solid curves represent the electron-plus-ion theory, while the broken curves give corresponding results for the electrons alone. For purposes of illustration, the ions were assumed to be of hydrogen; but this limitation is not a critical one because of the relatively slow change in the effects as the ion mass changes.

At any given frequency, and for any given direction of phase propagation, the ray direction is given by the normal to the n, θ curve. The broken curves illustrate the well-known prediction of the whistler theory, that the ray direction deviates from the field direction by small angles only, regardless of the direction of phase

propagation. With the ions included, the tendency towards rays directed along the field persists, but transverse and nearly-transverse ray directions are no longer excluded. Moreover, when θ approaches 90°, the actual ray direction may be nearly perpendicular to the direction predicted by the simpler theory.

One further point of interest revealed here concerns the dispersion of nearly-transverse waves. It is apparent from the figure that the lower frequencies propagate more rapidly than do the higher frequencies in this case, quite the reverse

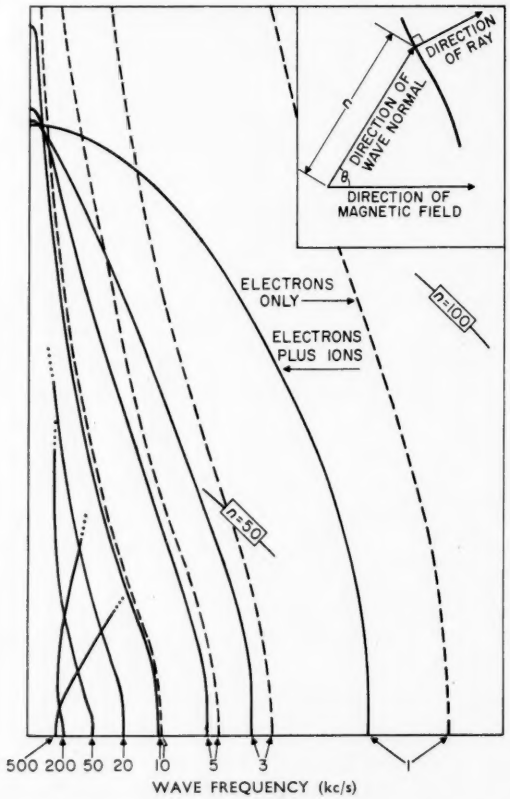

Fig. 1. Refractive index, n, as a function of wave direction and wave frequency, when
$G_e/2\pi = 918$ kc/s. $G_i/2\pi = 0{\cdot}5$ kc/s.
$\omega_e/2\pi = 2143$ kc/s. $\omega_i/2\pi = 50$ kc/s.

of the situation for longitudinal propagation in the same frequency range. This difference is emphasized by Fig. 2, where the group and phase refractive indices are plotted as functions of frequency in the two contrasting cases of longitudinal propagation and transverse propagation. (Group refractive index $= d\omega n/d\omega$.)

Conclusion

Conditions can be envisaged under which the transverse mode of propagation would play a significant observational part. Whether or not these conditions are to be found in practice is, for the moment, a matter of conjecture. What is certain,

is that many observed phenomena in the audio-frequency range await satisfactory interpretation, and that new mechanisms must be considered in seeking the interpretation. The transverse mode of propagation, with its previously unexpected characteristics, may help to provide some of the answers.

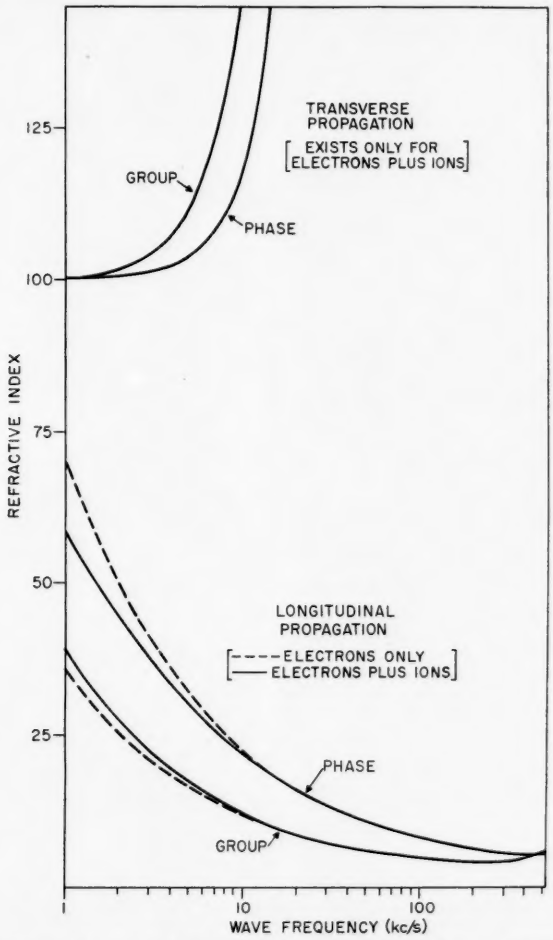

Fig. 2. Phase and group refractive indices as functions of wave frequency, when
$G_e/2\pi = 918$ kc/s. $G_i/2\pi = 0{\cdot}5$ kc/s.
$\omega_e/2\pi = 2143$ kc/s. $\omega_i/2\pi = 50$ kc/s.

Acknowledgement—The author would like to acknowledge many helpful discussions held with Dr L. R. O. Storey on the subject of whistler propagation; the investigation was undertaken at his suggestion. The work was performed under project PCC No. D48-95-11-01.

Appendix

Here are derived, in outline, the relations required for the full analysis of the heavy-ion effects considered in the main text. They pertain to electromagnetic

VOL. 11 1957

wave propagation through a homogeneous ionized medium, in the presence of a uniform magnetic field, with inter-particle collisons being ignored.

The electric field E is, from the outset, assumed to vary as $\exp i\omega t$, and the uniform magnetic induction B_0 is taken to lie along the ζ axis of a right-handed cartesian coordinate system ξ, η, ζ. In the absence of collisons, the current J is given by

$$J_\xi = i\omega\epsilon_0 a_2 E_\xi + \omega\epsilon_0 a_3 E_\eta \tag{3}$$

$$J_\eta = -\omega\epsilon_0 a_3 E_\xi + i\omega\epsilon_0 a_2 E_\eta \tag{4}$$

$$J_\zeta = -i\omega\epsilon_0 a_1 E_\zeta \tag{5}$$

where

$$a_1 = \sum_r \frac{N_r e_r^{\,2}}{\epsilon_0 M_r \omega^2}$$

$$a_2 = \sum_r \frac{N_r e_r^{\,2}}{\epsilon_0 M_r (G_r^{\,2} - \omega^2)}$$

$$a_3 = \sum_r \frac{N_r e_r^{\,2} G_r}{\epsilon_0 M_r \omega (G_r^{\,2} - \omega^2)}$$

with N_r = the number density of charged particles of the r^{th} type, e_r = the corresponding charge per particle (including sign), M_r = the corresponding mass per particle, $G_r = e_r B_0 / M_r$ = the corresponding circular gyrofrequency (including sign) and $\epsilon_0 = 8{\cdot}854 \times 10^{-12}$ farad/metre in the rationalized m.k.s. system $= 1/4\pi$ in the unrationalized Gaussian system. These relations can be obtained, for example, from equations (12) and (13) or (39) given by HINES (1953), by setting $K_r = 0$ for the present collision-free case. (While not pertinent to the present analysis, a correction to equation (39) of that paper may be noted for further application: the $i\omega$ factor in the numerator of the first summation should be replaced by $K_r + i\omega$; equation (41) there follows from the corrected formula only.)

Equations (3)–(5) can be replaced symbolically by

$$J_\mu = \sum_\nu \sigma_{\mu\nu} E_\nu \qquad \mu,\nu = \xi,\eta,\zeta \tag{6}$$

where $\sigma_{\mu\nu}$ = the conductivity matrix in the ξ, η, ζ coordinate system. Since the effects of charged particles are presented in this way, as a current, the displacement vector is simply that appropriate to a vacuum:

$$D = \epsilon^* E \tag{7}$$

where $\epsilon^* = \epsilon_0$ in the rationalized m.k.s. system and $= 1 = 4\pi\epsilon_0$ in the unrationalized Gaussian system of units. Equations (6) and (7) can be combined to yield an effective displacement vector,

$$\begin{aligned} D_{\text{eff}} &= D + (\epsilon^*/\epsilon_0) \int J\, dt \\ &= \epsilon^* [E - (i/\omega\epsilon_0) J]. \end{aligned} \tag{8}$$

This vector is related to E by an effective permittivity matrix in a manner analogous to (6). This matrix, in turn, yields the effective dielectric matrix

$$\kappa_{\mu\nu} = \begin{Vmatrix} \kappa_2 & -\kappa_3 & 0 \\ \kappa_3 & \kappa_2 & 0 \\ 0 & 0 & \kappa_1 \end{Vmatrix} \qquad \mu,\nu = \xi,\eta,\zeta$$

after division by ϵ^*. Here $\kappa_1(= 1 - a_1)$, $\kappa_2(= 1 + a_2)$, and $\kappa_3(= ia_3)$ are the "longitudinal," "transverse direct," and "transverse Hall" components. Both κ_1 and κ_2 are real, and κ_3 is pure imaginary, so $\kappa_{\mu\nu}$ is Hermitian: propagation will be lossless.

The refractive index and ray direction can be obtained quite readily with the use of $\kappa_{\mu\nu}$, following HINES (1951). This can be done most conveniently by reference to a new set of co-ordinates x, y, z, such that phase propagation is to occur in (say) the z direction. Without loss of generality, the z axis may be taken to lie in the η, ζ plane and to form angles $\pi/2 - \theta$ and θ with the η and ζ axes respectively, and the x axis may be taken to lie along the ξ axis. The dielectric matrix then transforms to

$$\kappa_{m,n} = \begin{Vmatrix} \kappa_2 & -\kappa_3 \cos\theta & -\kappa_3 \sin\theta \\ \kappa_3 \cos\theta & \kappa_1 \sin^2\theta + \kappa_2 \cos^2\theta & (\kappa_2 - \kappa_1)\cos\theta \sin\theta \\ \kappa_3 \sin\theta & (\kappa_2 - \kappa_1)\cos\theta \sin\theta & \kappa_1 \cos^2\theta + \kappa_2 \sin^2\theta \end{Vmatrix} . \quad m,n = x,y,z \qquad (9)$$

VOL. 11 1957

The refractive index n (which is not to be confused with the subscript in the foregoing relation) is then given as a solution of the equation

$$\alpha_4 n^4 + \alpha_2 n^2 + \alpha_0 = 0 \qquad (10)$$

where

$$\alpha_4 = \kappa_{zz}$$

$$\alpha_2 = \kappa_{zx}\kappa_{xz} + \kappa_{zy}\kappa_{yz} - \kappa_{zz}(\kappa_{xx} + \kappa_{yy})$$

and

$$\alpha_0 = \kappa_{xx}\kappa_{yy}\kappa_{zz} - \kappa_{xx}\kappa_{yz}\kappa_{zy} - \kappa_{yy}\kappa_{zx}\kappa_{xz} - \kappa_{zz}\kappa_{xy}\kappa_{yx} + \kappa_{yz}\kappa_{zx}\kappa_{xy} + \kappa_{zy}\kappa_{xz}\kappa_{yx}.$$

From (9), these reduce to

$$\alpha_4 = \kappa_1 \cos^2\theta + \kappa_2 \sin^2\theta \qquad (11)$$

$$\alpha_2 = -[\kappa_1\kappa_2(1 + \cos^2\theta) + (\kappa_2^2 + \kappa_3^2)\sin^2\theta] \qquad (12)$$

$$\alpha_0 = (\kappa_2^2 + \kappa_3^2)\kappa_1 \qquad (13)$$

in the present case. It will be seen that α_0 is independent of the direction of phase propagation, and examination will show that, in the conditions which are normally applicable to whistlers, the variation of α_2 with θ is essentially a $(1 + \cos^2\theta)$ variation which lacks any striking properties. It is for this reason that attention was directed away from α_0 and α_2 in the main text.

Again, in the conditions that pertain to whistlers, κ_1 is negative $(= 1 - \sum_r \omega_r^2/\omega^2$,

where $\omega_r = [N_r e_r^2/\epsilon_0 M_r^{\frac{1}{2}}]$ is the plasma frequency of the rth charge complex). On the other hand,

$$\kappa_2 = 1 + \sum_r \frac{\omega_r^2}{G_r^2 - \omega^2} \tag{14}$$

will take on both positive and negative values for ω's within the pertinent range. The situation is discussed most simply when there exist only electrons (number density N, charge $-e$, mass m) and a single type of singly ionized heavy ion (number density N, charge e, mass $M \gg m$). In practice, κ_2 can normally be approximated by the summation term in (14) alone, and, for ω's in the range $eB_0/M \ll \omega \ll eB_0/m$, it is then given by

$$\kappa_2 \simeq \frac{Ne^2/\epsilon_0 m}{(eB_0/m)^2} - \frac{Ne^2/\epsilon_0 M}{\omega^2} \tag{15}$$

which vanishes for

$$\omega^2 = (eB_0/m)(eB_0/M). \tag{16}$$

This is the transition value quoted in the main text.

The ray direction has direction cosines (in the x, y, z frame) proportional to $(\beta_4 n^2 + \beta_2, \gamma_4 n^2 + \gamma_2, 4\alpha_4 n^2 + 2\alpha_2)$, where

$$\begin{aligned}
\beta_4 &= \kappa_{zx} + \kappa_{xz} \\
\beta_2 &= \kappa_{xy}\kappa_{yz} + \kappa_{yx}\kappa_{zy} - \kappa_{yy}(\kappa_{zx} + \kappa_{xz}) \\
\gamma_4 &= \kappa_{yz} + \kappa_{zy} \\
\gamma_2 &= \kappa_{zx}\kappa_{xy} + \kappa_{xz}\kappa_{yx} - \kappa_{xx}(\kappa_{yz} + \kappa_{zy})
\end{aligned}$$

(cf. HINES, 1951). Substitution from (9) will show that $\beta_4 = \beta_2 = 0$ in the present case, and it will serve to determine γ_4 and γ_2. When (n,θ) curves are available in the form given in Fig. 1, however, the ray direction is most easily obtained by the geometrical construction indicated in the text.

REFERENCES

ASTROM E.	1950	*Arkiv. Fysik.* **2,** 443.
HINES C. O.	1951	*J. Geophys. Res.* **56,** 63.
HINES C. O.	1953	*Proc. Camb. Phil. Soc.* **49,** 299.
SCOTT J. C. W.	1951	*J. Geophys. Res.* **56,** 1.
STOREY L. R. O.	1956	*Canad. J. Phys.* **34,** 1153.

Journal of Atmospheric and Terrestrial Physics, 1957, Vol. 11 pp. 43 to 50. Pergamon Press Ltd., London

H_α emissions during aurorae over west-central Canada

R. MONTALBETTI* and A. VALLANCE JONES†
University of Saskatchewan, Saskatoon, Canada

(*Received* 18 *April* 1957)

Abstract—Observations of the occurrence of the H_α line in auroral spectra obtained at Saskatoon and at Churchill are reported. These observations are discussed with particular reference to the auroral theory of MARTYN. The diurnal dependence of the H_α emission does not seem to be in agreement with this theory. The dependence of H_α intensity on latitude and magnetic disturbance index suggests that the zone of maximum proton precipitation moves southwards as the magnetic disturbance becomes more intense. This observation is consistent with MARTYN's theory, and also with STÖRMER's theory and other theories derived from STÖRMER's analysis.

VOL. 11 1957

1. INTRODUCTION

THE discovery (VEGARD, 1939; GARTLEIN, 1948; MEINEL, 1950) that the Balmer lines of hydrogen appear strongly at times in the spectrum of auroral radiations, provided a very important clue to the interpretation of the aurora. The conclusive demonstration by MEINEL (1950) of the Doppler shift exhibited by the H_α line when aurora is viewed in the direction of the magnetic zenith, provided direct evidence of the entry of protons into the atmosphere with velocities of at least 3300 km/sec.

Some auroral theories proposed in recent years make predictions of the sign of the electrical charges of the particles which are presumed to provide the primary excitation of the auroral spectrum. This is particularly so for the theory of MARTYN (1951), which is an extension of the theory of magnetic storms of CHAPMAN and FERRARO (1931, 1932, 1933, 1940). A principal feature of this theory is the division of the main phase of auroral and magnetic disturbance into two stages.

In the primary stage (Fig. 3a) the earth is enveloped by a neutral stream of positive and negative particles travelling outward from the sun. MARTYN extended the treatment of CHAPMAN and FERRARO by proposing that the neutral stream should reunite on the dark side of the earth. The effect of the earth's magnetic field is first to polarize the neutral stream in the region near the forbidden zone encircling the earth (Fig. 3a), and secondly to cause a positive current to flow in a westerly direction around the polarized zone in the form of a ring encircling the earth in the equatorial plane. This situation is illustrated in Fig. 3(a). A component of the polarization field is then available to accelerate charged particles from the ring current along the lines of force of the earth's magnetic field.

In the second stage of the disturbance, the neutral stream of solar particles has passed beyond the earth, and the ring current maintains itself through its magnetic inertia. This situation is depicted in Fig. 3(b). The ring current is now polarized symmetrically. In both stages, positive and negative particles are presumed to

* Radio Physics Laboratory, Defence Research Board, seconded to Physics Department, University of Saskatchewan.

† The Research reported in this paper has been sponsored partly by the Geophysics Research Directorate of the Air Force Cambridge Research Center, Air Research and Development Command, under Contract AF19 (604)–1831, and partly by Radio Physics Laboratory, Defence Research Board.

leak away from the edges of the ring current, and to be accelerated toward the earth along the lines of magnetic force. As MARTYN showed, the calculated size and position of the ring current should cause these particles to reach the earth in the

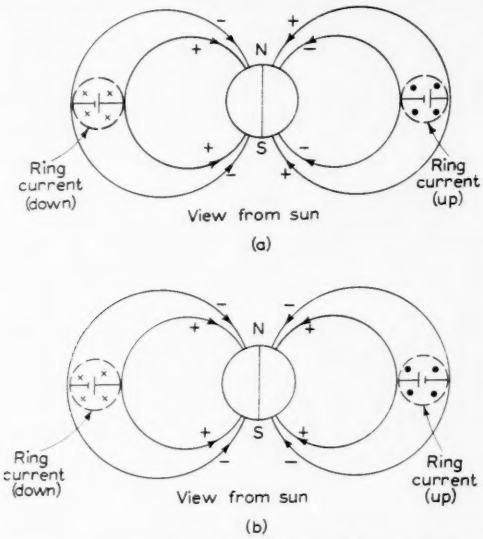

Fig. 3. Development of ring current according to MARTYN's theory of aurorae.
(a) Primary stage of main phase of disturbance.
(b) Secondary stage of main phase.

regions of the observed auroral zones. The signs of the particles precipitating north and south of the auroral zone of the Northern Hemisphere are set out in Table 1.

A programme of spectral observations to test these predictions was initiated at Saskatoon (geographic co-ordinates 51·1° N, 106·6° W, geomagnetic co-ordinates

Table 1. Sign of charge of particles according to MARTYN's theory

	Before midnight		After midnight	
	North	South	North	South
First stage of main phase of storm	+	−	−	+
Second stage	−	+	−	+
Total main phase	?	?	−	+

60·5° N, 48·9° W) and Churchill (geographic co-ordinates 58·8° N, 94·2° W, geomagnetic co-ordinates 69° N, 38° W). The northern auroral zone approximates to a circle of radius 23° centred on the north geomagnetic pole.

The testing of the theory involves two difficulties. The radius of the ring current, for an individual storm, and hence the location of the "auroral zone," is a function of the velocity and density of the particles of the neutral stream; and the two stages of the main phase of the disturbance cannot be distinguished from each

VOL.
11
1957

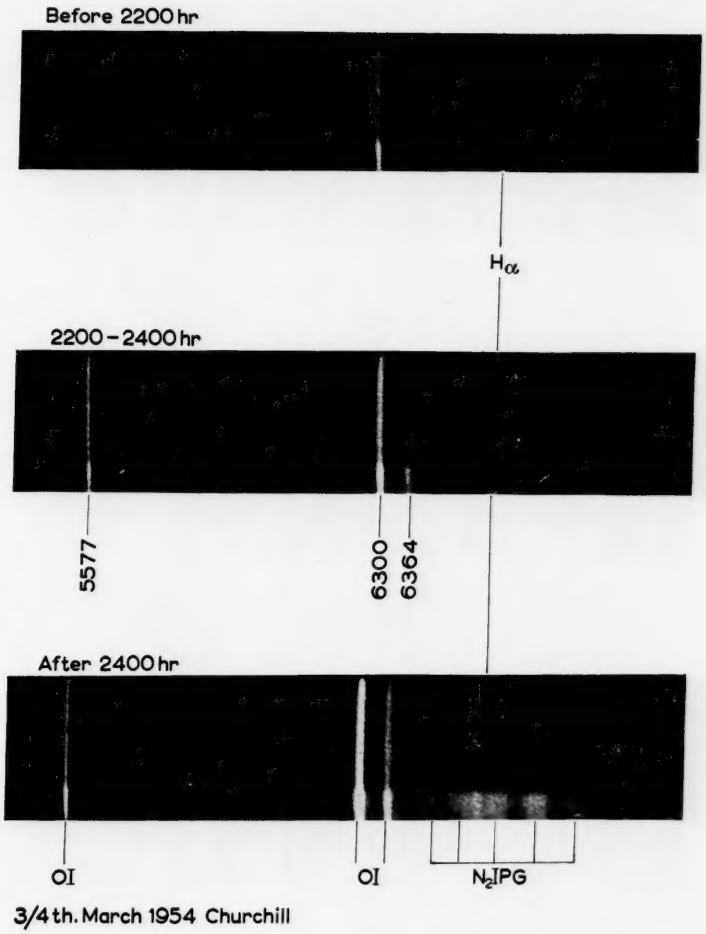

Fig. 1. Spectra of aurora obtained at Saskatoon, 28/29 April 1956.

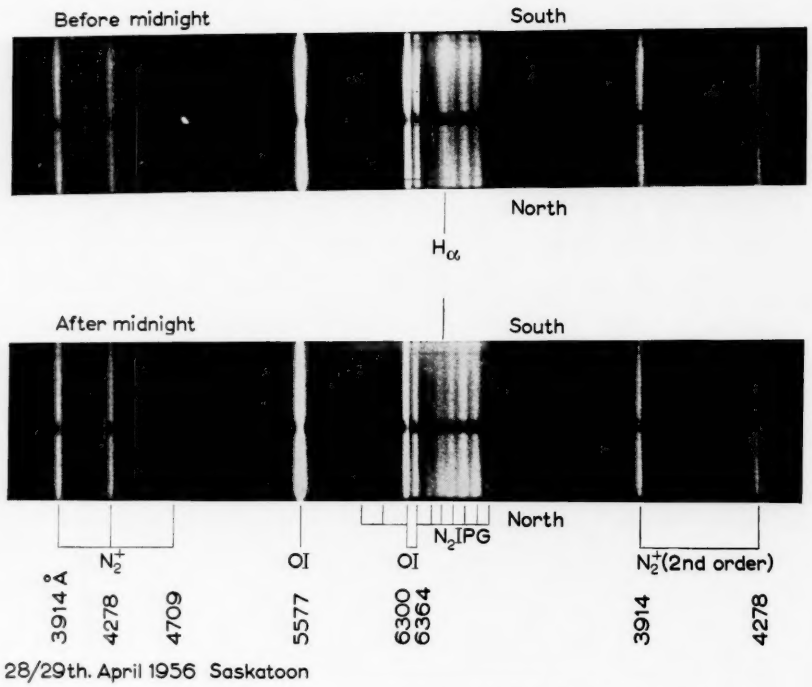

Fig. 2. Spectra of aurora obtained at Churchill, 3/4 March 1954.

other by reference to local magnetic records. There should, however, be differences in the observations for locations north and south of the auroral zone when they are averaged for each location over all periods of auroral activity. For example (see Table 1) there should be a clear distinction between the sign of the particles arriving to the north and to the south of the auroral zone for observations made after midnight. There should also be a preponderance of negative particles to the north of the auroral zone and of protons to the south for observations averaged over all times of the night. It should be noted, however, that the last prediction would also follow from other auroral theories, such as that of STÖRMER (1955), if the negative particles are electrons and the positive particles are protons.

2. INSTRUMENTATION

2.1. *Churchill*

The Churchill observations were made with a grating spectrograph with a relative aperature of $f/1{\cdot}6$ and a linear dispersion of 110 Å/mm. This instrument photographed the auroral spectrum from approximately 5560 Å to 6800 Å on 103a–F plates. It was constructed so that a maximum of six exposures could be made during any desired time-interval. An auroral exposure register as described by VALLANCE JONES and GUSH (1956) was built and mounted on the spectrograph. This records the integrated intensity of the auroral green line during each exposure.

Magnetic records of the horizontal component (H) were available from October 1955. The magnetometer was of the electronic flux-gate type.

2.2. *Saskatoon*

The Saskatoon observations from 15 October 1955 to 31 May 1956 were made with a grating spectrograph with a relative aperture of $f/1{\cdot}5$, and a linear dispersion of 300 Å/mm. This spectrograph photographed, on 103a-F plates, the auroral spectrum from 3900 Å to 7000 Å in the first order of a 600-line/mm transmission grating. A concave spherical mirror and a lens were used in conjunction with the spectrograph so that an image of a meridional strip of the sky was focused on the entrance slit. This arrangement was suggested by MEINEL (1954). The spectra obtained in this way show the variations in the auroral spectrum corresponding to different altitudes of the aurora all the way from the northern to the southern horizon. Some spectra were obtained between 19 February 1955 and 25 May 1955 with the same instrument but without the all-sky mirror system, the spectrograph being directed manually toward the brighter aurora.

Magnetic records from a three-component flux-gate magnetometer were available.

3. RESULTS

All times mentioned in this paper are local standard times, i.e. MST at Saskatoon and CST at Churchill. These times are respectively 7 and 6 hr behind GMT.

Table 2 gives the periods of observation and the total number of spectra secured in each period at Churchill and Saskatoon. At Churchill during the first period 3 spectra were generally obtained each night (one before 2200 hr, one between 2200 hr and 2400 hr, and one after 2400 hr). For the remaining two periods of observation, 2 spectra were usually taken each night (1 before local standard midnight and 1 after).

VOL. 11 1957

Table 2. Periods of observation and spectra obtained

Station	Period of observation	Number of spectra
Churchill	13 February 1954—21 April 1954	60
	23 December 1954—20 May 1955	48
	5 December 1955—13 May 1956.	162
Saskatoon	12 February 1955—3 December 1955	62*
	5 December 1955—31 May 1956	80

* These spectra were not included in the statistical analyses, but are included in the results discussed in Section 4.2.

At Saskatoon only 1 spectrum was obtained each night, except during a number of strong displays when 2 exposures were made as at Churchill. The Saskatoon spectra obtained before 15 October 1955 were not "all meridian" spectra, but were obtained by pointing the Saskatoon spectrograph at the brighter aurora without the all-sky mirror-lens system. The Churchill spectrograph was also used without an all-sky lens system, but was usually left pointing in a fixed direction during the course of a night.

Typical spectra obtained at Saskatoon are reproduced in Fig. 1. These spectra were obtained on the night of 28/29 April 1956. This was one night of a series of auroral displays which commenced on the night of 26/27 April. It may be seen that the spectrum taken before midnight shows the auroral emissions to have extended strongly from the northern to the southern horizon. The greatest intensity of the emission appears to be in the south. The H_α line is strongly developed in the before-midnight spectrum and shows the Doppler effect very strikingly as an apparent bending of the line towards shorter wavelengths near the zenith. The spectrum obtained after midnight shows very little trace of the hydrogen emission; it shows moreover that the auroral activity had retreated northward to some extent.

An example of spectra obtained at Churchill is shown in Fig. 2. These spectra were obtained during the night of 3/4 March 1954, and demonstrate a case where H_α was detected during the period before 2200 hr and after 2400 hr. H_α was not detected during the period 2200–2400 hr. From the intensity of the first positive nitrogen group and the 5577-Å line it is evident that the intensity of the aurora increased to a maximum during the interval after midnight.

4. Discussion of Results

4.1. *Diurnal variations*

On the basis of Martyn's theory (see Table 1) one would expect that south of the auroral zone the H_α emission should be slightly more frequent after midnight local time. North of the auroral zone there should be a strong tendency for H_α to occur before midnight.

In Table 3 the results bearing on this point are summarized. The results were obtained from pairs of spectra taken at Saskatoon or Churchill before and after midnight on the same night (there is, however, no correspondence between the

dates of obtaining the Churchill and Saskatoon spectra). Only spectra obtained during stronger auroral displays are included, so as to ensure that the Churchill results should refer to a station effectively north of the mean zone of precipitation.

These results do not support the MARTYN theory, since they show a tendency

Table 3. Diurnal variations of H intensity at Saskatoon and Churchill

	Number of nights	
	Saskatoon	Churchill
H_α more intense before midnight	9	11
H_α more intense after midnight	4	27
H_α present and equally intense in both periods	2	16
H_α not detected in either period	0	11

for H_α to occur more strongly before midnight at Saskatoon and after midnight at Churchill. Such a tendency is exactly the opposite to the predictions of the theory.

VOL. 11 1957

4.2. *Relations between spectra obtained at Saskatoon and Churchill on the same night*

The theory of MARTYN predicts a tendency for H_α to be relatively weak at Churchill and relatively strong at Saskatoon for those occasions when auroral spectra can be obtained simultaneously at both stations. On these occasions, Churchill and Saskatoon must straddle the effective "auroral zone" so that, as explained in the introduction, there should be a preponderance of protons to the south. This expectation is to some extent confirmed by the observations reported in Section 4.3. below. The data obtained from the relatively few occasions when spectra were obtained simultaneously are summarized in Table 4. The Table is divided into two sections, depending on whether the aurora was strong or weak at the southern station.

These observations show that there is a strong tendency for the H_α emission to be observed simultaneously at both stations during strong aurora. This result is not necessarily in contradiction to the observations of VEGARD (1955) that the intensity ratio of H_β to the 4709 Å N_2^+ band decreases with decreasing latitude. The spectra obtained in the present study were not suitable for making accurate comparisons of this ratio between the two stations, since the values depend on the slit-width and dispersion of the spectrograph at each station. The results obtained on 2/3 January and 21/22 March are noteworthy, although not apparently typical.

4.3. *Relation between magnetic activity and* H_α *intensity*

Definite predictions concerning the relationship which might be expected between magnetic disturbance and the intensity of the hydrogen emissions are difficult to make. If increasing magnetic disturbance is associated with the existence and possible contraction of the ring current, a shift southward of the zone

Table 4. Estimated (eye) intensities of auroral lines in spectra obtained simultaneously at Saskatoon and Churchill.

Date	Intensity [OI] 5577 Å		Intensity H_α		Remarks
	Churchill	Saskatoon	Churchill	Saskatoon	
Group I. Aurora strong at Saskatoon					
5/6 December 1955	11	12	6	7	
17/18 January 1956	11	12	8	8	
18/19 January	10	12	8	8	
21/22 January	11	12	7	7	
10/11 March	8	11	5	6	
13/14 March	9	10	6	7	
2/3 April	9	10	6	7	
Group II. Aurora weak at Saskatoon					
2/3 January 1956	10	8	0	6	
7/8 February	7	3	7	2	Magnetically disturbed at Churchill; quiet at Saskatoon. Aurora low in north at Saskatoon
8/9 February	9	3	6	2	
9/10 February	9	3	7	2	
20/21 February	9	7	6	3	
9/10 March	8	9	6	6	
19/20 March	8	7	2	6	
21/22 March	7	8	0	0	

of the most intense proton precipitation (except for the evening period of stage I) might be expected. As a result, the intensity of the hydrogen emissions might decrease at Churchill with increasing magnetic disturbance index, and increase and possibly pass through a maximum value at Saskatoon.

A test of these possibilities was carried out as follows:

(a) A magnetic-disturbance index was calculated for each night on which satisfactory auroral spectra had been obtained. The index for Churchill is given by the relation $N = \Delta H/200$, where ΔH is the maximum deviation of the horizontal magnetic field measured in γ. The index for Saskatoon was obtained in an essentially similar manner.

(b) The spectra obtained were divided into groups according to the value of the corresponding magnetic index.

(c) The average value of the intensity of H_α for each group of spectra was obtained. The results are set out in Table 5.

The average intensities shown in brackets are based on a very few observations, and hence are unreliable.

The striking result shown in Table 5 is the apparent negative correlation at Churchill between H_α intensity and magnetic activity contrasted with the positive correlation for Saskatoon. There is even a suggestion of a possible decline at

Table 5. Average intensities of H_α for different magnetic indices

	Magnetic index, N			
	0–1	1–2	2–3	>3
Churchill	4·3	3·9	2·7	(4·0)
Saskatoon	3·6	4·9	5·3	(2·0)

Saskatoon for high values of the magnetic index. As suggested at the beginning of this paragraph, this observation would be consistent with the MARTYN theory, although it would also be consistent with other mechanisms.

4.4. *Relations between magnetic-bay patterns and H_α intensity at Churchill and Saskatoon*

The Churchill data yielded some further interesting relations. The nights with aurora were divided into groups according to the nature of the magnetic disturbance—disturbed (magnetic storm), quiet, and quiet but with isolated magnetic bays. The nights in these groups were then checked for the occurrence of H_α. The spectra were then examined for the occurrence or absence of H_α for each of the nights. The results showed the following:

(a) For nights which were either magnetically quiet all night or quiet except for isolated magnetic bays after midnight, H_α was observed in almost all cases both before and after midnight. In only 1 case out of 68 was H_α not detected.

(b) For nights with isolated magnetic bays occurring before midnight, at midnight, or both before and after midnight, there was an equal likelihood of H_α appearing or not appearing before midnight, but only 1 case out of 16 where it was not detected after midnight.

(c) For nights showing continuous magnetic disturbance throughout the night (magnetic storms), H_α was never detected. During the period of observation, there were 12 such nights.

At Saskatoon, on the other hand, of 10 all-night magnetic storms, 5 showed strong H_α emission, while the remaining 5 exhibited no detectable H_α.

5. CONCLUSIONS

The observations presented in this paper provide information on the variability of the intensity of the H_α emission between Churchill and Saskatoon. This information makes possible a preliminary test of certain auroral theories. As far as they go, the observations do not support the detailed predictions of MARTYN's theory with regard to the diurnal variation of the sign of auroral particles.

Most of the observations can be fitted into the general picture of a zone of auroral activity, on the southern fringe of which the hydrogen emissions are strong and which moves southward with increased magnetic disturbance. Such a picture

VOL. 11 1957

is consistent with MARTYN's theory, but would also follow from STÖRMER's theory as modified by the assumption of an external ring current. It would also be consistent with the solar-ray bundle theory of VEGARD (1955).

One noteworthy feature of both the Saskatoon and Churchill observations is that strong auroral displays lasting several hours may yield spectra which show little or no traces of H_α radiation but do show strong first positive group nitrogen bands. The spectra shown in Fig. 1 provide an example of this. In cases such as this it seems almost necessary to assume that the primary exciting particles must be electrons. If a discharge type excitation is involved, one must consider a mechanism which embraces a very wide zone within the atmosphere and which can maintain itself for several hours.

Acknowledgements—The author (R. M.) wishes to express his thanks to Dr. GARTLEIN, Cornell University, for the loan of the spectrograph used at Churchill. The authors wish to express their appreciation of the interest and encouragement given to them by Dr. B. W. CURRIE and Dr. W. PETRIE.

REFERENCES

CHAPMAN S. and FERRARO V. C. A.	1931	*Terr. Magn. Atmos. Elect.* **36,** 77, 171.
	1932	*Terr. Magn. Atmos. Elect.* **37,** 147, 421.
	1933	*Terr. Magn. Atmos. Elect.* **38,** 79.
	1940	*Terr. Magn. Atmos. Elect.* **45,** 245.
GARTLEIN C. W.	1948	*Phys. Rev.* **74,** 1208.
MARTYN D. F.	1951	*Nature, Lond.* **167,** 92.
MEINEL A. B.	1950	*Astrophys. J.* **111,** 555.
	1954	Report of Aurora and Airglow Committee, U.S. National Committee for I.G.Y.
STÖRMER C.	1955	*The Polar Aurora* Clarendon Press, Oxford.
VALLANCE JONES A. and GUSH H.	1954	*Rev. Sci. Instrum.* **25,** 928.
VEGARD L.	1939	*Nature, Lond.* **114,** 1089.
VEGARD L.	1955	*Geophys. Publ., Dublin* **19,** No. 4.

Journal of Atmospheric and Terrestrial Physics, 1957, Vol. 11, pp. 51 to 53. Pergamon Press Ltd., London

An experimental verification of diffraction microscopy, using radio waves

G. L. Rogers
Department of Natural Philosophy, Marischal College,
University of Aberdeen

(*Received* 12 *March* 1957)

Abstract—An aircraft has been deliberately flown over the receivers of a station during Mitra recording. The contribution of the aircraft to the Mitra pattern has been isolated by diffraction microscopy, and a one-dimensional "image" of it has been recovered. The location of this image on the optical bench is in satisfactory agreement with the theory.

VOL. 11 1957

1. Introduction

The fading exhibited by radio waves reflected from the ionosphere has been interpreted as due to motion of the reflecting region. The technique of measuring the horizontal component of this movement, using three spaced receivers, originally due to Mitra (1949), has subsequently been employed by various workers (see Briggs and Spencer, 1954).

Rogers (1956, 1957) has advanced the hypothesis that diffraction microscopy can be applied to the interpretation of the fading record, using the spaced-receiver technique. This involves a number of subsidiary hypotheses, and an experiment has been devised to test some, but not all of these. The experiment particularly recommends itself, however, as a relatively direct and simple verification of the particular hypotheses tested.

The main hypotheses involved are: (1) that the ionosphere may, on some occasions, be regarded as a plane mirror, (2) that some at least of the features which contribute to the fading pattern are relatively local concentrations of absorption, phase shift, or abnormally high reflecting power, and (3) that such local concentrations can be localized in height upon reconstruction in the optical apparatus (ref. Rogers, 1952a). The experiment, which consists of flying an aircraft on a known course, height, and speed, recording the fading pattern which arises as it flies over the receivers, and attempting a reconstruction, does not in any way test the second hypothesis. In fact, it completely begs the question by using an object manifestly smaller than one wavelength. But it does enable the first question to be investigated and shows that the third hypothesis is also reasonable, the second condition being fulfilled.

In an attempt to shorten the labour involved in the optical analysis, the paper was run through the camera attached to the indicator at a lower speed than usual. This has the disadvantage that timings are less exact than is normal, and estimates of velocity from the records are not very accurate. The compensating advantages in the optical work did not come up to expectations. By using the known aircraft speeds, however, a self-consistent explanation of the phenomena can be built up.

2. The Radio Experiment

The arrangement of receivers and recording of the fading pattern was essentially the same as that used by Mitra (1949). The radio wavelength was 125 m.

The aircraft flight was made between 0930 and 1030 hours local time, a period when the signal intensity returned from the *E* layer was expected to be near its maximum. The organization required to bring the aircraft up did not allow, unfortunately, a period to be selected when there was not deep fading present. Such periods have not been able to be forecast, although they commonly occur over brief intervals, interspersed with periods of the more normal deep fading.

The aircraft, a DC-3, was flown on a course about 15 miles long, centred over the radio receivers. Two runs were made in opposite directions at each of two heights, 4000 and 8000 ft. An observer in the aircraft was in radio-telephone contact with the ground and gave an approximate indication of the start, overhead position, and end of each run. Owing to the presence of a variable amount of intervening cloud, and to the fact that a free R.T. channel was not available, the times coded on to the photographic record could not be relied on to better than ± 5 sec.

The calculation of ground speed was, however, much more accurate as a number of independent evaluations could be made on each run, and these did not vary by more than ± 1 m/sec about an average of about 75 m/sec.

The paper speed in the photographic recorded was reduced to 3 in./min, which allowed the pattern from a complete aircraft run to be displayed on about $1\frac{1}{2}$ ft of record, a convenient length for optical reduction.

3. The Optical Analysis

The first attempt at the optical analysis involved the photography of the three tracks through a combination of a spherical and a cylindrical lens, to cause a degree of variable area—variable density transformation without too much diffusion of the tracks into one another. In practice this did not prove satisfactory, as confusion of the tracks could not be avoided.

Consequently, the central aerial track was selected for tracing, and a single variable density track was produced from this by the use of a cylindrical lens alone (Rogers, 1952b). This "hologram" was examined carefully on the optical bench for visual foci, using mercury-green light $\lambda = 5461$ Å. Two were found with certainty, and one or two others rather doubtfully. Using a hologram with a scale of 53·3 μ/sec, the first of these came out at $12{\cdot}26 \pm 1{\cdot}85$ cm, or say ± 15 per cent. Assuming that the velocity of the pattern over the ground was essentially the same as that of the aircraft (being projected from a point over 200 km high) i.e. 75 m/sec, this visual focus corresponds to a radio focus of 1·05 km. The height of the aircraft on this run was 4000 ft or about 1·22 km. The agreement is therefore within the errors of measurement.

The second "disturbance" had a visual focal length of 1·8 m on this hologram, but is more exactly specified by a visual focal length of $14{\cdot}6 \pm 0{\cdot}6$ cm on another print of the same hologram at a scale of 15·5 μ/sec. But since the velocity of this disturbance could not be obtained from a single track, and could certainly not be assumed to be the same as that of the aircraft, its height could not be determined.

It is, however, interesting to note that this observation is not inconsistent with an ionospheric irregularity. A ground velocity of 300 m/sec, or an ionospheric velocity of 150 m/sec, would be sufficient to give a height of the object substantially in the ionosphere, in which case it might be a meteor trail just below ionospheric height. Owing to the reduced speed of the recording, neither the aircraft nor the proposed ground speed can be obtained by the Mitra technique with any accuracy.

4. Absorption Estimates

A rough visual estimate of the absorption of the above two objects gives the second substantially denser than the first, perhaps by a factor of 10. This at first sight seems surprising, as a DC-3 aircraft looks fairly substantial. But the projected plan area of a DC-3 is only about 130 m^2, and when it is compared with the area of the first Fresnel half-period zone—$\frac{1}{2}km^2$—the question is seen in a new light. The question, in fact, is why the aircraft absorbs so much.

Part of the answer is undoubtedly that the aircraft is metallic and distorts the radio field by virtue of induced currents, thereby absorbing energy from a larger area than its exact projected plan. But a great deal of the explanation lies in the very great sensitivity of the Gabor method. An object scattering 3 per cent of the *amplitude* of the main wave (i.e. 0·09 per cent of the *energy*) will produce noticeable fluctuations in the radio diffraction pattern, for the *amplitude* will fluctuate from 97 per cent to 103 per cent of the undisturbed amplitude of the wave, and the intensity from 94 per cent to 106 per cent of the intensity of the undisturbed background. This is easily picked up. Actually the "projected area" of the DC-3 aircraft is 0·028 per cent of that of the Fresnel half-period zone, and this is minimal for detection. A three-fold increase in effective projected area due to conduction would be ample to explain this result; and the use of a "circumscribing circle" round the aircraft would also fully explain its detection.

VOL. 11 1957

5. Location in Time

The reconstruction was photographed and put on a non-recording microphotometer. Careful tracking of this enabled the position of maximum absorption to be located to a precision of 0·65 sec. The recorded marks are not as good as this, and the registration in time is very satisfactory.

Acknowledgements—I am greatly indebted to the Director of Civil Aviation, Wellington, for authorizing this flight, and to Messrs. R. S. Unwin and C. L. Henderson of the Radio Group, Dominion Physical Laboratory, Lower Hutt, New Zealand, for organizing the flight and arranging the special recording.

References

Briggs B. H.	1951	*Proc. Phys. Soc. Lond.* **B64,** 255.
Briggs B. H. and Spencer M.	1954	*Rep. Progr. Phys.* **17,** 245.
Rogers G. L.	1952a	*Proc. Roy. Soc. Edinb.* **A63,** 193.
	1952b	*Proc. Roy. Soc. Edinb.* **A63,** 313.
Rogers G. L.	1956	*Nature, Lond.* **177,** 613.
Rogers G. L.	1957	*J. Atmosph. Terr. Phys.* **10,** 332.

Journal of Atmospheric and Terrestrial Physics, 1957, Vol. 11, pp. 54 to 58. Pergamon Press Ltd., London

Measurement of the gyro-frequency in the *F* region

G. R. Ellis*
Queensland University, Brisbane, Australia

(*Received* 23 *March* 1957)

Abstract—This paper describes a method of measuring the *F*-region gyro-frequency from *P'f* records, using the relation $f_H = f_x - f_z$. The observed values of the critical frequencies must be corrected for errors arising from lateral deviation and horizontal gradients of critical frequency.

It is shown that the lateral deviations of the *O*, *X*, and *Z* modes, calculated with an approximate value of f_H, and the observed values of f_x, f_o, and f_z, provide sufficient information to obtain both the horizontal gradient of critical frequency and the gyro-frequency. The results of an analysis of *P'f* records obtained at Hobart, Tasmania, are given. It was found that at a mean true height of 378 km, the mean gyro-frequency was 1·53 Mc/s, compared with an extrapolated value, using ground parameters, of 1·40 Mc/s.

Introduction

It is well known that the frequency difference between the ordinary and extraordinary, or between the extraordinary and *Z* critical frequencies of an ionospheric layer, provides in principle a method of determining the gyro-frequency and hence the geomagnetic field intensity in the layer.

We have (Mitra, 1948)

$$f_H = \frac{eH}{2\pi mc} = f_x - f_z \tag{1}$$

or

$$f_H = \frac{f_x^2 - f_o^2}{f_x} \tag{2}$$

where $f_{x,o,z}$ = critical frequencies, f_H = gyro-frequency, and H = geomagnetic field intensity.

As a practical way of measuring f_H, this method has a serious drawback which was pointed out by Scott (1950). Because of the different lateral deviations of extraordinary and ordinary wave packets, the reflection points will be horizontally separated, for vertical incidence. Scott showed that there is normally a sufficient horizontal gradient of electron density to cause large errors in the value of f_H calculated direct from equation (2). However, it is now known (Ellis, 1953, 1956) that *Z* echoes result from the oblique, quasi-longitudinal propagation of the ordinary mode, the critical angle of incidence being given by

$$\theta_i = \sin^{-1}\left[\left(\frac{y}{y+1}\right)^{\frac{1}{2}} \sin\theta_o\right]$$

where $y = f_H/f$ and θ_o = inclination of geomagnetic field.

The *Z* reflection point will be horizontally separated from both the ordinary

* Commonwealth Ionospheric Prediction Service and University of Queensland, Brisbane, Queensland, Australia.

and extraordinary reflection points, all three being in the magnetic meridian vertical plane.

Thus the three critical frequencies f_x, f_o, f_z refer to three horizontally separated points at the level of maximum ionization and there is sufficient information contained in the observed values of f_x, f_o, and f_z and in the observed vertical distribution of ionization to calculate both the horizontal gradient of critical frequency and the gyro-frequency.

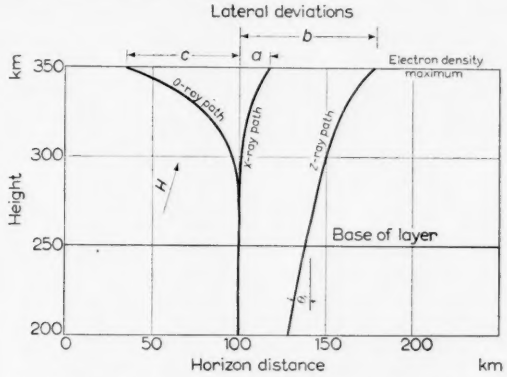

Fig. 1. Ray-paths for the different modes. Parabolic layer. Assumed gyro-frequency 1·53 Mc/s; inclination of geomagnetic field 18°; wave frequency 4·6 Mc/s.

VOL. 11 1957

Theory

If the horizontal separations of the x, z, and o reflection points from the vertical are a, b, and c respectively (Fig. 1), and the horizontal gradient of critical frequency is $df_o/ds = m$ (m is assumed constant) then the critical frequencies corrected for overhead reflection are

$$f_{x_v} \approx f_x - ma \tag{3}$$

$$f_{z_v} \approx f_z \cos\theta_i - mb \tag{4}$$

then from equation (1) we get

$$\begin{aligned} f_{H_v} &= f_{x_v} - f_{z_v} \\ &\approx f_x - f_z \cos\theta_i + m(b - a) \end{aligned} \tag{5}$$

To obtain m, we have (Mitra, 1948):

$$f_o^2 = f_x f_z \text{ for reflection at the same point.}$$

Taking this as the o-wave reflection point:

$$f_o^2 = [f_x - (a + c)m] \,.\, [f_z \cos\theta_i - (b + c)m] \tag{6}$$

Solving (6) for m, we get

$$m \approx \frac{f_x f_z \cos\theta_i - f_o^2}{\cos\theta_i \,.\, f_z(a + c) + f_x(b + c)}$$

if

$$\frac{f_o^2}{f_x f_z \cos\theta_i} \approx 1 \tag{7}$$

Hence, f_H follows from equation (5) if the lateral deviations a, b, and c are known. These will depend on the magnitude and inclination of the geomagnetic field and on the vertical distribution of ionization.

In principle, the intensity of the field can be found by successive approximations by assuming H and θ_o in order to calculate a, b, and c and then correcting with the value of H obtained from equation (5). In practice, the effect of a small change of H on a, b, and c is negligible and the initially calculated value of f_H is sufficiently close. The vertical distribution of ionization may be obtained from the $P'f$ curve in the usual way. However, in analysing a number of records it is more convenient to choose those for which a parabolic variation of electron density with height represents a good approximation to the actual distribution.

The lateral deviations may then be calculated for a parabolic layer of standard thickness for different critical frequencies and then corrected for the actual thickness and critical frequency (Fig. 2).

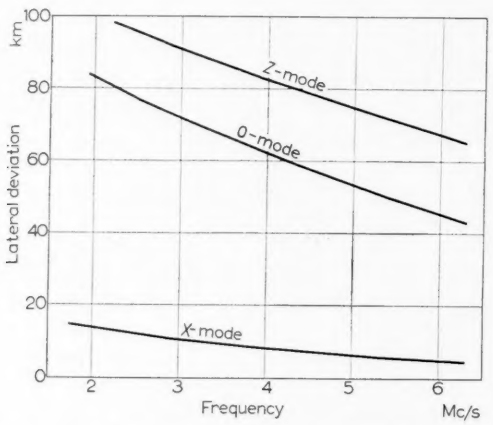

Fig. 2. Variation of lateral deviation with frequency with model of Fig. 1.

The value of f_H calculated is for the height of the electron density maximum. For a simple parabolic F layer this is obtained from the $P'f$ record at the frequency $0{\cdot}834\, f_o$ (Mitra, 1948).

Observations

A selection was made of routine, night-time $P'f$ records obtained at Hobart, Tasmania, during May 1956. The records were chosen for clarity, for absence of ionospheric disturbances during the same night, for low critical frequencies (to give an open-frequency scale), and for a $P'f$ trace which approximated that of a parabolic layer. Fig. 3 shows a typical example. The ordinary and extraordinary critical frequencies were scaled from the inside edge of the respective traces. The pulse width of the $P'f$ recorder transmitter was 100 μsec and the receiver bandwidth was 20 kc/s.

VOL.
11
1957

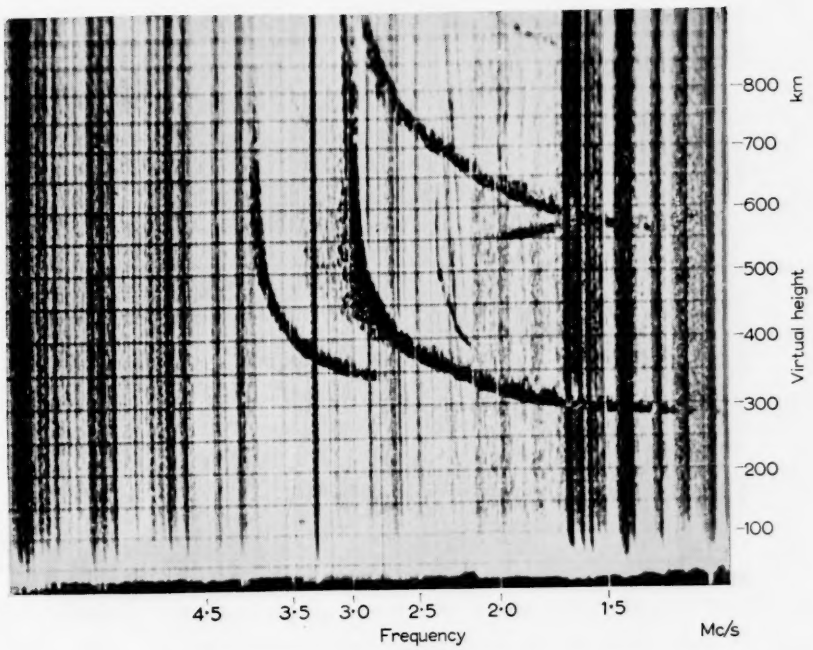

Fig. 3. Typical $P'f$ record. Hobart, 0440, 29 May 1956.

Table 1 shows the results of the analysis of the records, while Fig. 4 shows the calculated values of f_H plotted against height before and after correction for the lateral deviations.

Table 1.

Calculated values of the critical frequency gradient m and of the gyro-frequency f_H

Date	Local time (hr)	f_x (Mc/s)	f_o (Mc/s)	f_z (Mc/s)	True height (km)	m (c/s [km]$^{-1}$)	Corrected (Mc/s)
4/5/56	0520	3·9	3·0	2·45	325	305	1·53
5/5/56	0520	4·24	3·4	2·75	365	−190	1·55
	0530	4·15	3·29	2·63	370	−140	1·56
	0600	3·92	3·05	2·4	380	−285	1·55
	0640	4·45	3·59	3·02	365	350	1·54
6/5/56	0430	3·89	3·0	2·48	390	480	1·51
	0550	3·65	2·73	2·22	390	620	1·53
	0610	3·57	2·7	2·16	380	250	1·53
10/5/56	0620	4·28	3·40	2·78	325	67	1·56
19/5/56	0450	3·4	2·5	1·97	390	320	1·52
20/5/56	0310	3·8	3·0	2·27	410	690	1·525
	0320	3·85	3·01	2·33	400	360	1·53
	0410	3·3	2·4	1·85	440	275	1·52
21/5/56	0420	3·3	2·37	1·86	415	590	1·52
	0430	3·24	2·26	1·80	410	730	1·55
29/5/56	0120	3·88	3·02	2·43	370	122	1·51
	0230	3·8	2·98	2·26	370	−540	1·54
	0300	3·8	2·87	2·35	370	600	1·545
	0310	3·8	2·95	2·3	380	120	1·54
	0400	3·8	2·97	2·26	370	−410	1·545
	0430	3·8	2·92	2·32	378	180	1·535
	0440	3·76	2·91	2·32	380	60	1·505
1/6/56	0650	3·9	3·0	2·44	335	320	1·535

To a considerable extent the spread in the values of f_H has been reduced. It is interesting to note that all the final values are greater than that obtained by inverse cube extrapolation of the ground parameters of the geomagnetic field. As might be expected, in most cases the horizontal critical frequency gradient was from south to north.

Conclusion

It appears that a worthwhile increase in the accuracy of calculating f_H from $P'f$ records can be obtained by using the method described here. The method is obviously suitable only for places where triple splitting occurs reasonably often.

VOL. 11 1957

In general, this means geomagnetic latitudes of between about 50° and 70°. In the northern hemisphere triple splitting is a normal feature of $P'f$ records in Canada (Scott, 1950) and in Scandinavia (Rydbeck, 1951).

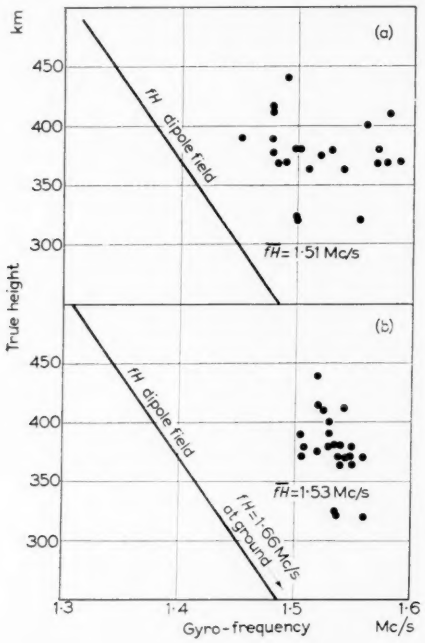

Fig. 4
(a) Calculated values of gyro-frequency plotted against true height of electron density maximum, corrected for oblique incidence of Z ray but not for lateral deviation.
(b) Values for gyro-frequency obtained after correcting for lateral deviation.

Furthermore, it is essential to have clear records with a minimum of spread F and, with higher critical frequencies, it would be necessary to use a $P'f$ recorder with a more open-frequency scale at the high end, than was available for this investigation.

References

Ellis G. R.	1953	*J. Atmosph. Terr. Phys.* **3,** 263.
Ellis G. R.	1956	*J. Atmosph. Terr. Phys.* **8,** 43.
Mitra S. K.	1948	*The Upper Atmosphere* p. 200.
Rydbeck O. E. H.	1951	*Trans. Chalmers. Inst. Tech.* No. 101.
Scott J. C. W.	1950	*J. Geophys. Res.* **55,** 65.

Journal of Atmospheric and Terrestrial Physics, 1957, Vol. 11, pp. 59 to 61. Pergamon Press Ltd., London

Magnetic activity following a solar flare

R. A. WATSON
Meteorological Office, Edinburgh

(*Received* 17 *May* 1957)

Abstract—Evidence is examined which suggests that either there is no increase of magnetic activity due to a solar flare or that the increase is a very rare event.

NEWTON and JACKSON (1951) surveyed the evidence produced by themselves and others connecting a solar flare and the occurrence of magnetic disturbance on the earth some 24 hr later. They came to the conclusion that there probably was a connection between a solar flare and increased magnetic activity on the earth one to two days later, at least in the case of the important flares designated 3_+. Their finding has been quoted very extensively with or without the qualifying cautions. It seemed desirable to check this result with the information published in the I.A.T.M.E. (now I.A.G.A.) annual bulletins 1949–1954. There is nothing new in the methods adopted both of which are used by NEWTON and JACKSON or by authors cited by them.

VOL. 11 1957

The time interval between a solar flare effect (S.F.E.) and a sudden commencement (S.C.)

The I.A.T.M.E. bulletins give lists of S.F.E. and doubtful S.F.E.s. Only the former were used in this note. There were 185 between 1949–1954. Sudden commencements following within three days of the S.F.E. were then picked out from the lists in the same journal and the time interval Time S.C.-Time S.F.E. tabulated. There were 255 such time intervals because although there may be no S.C. within three days (50 cases) there may also be several and all were listed. The numbers of cases following within any time interval were such as might be expected from a random distribution. For instance the numbers falling in each 12 hr interval following the time of the S.F.E. were:—

Hours	0–11·9	12–23·9	24–35·9	36–47·9	48–59·9	60–71·9
Cases	33	38	47	41	57	39

Applying the χ^2 test to these figures gives a high probability that the numbers in the intervals are "random." Other time intervals gave similar results.

It should be noted that the time intervals were calculated to the nearest minute.

The difference between this result and that quoted by NEWTON may be due to the different way of selecting material—NEWTON used only 3_+ flares—but it is more probably due to the very small number of cases considered by him.

The incidence of magnetic activity in each 3 hr period following a S.F.E.

Using the same list of S.F.E. as in the first method (except that if two S.F.E.s were recorded in one 3 hr period only one was used, which reduced the number from 185 to 180) a number representing the magnetic disturbance was written down for each of 25 3 hr periods beginning with the one previous to that in which the S.F.E. occurred.

The measure chosen for the 3 hr period was Ap. The meaning of Ap is explained in the I.A.T.M.E. Bulletins but approximately it is the Kp index of worldwide magnetic activity converted back to a hourly range (unit 2 γ) for a station having 500 γ as the lower limit for $K = 9$.

Table 1. Mean Ap for each 3 hr interval. S.F.E. occurs in first interval 1.
(The bracketed figures are explained later).

0	1	2	3	4	5	6	7	8	1	2	3	4	5	6	7	8	1	2	3	4	5	6	7	8
12	11	11	12	14	15	15	17	16	15	16	16	16	17	17	17	18	18	18	21	20	18	17	20	21
(12)	(12)	(11)	(12)	(14)	(16)	(17)	(19)	(18)	(16)	(18)	(18)	(18)	(20)	(19)	(21)	(21)	(22)	(21)	(23)	(24)	(22)	(20)	(24)	(26)

The mean Ap for all the months from which any S.F.E.s were chosen was 17 and the mean for all days 1949–1954 was also 17.

It is evident from the table that there is a steady rise of activity from the time of the S.F.E. until well into the third day following. There is certainly no evidence of a sudden increase about 24 hr after the S.F.E. In fact if the figure 17 can be taken as "normal" activity it is only towards the end of the second day that normality is reached and even after that is only slightly exceeded. (For those unfamiliar with this Ap measure of activity it can be stated that a big storm will produce Ap figures exceeding 100.) The really striking feature is the subnormal activity about the time of the S.F.E. Presumably this is due to the fact that it is only during magnetically quiet periods that a S.F.E. is likely to be distinguished as such. The simplest explanation of the figures in the table is that it demonstrates the slow recovery to normal activity from periods selected as being quiet.

There are many objections to the use of lists such as those which have been used but so far as is known data ideal for testing this point have not been conveniently tabulated.

It was mentioned above that in 50 cases there was no sudden commencement following the S.F.E. within three days. In view of the difference in behaviour which has been suggested between storms commencing gradually and those with a sudden commencement, it is of interest to repeat the investigation of the change of activity following the S.F.E. omitting the 50 cases not followed by a S.C. This has been done and the mean Ap for each 3 hr interval is placed in brackets in the table above. A distinctly steeper rise of activity is shown but certainly not the sort of rise if an appreciable magnetic storm were a frequent event at a more or less fixed time after a S.F.E. The difference in the two series is probably a mere sampling difference but the very marked "coherence" of Ap figures makes a satisfactory statistical test of this difficult.

The conclusion from this present analysis is that if a stream of particles is ejected from the sun at the time of a solar flare it is a rare event for the stream to cause an appreciable magnetic distrbance on the earth within three days.

References

I.A.T.M.E. or I.A.G.A. Bulletins (12c–12i). 1949–1954 *Geomagnetic Indices* K *and* C.

Newton H. W. and Jackson W. 1951 *Septième Rapport de la commission pour l'étude des relations entre les phénomènes solaires et terrestres.*

VOL. 11 1957

Journal of Atmospheric and Terrestrial Physics, 1957, Vol. 11, pp. 62 to 66. Pergamon Press Ltd., London

The time distribution of meteors

K. R. R. Bowden and J. G. Davies
Jodrell Bank Experimental Station, University of Manchester

(*Received* 21 *March* 1957)

Abstract—Observations have been made of transient echoes, using pulsed radio echo systems on 72 Mc/s and 36 Mc/s, and the records have been analysed with regard to the time of occurrence of echoes. Some authors have suggested that meteors, whose ionized trails cause such echoes, enter the atmosphere in groups, and also that many echoes are due to cloud discharges. No evidence is found to support either of these suggestions.

1. Introduction

It is well known to all observers of meteors, either visually or by radio techniques, that the events observed seem to occur in pairs or larger groups. Even when examining film or other records, the number of close groups repeatedly attracts the observer's attention. Some authors have concluded that this grouping is a real effect. For example, Wylie and Castillo (1956) have investigated the scattering of 20 Mc/s transmissions by meteor ionization over a 600 km baseline, and, with a mean echo rate of 2·9 per min, have found a significant excess of half-minute periods containing five or more echoes, over the number expected on the hypothesis of a random distribution. This they attribute to a bunching of meteors in space. Isted (1954, 1955) has observed trains of three or more echoes equally spaced in time, both on 11 Mc/s at vertical incidence and on 50 Mc/s over a 500 km baseline. He concluded that while some echoes are due to meteors, these trains, and the majority of all echoes observed at vertical incidence below 36 Mc/s, are probably caused by upwardly directed weather cloud discharges.

Shain and Kerr (1955) have used a vertically directed pulsed transmitter on 18 Mc/s in an investigation of the diurnal variation of the echo rate. Briggs (1956) has made observations similar to those of Isted on 50 Mc/s transmissions with a 500 km baseline. Neither found significant evidence for the marked grouping of echoes, in equally spaced trains or otherwise.

In this paper, a number of independent records obtained under widely differing conditions by the radio echo technique at Jodrell Bank are discussed.

2. Apparatus

All the data used were obtained using pulsed radio echo equipment. The first analysis was made of records obtained during the programme of velocity measurement of sporadic meteors by Almond, Davies, and Lovell (1951) on 72 Mc/s, using an aerial system with a gain of 50 for both transmission and reception. The equipment recorded about ten meteors per hr, mainly of magnitudes +5 and +6. The records in this case were individual frames on 35 mm film, the exposure of which was initiated by the radio echo itself. A clock giving time to 1 sec was photographed as part of the display.

More recently, a system operating on 36 Mc/s has been used, yielding rates of the order of 2000 per hr in the early morning and 200 per hr in the evening. The records in this case were photographed on film which moved through the camera at about 6 cm per min. Both amplitude-time and intensity-modulated range-time cathode-ray

VOL. 11 1957

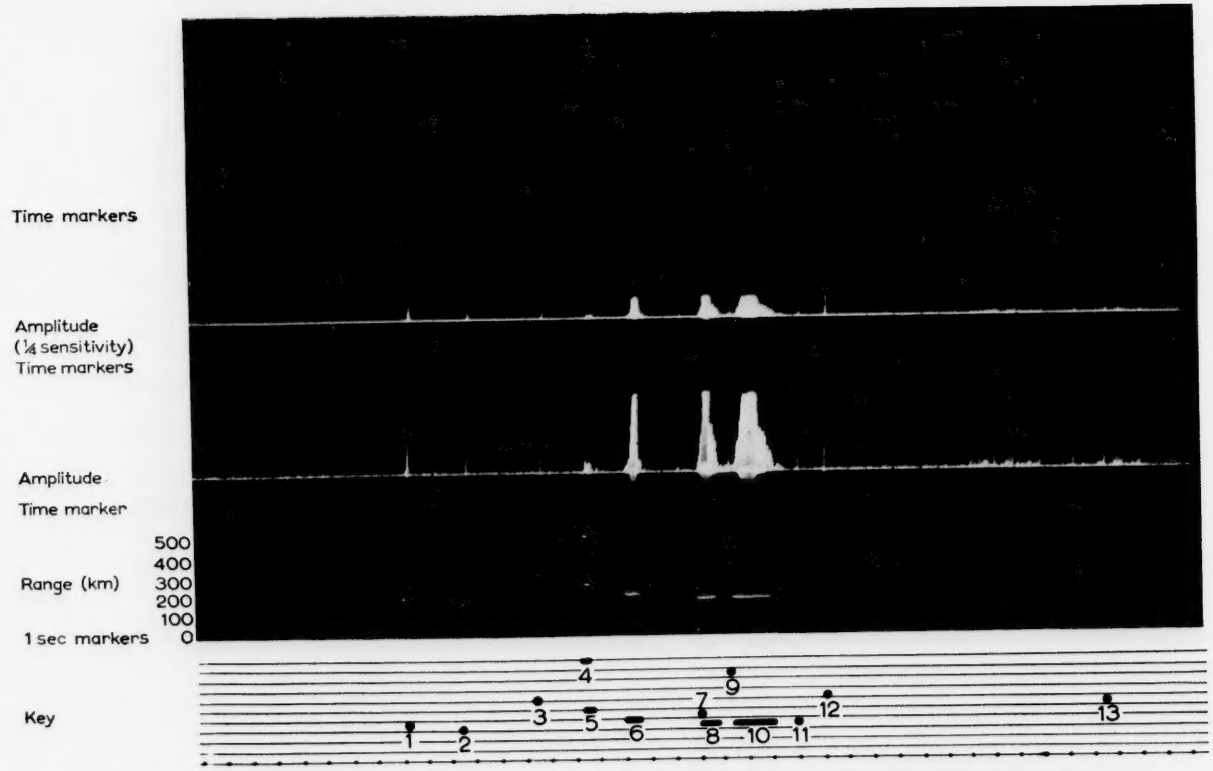

Fig. 1. A section of film record number 4, showing the importance of using a range-time display. Echoes 4 and 5 are separated with certainty, and echo 7 is clearly distinguished. It is also seen that echoes 8, 10, and 11 are all at 170 km range, and are probably all due to a single meteor trail; note the weak echo at the same range joining 8 and 10. The interference spike 12 gives a relatively fainter record on the range display, as there is no photographic integration such as occurs with constant-range echoes.

tube displays were photographed. Time markers at 1 sec intervals were also photographed and a system of lights giving the actual time was also available. With this system, time-intervals down to 0·1 sec could be estimated. This equipment was operated with two-element aerials, giving a wide beam at about 30° elevation, with a sensitivity approximately equal to magnitude +6.

A section of one of the records is given in Fig. 1.

3. Analysis

The time of commencement of each echo greater than a chosen amplitude, about three times the receiver noise-level, was read from the film. When necessary, the range display was used to distinguish between a single fluctuating echo and two or more separate echoes close together in time, and between echoes and interference (see Fig. 1).

The meteor-echo rate has a diurnal and annual variation and at times is strongly influenced by the occurrence of showers. The most rapid known fluctuation of this sort recorded on a radio echo system is that of the Giacobinid meteor stream, with activity confined to about 3 hr, and a sharp peak lasting only a few minutes (Davies and Lovell, 1955). In order to remove all such effects from the present analysis, the number of echoes in 10 min intervals was counted, and the periods selected were such that no significant variation occurred in this 10 min rate.

VOL. 11 1957

Four methods of analysis were used. In the first the observations were divided into periods of half a minute, and the number of echoes in each period was noted. The number of periods containing n echoes, where $n = 0, 1, 2, 3$, etc., was compared with that expected from the Poisson distribution which would result from the random occurrence of echoes, which is

$$Me^{-z}\frac{z^n}{n!} \tag{1}$$

where M is the total number of half-minute periods, and z is the average number of echoes observed in half a minute. This method is identical with that of Wylie and Castillo.

From an examination of the records, it seemed that the duration of the apparent groups was only of the order of a few seconds, and much less than half a minute. The data were therefore subjected to a second analysis, in which the time-interval between one echo and the next was noted, and the frequency distribution of these intervals was compared with that expected from randomly occurring echoes, when the probability of an interval having a value between t and $t + \delta t$ would be

$$\frac{\delta t}{T}e^{-t/T} \tag{2}$$

where T is the average interval, and the expected number of such intervals would be

$$N\frac{\delta t}{T}e^{-t/T} \tag{3}$$

where N is the total number of intervals.

The χ^2 test was used to estimate the significance of departures from the expected distributions.

A third method of analysis used was the calculation of the correlation between successive intervals, which would be zero for a random distribution of echoes. The correlation coefficient ρ was calculated using the formula

$$\rho = \frac{\Sigma t_n t_{n+1} - NT^2}{\Sigma t_n{}^2 - NT^2} \pm \frac{1}{\sqrt{N}} \tag{4}$$

where t_n is the duration of the nth interval, N is the total number of intervals, and T is the average interval, as before. This test would also reveal any slow change in the echo rate during the period.

The number of trains of three equally spaced echoes was also found, and compared with the number expected by chance. The probability that an interval between t and $t + dt$ should be followed by an interval of equal length, within an accuracy of measurement $\delta t'$, is given by

$$\frac{dt}{T} e^{-t/T} \cdot \frac{\delta t'}{T} e^{-t/T} \tag{5}$$

from (2) above. By integration of this over all values of the interval t, the probability of two successive intervals being equal, without regard to the actual interval, is obtained as $\frac{1}{2}\delta t'/T$. The number of pairs of intervals is $N - 1$, and the number of equal pairs expected by chance is therefore $\frac{1}{2}(N - 1)\delta t'/T$. Thus, for large values of N, the number of equal pairs should be

$$\tfrac{1}{2} N \frac{\delta t'}{T} . \tag{6}$$

The last three methods of analysis are identical with those used by Briggs.

4. Results

Four records were analysed, containing a total of over 3000 echoes. The first was obtained with the 72 Mc/s equipment over a period from September to November 1948. The three remaining were obtained with the 36 Mc/s equipment, one of them on 9–10 August 1954 during the Perseid meteor shower.

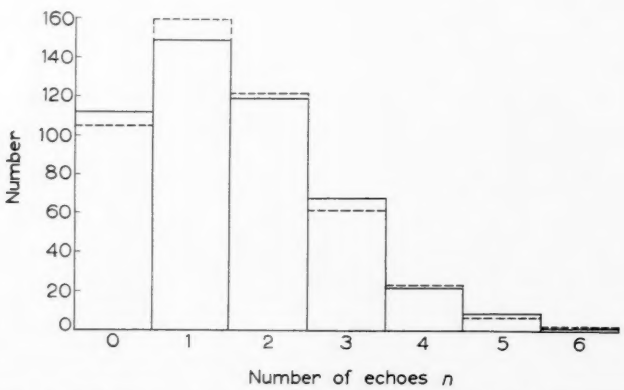

Fig. 2. Distribution of the numbers of echoes in half-minute periods, from record 3. The theoretical random distribution is shown by the dotted lines.

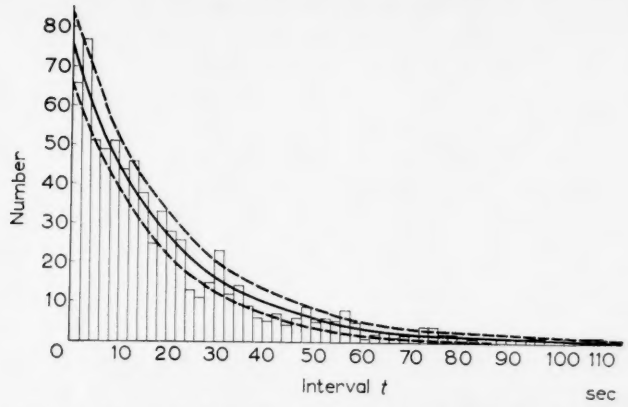

Fig. 3. Distribution of intervals between successive echoes, from record 3. The theoretical random distribution is shown by the continuous curve, with the r.m.s. error indicated by the dotted curves.

Histograms for the distributions of n, the number of echoes in half-minute periods, and t, the interval between successive echoes, for record 3, are shown in Figs. 2 and 3, together with the distributions expected for randomly occurring echoes. A summary of the results from the four records is given in the table below. These results show no significant departure from a random distribution.

VOL. 11 1957

Record number	1	2	3	4
Date	Sept./Nov. 1948	9–10 Aug. 1954	16 Aug. 1956	18 Aug. 1956
U.T.	approx. 0600–0900	2335–0215	1735–2135	0455–0615
Number of echoes	537	689	730	1179
Average rate (per min)	0·22	4·32	3·04	14·76
Probability of n distribution	0·3	0·2	0·7	0·4
Probability of t distribution	0·8	0·4	0·1	0·8
Correlation coefficient	$-0·044$ $\pm 0·045$	$-0·036$ $\pm 0·038$	$-0·052$ $\pm 0·037$	$+0·018$ $\pm 0·029$
Timing accuracy $\delta t'$	0·5 min	0·1 sec	0·1 sec	0·1 sec
Groups of three: theoretical number	25	2	2	14
Groups of three: experimental number	27	2	3	11

5—12 (pp.)

5. Discussion

It should be noted that the equipment as used would not resolve two meteors with a separation of less than about 5 km, so that very recent disintegrations would not be detected. Also, for two meteors to be observable by radio echo methods at the same station, the separation cannot be greater than a few hundred kilometres. Calculation shows that two meteors of density 4 g/cm^3, having radii of 0·05 and 0·1 cm, initially in the same orbit, will be separated by this distance by the Poynting-Robertson effect, in a typical orbit, in a period of the order of a year. Even if such pairs were sometimes formed by the break-up of a meteor, it is therefore unlikely that they would remain associated long enough to be observed together.

A group may be defined as an increase in the meteor rate, other than the statistical fluctuation, for a period of short duration compared with the daily variation. No evidence was found, in any of the records analysed, to support the theory that meteors enter the atmosphere in such groups. We believe that the equipment of Wylie and Castillo was not capable of distinguishing satisfactorily between fluctuating echoes and close groups, and that this has led to an excess of apparent groups in their results. In the present work the use of a range display has resolved this difficulty.

Trains of echoes, of the type observed by Isted, were not found more often than expected by chance. It may be concluded that the discharge mechanism he proposes was not the cause of an appreciable fraction of the echoes observed by us.

Acknowledgements—The work described was carried out at the Jodrell Bank Experimental Station, University of Manchester, under the direction of Prof. A. C. B. Lovell. One of the authors (K. R. R. B.) is in receipt of a maintenance grant from the Department of Scientific and Industrial Research.

References

Almond M., Davies J. G., and Lovell A. C. B.	1951	*Mon. Not. Roy. Astr. Soc.* **111,** 585.
Briggs B. H.	1956	*J. Atmosph. Terr. Phys.* **8,** 171.
Davies J. G. and Lovell A. C. B.	1955	*Mon. Not. Roy. Astr. Soc.* **115,** 23.
Isted G. A.	1954	*Marconi Rev.* **17,** 37.
	1955	*The Physics of the Ionosphere* p. 150. Physical Society Report of Cambridge conference.
Shain C. A. and Kerr F. J.	1955	*J. Atmosph. Terr. Phys.* **6,** 280.
Wylie L. R. and Castillo H. T.	1956	Private communication.

RESEARCH NOTES

Correction for Rayleigh-scattered light of sodium observations in twilight*

(*Received* 6 *March* 1957)

Abstract—It is pointed out that observations of sodium in twilight must always be corrected for Rayleigh-scattered white light and that the presence of the Fraunhofer lines must be allowed for. Otherwise they will effectively subtract from the sodium scattering and give a low value of the line brightness, particularly in early twilight. It is likely that this effect will mask the one recently treated by DONAHUE (1956), even after corrections have been made as well as possible. In any case, a small modification of the correction procedure will automatically take his effect into account to a good approximation.

VOL. 11 1957

IN A recent paper, DONAHUE (1956) has pointed out that the Rayleigh-scattered light observed along with twilight sodium lines contains a telluric absorption line along with the solar Fraunhofer line, and has calculated the magnitude of the effect. All observations are affected by the white light and must be corrected for it with proper allowance for the absorption lines. If this allowance is not made, the brightnesses will be too small and in early twilight may even become negative. We should like to emphasize that the effect of the solar line is much greater than that of the telluric line treated by DONAHUE, but is very similar; in fact, both effects may be allowed for together. For convenience, we shall call this process the "Fraunhofer correction." It is the presence of the white light and the necessity for the correction that causes most of the difficulties in observing the twilight sodium emission.

Twilight observations are usually made with a spectrograph, a spectrometer, or a sodium-vapour detector (BLAMONT, 1953, 1956). The effect of white light is large in the first two, and small but not zero in the last. All three give effectively a negative response to white light because of the Fraunhofer line. This is true of the dispersing instruments when the line intensity is read from the level of the continuum, and the presence of the effect is then very obvious. That the same is true of BLAMONT's detector may be seen in Fig. 2 of the first paper quoted, or Fig. 3 of the second. To make the Fraunhofer correction, the intensity of the white light must be recorded along with that of the sodium light. A suitable fraction of the white intensity is then added to the sodium intensity (as measured above the continuum) to give the corrected sodium intensity. The fraction to be added is determined in a separate measurement made in the daytime or very early twilight. The method is discussed by HUNTEN and SHEPHERD (1954) and in more detail by HARRISON and VALLANCE JONES (1956). If the determination is made in early twilight, the correction of DONAHUE will be automatically included to a very good approximation. This is true because the Rayleigh scattering is by the lower atmosphere and the path by which this is illuminated traverses the sodium layer at the same angle all through the twilight, then grazing the earth's surface, and finally illuminating the region under observation. For the same reason, the measurements of the telluric lines just before sunset made by SCRIMGER and HUNTEN (1956) allow the magnitude of the effect to be estimated. Since the lines were just barely detectable, and since this method effectively used an artificial "sodium twilight" similar to the natural one, it follows that the telluric Fraunhofer correction is so small as to be nearly negligible.

* The research reported in this paper was supported by the Geophysics Research Directorate of the Air Force Cambridge Research Center, Air Research and Development Command, under Contract AF 19 (604)–1839.

The sodium-vapour detector records emission even in early twilight, and therefore the Fraunhofer correction must be determined in the daytime. However, this very fact means that the correction is small, and DONAHUE's effect must be even smaller. The best procedure would be to make the determination just before sunset on direct sunlight (attenuated, of course) rather than on sky light, which might still show an appreciable emission component.

The appearance of raw observations without the Fraunhofer correction may be of interest. Two such runs have been published by BLAMONT and KASTLER (1951); they were taken with a quartz birefringent filter. Negative intensities are shown for early twilight; the authors explained the reason, but did not attempt to make a correction, probably because they had no record of the white-light intensity. Our own results behave in much the same way; the apparent intensity is about 10 per cent low during the main part of the twilight, but falls much lower in the early part, going negative when the solar depression is less than about 4°30′. With the correction included, no drop in intensity has ever been found in about one-hundred examples, although the scatter of the points is often large, because the correction gives nearly the whole result. A good example of a corrected run has been published by HUNTEN and SHEPHERD (1954, Fig. 3).

The observations published by BLAMONT (1956) were made with the sodium-vapour detector and have had no Fraunhofer correction applied. There are indications that it is negligible as long as the solar depression is greater than about 5°, but for smaller angles it may be appreciable. We hope to make a closer study of the question in co-operation with BLAMONT, who has been most generous with his data and in discussion.

In addition, we should like to acknowledge discussions and correspondence with CHAMBERLAIN and DONAHUE; the latter also kindly sent a copy of his paper before it was published.

D. M. HUNTEN

University of Saskatchewan,
Saskatoon, Canada

REFERENCES

BLAMONT J. E.	1953	*C. R. Acad. Sci. Paris.* **237**, 1320.
	1956	*The Airglow and the Aurorae* (Edited by B. E. ARMSTRONG and A. DALGARNO) p. 99. Pergamon Press, London.
BLAMONT J. E. and KASTLER A.	1951	*Ann. Géophys.* **7**, 73.
DONAHUE T. M.	1956	*J. Atmosph. Terr. Phys.* **9**, 262.
HARRISON A. W. and VALLANCE JONES A.	1956	*The Airglow and the Aurorae* (Ed. E. B. ARMSTRONG and A. DALGARNO) p. 95. Pergamon Press.
HUNTEN D. M. and SHEPHERD G. G.	1954	*J. Atmosph. Terr. Phys.* **5**, 57.
SCRIMGER J. A. and HUNTEN D. M.	1956	*Nature, Lond.* **178**, 753.

On the remarks of V. I. Krassovsky regarding the O_3 and O_2* hypotheses of the OH airglow

(*Received* 28 *March* 1957)

KRASSOVSKY (1957) claims that the rocket investigations of KOOMEN, SCOLNIK, and TOUSEY (1956) on the nocturnal radiation near 5300 Å have established that the Meinel

hydroxyl emission originates from about the 100 km level. This claim is unjustified. Thus, KOOMEN *et al.* state: " Some of the [5300] radiation may be from OH, though the 9-2 and 6-0 bands were located well away from the wavelength of maximum transmission of the filter." Again, HUNAERTS and NICOLET (1950) do not, as asserted by KRASSOVSKY, suppose that the 5300 Å radiation *consists* of the 9-2 and 6-0 bands—they merely point out that these bands *are present*. Their intensity is in fact low (cf. BARBIER, DUFAY, and WILLIAMS, 1951; BARBIER, 1956).

In the remainder of his note, KRASSOVSKY contests the views put forward by us (BATES and MOISEIWITSCH, 1956). We shall not take space by reiterating our arguments, but there are several points on which comment is desirable, since misunderstanding appears to have arisen.

(i) The excitation of the tenth vibrational level of OH by

$$O_3 + H \rightarrow O_2 + OH^* \qquad (1)$$

requires the availability of about 5 kcal of kinetic energy/mole and therefore cannot occur to an observable extent at ordinary temperatures. Further, the studies of GARVIN and MCKINLEY (1956) confirm that the activation energy of (1) is low, as assumed by BATES and NICOLET (1950)—indeed, its value appears to be less than 3 kcal/mole.†

(ii) KRASSOVSKY takes the rate coefficient of

$$O + O_2 + M \rightarrow O_3 + M \qquad (2)$$

to be $10^{-33}\ T^{\frac{1}{2}}$ cm^6/sec, as estimated by ENIKOLOPJAN and NALBANDJAN (1950). This is approximately the gas kinetic value and hence seems to us improbably large. ENIKOLOPJAN and NALBANDJAN obtained their estimate by a very indirect method. Their work provides no justification for discarding the value based on the measurements of EUCKEN and PATAT (1936).

(iii) There is no inconsistency in using different effective solar temperatures when considering the two rival hypotheses. It is necessary to do so, since the O_3 hypothesis depends mainly on photo-dissociation by the *Herzberg* continuum deep in the atmosphere, whereas the O_2* hypothesis depends mainly on photo-dissociation by the *Schumann-Runge* continuum high in the atmosphere. Rocket scientists (cf. FRIEDMAN, 1956) find that the effective solar temperature is a rapidly decreasing function of the frequency in the spectral region concerned.

(iv) Deactivation by the atom-atom interchange process cannot be dismissed on the grounds that the process "need not necessarily be accompanied by a change of vibrational quantum number," since there is no reason why collisions in which this quantum number is preserved should be favoured.‡

D. R. BATES
B. L. MOISEIWITSCH

Department of Applied Mathematics,
The Queen's University of Belfast

VOL. 11 1957

REFERENCES

BATES D. R. and MOISEIWITSCH B.L. 1956 *J. Atmosph. Terr. Phys.* **8,** 305.
BATES D. R. and NICOLET M. 1950 *J. Geophys. Res.* **55,** 301.
BARBIER D. 1956 *Ann. Géophys.* **11,** 67.§
BARBIER D., DUFAY J., and WILLIAMS D. R. 1951 *Ann. Astrophys.* **14,** 399.¶

† Private communication (Dr. McKinley).

‡ We did not misquote KRASSOVSKY's estimate of the half-life of atomic oxygen at 70 km, as his final footnote suggests—the erroneous value, 5 sec, appears in his papers (KRASSOVSKY, 1954, 1956). As regards the critical vibrational quantum numbers of O_2*, the values 25 and 26 result from a calculation by us, using an expression given by CURRY and HERZBERG (1934).

§ See, in particular, p. 75 *et seq.*

¶ See, in particular, p. 428.

Curry J. and Herzberg G.	1934	*Ann. Phys. Lpz.* **19,** 800.
Enikolopjan N. S. and Nalbandjan A. B.	1950	*The Kinetics of Chain Oxidation Reactions.* (Ed. by A. B. Nalbandjan and N. M. Amanouel) p. 38. Publishing House of the Acad. of Sciences, U.S.S.R.
Eucken A. and Patat F.	1936	*Z. Phys. Chem.* **33,** 459.
Friedman H.	1956	*Ann. Géophys.* **11,** 60.
Garvin D. and McKinley J. D.	1956	*J. Chem. Phys.* **24,** 1256.
Hunaerts J. and Nicolet M.	1950	*Ciel et Terre* **66,** 213.
Koomen M., Scolnik R., and Tousey R.	1956	*J. Geophys. Res.* **61,** 304.
Krassovsky V. I.	1954	*Dokl. (U.S.S.R.)* **99,** 979.
Krassovsky V. I.	1956	*The Airglow and the Aurorae.* (Ed. by E. B. Armstrong and A. Dalgarno) p. 197. Pergamon Press, London.
Krassovsky V. I.	1957	*J. Atmosph. Terr. Phys.* **10,** 49.

Nuclear explosions and a possible secular variation of the potential gradient in the atmosphere

(*Received* 2 *May* 1957)

The fair-weather aspects of atmospheric electricity may be considered as resulting from two factors. The first is the presence of a conducting or "equalizing" layer, at a height H in the atmosphere, which is maintained at a potential V_H, with respect to the earth, by the action of thunderstorms. Secondly, as a result of certain ionizing radiations, the air between the equalizing layer and the ground is a conductor. An air-earth current therefore flows whose magnitude is independent of height, since there is no accumulation of charge at any point. The resistance, R_H, of a column of air of unit cross-section extending from the ground to the equalizing layer is given by

$$R_H = \int_0^H \frac{1}{\lambda_h} \cdot dh \tag{1}$$

where λ_h is the local conductivity at height h; the local potential gradient, F_h, at the same level may be written as

$$F_h = \frac{V_H}{R_H} \cdot \frac{1}{\lambda_h} \tag{2}$$

The suffix h may now be dropped, it being understood, however, that λ and F vary with height.

The conductivity is due to the ionization present, and

$$\lambda = \Sigma\, n_i k_i e_i \tag{3}$$

where n_i, k_i, and e_i, are respectively the number per unit volume, the mobility, and charge, of ions of a particular kind; the summation is to cover all the ions present. Near the ground, two main kinds of ion, the large and the small, exist. The concentration of the small ions is perhaps only a tenth of the corresponding figure for large ions, but the small-ion mobility is about 10^4 times as great as that of large ions; hence the conductivity is almost entirely

due to small ions. Assuming that the concentrations and mobilities of positive and negative small ions are roughly equal, (3) simplifies to

$$\lambda \approx 2nek \tag{4}$$

where n is the number of small ions of one sign per unit volume.

If q is the production of ionization expressed in ion-pairs per unit volume per second, well-known balance equations govern the production and disappearance of small and large ions. Near the ground, where n is appreciably less than N or N_0, the concentrations of large ions and uncharged nuclei, respectively, the balance equations may be rearranged to give

$$q \approx 2\eta_0 n N_0 \tag{5}$$

where η_0 is the coefficient for combination between small ions and nuclei. Using (4) and (5), (2) becomes

$$F \approx \frac{V_H}{R_H} \cdot \frac{\eta_0 N_0}{ek} \cdot \frac{1}{q} \tag{6}$$

q is due to the combined effects of cosmic rays (q_c), of radioactive matter in and on the earth (q_E), and of radioactive gases in the atmosphere (q_A).

Evidence has recently been growing that radioactive fall-out after nuclear explosions is producing a semi-permanent contamination of the earth's surface. The recent work of Hess, Parkinson, and Miranda (1953), for instance, has shown a steady and considerable

VOL. 11 1957

Table 1. Mean annual value of potential gradient (V/m) for undisturbed days

Year	Lerwick Observatory	Eskdalemuir Observatory
1928-1937 (average)	167	237
1946	184	223
1947	173	210
1948	180	219
1949	168	193
1950	179	201
1951	188	224
1952	154	188
1953	190	182
1954	206	153
1955	172	143
1956	—	133

secular increase in q_E. Considering (6), a change in q caused by an increase in q_E would be expected, to a first approximation, to produce a proportionate alteration in F; the effect on R_H, the only other factor in (6) that is involved, is of secondary importance, since the ionizing radiations concerned in q_E are of limited range.

The potential gradient at a height of a metre has been measured for many years at many observatories throughout the world. It is therefore interesting to examine whether there are any recent variations corresponding to those anticipated in q. Mean annual values of potential gradient for undisturbed (Oa) days are given in Table 1 for two observatories in the British Isles.

For Eskdalemuir, it is apparent that a pronounced secular variation has occurred in recent years. Furthermore, the annual rate of decrease of field has intensified of late, this being perhaps indicative of the steady increase in the magnitudes of nuclear explosions. Quantitatively, extrapolation of the data of HESS *et al.* indicates a change by a factor of 2 in q between 1945 and 1956; the alteration in potential gradient at Eskdalemuir between the same years is in surprisingly good agreement with this value.

For Lerwick, on the other hand, there is no sign of any secular change in potential gradient, and the evidence in this respect is in disagreement with that for Eskdalemuir. Further investigation on a world-wide basis therefore seems desirable; such work might yield valuable information on the geographical distribution of the radioactive fall-out from nuclear tests.

I am indebted to the Director of the Meteorological Office and the Superintendents of Eskdalemuir and Lerwick Observatories for supplying the potential gradient information.

Cavendish Laboratory
Cambridge

E. T. PIERCE

REFERENCE

HESS V. F., PARKINSON W. D., and MIRANDA H. A. 1953 *Beta ray ionization from the ground* Fordham University, Department of Physics, Contract AF 19(122)-409, Scientific Report No. 4.

Quelques intéressantes variations du souffle de fond observées sur les fréquences de 17·6 Mc/s

(*Received* 7 *May* 1957)

Abstract—Observations of static noise on 17·6 Mc/s extending over a long period reveal that cosmic signals registered one hour before sunset and one hour and three hours after sunset present on this frequency a difference l in intensity of the order of 0·6 dB, the after sunset signal being the weaker. For working frequencies closer to the critical frequency the effect is reversed. This effect may be explained by the closing up of the reception cone for a given critical frequency as a result of the diminishing of the altitude of the F region with the coming of the night. This effect is not appreciable when the presence of the centre of the Galaxy in the cone counterbalances the loss, i.e. during the summer months.

DES enregistrements du souffle de fond total sur 17·6 Mc faits par M. CRAMET à St. Omer (Pas-de-Calais) suivant un programme établi par M. LAFFINEUR, Chef du Laboratoire de Radio Astronomie de l'Institut d'Astrophysique avant et après le coucher du Soleil à des intervalles d'abord de 2 heures (1 heure avant et 1 heure après le coucher du Soleil) et ensuite de 4 heures (1 heure avant, 3 heures après) ont revélé, surtout dans ce dernier cas, un leger affaiblissement du souffle de fond après le coucher du Soleil. Tout en etant faible, de l'ordre de 0·6 dB, cet effet semble persister pendant l'hiver et le printemps pour disparaître entre Juillet et Septembre, inclus. Il est a noter que pour des fréquences voisines de la fréquence critique un effet contraire a été observé. Pendant mon séjour à l'Institut d'Astrophysique j'ai éssayé, sur la demande de M. LAFFINEUR, d'établir l'explication théorique de cet effet.

Instruments. La déscription detaillée du recepteur de M. CRAMET a parue dans la Revue Francaise des Ondes courtes (Radio REF) du 1er Décembre 1954, p. 632. Son antenne est isotrope et consiste en un dipôle a peu prés dem-ionde d'une longueur totale

de 10·10 m, horizontal, sur mât de 18 m et orienté du NE au SW. Le contour de reception est un tore dont le plan de symmetrie équatorial est un cercle azimuthal passant par les points SE et NW de l'horizon. Dans ce plan la receptivité de l'antenne s'étend jusqu'à l'horizon sans changement, tandisque dans la direction du bipôle elle peut étre considerée comme trés éfficace jusqu'à $z = 80°$ environ.

Travail. L'enregistrement du souffle total sur 17·6 Mc à St. Omer (latitude: 50° 45′ N.) se faisait de la maniére suivante: La premiére écoute une heure avant le coucher du Soleil; la seconde écoute se faisait, pendant l'année 1954, 1 heure aprés le coucher, et, en 1955, 3 heures après. Dans le premier cas l'effet est appreciable, mais dans le second cas il devient extrêmement net et l'affaiblissement peut atteindre 0·8 dB. Il est évident que 1 heure aprés le coucher du Soleil une partie de la couche *F* est encore ensoleillée, son étendue ne depassant pas la region du ciel s'étendant de l'horizon Ouest à une hauteur de 45°, environ. A la seconde écoute de la seconde serie d'observations, celles de 1955 (3 heures aprés le coucher du Soleil), la couche *F* se trouve pratiquement dans l'obscurité d'un horizon a l'autre de l'observateur. L'éxistence d'un effet partiel plus faible dans le premier cas s'explique par le fait que l'illumination partielle de la couche *F* dans la partie Ouest du ciel n'empêche nullement un régime nocturne de s'établir sur le reste, et la plus grande partie de la couche *F*, entourant l'observateur. Il est intéressant que dans ce cas l'effet d'affaiblissement du souffle de fond total commence a s'ébaucher pour devenir très marqué lorsque la totalité de la couche *F*, autour et au dessus de l'observateur, se trouve dans l'obscurité.

VOL. 11 1957

Par contre l'enregistrement du souffle total sur 5·0 Mc, fait par le même observateur, aux mêmes heures a revelé l'existence d'une effet exactement opposé. Le signal, à la seconde écoute, est plus intense. Ceci écarte tout soupçon que la cause de l'effet sur 17·6 Mc, ou effet d'affaiblissement, peut être instrumentale, telle que, p.e., chute systematique du voltage d'alimentation. Nous pensons que l'éxplication doit en être recherchée dans la variation de l'angle solide du cône d'acceptance.

Deplacement de la couche F. *Variations de* N_e. Pour une frequence critique de, par exemple, $f = 5{\cdot}0$ Mc et une fréquence de travail, $f_t = 17{\cdot}6$ Mc nous avons un cône d'acceptance ayant pour ouverture le demi-angle solide, a,

$$\cos a = f_c/f_t, \qquad a = 73° 30';$$

ou

$$f_c = N_e/1{\cdot}12 \,.\, 10^2 = 5{\cdot}0 \text{ Mc}$$

On établit sans difficulté que la diminution de N_e, qui suit le coucher du Soleil sur la couche *F* entrainerait une diminution de f_c et un accroissement de a pourvu que f_t soit bien superieure à f_c. A part cette cause physique influençant, a, il éxiste une cause géometrique, soit la hauteur de la couche *F* qui entre en jeu pour les f_t elevées. La Fig.1

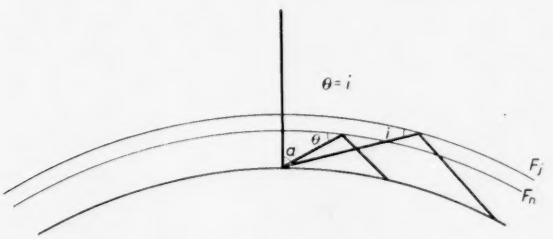

Fig. 1. L'abaissement nocturne de la couche *F* retrecit le cône d'acceptance pour une fréquence critique donnée, pourvu que la fréquence de travail en est tres éloignée

montre comment les déplacements de F en hauteur modifie a, donc la quantité totale d'énergie du bruit cosmique recue par l'antenne isotrope.

Lorsque f_t se rapproche de f_c le cône d'acceptance devient de plus en plus mal defini pour disparaître lorsque $f_t = f_c$. Dans ce cas l'importance des considerations géometriques va en diminuant au profit de la densité éléctronique laquelle acquiert le rôle préponderant. L'effet contraire, ou renforcement du second signal, observé par le même observateur pour $f_t = 5{\cdot}0$ Mc serait dû a l'inéxistence aux basses fréquences de travail d'un cône d'acceptance, le bruit, ou energie recue, etant determiné exclusivement par la N_e de la couche F qui diminue lorsque F cesse d'être ensoleillée.

Il est intéréssant de constater que ces fluctuations sur 17·6 Mc disparaissent, ou presque, pendant les mois d'été. En effet pendant Juillet, Aout, et Septembre le centre de la Galaxie dont la declinaison moyenne est environ $-23°$ émérge à l'heure de la seconde écoute au dessus du bord du cône d'acceptance. La latitude de St. Omer etant, 50° 45′ N. la distance zénithale moyenne de la region émissive du centre de la Galaxie est, au meridien, $z = 73° 45'$. Donc cette region frôle le bord du cône et, en partie émérge au dessus du bord qui la sectionne. Il suffit de consulter le travail de Shain et Higgins sur la distribution générale du bruit de fond sur 18·3 Mc, fréquence très voisine de notre fréquence de travail, pour apprecier l'importance de la contribution de la region du Sagittaire au bruit général, même si celle ci n'émérge qu'en partie au dessus du bord du cône. Cette contribution offerte par le centre de la Galaxie à son passage au meridien de St. Omer contrebalancerait les pertes d'énérgie dues au retreçissement du cône d'acceptance lors de la seconde écoute pendant les mois d'été.

Les effets decrits ci-dessus offrent un sujet intéressant ouvert a l'étude.

W. N. Abbott

Université d'Athènes,
Institut d'Astrophysique, Paris

Bibliographie

Shain and Higgins 1944 *Aust. J. Phys.* **7**, 130-149, 150-163.

Journal of Atmospheric and Terrestrial Physics, 1957, Vol. 11, pp. 75 and 76. Pergamon Press Ltd., London

Indices of geomagnetic activity

of the Observatories HARTLAND (*Ha*), ESKDALEMUIR (*Es*) and LERWICK (*Le*)

April to May 1957

THE K-indices etc. for April are derived from the new Magnetic Observatory at Hartland (Lat. 50° 59·7′ N; Long. 4° 29′ W) following the closing of the Abinger Magnetic Observatory on 18th April, 1957.

In estimating the K-indices the Abinger Sq curves have been used as a guide.

April 1957

Day	*Ha* Range for $K = 9 : 500\gamma$			*Es* Range for $K = 9 : 750\gamma$			*Le* Range for $K = 9 : 1000\gamma$			*Day*
	K-Indices		*Sum*	*K-Indices*		*Sum*	*K-Indices*		*Sum*	
1	4323	3334	25	3332	3343	24	5333	3444	29	1
2	4233	3333	24	3122	2333	19	5222	2333	22	2
3	3333	2344	25	3123	2344	22	4112	3446	25	3
4	3432	3243	24	3321	3342	21	4432	3343	26	4
5	4334	4425	29	3224	5424	26	4323	4435	28	5
6	5443	2112	22	5443	3211	23	5543	3211	24	6
7	0333	2211	15	1122	1111	10	1011	1101	6	7
8	2332	3223	20	2232	3233	20	2122	3333	19	8
9	2433	3344	26	2332	4334	24	3332	5446	30	9
10	5554	3433	32	5654	4432	33	7765	5541	40	10
11	2324	3223	21	2224	4223	21	3113	4323	20	11
12	2232	3333	21	1131	2332	16	1221	1343	17	12
13	3332	3212	19	3232	3312	19	3222	2221	16	13
14	0121	0321	10	1110	0322	10	1110	1211	8	14
15	0343	3235	23	0123	3335	20	1112	3337	21	15
16	4434	3333	27	4224	3333	24	5322	3443	26	16
17	3333	5457	33	2334	5456	32	3334	4348	32	17
18	6333	3544	31	6323	3554	31	6223	2656	32	18
19	5553	3544	34	5553	4554	36	7753	5455	41	19
20	4322	2322	20	3331	3322	20	4522	3322	23	20
21	3322	2433	22	3332	3433	24	3332	4343	25	21
22	1222	2221	14	1011	1331	11	1101	1331	11	22
23	3322	3323	21	3222	3223	19	3221	3223	18	23
24	3233	5544	29	3233	5434	27	3322	4433	24	24
25	3232	3332	21	3122	2332	18	3112	3331	17	25
26	2334	3443	26	2233	4433	24	1233	5534	26	26
27	4433	3222	23	4333	3322	23	6543	3322	28	27
28	2233	3344	24	1122	3454	22	2122	4654	26	28
29	3333	3321	21	3323	2221	18	3423	4331	23	29
30	2333	2333	22	2322	3433	22	2322	2333	20	30

VOL. 11 1957

K-indices

May 1957

Day	*Ha* *Range for K = 9 : 500γ*		*Es* *Range for K = 9 : 750γ*		*Le* *Range for K = 9 : 1000γ*		*Day*
	K-Indices	*Sum*	*K-Indices*	*Sum*	*K-Indices*	*Sum*	
1	4433 3322	24	3432 2311	19	3443 2210	19	1
2	2343 2222	20	1333 3212	18	2232 2113	16	2
3	2212 2334	19	2212 3334	20	2211 3344	20	3
4	2232 33 loss of record	loss of record	1121 3332	16	1122 3343	19	4
5	loss of record 3323		3212 2312	16	3122 2222	16	5
6	3234 3232	22	3233 3222	20	3323 3222	20	6
7	3323 2322	20	2222 2321	16	3322 2331	19	7
8	1122 2434	19	0122 2334	17	1112 2324	16	8
9	2344 4332	25	3333 3332	23	4543 3332	27	9
10	2222 2334	20	2212 2333	18	1112 2224	15	10
11	2222 3223	18	2211 2223	15	3211 2324	18	11
12	2123 3202	15	2111 2212	12	3111 1201	10	12
13	3323 3333	23	3212 3332	19	3322 3332	21	13
14	1223 2232	17	1222 2232	16	2212 2221	14	14
15	2121 3222	15	1111 2222	12	1112 2222	13	15
16	0022 2330	12	1010 1331	10	1112 1331	13	16
17	0233 2432	19	1222 1422	16	1222 2422	17	17
18	2131 3222	16	1122 3232	16	2132 3322	18	18
19	2122 4443	22	2122 4443	22	2122 3443	21	19
20	3433 3432	25	3333 3432	24	3333 4432	25	20
21	3333 3332	23	3223 3332	21	3323 3332	22	21
22	2222 2311	15	2322 2311	16	1212 2211	12	22
23	2222 3231	17	2122 3341	18	3222 3342	21	23
24	2123 3220	15	1123 3220	14	1022 2121	11	24
25	2233 3333	22	1232 3333	20	2222 3233	19	25
26	3344 4433	28	3344 3433	27	4444 3433	29	26
27	3232 2212	17	2223 2212	16	2222 2222	16	27
28	1122 2322	15	2122 3322	17	1122 3313	16	28
29	1221 1322	14	1121 2321	13	2122 3311	15	29
30	3234 4433	26	2123 4532	22	3224 4553	28	30
31	3322 1322	18	3332 1232	19	3323 1211	16	31

Journal of Atmospheric and Terrestrial Physics, 1957, Vol. 11, pp. 77 to 82. Pergamon Press Ltd., London

Electric field measurements in the stratosphere

C. G. Stergis, G. C. Rein, and T. Kangas
Geophysics Research Directorate, Air Force Cambridge Research Center,
Air Research and Development Command, Bedford, Mass., U.S.A.
and Minneapolis-Honeywell Regulator Company*

(*Received* 2 *April* 1957)

Abstract—The electric field in the atmosphere from ground up to 90,000 ft was measured during a series of twenty balloon flights made in 1955 and 1956. The tests indicate that the electric field in the atmosphere, above the exchange layer, decreases monotonically with height up to the maximum height at which measurements were made. The measured values of electric field agree very well with the values calculated from conductivity data and the assumption of an approximately constant air-earth current density.

VOL. 11 1957

1. Introduction

Prior to our measurements, the only measurements that were made, to our knowledge, of the electric field in the stratosphere were those of Koenigsfeld (1953) and Venkiteshwaran (1956). These investigators have found that, in general, the electric field diminishes rapidly with increasing height above the surface of the earth. However, at some altitude from 15,000 to 30,000 ft, the electric field appears to stop decreasing and remains constant to the highest regions reached by their instruments. Furthermore, this constant value is sometimes of the order of 20 to 50 V/m, which is a fairly substantial electric field. These results are in direct contradiction to atmospheric electricity theory, as will be shown below. As part of a larger programme in atmospheric electricity research, we had occasion in the summers of 1955 and 1956 to measure the electric field in the stratosphere. Consequently, we present our results in an effort to shed some light on the above discrepancy.

2. Theoretical Considerations

According to present theories of atmospheric electricity, thunderstorms act as giant generators of electricity sending positive current to the ionosphere and maintaining the potential of the ionosphere at several hundred kV positive with respect to the earth. In fair-weather regions, positive current flows from the ionosphere to the earth, and the current density is given by

$$i = \frac{V}{r} \tag{1}$$

where V represents the potential of the ionosphere with respect to the earth, i the current density; i.e. the current flowing in a vertical column of the atmosphere of unit area cross-section and extending from the earth to the ionosphere, and r the resistance of this column.

* The second author is with Minneapolis-Honeywell and the others are with Geophysics Research Directorate.

The current density may be obtained directly by measuring the quantity of charge arriving at a plate of unit area in unit time or indirectly by measuring the electric field and the conductivity. The product of these two quantities gives the current density. Thus

$$i = (\lambda_1 + \lambda_2)E = \lambda E \tag{2}$$

where λ_1 represents the conductivity due to positive ions, λ_2 the conductivity due to negative ions, λ the total conductivity, and E the electric field at the region of measurement. The direct method measures the total current density, which consists of the conduction current and the convection current. The indirect method determines the conduction current only. Experiments by NOLAN and NOLAN (1937), however, have shown that there is very little convection current; and hence, the conduction current is approximately equal to the total current.

In the electric current flow system from ionosphere to earth, the equation of continuity states that

$$\Delta \cdot i + \frac{\partial \rho}{\partial t} = 0 \tag{3}$$

where ρ represents the charge per unit volume at the region in question. Under steady-state conditions, this leads immediately to a constant current density between ionosphere and ground. From equation (2) we see then that the product of conductivity and electric field should be a constant under steady-state conditions. Measurements of conductivity in the stratosphere by STERGIS *et al.* (1955) have shown that the conductivity increases monotonically with height. Therefore, to maintain a constant current density, it is necessary that the electric field decrease monotonically with height. The absence of steady-state conditions would mean a varying current density. A varying current density, as is seen from equation (1), may be due to a variation in one of two factors: (a) the potential of the ionosphere, which may vary due to a change in the electrical activity of thunderstorms, and (b) the columnar resistance, which may change due to the introduction or removal of pollution particles in the lower layers of the troposphere. Let us estimate how far the current density may deviate from a constant value during the time required to make a complete measurement of electric field with altitude which, by balloon methods, is of the order of 1 hr.

An examination of the current density data taken at Tucson, Arizona, during the period 1935 to 1951, as reported by WAIT and PARKINSON (1953), indicates that in fair weather during the afternoon hours (the period during which our experiments were conducted) the variation in current density over a period of 1 hr is seldom greater than 25 per cent. To account for the increase in conductivity from 30,000 to 60,000 ft, as given in Fig. 1, without any change in the electric field values, would require an increase in the electric current density of 500 per cent. This never happens in fair weather. We must, therefore, conclude that, since during the period of 1 hr the current density remains constant within 25 per cent, the increase in conductivity obtained experimentally must be accompanied by a corresponding decrease in electric field.

According to GISH (1951), the total electric current from air to earth for all fair-weather areas is about 1800 A. The average current density then becomes 10^{-6}

e.s.u. Using this value of current density, the experimental conductivity data given in Fig. 1, and equation (2), we calculated the values of electric field as a function of altitude. The results of the calculations are given in Fig. 2. It remains to compare the expected values of electric field with the experimental data.

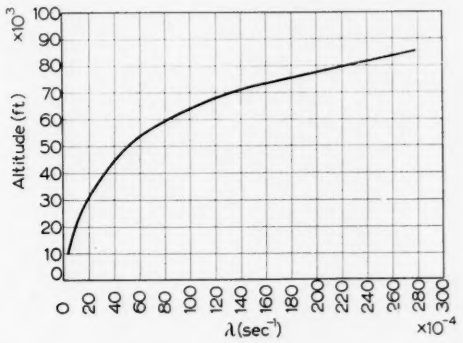

Fig. 1. Average negative conductivity vs. altitude for flights on 10, 12, and 16 July 1955.

VOL. 11 1957

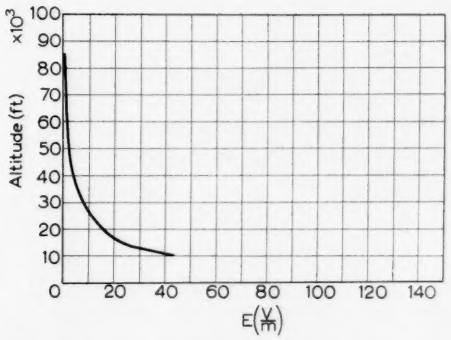

Fig. 2. Calculated electric field vs. altitude based on conductivity data of Fig. 1.

3. Experimental Method

The method of measuring the conductivity in the stratosphere has been described previously by Stergis *et al.* (1955). The instrument used for measuring the electric field in the stratosphere has been described by Rein *et al.* (1957). It consists essentially of two radioactive probes (polonium-210) separated by a distance of 1 m. These probes quickly attain the potentials of their surroundings, and the voltage across them is measured by a cathode-follower type of electrometer

circuit. The electrometer drives a standard radiosonde transmitter operating at 1680 Mc/s. The signals from this transmitter are received at the ground and automatically recorded. The instrument also telemeters altitude information to the ground receiver.

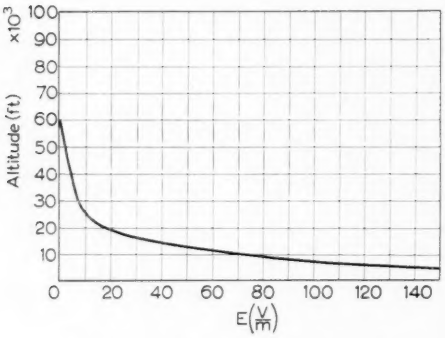

Fig. 3. Electric field vs. altitude for flight on 4 August 1955.

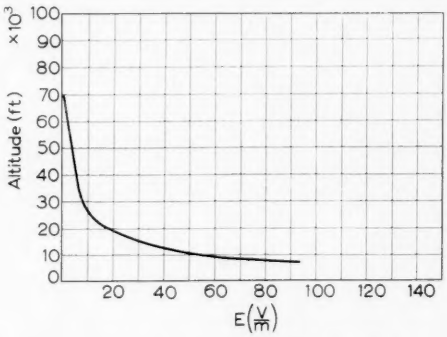

Fig. 4. Electric field vs. altitude for flight on 5 August 1955.

The electric-field meter is carried aloft at an average rate of 1000 ft per min by means of a polyethylene balloon. To minimize the electrostatic effects of the balloon on the electric-field meter, the instrument was suspended 200–300 ft below the balloon.

4. Experimental Results

All the flights were made during the afternoon hours at Cape Canaveral, Florida, in the summers of 1955 and 1956. Three conductivity flights and twenty electric-field flights were successfully accomplished. Fig. 1 shows some of the conductivity data, and Figs. 3, 4, 5, and 6 show some of the electric-field data. The remaining flights showed similar results. It is observed that the electric field not only decreases rapidly in the first few thousand feet above the ground, as found by other investigators, but that it continues to diminish to the highest altitude at which measurements were made. Comparison with the theoretical curve of Fig. 2 shows that the experimental values of electric field agree very closely with the calculated average values.

Fig. 7 shows the electric-field results in detail for the first 20,000 ft for one particular flight. It is observed that a sharp decrease in electric field occurs at 4,000 ft. This is evidently the top of the exchange layer, which has been investigated quite extensively by Sagalyn and Faucher (1954). In their measurements, the top of the exchange layer shows a very sharp increase in conductivity. Our measurements then are in agreement with their data along with the assumption of a constant current density. Variations in the electric field are present in the exchange layer, as would be expected from Sagalyn's results on the variations in conductivity that are found in the exchange layer.

It is also observed from the figures that the electric field in the stratosphere does vary from day to day, sometimes by as much as 25 per cent. This would be expected from: (a) variations in the air-earth current density as indicated previously, and (b) variations in the conductivity in the stratosphere due to the time variations of the cosmic-ray intensity at high altitudes, as given by NEHER (1953).

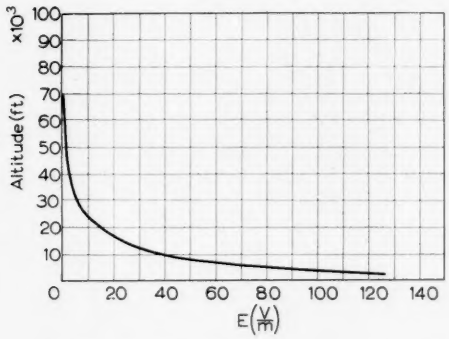

Fig. 5. Electric field vs. altitude for flight on 24 July 1956.

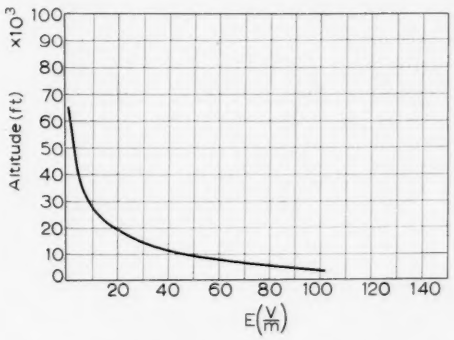

Fig. 6. Electric field vs. altitude for flight on 25 July 1956.

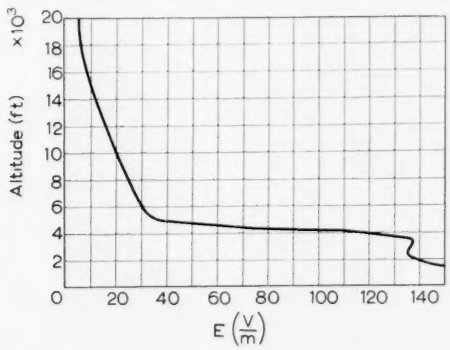

Fig. 7. Electric field vs. altitude for flight on 2 August 1956.

5. CONCLUSIONS

From the experimental results and theoretical calculations, we may make the following conclusions:

(1) During fair weather, the electric field in the atmosphere, above the exchange layer, decreases monotonically with height up to 100,000 ft above sea-level.

(2) The measured values of electric field agree very well with the calculated values based on the assumption of an approximately constant air-earth current density.

REFERENCES

GISH O. H. 1951 *Compendium of Meteorology.* American Meteorological Society, Boston, Mass.

VOL. 11 1957

Koenigsfeld L.	1953	*Thunderstorm Electricity.* University of Chicago Press.
Neher H. V., Peterson V. Z., and Stern E. A.	1953	*Phys. Rev.* **90,** 655.
Nolan J. J. and Nolan P. J.	1937	*Proc. R. Irish Acad.* **43,** 79.
Rein G. C., Stergis C. G., and Kangas T.	1957	Instrumentation Conference of Institute of Radio Engineers, Dec. 1956.
Sagalyn R. C. and Faucher G. A.	1954	*J. Atmos. Terr. Phys.* **5,** 253.
Stergis C. G. *et al.*	1955	*J. Atmos. Terr. Phys.* **6,** 233.
Venkiteshwaran S. P. and Huddar B. B.	1956	*Indian J. Met. Geophys.* **7,** 61.
Wait G. R. and Parkinson W. D.	1953	*Investigations of Electrical Properties of the Atmosphere.* Department of Terrestrial Magnetism, Carnegie Institution of Washington.

Journal of Atmospheric and Terrestrial Physics, 1957, Vol. 11, pp. 83 to 90. Pergamon Press Ltd., London

Electric field measurements above thunderstorms

C. G. Stergis, G. C. Rein, and T. Kangas
Geophysics Research Directorate Air Force Cambridge Research Center, Air Research and Development Command, and Minneapolis-Honeywell Regulator Company*

(*Received* 17 *May* 1957)

Abstract—The electric field and conductivity of the atmosphere were measured above thunderstorms in the central Florida area in a series of twenty-five balloon flights made at altitudes ranging from 70,000 to 90,000 ft above sea level. These tests indicate that at these altitudes and for the storms investigated there is a positive current of approximately 1·3 A, on the average, flowing upward from the top of the thunderstorm toward the ionosphere and confirm Wilson's hypothesis that thunderstorms are the generators which supply the electric current necessary for maintaining the earth's negative charge.

VOL. 11 1957

1. Introduction

It has been known for many years that the earth has a negative electrical charge and that this charge would leak away, due to the conductivity of the air, in a few minutes were it not for some source which supplies charge to the earth at a rate sufficient to compensate for the loss due to conduction. It was Wilson (1920) who first suggested that thunderstorms might be the generators which supply the electrical current necessary for maintaining the earth's charge. A confirmation of this hypothesis was obtained in 1948 when Gish and Wait (1950) flew an aircraft at 40,000 ft over twenty-one thunderstorms in the central United States. They found that for these storms there was a current of 1/2 A, on the average, flowing from the top of the thunderstorms upward. This current is in the right direction and of the order of magnitude required for Wilson's hypothesis.

Further confirmation of Wilson's hypothesis was deemed desirable because of the following considerations. First, Gish and Wait's experiment was performed just over the thunderstorms and, in some cases, inside the upper portion of the thunderstorms. The question immediately arises as to what fraction of the upwardly directed current flows to the ionosphere since, conceivably, part of this current may be flowing in a local circuit such as between two charge poles in the cloud. Second, the question arises as to how representative are these storms in the central United States. It is known that tropical thunderstorms attain much greater heights than do thunderstorms in the temperate climates. Are these higher elevation storms more active electrically? Third, a question was raised by Gunn (1935) as to whether cloud-ground strokes are necessary for the generation of appreciable upward currents. An experiment on thunderstorms which have very few cloud-ground strokes was considered desirable.

Therefore, in the summers of 1955 and 1956, twenty-five balloon flights were made over thunderstorms in central Florida. The altitudes of these flights were

* The second author is with Minneapolis-Honeywell and the others are with Geophysics Research Directorate.

from 70,000 to 90,000 ft above sea level. The storms investigated had maximum heights ranging from 30,000 to 60,000 ft above sea level and cloud-ground strokes comprised approximately 25 per cent of the total number of lightning strokes occurring.

2. Experimental Method

The electric current flowing above thunderstorms was determined by measuring the conductivity and the electric field, since the product of these two quantities gives the conduction current.

The method of measuring the conductivity in the stratosphere was described previously by Stergis *et al.* (1955). The conductivity chamber consists essentially of two concentric cylinders across which a given voltage is applied. A fan attached at one end of this chamber draws air through the chamber at a rate of about 3000 ft/min. As the air passes through the chamber, it gives up a fraction of its electric charge to the inner electrode which is connected to a d.c. electrometer-amplifier. This in turn drives a standard radiosonde transmitter operating at 1680 Mc/s. The signals from this transmitter are received at the ground and automatically recorded.

The method of measuring the electric field in the stratosphere has been described by Rein *et al.* (1957). The electric field meter consists essentially of two radioactive probes (polonium 210) separated by a distance of 1 m. These probes quickly attain the potentials of their surroundings, and the potential difference between them is measured by a cathode-follower type of electrometer circuit. The electrometer drives a standard radiosonde transmitter which sends the desired information to a ground receiver.

The conductivity chamber or the electric field meter is transported into the stratosphere by means of a polyethylene balloon at an average rate of 1000 ft/min. To minimize the electrostatic effects of the balloon on the measurements, the instrument is suspended 200–300 ft below the balloon.

The balloon is launched on the east coast of Florida in advance of forecasted thunderstorm formation. The balloon ascends to a height of 70,000 to 90,000 ft, depending on the size of the balloon and on the load. It then floats toward the west coast of Florida, since the upper air winds in Florida during the summer months are invariably from east to west. The magnitude of the wind in this region of the stratosphere is from 35 to 55 m.p.h. In its passage across Florida, the balloon usually encounters one or more thunderstorms (assuming a correct forecast was made in the first place). The electrical measurements above thunderstorms are made by the instrument suspended below the balloon and the information is telemetered to the ground. When the balloon arrives at the west coast of Florida, it is cut down automatically and the instrument descends by parachute.

The radiosonde receiver not only picks up the signal from the balloon transmitter but also tracks the balloon in its flight, automatically recording the azimuth and elevation. This information, in addition to the altitute information transmitted by the measuring instrument, is sufficient to locate the instrument at all times.

The location of all thunderstorms in the vicinity of the balloon must also be known, and this is done by conventional radar techniques.

3. Results

Three conductivity flights were made over thunderstorms with the results of one of the flights shown in Fig. 1. The other two flights showed similar results. It is observed that there is no detectable difference in conductivity between regions above a thunderstorm and regions away from a thunderstorm. One may ask how

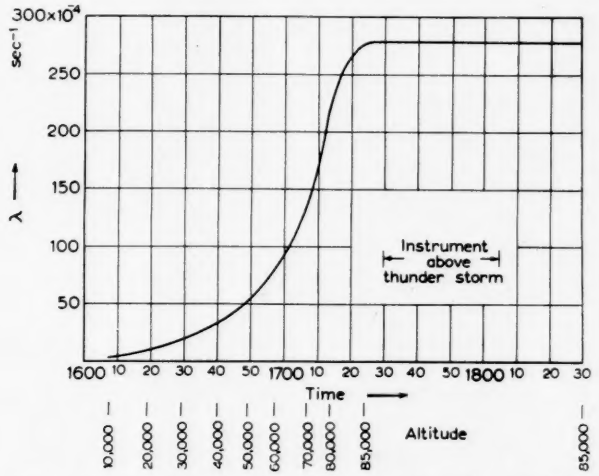

Fig. 1. Negative conductivity of the atmosphere above a thunderstorm.

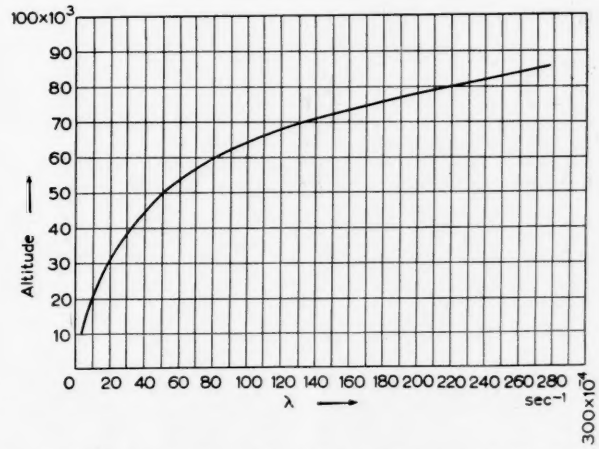

Fig. 2. Average negative conductivity as a function of altitude for flights on 10, 12 and 16 July 1955.

definite it is that the conductivity chamber went over thunderstorms and not to one side of them. The radar information on these days indicated a line of thunderstorms active during each balloon flight and the balloon could not fail to traverse this line.

VOL. 11 1957

This result, although a purely negative one, enables us to determine the current flowing above thunderstorms merely by measuring the electric field and using the value of conductivity obtained previously for the particular altitude of the flight. Fig. 2 shows the average value of conductivity obtained on three flights in the

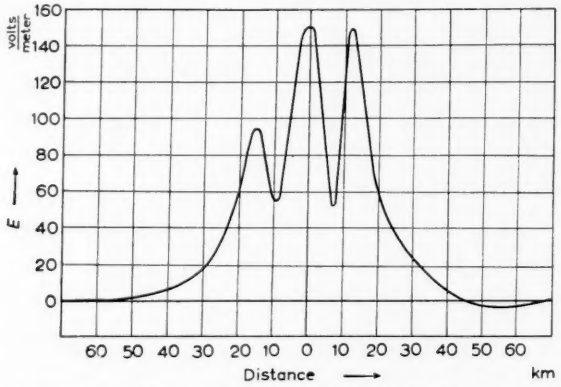

Fig. 3. Electric field at an altitude of 70,000 ft for flight on 21 July 1956.

Florida area, and these values of conductivity were used in calculating the electric current.

Figs. 3, 4, 5, and 6 show the electric field results obtained on four of the flights made. The abscissa on these figures represents distance from an arbitrary reference

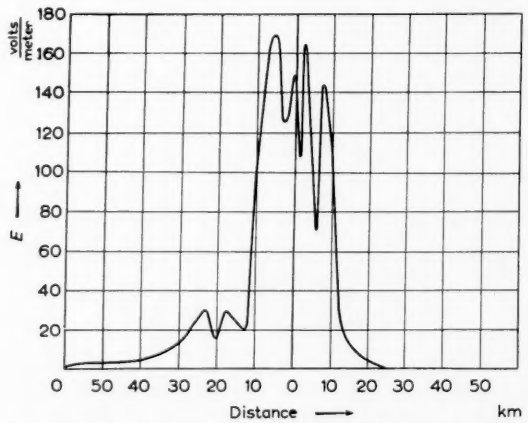

Fig. 4. Electric field at an altitude of 71,000 ft for flight on 30 July 1956.

point, and this point does not necessarily correspond to a point directly above the centre of the storm. The ordinates represent the average electric field measured. Superimposed on this average were numerous field changes due to lightning discharges, but these changes were omitted from the figures for the sake of simplicity.

An examination of the figures indicates that there is a considerable amount of electrical structure to the storms. This is due to two factors. First, at any given time, the storm is not a simple dipole but consists of a complicated configuration of

charges. Second, the activity of individual cells within a storm varies with time. For example, an examination of the radar information for the flight shown on Fig. 4 showed several cells which increased in intensity and then decreased again while the field meter was still near enough to record electrical effects.

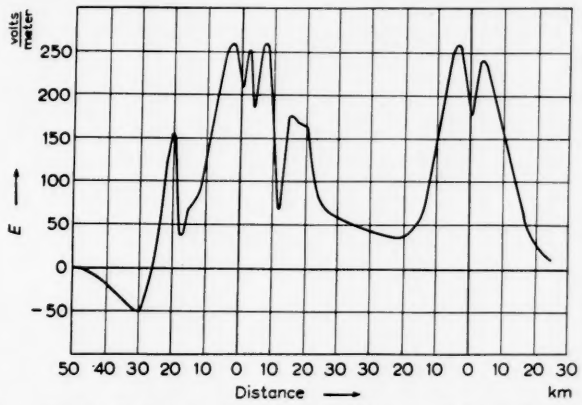

Fig. 5. Electric field at an altitude of 70,000 ft for flight on 3 August 1956.

VOL. 11 1957

Several of the figures show a reversal in the electric field which would always be expected from the electric field due to a simple dipole. Again, the absence of a reversal in the field in some of the flights probably indicates a charge configuration different from that of a simple dipole.

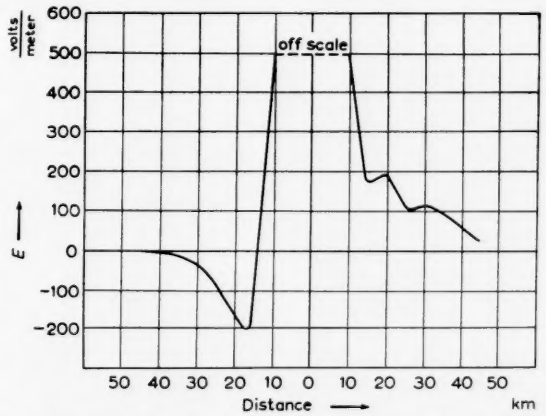

Fig. 6. Electric field at an altitude of 76,000 ft for flight on 20 July 1956.

It is observed that the maximum value of field obtained varies from flight to flight. This is due to storms of different intensities and also to the fact that the balloon did not always go directly over the storm in question. From the radar information, it was deduced that the balloon went directly over a very intense line of storms on the flight shown in Fig. 6, went within 7 miles of the centre of the storm in Fig. 3, within 3 miles in Fig. 4, and within 8 miles in Fig. 5. Also, Fig. 5 shows the passage of the instrument over two distinct thunderstorms.

4. Calculations

The horizontal distribution of the electric field above an electrical dipole immersed in a medium of conductivity exponentially increasing with height was calculated, using Holzer and Saxon's (1952) solution, which is

$$\phi = q_0 e^{-k(z-z_0)} \left(\frac{e^{-kR_0}}{R_0} - \frac{e^{-kR_0'}}{R_0'} \right)$$

where ϕ represents the potential at a point P having co-ordinates x, y, z; q_0 the magnitude of the charge; z_0 the height of the charge; k the factor which gives the variation of conductivity with height; R_0 the distance from q_0 to P; and R_0' the distance from the image of q_0 to P.

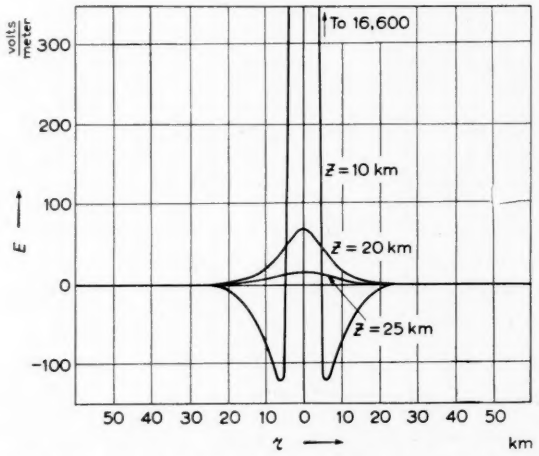

Fig. 7. Theoretical electric-field distribution at 10, 20, and 25 km above sea level when there exists a dipole of 37·5 C at 8 km and −20 C at 5 km.

Differentiating ϕ with respect to z, we obtain the vertical component of the electric field which for charges of opposite sign at z_0 and z_1 becomes

$$E_z = q_0 e^{-k(z-z_0)} \left\{ \left[e^{-kR_0} \left(\frac{k}{R_0} + \frac{k(z-z_0)}{R_0^2} + \frac{z-z_0}{R_0^3} \right) - e^{-kR_0'} \left(\frac{k}{R_0'} + \frac{k(z+z_0)}{(R_0')^2} + \frac{z+z_0}{(R_0')_3} \right) \right] - e^{-k(z_1-z_0)} \times \left[e^{-kR_1} \left(\frac{k}{R_1} + \frac{k(z-z_1)}{R_1^2} + \frac{z-z_1}{R_1^3} \right) - e^{-kR_1'} \left(\frac{k}{R_1'} + \frac{k(z+z_1)}{(R_1')^2} + \frac{z+z_1}{(R_1')^3} \right) \right] \right\}$$

This equation is plotted in Fig. 7 for $q_0 = -20$ C, $z_0 = 5$ km, $z_1 = 8$ km, $k = 0{\cdot}1$ km^{-1}, and $z = 10$, 20, and 25 km. The reversal of electric field is easily seen for the 10 km curve, although it is present in the other curves but not discernible because of the scale of the drawing. It is observed from these curves that flights made near the top of the dipole would show a very rapid change of field with distance; whereas, flights made at great distances above the dipole show a very

gradual field change with distance. In fact, at a 25 km flight, the instrument could be 10 km away from the vertical axis of the dipole and still have only a 50 per cent decrease in field. Consequently, because of the high altitude of our flights, even though in some of the flights we did not pass directly over the centre of the thunderstorm, we may still make a fairly good estimate of what the field would be directly above the storm.

The current density above the thunderstorms was calculated from the relation

$$i = (\lambda_1 + \lambda_2)E = \lambda E$$

where i represents the current density, λ_1 the conductivity due to positive ions, λ_2 the conductivity due to negative ions, λ the total conductivity, and E the electric field in the region of measurement. λ was obtained from Fig. 2 and E from figures similar to Figs. 3 to 6.

The total current I due to a single thunderstorm was calculated by integrating the current density curves (similar to the electric field curves of Figs. 3 to 6) over the distance at which the current density could be detected and assuming electrical symmetry for the current density distribution around a thunderstorm. An examination of the radar pictures of the storms and the path of the balloons with respect to the storms indicated that in every case the assumption of electrical symmetry resulted in a calculated value of I which is low, perhaps by as much as 50 per cent. Hence, the calculated values of I listed below are to be considered as lower limits to the actual values of I. Table 1 gives the results obtained for the four flights which gave the data of Figs. 3 to 6.

VOL. 11 1957

Table 1

Date	I (A)
20 July	>4·3
21 July	0·6
30 July	1·1
3 August	2·7 (first storm)
3 August	0·8 (second storm)

The remaining flights gave values of I which ranged between the extremes of 0·6 and 4·3 given above. The average value of I for twenty storms that were investigated was 1·3 A. The direction of I in all cases was positive, that is, positive current flowing from the top of the thunderstorm toward the ionosphere.

5. Conclusions

From the experimental results obtained on 25 balloon flights over thunderstorms in the central Florida area we may make the following conclusions:

(1) There is no detectable difference in the conductivity of the atmosphere between the region above a thunderstorm and regions away from a thunderstorm.

(2) Above thunderstorms there is a positive current flowing from the top of thunderstorms toward the ionosphere.

(3) For the storms investigated, the magnitude of the current flowing upward in the region of the stratosphere between 70,000 and 90,000 ft is approximately 1·3 A, on the average.

(4) Cloud-ground lightning discharges are not necessary for an appreciable flow of current upward from the top of a thunderstorm.

In summary, we may say that these experiments have given added confirmation to Wilson's thunderstorm hypothesis and that, although thunderstorms may not be the only sources which supply the electric current necessary for maintaining the earth's negative charge, they are certainly powerful enough electrically to produce the greatest portion of the required current.

References

Gish O. H. and Wait G. R.	1950	*J. Geophys. Res.* **55,** 473.
Gunn R.	1935	*Terr. Magn. Atmos. Elect.* **40,** 79
Holzer R. E. and Saxon D. S.	1952	*J. Geophys. Res.* **57,** 207.
Rein G. C., Stergis C. G. and Kangas T.	1957	*Instrumentation Conference of Institute of Radio Engineers* Dec. 1956.
Stergis C. G. *et al.*	1955	*J. Atmos. Terr. Phys.* **6,** 233
Wilson C. T. R.	1920	*Trans. Roy. Soc.* **A221,** 73

Journal of Atmospheric and Terrestrial Physics, 1957, Vol. 11, pp. 91 to 101. Pergamon Press, Ltd., London

Ionospheric irregularities causing random fading of very low frequencies*

S. A. Bowhill
Ionosphere Research Laboratory, The Pennsylvania State University,
University Park, Pennsylvania, U.S.A.

(*Received* 29 *April* 1957)

Abstract—The process by which random irregularities in the ionosphere cause random fading in a reflected radio wave at the ground may be divided into two parts: the scattering process within the layer which builds up an inhomogeneous field in free space immediately beneath it, and the diffraction process by which this field propagates to the earth's surface, possibly changing in form as it travels.

The extent of this change is evaluated by finding the correlation coefficients for three pairs of quantities measured experimentally at 75 and 150 kc/s frequency. These are

(a) the signal amplitude at two horizontally separated receivers
(b) the amplitudes of the first and second reflections
(c) the amplitude and phase of the first reflection.

The diffractive changes are found to be considerable, but the wave emerging from the layer is probably modulated in phase rather than amplitude.

A study of the variation of fading speed at 75 kc/s with height of reflection appears to confirm existing ideas concerning the presence of small-scale irregularities above a critical height in the lower *E*-region.

VOL. 11 1957

1. Introduction

The broad principles which govern the fading of radio waves of medium and low frequencies are now well understood. This paper describes some experiments towards the evaluation of the detailed process by which random fading is produced. This process can be divided into two parts. The incident wave first interacts with the random inhomogeneities of ionization within the layer to produce a scattered signal in free space immediately below the layer, together with a specularly reflected signal. These two signals then propagate to the earth's surface, changing as they do so, by the process of random diffraction.

It is convenient to adopt this division between the processes of scattering and diffraction. This is particularly true as the random diffraction process is now well understood, since the work of Booker, Ratcliffe, and Shinn (1950) and Hewish (1951, 1952). The study of processes of random scattering on the other hand, is only just beginning (Booker, 1955; Ratcliffe, 1956).

The properties of randomly fading radio waves measured at the ground have been studied at medium frequencies by Briggs and Phillips (1950) and by many others. Low frequency studies have been made by Millman (1952), Harwood (1953), Bowhill (1956) and Sales (1956).

2. Outline of Diffraction Theory

The theory of the diffraction of a shallowly phase or amplitude modulated random signal, anisotropic in two dimensions, has recently been treated by the

* The research described in this paper has been sponsored in part by the Geophysical Research Directorate of the Air Force Cambridge Research Center, Air Research and Development Command, under Contract AF19(604)–1304, and in part by the National Science Foundation, under Grant G–1969.

author. The method used, details of which will be published elsewhere, permits the calculation of all the detailed statistical parameters of the random phase and amplitude variation in the diffraction pattern.

In most ionospheric pulse experiments the ray path is normal to the ionosphere. It is therefore convenient as a first approach, to consider the wave incident on the ionosphere as having a plane wave-front, parallel to the plane of stratification of the ionosphere. There is then an equivalence theorem which compensates for the sphericity of the waves actually incident on the reflecting layer. This is stated without proof in the appendix.

When a plane wave passes into, and is reflected from, an ionized medium containing random irregularities in ionization, a random field is produced just below the lower boundary of the medium. It is important for an understanding of the nature of the irregularities that the form of this variation should be known. For

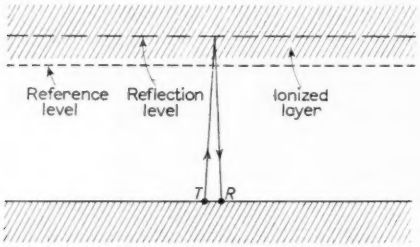

Fig. 1. The geometry of the reflection.

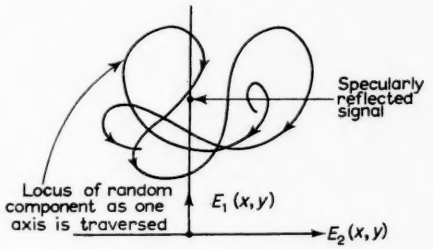

Fig. 2. A possible phase-amplitude diagram for the diffracted signal a long way from a random screen.

instance, irregularities situated at low heights in the ionized region will primarily affect the absorption of the wave, while irregularities near the height of reflection will primarily change the phase of the wave (Jones, Millman, and Nertney, 1953). In the former case the wave immediately below the region will be amplitude modulated, while in the latter it will be phase modulated.

At low frequencies it is found experimentally that the reflected signal received at the ground is modulated shallowly in amplitude and phase. The vector mean of the signal can be regarded as due to a specular reflector at the apparent height of reflection: it is called the "specular" component. The remaining component, the random signal, can then be treated separately.

Consider a plane immediately below the ionized region, and let this be the reference plane $z = 0$ (see Fig. 1). At any horizontal plane at a distance z from the reference plane, the random signal $\bar{E}(x,y,z)$ can be resolved into phase-components $E_1(x,y,z)$, and $E_2(x,y,z)$, which are respectively in phase and in quadrature with the specular signal at the plane. As can be seen from Fig. 2, the component $E_1(x,y,z)$ gives variations in the amplitude of the total signal, while $E_2(x,y,z)$ produces variations in its phase.

Two special cases are of importance, corresponding to a signal at the reference level which is purely amplitude-modulated, i.e. $E_2(x,y,0) = 0$, or purely phase-modulated, for which case $E_1(x,y,0) = 0$. The signal at all points below the reference level (ignoring the up-going incident wave) can then be regarded as due to an

idealized shallowly modulated diffracting screen, described respectively as an amplitude screen or a phase screen, situated at the reference level.

Since the diffraction of the random signal $\bar{E}(x,y,0)$ does not depend on the phase of the specular signal, there is an equivalence between the results for a phase and an amplitude screen. Relationships between E_1 and E_2 for an amplitude screen also hold between E_2 and $-E_1$ for a phase screen: so all results will be quoted for an amplitude screen.

A Gaussian form is assumed for the spatial correlogram of $E_1(x,y,0)$:

$$\rho(\alpha) = \exp(-\alpha^2/2D^2)$$

where ρ is the correlation between $E_1(x,y,0)$ at two points a distance α apart at the reference level, and D is defined as the structure size of the random variations of signal. The justification for this choice of correlation function is that it is found experimentally to hold at low frequencies (BOWHILL, 1956).

Theoretical analysis shows that there is a critical distance $\pi D^2/\lambda$ from the reference level (where λ is the wavelength of the frequency used) within which geometric optics applies. For $z \gg \pi D^2/\lambda$ diffraction theory must be used to calculate the signal. It is convenient to define a quantity $a = \lambda z/\pi D^2$ which gives a scale for z in terms of this critical distance.

The depth of fading can be expressed by the mean square values of $E_1(x,y,z)$ and $E_2(x,y,z)$. If, at the reference level, we define the specular signal as having unit amplitude, and also define

$$\left.\begin{aligned}\overline{E_1^2(x,y,0)} &= B \\ \overline{E_2^2(x,y,0)} &= 0\end{aligned}\right\} \quad (B \ll 1)$$

then, a long way from the screen,

$$\overline{E_1^2(x,y,\infty)} = \overline{E_2^2(x,y,\infty)} = B/2$$

and the variation occurs equally in phase and amplitude. At intermediate distances the depths of fading of the two phase-components vary as shown in Fig. 3.

The structure size d of the random variations of E_1 or E_2 at any distance z is defined as the analogous parameter to D, for the Gaussian curve which best fits the actual spatial correlogram of $E_1(x,y,z)$ or $E_2(x,y,z)$ for small values of α. The variation of d with a is illustrated in Fig. 4.

The cross-correlation ρ_{12} between $E_1(x,y,z)$ and $E_2(x,y,z)$ can be shown to have the form

$$\rho_{12} = (2 + a^2)^{-1/2}$$

It is shown, in the appendix, that if a wave is multiply reflected from a region containing irregularities, and the reference level is near to the level of reflection, the correlation between the values of $E_1(x,y,z)$ for the first and second reflected signals can be calculated very simply: as can the corresponding correlation for $E_2(x,y,z)$. The variation of this correlation with a for E_1 and E_2 is given by the curves of Fig. 5.

The significance of the value of a can be seen from Fig. 6, which gives the correlation ρ_{11} between the signal at the reference level and at the ground as a

VOL. 11 1957

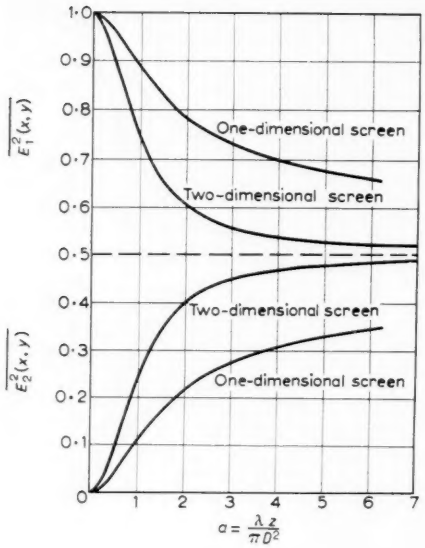

Fig. 3. Variation of mean-square diffracted signal with distance from two kinds of random screen.

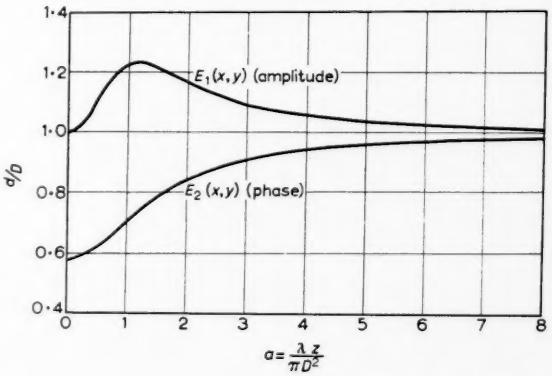

Fig. 4. Variation of structure size d with distance from a two-dimensional amplitude screen.

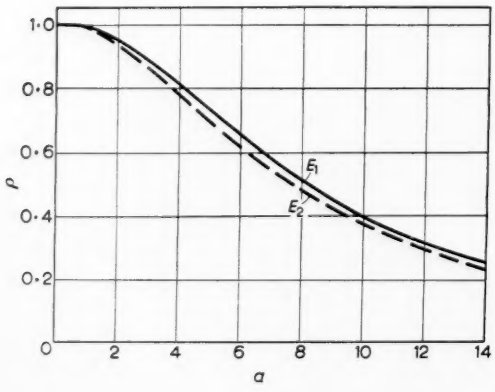

Fig. 5. Variation of multiple reflection correlation with α.

function of a. For large values of a the two signals are seen to be substantially unrelated.

With this brief summary of the theory, some experiments will now be described which put limits on the values of a at low frequencies.

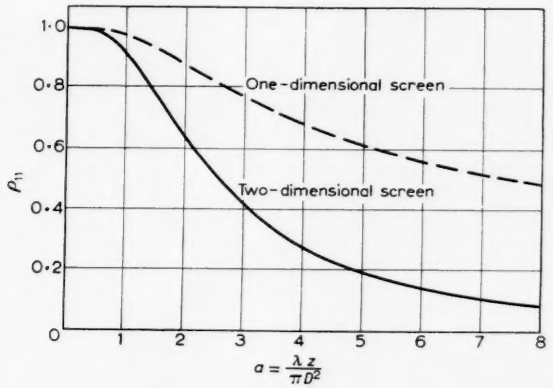

Fig. 6. Variation of the correlation of the diffraction pattern amplitude at the screen as a function of distance for one- and two-dimensional screens.

VOL. 11 1957

3. Three Correlation Methods

There are three types of experimentally measured correlation which give information about the value of a. They are described separately below.

(a) *Spatial correlation.* Three workers have observed the night-time correlation between the signals received at close-spaced receivers at very low frequencies. The values of d inferred by assuming a Gaussian form for the spatial correlogram are given in Table 1.

Table 1

Frequency (kc/s)	Reference	d (km)	Variation at reference level	a
75	Sales (1956)	4·5	Amp	11·3
			Phase	11·3
71	Bowhill (1956)	6·0	Amp	6·8
			Phase	6·6
16	Harwood (1953)	31	Amp	1·5
			Phase	0·36

Using Fig. 4, these values of d can be used to calculate the value of a. Allowance has been made for the fact that the waves incident on the layer are spherical, using the result stated in the appendix. The values of a depend upon whether the variation is supposed to be in amplitude or in phase at the reference level, and separate entries have been made in Table 1 accordingly.

It is clear that at 71 kc/s and above, $a \gg 1$. This means that measurements on the signal at the ground can never decide for these frequencies whether the signal at the reference level is modulated in amplitude or in phase. At 16 kc/s, however, it appears possible in principle to resolve these two possibilities.

(b) *Cross-correlation between phase and amplitude.* The cross-correlation ρ_{12} between the phase and amplitude of a signal, mentioned in section 2, affords a direct method of distinguishing between a phase and an amplitude variation at the

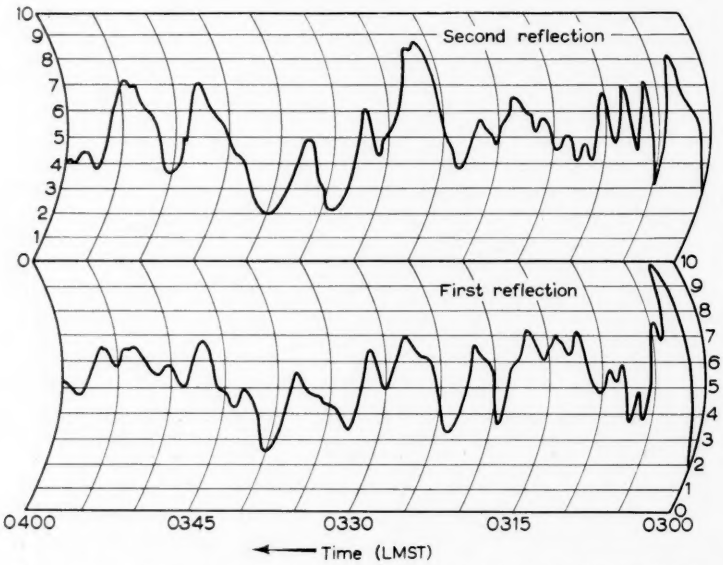

Fig. 7. Simultaneous amplitude records for first and second reflected signals: 1 March 1956.

reference level. It can be shown to be positive in sign for a phase variation, and negative for an amplitude variation. Since $a \gg 1$ for frequencies of 71 kc/s and above at night, this correlation is very small. However, day-time measurements by Jones, Millman, and Nertney (1953) gave small *positive* values for ρ_{12}. This indicates that the signal at the layer is probably modulated in phase rather than in amplitude.

(c) *Multiple reflection correlation.* Two comparisons have been made between the properties of the first and second reflected signals. Records of the phase of the two orders of reflection obtained by Jones (1952) were correlated for periods of 30–60 min, at times when the phase was free from slow, large-scale variations. Times when the RMS deviation of the phase from its mean were more than 1 radian were rejected, as these did not correspond to a shallowly fading signal. Records of amplitude recently obtained by the author at 75 kc/s frequency were analysed in the same way. Results for the average correlation are given in Table 2, and a sample pair of amplitude records is shown in Fig. 7.

The value of a can then be calculated from Fig. 5. This is found to be about 7 at 150 kc/s, and about 9 at 75 kc/s, in approximate agreement with the results obtained in previous sections.

4. The Heights of Irregularities Causing Fading

It has previously been shown (Bowhill, 1956) that in the neighbourhood of 100 kc/s frequency, two periods of fading are present in the reflected wave at night:

Table 2

Frequency (kc/s)	Reference	Average correlation	Hours of observation
150	Jones (1952)	0·59	4
75	Bowhill (1953)	0·44	6

a slow component with about 7 min quasi-period, and a faster fading component with about 1 min quasi-period. The signals used in that analysis, however, were continuous-wave transmissions, and there was the possibility that the presence of two distinct fading signals might be connected with the presence of multiple reflections.

The use of pulsed transmissions removes this possibility. The results of nearly 400 hr of night-time records are summarized in the fading speed frequency distribution of Fig. 8. Four sample records *A*, *B*, *C* and *D*, which fall in the main distribution at the points indicated on Fig. 8 are illustrated in Fig. 9. It is evident

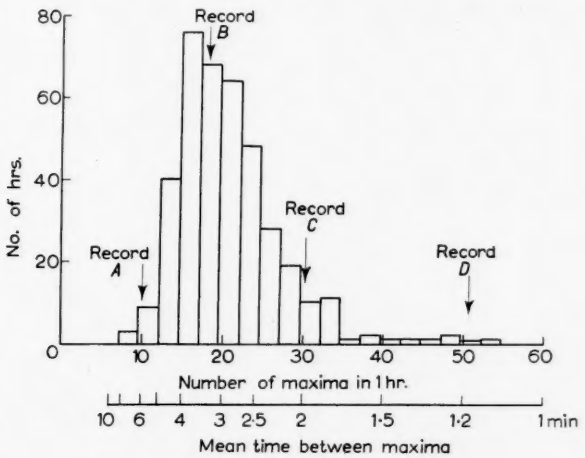

Fig. 8. Overall frequency distribution of 75 kc/s fading speed.

from these records that the differences in fading speed between them can be attributed to the presence of different amounts of the faster fading signal, in combination with a constant amount of the slower fading signal. This confirms the continuous-wave observations.

VOL. 11 1957

On examining the diurnal variation of mean fading speed (Fig. 10a), it was found to resemble the curve for the diurnal variation of group height at 75 kc/s (Fig. 10b) as determined at the same time by Ross (private communication). It appeared that this fact might offer confirmation of the idea that the faster fading was due to irregularities situated at greater heights. However, the fact that two

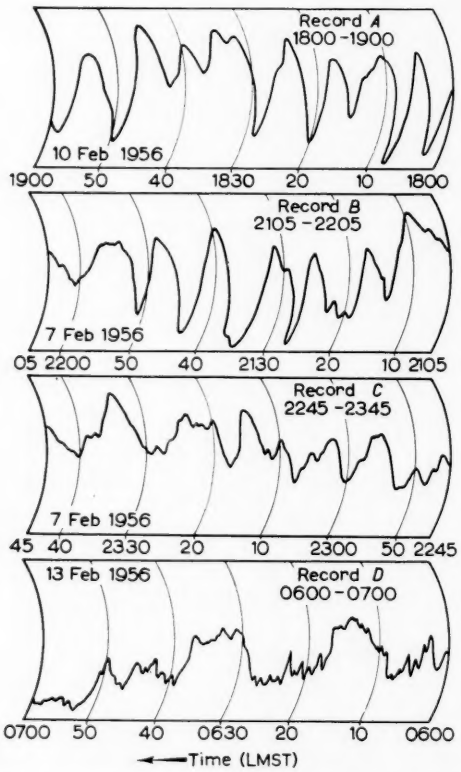

Fig. 9. Typical 75 kc/s amplitude records showing various amounts of rapid fading.

quantities have similar diurnal variations does not establish a causal relationship between them. They must necessarily both have diurnal variations, and the agreement might be merely fortuitous.

To decide this possibility, 118 hr were analysed in which records were available both of fading and of group height. The diurnal variation was then removed from the fading speed figures, by dividing each hourly figure by the average fading speed for that hour, to give a fading index which had an overall average value of unity. As the variations in this index are quite unsystematic, any correlation between it and the reflection height makes a connexion between them overwhelmingly probable.

The average index for height ranges above 100 km was found to be $1{\cdot}10 \pm 0{\cdot}05$ and the overall average for the remaining observations was $0{\cdot}96 \pm 0{\cdot}04$. Applying

a rigorous statistical test to determine whether the means of these two groups are significantly different, the parameter t of Student's distribution is 2·7 with 116 degrees of freedom. The probability of this occurring by chance is less than 0·01.

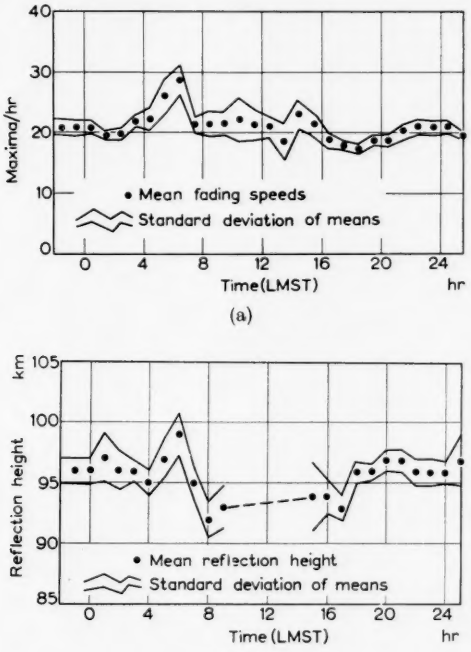

Fig. 10.
(a) Average diurnal variation of 75 kc/s fading speed: winter 1955–6.
(b) Average diurnal variation of 75 kc/s group reflection height: February 1956.

This appears to bear out the previous suggestion by Bowhill (1956) that the more rapid fading arises due to irregularities situated above about 100 km.

5. Summary

It has been shown that the night-time randomly fading signal at the ground is uncorrelated with the signal at the layer for frequencies of 75 kc/s and above. This observation conflicts with the theoretical surmises of Jones, Millman, and Nertney (1953).

Simultaneous measurements of fading speed and group reflection height at 75 kc/s confirm the suggestion made by Bowhill (1956) that there are irregularities of small size situated just above the normal night-time reflection height for 71 kc/s.

References

Booker H. G. 1955 *J. Atmos. Terr. Phys.* **7**, 343.

Booker H. G., Ratcliffe J. A., and Shinn D. H. 1950 *Phil. Trans.* **A242**, 579.

Bowhill S. A. 1953 Ph.D. Thesis, Univ. of Cambridge.

VOL. 11 1957

Bowhill S. A.	1956	*J. Atmos. Terr. Phys.* **8,** 129.
Briggs B. H. and Phillips G. J.	1950	*Proc. Phys. Soc.* **B63,** 907.
Harwood J.	1953	*Instn. Elect. Engrs. Monograph. No.* 86.
Hewish A.	1951	*Proc. Roy. Soc.* **A209,** 81.
Hewish A.	1952	*Proc. Roy. Soc.* **A214,** 494.
Jones R. E.	1952	*Scientific Report No.* 41. The Pennsylvania State University, Ionosphere Research Laboratory.
Jones R. E., Millman G. H., and Nertney R. J.	1953	*J. Atmos. Terr. Phys.* **3,** 79.
Millman G. H.	1952	*Ann. Geophys.* **8,** 365.
Ratcliffe J. A.	1956	*Rep. Prog. Phys.* **19,** 188.
Sales G. S.	1956	*Scientific Report No.* 88. The Pennsylvania State University, Ionosphere Research Laboratory.

Appendix

If a thin plane random diffracting screen is illuminated by radiation from a point source at a distance z' from it, and the diffracted signal at a distance z on the other side of the screen is denoted by $E(z',z,d)$, where d is the structure size of the random variations at the level z, then it can be shown (Bowhill, 1953) that the following statement holds.

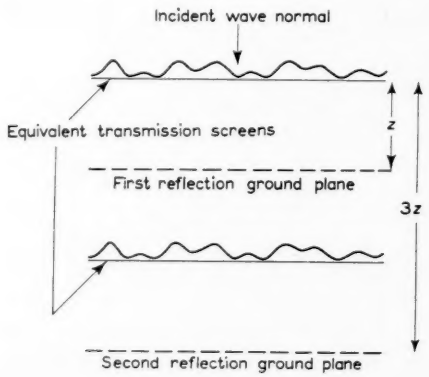

Fig. 11. The diffraction of the second reflected signal.

The signal at a distance z from the screen if the source of waves is z' from it is exactly what would be obtained at a distance $zz'/(z + z')$ from the screen if the source were removed to infinity; provided that the whole diffraction pattern is expanded (away from the intersection with the screen of the normal drawn to it from the source) by a factor $(z + z')/z$:1 This can be written symbolically as $\bar{E}(z',z):1 = \bar{E}(\infty,zz'/(z + z')):(z + z')/z'$ the term after the colon representing the scale factor to be applied to the signal variations.

This equivalence is seen to be physically plausible by taking the limit as λ becomes small: the factor $z'/(z + z')$ then becomes evident from geometrical optics.

The geometry of multiple reflection is illustrated in Fig. 11. Assuming that the reference plane is not too far from the reflection level, the effect of the ionosphere

can be approximated by two identical diffracting screens situated at the reference level, and at its image in the ground plane.

The first reflected signal is given by

$$\bar{E}(z,z):1 = \bar{E}(\infty,z/2):2$$

The second reflected signal may be calculated very simply, if the signal at the reference level is shallowly modulated—i.e. if there is a large specular component present. The angular spectrum of the second reflected signal at the reference level then consists of the diffracted parts of the specular component due to the two equivalent screens, the specular component itself, and a negligible contribution due to the diffraction (on the second reflection) of the already diffracted signal. Neglecting this latter contribution, the second reflected signal at the ground becomes

$$\bar{E}(z,3z):1 + \bar{E}(3z,z):1 = \bar{E}(\infty,3z/4):4 + \bar{E}(\infty,3z/4):4/3$$

If the specular wave from the transmitter to the receiver is incident normally on the reflecting layer, it follows that the difference in structure size of the two terms is irrelevant: so they are necessarily equal. The correlation between the first and second reflected signals is therefore just given by the correlation between $\bar{E}(\infty,3z/4)$ and $\bar{E}(\infty,z/2)$. This can easily be calculated by diffraction theory, and is plotted in Fig. 5.

VOL.
11
1957

Journal of Atmospheric and Terrestrial Physics, 1957, Vol. 11, pp. 102 to 110. Pergamon Press Ltd., London

Self-distortion of radio waves in the ionosphere, near the gyro frequency

F. H. Hibberd
Department of Physics, University of New England, Armidale, N.S.W., Australia

(*Received* 2 *May* 1957)

Abstract—In a previous paper (Hibberd, 1956) the self-distortion (or self-interaction) of a low frequency radio wave in the ionosphere was considered, neglecting the earth's magnetic field, and it was shown that self-distortion results in a small reduction of the modulation depth of a modulated wave. The theory is extended here, with the inclusion of the magnetic field, for frequencies near the gyro frequency. It is shown that the reduction in modulation depth varies only slowly with wave frequency near the gyro frequency, and shows no resonant-like variation. The reduction is proportional to the power radiated, is greatest for low modulation frequencies and decreases rapidly as the modulation frequency is increased. With 100 kW radiated, the fractional reduction in modulation depth of a modulated gyro wave is expected to be of the order of 1 part in 100. Recent experiments that have been claimed to have demonstrated large self distortion effects near the gyro frequency are discussed.

1. Introduction

In a previous publication (Hibberd, 1956—hereafter referred to as (A)) a theory was developed for the self-distortion, or self-interaction, of a radio wave in the ionosphere, when the effects of the magnetic field of the earth could be neglected. This theory is applicable for wave frequencies well removed from the gyro frequency and has recently received confirmation by experiments of King (1957) but it is not directly applicable close to the gyro frequency. The present paper is a sequel to (A) and is concerned with self-distortion very near the gyro frequency, at night, in the E-layer.

It will be recalled that one of the manifestations of self-distortion is a reduction in the modulation depth of a powerful modulated wave during its passage through the ionosphere. Energy absorbed from the wave changes the electron collision frequency and hence changes the absorption. For low modulation frequencies the increase in absorption is greatest near the crests of the modulation envelope and least near the troughs and the modulation depth is thereby reduced.

2. Properties of Gyro Waves

In discussing self-distortion near the gyro frequency it is convenient to consider separately the effects of the ordinary and extraordinary components of the wave. To facilitate discussion the respective absorption coefficients k_o and k_e and the refractive indices μ_0 and μ_e have been computed for a gyro wave in the lower part of the E-layer at night, for two typical directions of propagation relative to the magnetic field. The model adopted for the layer assumes exponential variations of electron density and collision frequency with height. It is sufficiently typical for the purpose and the argument does not depend on the details of the model. The results of the computations are given in Table 1.

Table 1 shows that k_e is very much greater than k_o for both angles relative to the field, and at all heights. Further, it can be shown that the attenuation factor

$\int_0^s k_e\, ds$, where s is the path length, becomes sufficiently large after the wave has proceeded through a vertical distance of some 5 or 6 km into the layer that the extraordinary component has by then been almost completely attenuated. Table 1 also shows that this region in which the extraordinary is absorbed is a non-deviating region for both components. These conclusions are true also for a wave whose frequency lies within, say, 20 per cent of the gyro frequency. It is thus seen that a gyro wave emerging from the E-layer consists entirely of ordinary component.

Table 1. Values of absorption coefficient k and refractive index μ for a wave whose frequency is equal to the gyro frequency (taken as 1·53 Mc/s) at various heights h above the lower boundary of the E-layer at night. θ is the angle between the direction of propagation and the earth's magnetic field.

h (km)		0	2	3	4	5	6
N (cm^{-3})		1	7·4	20·1	54·6	148	403
$\nu \times 10^{-5}$ sec^{-1}		11	9·0	8·2	7·4	6·7	6·0
$\theta = 30°$	k_o	$2{\cdot}3 \times 10^{-10}$	$1{\cdot}4 \times 10^{-9}$	$3{\cdot}4 \times 10^{-9}$	$8{\cdot}3 \times 10^{-9}$	$2{\cdot}1 \times 10^{-8}$	$5{\cdot}1 \times 10^{-8}$
	k_e	$4{\cdot}2 \times 10^{-8}$	$3{\cdot}8 \times 10^{-7}$	$1{\cdot}1 \times 10^{-6}$	$3{\cdot}4 \times 10^{-6}$	$1{\cdot}0 \times 10^{-5}$	$3{\cdot}1 \times 10^{-5}$
	μ_o	1·000	1·000	1·000	0·999	0·999	0·996
	μ_e	1·000	1·000	1·000	1·001	1·002	1·004
$\theta = 60°$	k_o	$4{\cdot}6 \times 10^{-10}$	$2{\cdot}8 \times 10^{-9}$	$6{\cdot}9 \times 10^{-9}$	$1{\cdot}7 \times 10^{-8}$	$4{\cdot}2 \times 10^{-8}$	$1{\cdot}0 \times 10^{-7}$
	k_e	$3{\cdot}0 \times 10^{-8}$	$7{\cdot}5 \times 10^{-8}$	$8{\cdot}2 \times 10^{-7}$	$2{\cdot}5 \times 10^{-6}$	$7{\cdot}3 \times 10^{-6}$	$2{\cdot}2 \times 10^{-5}$
	μ_o	1·000	1·000	1·000	0·999	0·998	0·994
	μ_e	1·000	1·000	1·000	1·000	1·000	1·005

From the point of view of self-distortion experiments made to determine the reduction in modulation depth suffered by a gyro wave it is therefore only necessary to consider the reduction suffered by the observable, ordinary component. This reduction will be due to the ionospheric effects of (*i*) the extraordinary component and (*ii*) the ordinary component. The former effects are confined to the narrow region in which the extraordinary is absorbed; the latter occur over an extended region of the ionosphere. We shall proceed to consider the distortion of the ordinary component by the extraordinary and then consider the distortion of the ordinary by itself.

3. Effect of the Extraordinary Component

The distortion of the ordinary by the effects of the extraordinary may be regarded simply as interaction in which the two components take respectively the roles of "wanted" and "disturbing" waves.

We first determine the modulation that would be impressed on a hypothetical unmodulated ordinary component by a modulated extraordinary component. It

VOL. 11 1957

was shown in (A) that the time variation $\Delta\nu$ of the collision frequency ν at a point in the ionosphere produced by a sinusoidally modulated wave is

$$\Delta\nu = \frac{\nu^2 wM}{Q[(G\nu)^2 + \omega^2]^{\frac{1}{2}}} \cos(\omega t - \phi) \tag{1}$$

where w is the mean work done by the wave on an electron per collision,

M and ω are respectively the depth and angular frequency of the modulation,

Q is the mean thermal kinetic energy of the electrons,

G is the energy loss factor for collisions between electrons and molecules, and

$\phi = \tan^{-1}(\omega/G\nu)$ is the phase difference between $\Delta\nu$ and the original modulation.

The depth of modulation M_i impressed on an unmodulated wave, of absorption coefficient k_o, after it has travelled a distance s through a region disturbed by a modulated wave, is given by

$$M_i = \left| \int_0^s \frac{\partial k_o}{\partial \nu} \Delta\nu \, ds \right| \tag{2}$$

In order temporarily to eliminate from the following argument the details of the modulation we shall denote by D the value of $|\Delta\nu|$ when $M = 1$ and $\omega \to 0$. Thus, from (1)

$$D = \frac{\nu w}{QG}$$

or

$$|\Delta\nu| = \frac{DMG\nu}{[(G\nu)^2 + \omega^2]^{\frac{1}{2}}} \tag{3}$$

We estimate the magnitude of the modulation impressed on the unmodulated ordinary component by the modulated extraordinary component by using a method similar to one used by Shaw (1951). It is emphasized that the procedure is applicable here because the interaction occurs in a region in which both components are undeviated.*

The power supplied to the electrons per unit volume in the ionosphere by a plane wave is equal to the negative gradient of the energy flux U; thus, for the extraordinary component,

$$N\nu w = -\frac{\partial U}{\partial s} \tag{4}$$

where N is the electron density, w and U here refer to the extraordinary component, and s is the distance travelled by that component. When equilibrium exists between the electrons and molecules in the presence of the wave, with $\omega \to 0$. the mean energy acquired by an electron from the wave between collisions is equal to the mean energy lost per collision to the molecules. Therefore

$$w = G(Q - Q_0) \tag{5}$$

* Shaw's application of his procedure to estimate the magnitude of the modulation impressed by a gyro wave onto another wanted wave, while correct for the situation considered by him, can lead to false *general* conclusions concerning gyro interaction because the paths of wanted and disturbing waves are not, in general, simply related to each other.

where Q and Q_0 are the respective electron and molecular thermal kinetic energies. We can write

$$Q = \tfrac{1}{2} mv^2 = \tfrac{1}{2} ml^2\nu^2$$

where m and l are the electron mass and mean free path. On making the usual assumption that l is independent of Q for $Q - Q_0 \ll Q_0$, we obtain

$$\frac{Q}{Q_0} = \frac{\nu^2}{\nu_0^2}$$

where ν_0 is the value of ν in the absence of the disturbing (extraordinary) wave. Therefore, when $Q - Q_0 \ll Q_0$ and $\omega \to 0$,

$$\begin{aligned} Q - Q_0 &= (2Q/\nu)(\nu - \nu_0) \\ &= (2Q/\nu)D \end{aligned} \tag{6}$$

Equations (4), (5) and (6) together then yield

$$D = -\frac{1}{2GQN}\frac{\partial U}{\partial s} \tag{7}$$

For $M = 1$ and $\omega \to 0$, the depth of modulation imposed on the ordinary component will be denoted by M_D, so that equation (2) for the present situation becomes

$$M_D = \int_0^s \frac{\partial k_o}{\partial \nu} D\, ds \tag{8}$$

and therefore, by (7),

$$M_D = -\frac{1}{2GQ}\int_0^s \frac{\partial k_o}{\partial \nu}\frac{1}{N}\, dU \tag{9}$$

since the paths s of both components are coincident in the region considered. The absorption coefficient k_o for the ordinary component of a gyro wave in a non-deviating region may be represented by

$$k_o = fN\nu \tag{10}$$

where, to a very close approximation, f is independent of N and ν. The value of f may be computed exactly from the complete magneto-ionic equations. Substitution of (10) into (9) yields

$$\begin{aligned} M_D &= \frac{f}{2GQ}(U_i - U_s) \\ &= \frac{fU_i}{2GQ} \end{aligned} \tag{11}$$

where U_i is the incident energy flux in the extraordinary component. U_s is zero because the extraordinary component is always completely absorbed below the level at which the ordinary component is reflected.

VOL. 11 1957

The modulation terms M and ω are now restored to (11) by comparing (8) with (2), and noting (3), to give

$$M_i = \frac{fU_i}{2GQ} \frac{MGv}{[(Gv)^2 + \omega^2]^{\frac{1}{2}}} \tag{12}$$

This is the depth of the modulation that would be impressed on an initially unmodulated ordinary component by the modulated extraordinary component. We must now consider what the resultant modulation would be when the ordinary component is initially modulated to a depth M with modulation that is in phase with the disturbing modulation of the extraordinary component. The collision frequency variation $\Delta\nu$ lags the initial modulation by a phase angle ϕ and the variation of k_o lags $\Delta\nu$ by π. The resultant modulation on the ordinary component is therefore described by

$$\begin{aligned} &(1 + M \cos \omega t)\,[1 + M_i \cos (\omega t - \pi - \phi)] \\ &= (1 + M \cos wt)\,[1 - M_i \cos (\omega t - \phi)] \end{aligned}$$

On neglecting the small second harmonic terms, this may be written in the form

$$1 + M'' \cos (\omega t - \alpha)$$

where

$$\begin{aligned} M'' &= \frac{M - M_i \cos \phi}{1 - \frac{1}{2} M M_i \cos \phi} \\ &= M - M_i(1 - \tfrac{1}{2}M^2) \cos \phi, \quad \text{for } M_i \ll 1 \end{aligned}$$

and M'' is the resultant modulation depth on the ordinary component taking account of the effects of the extraordinary alone. Also

$$\tan \alpha = \frac{M_i \sin \phi}{M - M_i \cos \phi} = M_i \sin \phi, \quad \text{for } M_i \ll 1.$$

Noting that $\tan \phi = \omega/Gv$, it is seen that the reduction in modulation depth of the ordinary component, in its upward travel, as a result of the effect of the extraordinary is

$$M - M'' = M_i\,(1 - \tfrac{1}{2}M^2) \cos \phi = \frac{fU_i\,M\,(1 - \frac{1}{2}M^2)\,(Gv)^2}{2GQ[(Gv)^2 + \omega^2]} \tag{13}$$

A further reduction of modulation depth is experienced by the ordinary component in its downward travel through the disturbed region. This further reduction is given by an expression similar to (13) provided that U_i is assigned the value appropriate to the point of exit of the ordinary component and one includes in the phase angle ϕ the phase delay of the modulation corresponding to the path length of the ordinary component to and from the F-layer where, for small angles of incidence, it is reflected. For vertical incidence, the corresponding change in $\cos \phi$ is not significant for modulation frequencies below about 300 c/s and the overall reduction of M in passing twice through the disturbed region is very nearly equal to twice the value of the right hand side of (13). For oblique incidence the reduction will also depend on the radiation pattern of the transmitting aerial and the angle

between the down-coming ordinary and up-going extraordinary components and it will generally be somewhat less than for vertical incidence.

Equation (13) shows that the reduction varies with wave frequency p and angle of incidence in the same manner as f and therefore as the absorption coefficient k_o of the ordinary component, provided that p is sufficiently close to p_H for the energy in the extraordinary component to be almost completely absorbed in a region that is non-deviating for both components. The variation of k_0 with p is very slow, so that we expect no rapid variation of $M - M''$ as p is varied about the gyro frequency.

The magnitude of the effect under the favourable conditions of vertical incidence, with $M \approx 1$ and $\omega^2 \ll (G\nu)^2$ will be calculated. Here, from (13), including upward and downward paths,

$$M - M'' = \frac{f\, U_i}{GQ}$$

Because the change in electron energy is small, $Q \approx Q_0 = 4{\cdot}5 \times 10^{-14}$ ergs for a temperature of 220°K. Also, $G \approx 1{\cdot}7 \times 10^{-3}$. From Table 1 we obtain for $p = p_H$ and $\theta = 60°$, that $f = 4{\cdot}2 \times 10^{-16}$. With 100 kW radiated from a half-wave horizontal dipole a quarter of a wavelength above a conducting ground, and assuming that approximately half of the energy goes into the extraordinary component, it may be computed that $U_i = 1{\cdot}4 \times 10^{-3}$ erg cm^{-2} sec^{-1} at a height of 90 km. Therefore,

$$M - M'' = 8 \times 10^{-3} = 0{\cdot}8 \text{ per cent.}$$

Thus the effect of the extraordinary component in the ionosphere reduces the modulation depth of the ordinary component by less than one part in one hundred.

VOL. 11 1957

4. Effect of the Ordinary Component

The distortion of the ordinary component by itself is now considered. For both vertical and fairly steep incidence an argument identical to that in section 3 is applicable (except at the top of the trajectory) provided that U_i is interpreted throughout as the energy flux of the ordinary component. At night the E-layer is penetrated and reflection takes place from the F-layer. Equation (10) is valid over the whole path except in the deviating region near the top of the trajectory. Even here (10) is probably not seriously incorrect. Since the magnitudes of the incident energy fluxes of the two components are generally of the same order it is to be expected that the magnitude of the effect of the odinary on itself is not greatly different from the effect of the extraordinary on the ordinary.

For angles of incidence sufficiently oblique that the E-layer is not penetrated, the self-distortion of the ordinary component may be treated by the method used in (A), since that theory requires only that k_o be proportional to ν. The relevant equation is equation (21) of that paper, namely

$$M - M' = \frac{(2 - M^2)\, MG\nu^2}{[(G\nu)^2 + \omega^2]} \int_0^s \frac{w\nu}{Q} \frac{\partial k_o}{\partial \nu}\, ds \qquad (14)$$

in which $w\nu$ is written for the w_0 of (A). M is the original depth of modulation and

M' is the modulation depth when the wave emerges after undergoing self-distortion. It may be noted that the reduction $M - M'$ is proportional to w, which in turn is proportional to the power radiated.

It was shown in (A) that a wave radiated obliquely from a typical 100 kW transmitter on 500 kc/s, modulated at a low frequency with $M = 0{\cdot}8$, and reflected in the E-layer, would have the modulation depth reduced to a value M' such that $(M - M')/M$ lies between 0·15 and 0·02. To compute the value of $M - M'$ for the gyro ordinary component, where M' is the final modulation depth resulting from the effects of the ordinary component alone, we note first that only about one half of the total radiated power goes into this component. Further, for the gyro ordinary component, with $p^2 \gg \nu^2$, w varies with frequency roughly as $(p + p_H)^{-2}$ and $\partial k_o/\partial \nu$ also varies as $(p + p_H)^{-2}$. We assume that the average values of w and k for the 500 kc/s wave also depend on frequency in much the same manner. Then with $p_H/2\pi \sim 1{\cdot}5$ Mc/s,

$$\frac{M - M' \quad \text{(gyro ord)}}{M - M' \quad \text{(500 kc/s)}} \sim \frac{1}{2}\left(\frac{3}{2}\right)^{-4} \sim \frac{1}{10}$$

Thus, for the gyro ordinary component with $M \approx 1$, $M - M'$ lies between about 0·015 and 0·002, so that the reduction in modulation depth lies between 1·5 and 0·2 per cent. Although this computation is crude it nevertheless indicates the order of magnitude to be expected, namely a reduction in modulation depth of about one part in one hundred.

5. Summary of Total Effects

The total reduction in the modulation depth of a down-coming gyro wave, which as has been seen is purely ordinary component, is the sum of the reductions caused by the effects of the two components in the ionosphere. It has been shown in sections 3 and 4 that for a gyro wave radiated with 100 kW at a low modulation frequency with $M \approx 100$ per cent, the reductions produced by the effects of the two components are each somewhat less than 1 per cent. The maximum total reduction to be expected under favourable conditions is thus of the order of 1 or 2 per cent.

From equations (13) and (14) it is seen that the total reduction is proportional to the radiated power and also almost proportional to the original depth of modulation.

The reductions given by (13) and (14) both depend on the modulation frequency in the same manner, namely the reduction is proportional to

$$\frac{1}{(G\nu)^2 + \omega^2}$$

so that the reduction rapidly becomes less as the modulation frequency is increased. The reduction at 300 c/s, for instance, is about half that at 100 c/s.

Within a range of ± 20 per cent of the gyro frequency there is a slight decrease in the magnitude of the reduction as the wave frequency increases but for both components there is no marked dependence on wave frequency, and certainly no "resonant-like" behaviour.

6. Review of Experiments on Gyro Self-distortion

Cutolo (1952, 1953) has described a number of experiments in which the depths of modulation of gyro waves have been measured after reflection at very oblique incidence in the ionosphere. With radiated powers of 3 and 5 kW it was observed that a wave which was radiated with a modulation depth of 80 per cent had apparently had its modulation depth reduced to about 50 per cent after reflection. The individual results varied widely and much fading was observed but it is claimed that the reduction is greatest at the gyro frequency. Further, the experiments appear to show that the reduction is least for low modulation frequencies and increases rapidly as the modulation frequency is increased. Cutolo called the effects "self-gyro interaction," presumably implying that they were due to a change in electron collision frequency produced by a gyro wave. He appears to have interpreted his results by an imperfect analogy with the interaction of a gyro wave and another "wanted" wave.

Aitchison and Goodwin (1955) carried out experiments at near vertical incidence using a modulated continuous wave and selected the reflected sky wave for measurement. The modulation depth was measured by comparison with that of the ground wave. They found that, with a gyro wave radiated at 5 kW with a modulation depth of 20 per cent, the reflected wave commonly had a modulation depth of about 16 per cent, which did not vary appreciably with modulation frequency. They reported that usually both E and F reflections were present and that fading was very troublesome.

VOL. 11 1957

Mitra (1955) reported receiving at a single site waves from fifteen transmitters with frequencies between 590 and 1480 kc/s modulated at 1000 c/s to a depth of 80 per cent. He found that the received modulation depth was considerably less than 80 per cent. The reduction had a sharp maximum at 1020 kc/s, which Mitra interpreted as the gyro frequency (although this differs considerably from the gyro frequency of 1330 kc/s at the ground).

It is quite clear that the effects observed cannot be due to changes caused in the ionosphere by a wave and that they are therefore not self-distortion effects of the type discussed in the present paper. The experimental study of self-distortion presents considerable difficulties, the most serious of which is the recognition and elimination of spurious results caused by the selective fading that occurs when two modulated signals arrive at a point with a phase difference between them. Some simple precautions that should be taken in such experiments have been given by Hibberd (1956).

Some recent experiments by Anderson and Goldstein (1955) in which microwaves were propagated through a plasma contained in a waveguide, with and without an applied magnetic field, appear to be true self-distortion effects in an ionized medium. However, it is not permissible in interpreting these experiments to assume that the strongly absorbed mode does not reach the detector. The results of these experiments do not therefore invalidate the conclusions of the present paper concerning self-distortion effects in the ionosphere.

It would appear that ionospheric self-distortion near the gyro frequency has not yet been observed. Because of the small magnitude of the effect and the absence of any special features at the gyro frequency it would seem that, in general, it

would be more convenient, in investigating the ionosphere by means of self-distortion, to work at lower frequencies.

References

Anderson J. M. and Goldstein L.	1955	*Phys. Rev.* **100,** 1037.
Aitchison G. J. and Goodwin G. L.	1955	*Nuovo Cim.* **1,** 722.
Cutolo M.	1952	*Nuovo Cim.* **9,** 687.
	1953	*Nature, Lond.* **172,** 774.
		Nuovo Cim. **10,** 915.
Hibberd F. H.	1955	*J. Atmos. Terr. Phys.* **6,** 268.
	1956	*J. Atmos. Terr. Phys.* **8,** 120.
King J. W.	1957	*J. Atmos. Terr. Phys.* **10,** 166.
Mitra S. N.	1954	*Proceedings of Conference on The Physics of the Ionosphere* p. 71. The Physical Society.
Shaw I. J.	1951	*Proc. Phys. Soc.* **B54,** 1.

Journal of Atmospheric and Terrestrial Physics, 1957, Vol. 11, pp. 111 to 117. Pergamon Press Ltd., London

Short-range echoes observed on ionospheric recorders

R. L. Dowden
Antarctic Division, Department of External Affairs, Melbourne

(*Received* 15 *May* 1957)

Abstract—Strong echoes from the 20–100 km region previously reported from several ionospheric stations near the sea have been examined at Macquarie Island and found to arrive from very low angles of elevation and with vertical polarization. It is shown that the echoes are therefore not ionospheric but are produced by coherent back-scatter of surface propagated waves by sea waves of length $L = \lambda/2$.

VOL. 11 1957

1. Introduction

Various investigators have reported pulse reflections from *D*-region heights on frequencies much greater than the critical frequency. Ellyett (1947) reported strong echoes (voltage reflection coefficient $>10^{-2}$) at heights down to 20 km from Pitcairn, Raoul, and Christmas Islands. He suggested that these reflections might be characteristic of a tropical region. Similar reflections however, have been observed from Campbell Island ($52\frac{1}{2}^\circ$ S) and Macquarie Island ($54\frac{1}{2}^\circ$ S). Major (1955) concluded that the reflections were peculiar to island observatories. An example of these "island echoes" is shown in Fig. 1.

Inland, weak reflections (voltage reflection coefficients around 10^{-4}) from the *D*-region of the ionosphere from 60 km and upwards have been described by Dieminger (1952), Gardner and Pawsey (1953) and others. The latter used simple direction-finding tests to establish that their "low" echoes were arriving from near overhead.

This paper describes similar direction-finding tests made by the author at the Australian National Antarctic Research Expedition's station at Macquarie Island at 7 Mc/s which demonstrate that the "low" island echoes were arriving, not from overhead, but at very low angles of elevation. An ionospheric mechanism is obviously ruled out.

At the observed ranges the only possible reflecting objects were tropospheric irregularities and the sea surface. From echo strength considerations the former is immediately rejected. However the latter mechanism is consistent with the strong echoes observed and also agrees with recent C.W. observations of sea reflections at 13 Mc/s made by Crombie (1955) in New Zealand.

This apparently clears up an anomaly of long standing, viz. the conflicting reports on low echoes as summarized by Ellyett (1947). Instead of yielding data on the ionosphere it is probable that this type of observation could be developed to give information on sea waves and so provide a useful tool in oceanographical research.

2. Observations

The equipment used was the Macquarie Island ionospheric recorder described elsewhere (Callow, 1956). The transmitter "delta" aerial was used throughout the experiments and initially the usual receiver delta was used also. In addition three

half-wave dipoles—two horizontal and one vertical—were erected a quarter wavelength above the ground. The two horizontal aerials had their wire axes pointing approximately north–south and east–west respectively. Any one of these aerials could be quickly connected to the receiver of the ionospheric recorder by a rotary switch.

2.1. *Angle of arrival.* A large number of *A*-scope photographs of echoes received by each of the above aerials were taken. A typical series is shown in Fig. 2. The amplitudes and ranges of the strongest maxima of the short-range echo and the amplitude of the *F*2 echo were scaled from these photographs. The ratios of the echo amplitude on a horizontal aerial to that on the vertical aerial (i.e. H/V ratio) were then calculated. The mean ratios for each type of echo for both horizontal aerials are shown below in Table 1. The three range classifications of short-range echo are purely arbitrary.

Table 1

Echo	Mean range	H/V for N–S	H/V for E–W	No. of obs.
*F*2	—	6·0	6·7	24
<30 km	22 km	0·032	0·067	19
30–49 km	37 km	0·034	0·091	45
>49 km	58 km	0·036	0·067	24

Now the horizontal aerials have their maxima directed vertically upwards and the vertical one horizontally. Thus the high value of the H/V for the *F2* is to be expected. But the values of H/V for the short-range echoes are about 1 per cent of those for *F2* and are completely inconsistent with arrival from overhead. The short-range echoes must arrive from within a few degrees of the horizontal and must be vertically polarized.

Further the higher average intensity on the east-west aerial compared with the north-south one appears to indicate a preference for an easterly or westerly direction. The east-west aerial would have its maximum sensitivity for vertically polarized waves from the east and west. The transmitting delta aerial which is oriented about 30° west of north should radiate in the horizontal direction somewhat less in the E–W direction than N–S. Since the prevailing wind is E–W this direction of arrival is perpendicular to the dominant sea waves.

2.2. *Apparent reflection coefficient.* The "apparent reflection coefficient" for any echo mechanism can be defined in terms of an equivalent smooth infinite plane surface of voltage reflection coefficient ρ. The power of the received echo at a distance "R" from such a surface can be found from the "radar equation" to be (in the usual notation):

$$p = \frac{GPA}{8\pi^2} \cdot \frac{\pi\rho^2}{R^2}$$

$$= K \frac{\pi\rho^2}{R^2} \qquad (1)$$

VOL. 11 1957

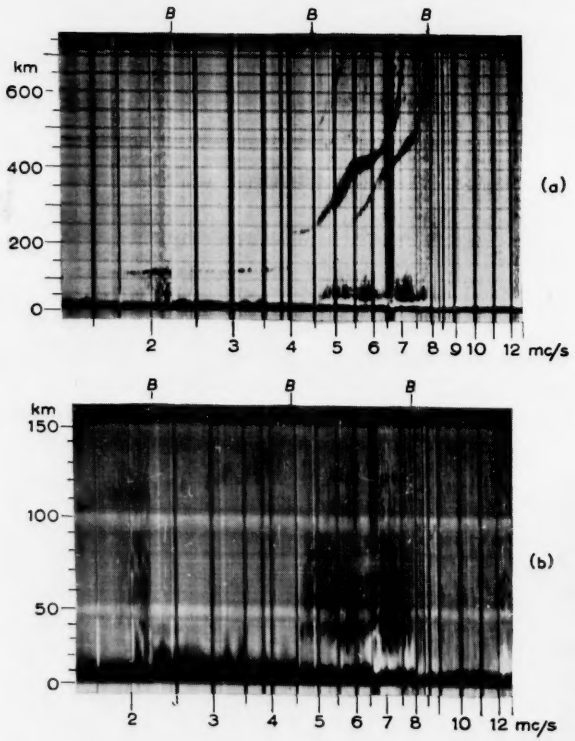

Fig. 1. (a) Typical $p'f$ record showing strong short-range echoes up to about 7·5 Mc/s. Band changes occur at points marked B. (b) Similar record using faster time base to expand range scale.

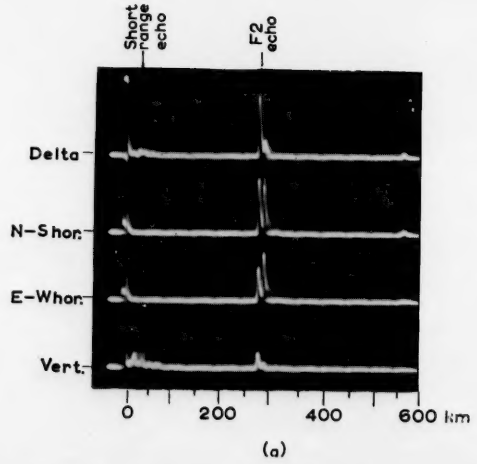

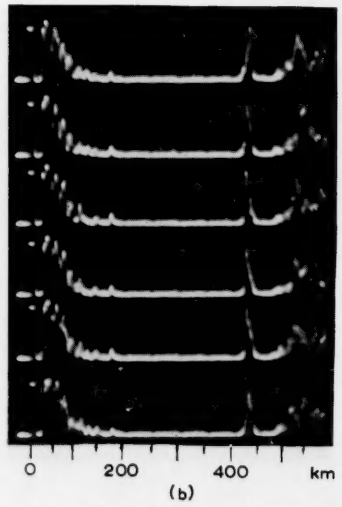

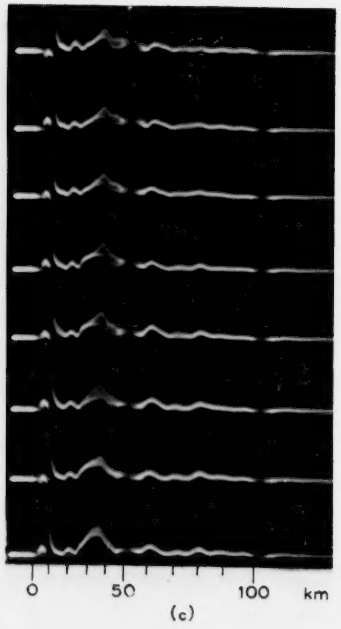

Fig. 2. (a) Typical series of A-scope traces taken about a few seconds apart using each of the aerials in turn. (b) Record showing very strong short-range echoes (vertical aerial). (c) Series of traces taken about a second apart using vertical aerial and fast time base.

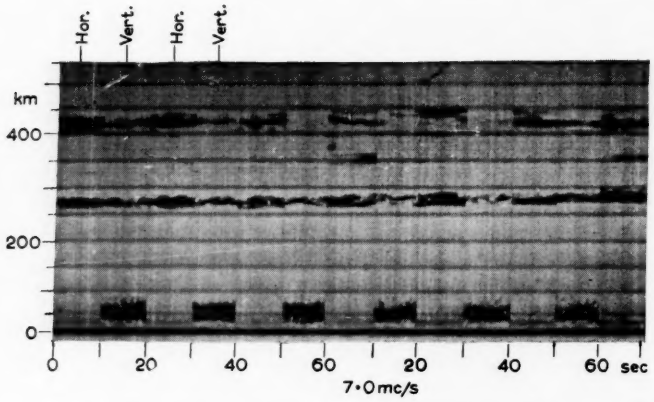

Fig. 4. *P't* record using vertical and horizontal aerials alternately. Note fading pattern in first sample using vertical aerial.

The reflection coefficient of a horizontal layer can be found experimentally (MITRA, 1952) using multiple reflections from some other layer. Since all echoes come from the same direction, the equipment and aerial constants (the K term above) cancel. At first the short range-echoes were presumed at vertical incidence and ρ was computed to be $1{\cdot}5 \times 10^{-2}$. As this is not the case, the apparent reflection coefficient is probably nearer 10^{-1}.

2.3. *Echo structure.* The amplitudes and ranges of 152 maxima from a series of 16 A-scope photographs taken over a period of about a minute on 14 August are shown plotted in Fig. 3. For ranges less than about 30 km it is likely that the receiver sensitivity is considerably reduced by ground pulse paralysis. Beyond this it is believed there is no strong variation of gain with range although this was not accurately checked. The spread of observations in Fig. 3 indicates no tendency to

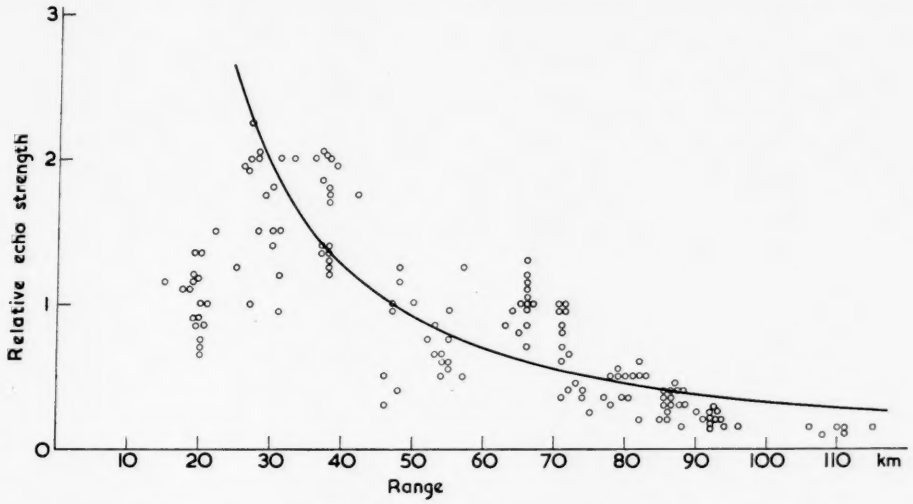

Fig. 3. Echo maxima from a series of A-scope photographs taken on 14 August. The full line is the $R^{-3/2}$ relationship expected for back-scatter from one-dimensionally extended objects (e.g. wave crests).

form layers. Also the echo amplitude falls fairly slowly with range up to about 70 or 80 km and then more rapidly.

2.4. *Fading.* Slow fading of the different peaks of the echo was often noticed and is clearly shown in Fig. 4, obtained at a constant frequency of 7·0 Mc/s on moving film in a similar manner to the routine $p'f$ records. The receiver has been alternately switched from the vertical dipole to the north-south horizontal dipole every 10 sec. The first sample using the vertical dipole in Fig. 4 shows this fading very clearly and the fading period is seen to be very nearly 2 sec. Unfortunately this was the only observation actually recorded.

2.5. *Apparent diurnal variation.* The intensity of the echo appearing on the standard $p'f$ records was visually estimated on an arbitrary 0–4 scale according to the area of $p'f$ record covered. The mean hourly intensities for each of the two months (January and February 1956) for which this was done showed that the echo was usually just detectable at night but apparently strengthened rapidly around

VOL. 11 1957

sunrise to an intensity such as that shown in Fig. 1. Around sunset the echo rapidly waned. This pattern is similar to that reported by Ellyett and others.

This effect may be instrumental. The diurnal variation of the background of interference which is controlled by the absorption of the *D*-layer may have introduced a strong diurnal variation of effective receiver sensitivity. At the time it was not possible to check this.

3. Discussion

We now consider possible objects of reflection in the observed ranges of 15 to 100 km. Obviously the echoes are non-ionospheric and, as the maximum dimension of the Island is about 30 km, they are equally obviously not due to fixed objects. This leaves back-scatter from tropospheric irregularities or back-scatter from sea waves as the only possible mechanisms.

3.1. *Tropospheric back-scatter.* A patchy plane surface (i.e. irregularities much smaller than a wavelength, 40 m) might conceivably give rise to our type of echo, the longer delay time components corresponding to lower angles of elevation. Echoes from higher angles would correspond to delay times well within the paralysis region and would not be seen.

To derive an upper limit for the echo strength due to this mechanism we might consider a layer of small spheres of saturated air in dry air and choose the diameter of the spheres to give maximum back-scatter. The apparent reflection coefficient can then be estimated from the Rayleigh scattering law for 30 km echoes to be about 10^{-7}. If the scatterers were somehow arranged to produce coherent scattering, then this value might be increased to about 10^{-4}, but this is still two or three orders of magnitude lower than the experimental value.

3.2. *Sea back-scatter.* Sea echoes on centimetre and decimetre wavelengths have been studied in detail (Kerr, 1951). At such frequencies however, fine scale irregularities are important, so the mechanism cannot be considered similar to ours. Back-scatter of dekametre wavelengths by the sea have since been reported by Crombie (1955) and McCue (1956). The latter was concerned with fairly high angle back-scatter via the ionosphere and so his results are not readily comparable with ours.

By measuring the Doppler shifts of sea echoes at 13·56 Mc/s Crombie (1955) found a strong resonance effect for sea wavelengths equal to half the wavelength of his radio waves, i.e. for $L = \lambda/2$. He found a smaller effect for the $L = \lambda$ case. This suggests that resonant or coherent scattering is the most important mechanism: of the large spectrum of sea waves normally present the radio wave selects those exactly half its length and in a direction perpendicular to the direction of propagation to yield most of the back-scatter.

The intensity of the back-scattered radiation can be expressed as the product of two factors, one giving the scattering produced by a single sea wave and the other depending on the arrangement of the sea waves. For grazing incidence and back-scatter, neglecting multiple scattering, the latter factor is of the form (Ditchburn, 1952):

$$F(L) = \frac{\sin^2 2\pi NL/\lambda}{\sin^2 2\pi L/\lambda}$$

where N is the number of sea waves contained in the distance corresponding to the transmitter pulse length. Since this is about 70 μsec, N is about $(2/L) \cdot 10^4$. Principal maxima are obtained for $L/\lambda = \frac{1}{2}, 1, \frac{3}{2}, 2, \ldots$ etc. Most of the echo is therefore due to sea waves of length $L = \lambda/2$, the intensity of the $L = \lambda$ component being about one quarter as much.

The scattering produced by a single wave is more difficult to calculate and only the order of magnitude is estimated. Since the height to wavelength ratio of sea waves is small ($\sim 1/20$) suppose we consider the waves to be triangular. As a further simplification we will neglect that part of the wave facing away from the transmitter, so that each sea wave becomes a "thin" ribbon, inclined (say) 6° to the horizontal towards the transmitter. Expressions for the scattering of waves by thin ribbons have been obtained by MORSE and RUBENSTEIN (1938) in terms of Mathieu functions. From these, the power of the received echo at a distance R from N such scatterers spaced $\lambda/2$ apart is found from the "radar equation" to be:

$$p = \frac{GPA}{8\pi^2} \cdot \frac{N^2 h}{R^3} \times 10^{-2}$$

$$= K \cdot \frac{N^2 h}{R^3} \times 10^{-2}$$

VOL. 11 1957

To find the "apparent reflection coefficient" we substitute in equation (1) (page 112):

$$\frac{\pi \rho^2}{R^2} = \frac{N^2 h}{R^3} \times 10^{-2}$$

For 30 km echoes, $L = \lambda/2 = 20$ m, $N \approx 10^3$, $H = 2$ m, we find $\rho \approx 0{\cdot}4$, in reasonable agreement with the experimental value of roughly 0·1.

This estimate is probably an overestimate since it includes end effects of the postulated ribbons which would be absent for real waves; further the wave height of 2 m is large for waves of a particular wavelength which need not be that of the principal waves. However it gives the right order of magnitude and the $R^{-3/2}$ law suggested by Fig. 3.

3.3. *Propagation.* To produce echoes from ranges of up to 100 km, the 7 Mc/s pulse must be confined to the earth's surface for about one degree of arc for both the outgoing and returning trip. We consider three mechanisms for this.

The average ray curvature given by the rate of change of refractive index with respect to height for the layer of air between the ground and the 900 mb level at Macquarie Island was calculated from radiosonde data (ANARE, 1955). That for the best day found on inspection of a number of months was only 15 min of arc in 100 km. Superrefraction if therefore ruled out.

There is evidence (FRIEND, 1941) of sharp tropospheric discontinuities in temperature and humidity which usually escape detection because of the slow response of radiosondes. Even at vertical incidence, FRIEND reports voltage reflection coefficients of up to 10^{-4} which would be considerably augmented for grazing incidence. However an attenuation of one or two orders of magnitude over that for free space would be introduced.

The ratio of the strength of the surface wave to that expected for a free wave (inverse distance) for various distances travelled over a smooth sphere of various surfaces is given in Table 2 below (obtained from curves after TERMAN, 1943) for a frequency of 5·0 Mc/s.

Table 2

Distance	Sea	Good earth	Poor earth
40 km	0·9	10^{-2}	2×10^{-3}
80 km	0·8	5×10^{-3}	6×10^{-4}
160 km	0·4	10^{-3}	10^{-4}

For echo ranges up to 70 or 80 km over sea the attenuation is scarcely more than the free space wave. This is in agreement with the more rapid decrease in amplitude for echoes beyond 70 or 80 km noticed in Fig. 3. This also explains the association of the echo with islands. Over land, ground objects are highly reflecting but the surface waves are attenuated some hundreds of times more.

3.4. *Fading.* As mentioned above, CROMBIE using C.W. observed a Doppler beat between the ground wave and the sea echo. Since the velocity v of a sea wave of length L is given by $v = \sqrt{\frac{g}{2\pi}}L$, g being the acceleration due to gravity, then the Doppler shift Δf produced by sea waves of length $L = \frac{\lambda}{2}$ travelling radially to the observer will be

$$\Delta f = \frac{2v}{\lambda} = \frac{2}{\lambda}\sqrt{\frac{g}{2\pi} \cdot \frac{\lambda}{2}} = \sqrt{\frac{g}{\pi} \cdot \frac{1}{\lambda}}$$

At 7 Mc/s, $\Delta f = 0{\cdot}27$ c/s and the observed fading of about $2\Delta f$ ($\approx 0{\cdot}5$ c/s) would fit the beat between reflections from opposite sides of the island.

3.5. *Apparent diurnal effect.* The observed diurnal variation is inconsistent with the sea-echo hypothesis. As mentioned above the effect is probably instrumental.

4. CONCLUSIONS

The short-range echoes observed on ionospheric recorders at Macquarie Island and other island observatories, and formerly attributed to reflections from the lower ionosphere have been shown to be due, not to ionospheric effects, but to back-scatter from the sea propagated along the surface.

Most of the back-scatter is produced by sea waves of length $L = \lambda/2$. The back-scatter and hence the relative amplitude of other sea wavelengths can be found by varying λ. Hence observations of this type should provide a useful tool in oceanographical research.

Acknowledgements—The author wishes to express thanks to the Ionospheric Prediction Service for the use of equipment, to Australian National Antarctic Research Expedition members for assistance with observations and to Drs. F. F.

GARDNER and J. L. PAWSEY of the Radiophysics Division, and Dr. G. H. MUNRO of the Research Board, C.S.I.R.O. for many valuable criticisms and suggestions to the draft paper.

REFERENCES

Australian National Antarctic Research Expedition	1955	*Meteorology* VI Series D.
CALLOW D. R. L.	1956	*Interim Report No.* 13. Australian National Antarctic Research Expedition.
CROMBIE D. D.	1955	*Nature, Lond.* **175,** 681.
DIEMINGER W.	1952	*J. Atmos. Terr. Phys.* **2,** 340.
DITCHBURN R. W.	1952	*Light* p. 175. Blackie, London.
ELLYETT C. D.	1947	*Terr. Magn. Atmos. Elect.* **52,** 1.
FRIEND A. W.	1941	*Bull. Amer. Met. Soc.* **22,** 53.
GARDNER F. F. and PAWSEY J. L.	1953	*J. Atmos. Terr. Phys.* **3,** 321.
KERR D. E.	1951	*Propagation of Short Radio Waves* p. 481. McGraw-Hill, New York.
MCCUE C. G.	1956	*Aust. J. Phys.* **9,** 454.
MAJOR G.	1955	*Nature, Lond.* **175,** 862.
MITRA S. K.	1952	*Upper Atmosphere* p. 249. Asiatic Society.
MORSE P. M. and RUBENSTEIN P. J.	1938	*Phys. Rev.* **54,** 895.
TERMAN F. E.	1943	*Radio Engineer's Hand Book* pp. 681–683. McGraw-Hill, New York.

VOL.
11
1957

Journal of Atmospheric and Terrestrial Physics, 1957, Vol. 11, pp. 118 to 127. Pergamon Press Ltd., London

Radio-star ridges

M. DAGG*
Jodrell Bank Experimental Station, University of Manchester

(*Received* 20 *October* 1956)

Abstract—A radio-star "ridge" effect has been investigated which is quite different in character from the usual radio-star scintillations. The occurrence of ridges correlates more closely with ionospheric inhomogeneities in the *E* region than in the *F* region. A divergent-lens mechanism for the production of ridges is proposed which gives a qualitative explanation of the main features.

1. INTRODUCTION

IT HAS been known since 1950 (SMITH, LITTLE, and LOVELL, 1950), that inhomogeneities in the electron density of the ionospheric *F* region cause the intensity of the metre wavelength radiation from radio stars to scintillate (RYLE and HEWISH, 1950; LITTLE and MAXWELL, 1951; LITTLE, 1951). Australian workers have claimed that *E*-region ionospheric irregularities also cause radio stars to fluctuate when observations are made on radio sources at low angles of elevation towards the equator (BOLTON, SLEE, and STANLEY, 1953), but no such effects have been reported by observers in the northern hemisphere.

In the course of a long-term investigation of radio-star scintillations at Jodrell Bank, the radiation at 79 Mc/s from the radio source in Cassiopeia has been recorded continuously since June 1954: during the summer months of 1954 and 1955 large-scale variations in the intensity of radiation were observed which were quite different in character from the usual scintillations and lasted for periods of only about 30 min. This paper gives an account of these distinctive variations and of the attempt to correlate them with inhomogeneities in the *E* and *F* regions. They have been designated radio-star "ridges" in view of their similarity with the "ridge" effects on radio stars observed by WILD and ROBERTS (1956) with the radio spectrometer in Australia.

2. EQUIPMENT

The observations were made using an equatorially mounted broadside array consisting of six full-wave dipoles and reflector. The axis of the mounting was driven so that the main beam of the aerial was continuously directed at the radio source in Cassiopeia. The receiver was of conventional superheterodyne design, similar to that described by MAXWELL and DAGG (1954). The output of the receiver was recorded on a pen-recording milliameter. The receiver was calibrated by using a noise diode and the gain of the aerial system was calculated from its dimensions.

* Now at East African Agricultural and Forestry Research Organization, Kenya.

3. Description of Ridges

Representative examples of the ridge effects are shown in the facsimiles of the pen-recorder charts in Fig. 1(a), (b), and (c). The radio-star ridges can be conveniently classified into three groups; although they are probably all manifestations of the same type of ionospheric irregularity. The groups are labelled *A* regular, *B* irregular, and *C* "twinned" ridges as follows:

Fig. 1(a) *A*. Regular ridges have a quasi-sinusoidal form inside a fairly smooth envelope. The fluctuation rate (number of maxima per minute) is slow, about 0·3 min^{-1}, and the whole disturbance lasts about 20 min.

Fig. 1(b) *B*. Irregular ridges do not have so smooth an envelope, and the fluctuation rate is higher, about 0·8 min^{-1}. The disturbance lasts about 30 min.

Fig. 1(c) *C*. "Twinned" ridges show a steep-sided envelope and often occur in pairs forming a twinned group. The average fluctuation rate is higher still, about 2 min^{-1}, and the overall duration is about 30 min.

The majority of ridges usually showed maximum peak-to-peak variations greater than the mean intensity of the source, and some had peak-to-peak variations of twice the mean intensity of the source. A notable feature of all the observations of groups *A* and *B* was a minimum source-intensity at the point of maximum depth of the envelope.

VOL. 11 1957

4. Distribution of the Incident Energy

A characteristic of radio-star scintillations is the constancy of the mean intensity of the source (Hanbury Brown and Hazard, 1951). The irregularities merely redistribute the incident energy. The ridges were investigated to determine whether or not they represented any net enhancement or absorption of the source.

An estimated undisturbed base line was drawn through the ridge, and the area under the ridge compared with that under the undisturbed base line by using a planimeter. The lower limit of the area was the estimated level of radio noise minus the contribution due to the Cassiopeia source. Thus, any difference in the areas would represent a net change in the intensity of the source. The results are given in Table 1.

Table 1. Planimeter measurements on ridges

Date 1955	Ridge group	Area under mean level (planimeter units)	Area under ridge	Difference in area (enhancement)
13 June	*A*	864 ± 1	848 ± 3	−16 (−2%)
30 June	*A*	870 ± 1	894 ± 3	+24 (+3%)
29 June	*A*	668 ± 1	657 ± 4	−11 (−2%)
3 July	*B*	811 ± 1	858 ± 4	+47 (+6%)
3 July	*B*	743 ± 1	756 ± 3	+13 (+2%)
20 July	*B*	359 ± 1	356 ± 2	−3 (−1%)
15 July	*C*	443 ± 1	430 ± 5	−13 (−3%)

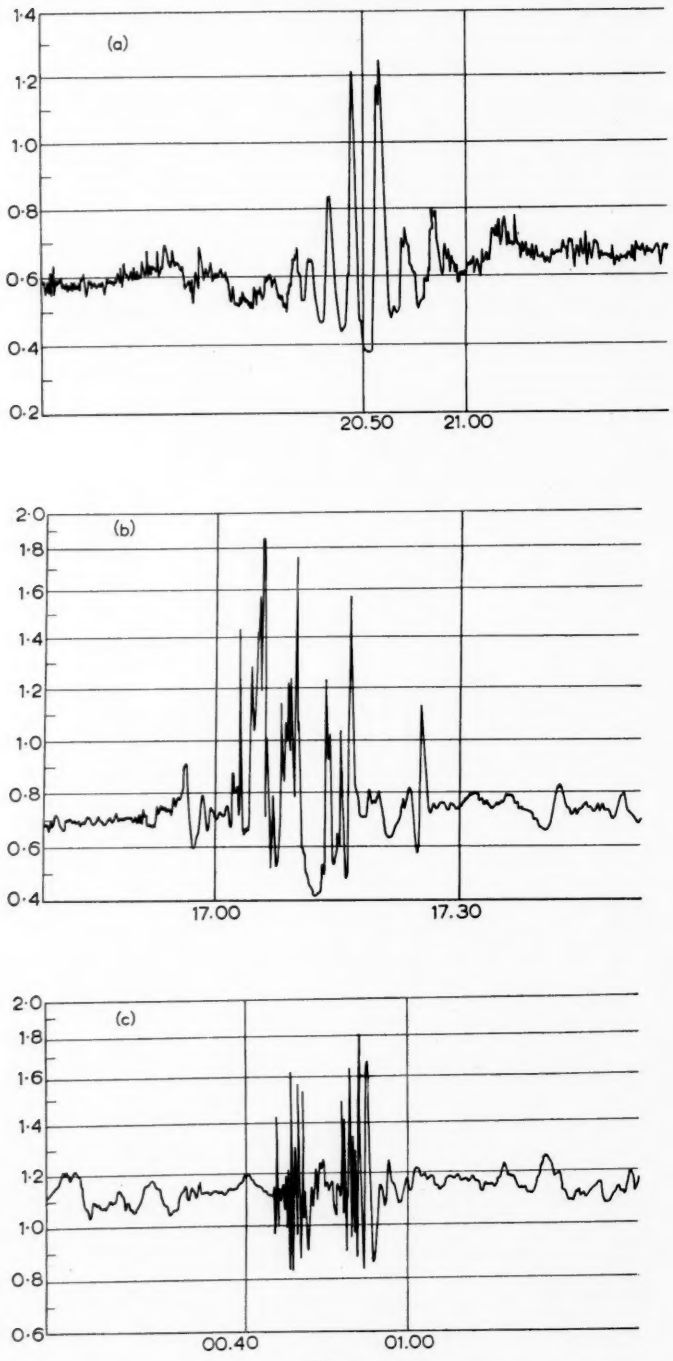
(a)
1·4
1·2
1·0
0·8
0·6
0·4
0·2
20.50
21.00
(b)
2·0
1·8
1·6
1·4
1·2
1·0
0·8
0·6
0·4
17.00
17.30
(c)
2·0
1·8
1·6
1·4
1·2
1·0
0·8
0·6
00.40
01.00

Fig. 1

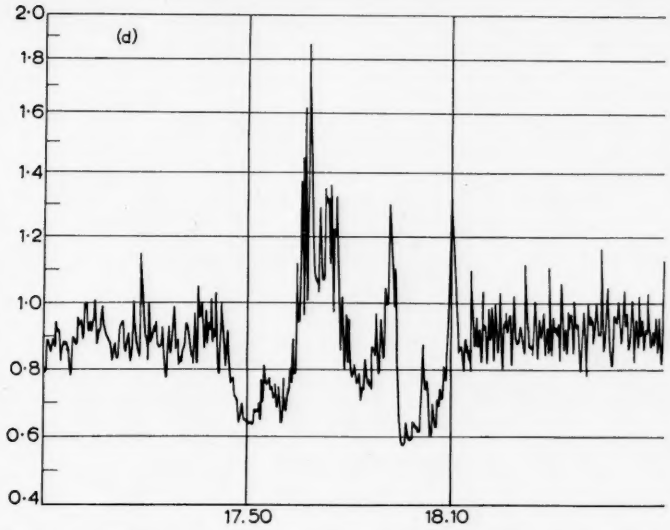

Fig. 1. Radio-star ridges. (Ordinates = amplitude in arbitrary units. Abscissae = time.)
(a) Regular ridge, *A*. 13 June 1955, 2050.
(b) Irregular ridge, *B*. 3 July 1955, 1710.
(c) Twinned ridge, *C*. 10 July 1954, 0050.
(d) Ridge with scintillations. 28 May 1955, 1800.

VOL. 11 1957

It is clear that the mean intensity of the source remains constant to within 3 per cent while the peak to peak intensities vary by as much as 200 per cent, and that the ionospheric irregularities causing ridges merely redistribute the energy from the source as in the case of the normal scintillations.

Additional evidence on this point was provided by the few clear cases when ridges occurred at the same time as normal scintillations (Fig. 1d). It was found that at the ridge peaks the scintillation amplitude increased in accordance with the increase in source intensity due to the ridge, and at the ridge troughs the scintillation amplitude was correspondingly reduced. This suggested that two effects were influencing the source independently.

5. Diurnal and Seasonal Variation

The seasonal variation of the occurrence of ridges was very pronounced. Of 99 total observations of ridges between July 1954 and July 1955 (inclusive), 80 occurred in June and July and 19 in the rest of the year; of the latter, 9 were in May and none at all were observed from December to April, inclusive. The diurnal variation of occurrence of ridges is shown in Fig. 2(a). All three groups showed the same characteristics with two diffuse peaks at 1200 and 1800.

Most of the observations of ridges (95 per cent) were made at angles of elevation between 45° and 23°. Radio-star scintillation diurnal and seasonal effects are confused by the variation of the position of the radio source during the day and year. No such confusion of this kind appears to be present in this case, as the months of August to November are as suitable as June and July for day-time observations at angles of elevation less than 45°. Very few ridges were observed

in the autumn months, and it is not likely, therefore, that the angle of elevation is a major factor in the frequency of occurrence of the observation of ridges.

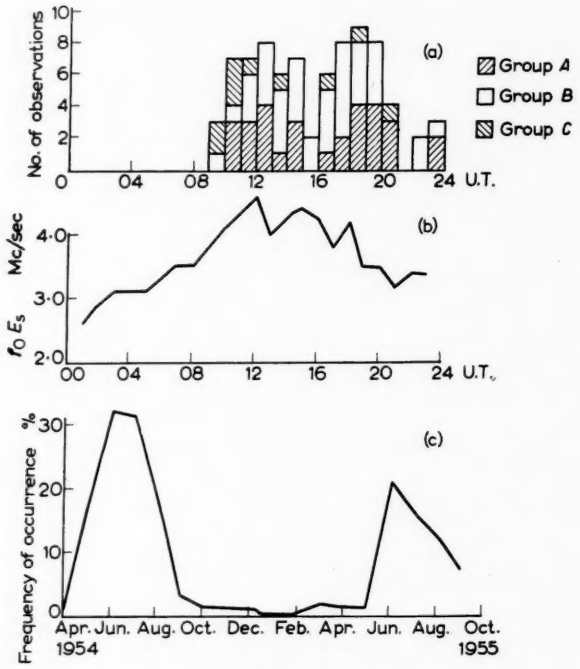

Fig. 2.
(a) Diurnal variation of occurrence of radio-star ripples.
(b) Diurnal variation of f_0E_s, June 1955, Inverness.
(c) Seasonal variation of sporadic E, Inverness.

6. Correlation with Other Ionospheric Phenomena

No correlation was found between the occurrence of ridges and either spread F or geomagnetic K index. However, a positive correlation was found between the occurrence of ridges and sporadic E activity as follows:

(i) The monthly mean diurnal variation of sporadic E at Inverness for June 1955 is shown in Fig. 2(b). The form of the curve is broadly similar to that of Fig. 2(a).

(ii) The seasonal variation of the occurrence of sporadic E echoes at frequencies greater than 4 Mc/s is shown in Fig. 2(c). The marked peak in June and July agrees well with the seasonal variation of occurrence of radio-star ridges.

The ridge correlation with ionospheric phenomena was based on 63 observations. On 43 occasions, the sporadic E critical frequency was greater than 4 Mc/s. The relative frequency of occurrence of ridges and f_0E_S greater than 4 Mc/s is shown in Table 2. The table shows that ridges are not always observed when f_0E_S is greater than 4 Mc/s, but the ratios of occurrence on different months

are very similar for ridges and sporadic E: these are shown by the figures in parentheses.

Table 2. Frequency of occurrence $= \dfrac{\text{Number of occasions}}{\text{Total number of hours of observations}}$

Month	All ripples	Groups of ripples	$f_0E_s > 4{\cdot}0$ Mc/s
July 1954	0·0825 (2)	0·055 (1·9)	0·303 (1·8)
June 1955	0·0525 (1·3)	0·035 (1·2)	0·219 (1·3)
July 1955	0·041 (1)	0·029 (1)	0·165 (1)

7. Spaced Receiver Measurements

On 23 June 1956 a measurement of the velocity of movement of an irregularity producing a ridge effect was obtained using the three-spaced-receiver technique (Maxwell and Dagg, 1954). A tracing of the three-receiver recording is shown in Fig. 3. There was little correlation in the initial phase, but from the time differences between the clearly correlated features, numbers 1 to 5, the velocity of the ground pattern was calculated to be 16 $\pm$ 3 m/sec in a direction 220° E of N. (No correction for star motion was included in the above velocity.

VOL. 11 1957

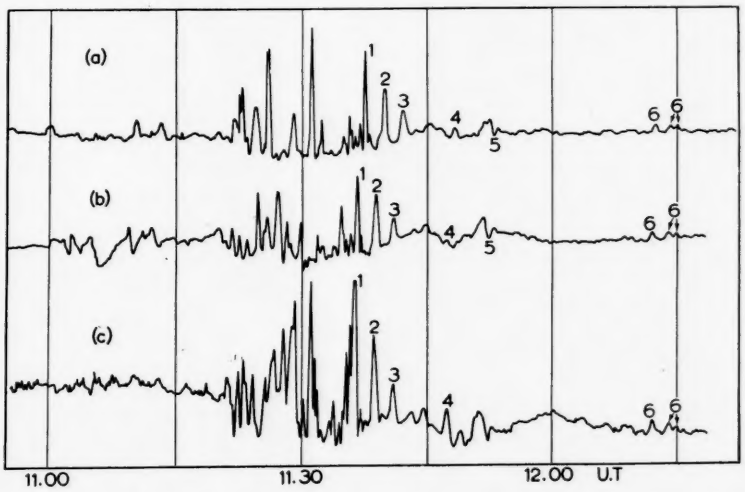

Fig. 3. Spaced-receiver record of a radio-star ridge.
Ordinates = amplitude in arbitrary units.
Abscissae = time.
(a) From Jodrell Bank home receiver.
(b) From remote receiver east of home station, spacing approximately 1 km.
(c) From remote receiver 20° east of north from home station, spacing approximately 1 km.

The small fluctuations denoted by the number 6 in Fig. 3 are believed to be normal scintillations caused by F-region irregularities. Measurements of the time

differences for these fluctuations indicate a velocity of 60 m/sec 226° E of N. This is markedly different from the measured ridge velocity and supports the suggestion that the ridges are not caused by F-region phenomena. At the Inverness ionospheric sounding station during the hours 1100 to 1200 on 23 June, f_0E_S was 6·1 Mc/s; f_0E was not observed because of blanketing, but the mean for the month was 3·7 Mc/s.

8. Discussion

The observations described above agree in fair detail with the normal type of "ridge" fluctuations found by Wild and Roberts in Australia in their observations on the Cygnus radio source at low angles of elevation, using the radio spectro-

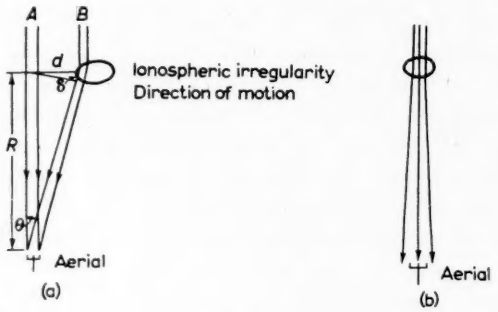

Fig. 4.
(a) Mechanism of production of radio-star ridges.
(b) Irregularity overhead.

meter. However, the ridges they observe appear to occur almost continuously over long periods, and not as distinct, isolated bursts as found in the present work.

Wild and Roberts arrived at the conclusion that their results could not be interpreted in terms of a diffracting screen, but must be interpreted in terms of refraction. They suggested that each ridge was due to the focusing effect of a single atmospheric lens consisting of a region of relatively low-electron density, i.e. high refractive index, and that the fine structure of the "ribbed" patterns (group C ridges) was due to interference by a Fresnel biprism effect of wedges of ionization in the atmosphere.

(a) *Convergent-lens mechanism*

The Jodrell Bank results were therefore first examined in terms of a focusing mechanism. The total duration of a disturbance, 30 min, suggested dimensions of about 50 km, assuming an ionospheric velocity of about 30 m/sec. However, even assuming the most favourable conditions, with a spherical irregularity with dimensions corresponding to the fine structure of a ridge, about 2 km (at a velocity of 30 m/sec) and an electron deficiency equal to the maximum electron density of the E region, the focal length of such a lens at 79 Mc/s is still about 5000 km, which would have a negligible effect on observations made at a distance

of about 200 km. Moreover, it is not at all clear how fine structure could arise in the observed pattern at the ground. Nor is it clear how a deficiency of ionization of these dimensions could return 4 Mc/s sporadic E echoes. Finally, any focusing effect might be expected to give a maximum source intensity at the centre of the envelope, whereas a minimum is observed. A focusing mechanism for the ridges was therefore rejected.

(b) *Divergent-lens mechanism*

Attention was turned to the effect on radio-star radiation of an extra ionized irregularity capable of returning echoes at 4 Mc/s. This requires an increase of electron density relative to its surroundings of 4 if the critical frequency of the E region is 2 Mc/s. The following mechanism is therefore suggested to explain radio-star ridges.

Representative rays from a radio star are shown in Fig. 4(a). If a localized region with an electron density above that of its surroundings approaches the line of sight to the star, then rays such as B will be refracted and will interfere with the direct ray A, as there will be a path difference, δ, between them. As the irregularity moves further into the line of sight, the path difference will vary systematically and the received signal will show maxima and minima accordingly, until a position as represented in Fig. 4(b) is reached. The concave-lens effect will then produce a *minimum* intensity when the irregularity is in the direct line of sight to the star source (Figs. 1a and b). A radio-star ridge of group A will therefore be produced by a "uniform irregularity," whereas a group B ridge will be produced by an irregularity more intensely ionized or disturbed. Finally, if the irregularity is so large that at its central passage its upper and lower surfaces are flat, then no fluctuation in source intensity will be seen although deviation at its edges will cause fluctuations, as observed in type C ridges (Fig. 1c).

VOL. 11 1957

It is possible to calculate the angular deviation of a ray that will be introduced by a spherical ionospheric irregularity. For a ray incident at an angle θ_1 on a discontinuity in a layer of ionized gas, the angle θ_2 at which it is refracted is given by

$$\frac{\sin \theta_1}{\sin \theta_2} = \frac{\sqrt{[1 - (N_2 e^2/\pi m f^2)]}}{\sqrt{[1 - (N_1 e^2/\pi m f^2)]}}$$

where $N_{1,2}$ are the electron densities on the 1,2 sides, f is the operating frequency (79 Mc/s), and e and m are the electronic charge and mass respectively.

For sporadic E reflecting 4 Mc/s pulses in an E region with a critical frequency of 2 Mc/s,

$$\frac{\sin \theta_1}{\sin \theta_2} = 0{\cdot}9994$$

Table 3 shows the deviation, for varying angle of incidence, introduced by a spherical irregularity with a critical frequency of 4 Mc/s in surroundings where

the critical frequency is 2 Mc/s. At a range R the path difference introduced between the direct and deviated ray is

$$\delta = R\left(1 - \frac{1}{\cos\theta}\right)$$

$$\simeq R\,\frac{\theta^2}{2}$$

At a range of 200 km this path difference is

$$\delta = 200 \text{ m} \quad \text{for} \quad \theta = 4^\circ$$

$$\delta = 0{\cdot}02 \text{ m} \quad \text{for} \quad \theta = 2'$$

On this simple picture it is possible to obtain sufficiently large path differences to cause interference at a wavelength of 3·7 m, provided the angle of incidence is fairly large.

Table 3.

Angle of incidence	Deviation by spherical irregularity
90°	4°
85°	48′
80°	24′
60°	4′
30°	2′
10°	1½′

(c) *Discussion of spaced-receiver measurements*

The divergent lens mechanism can be tested quantitatively from the three-station measurement of the velocity of a ridge effect at the ground, if f_0E and f_0E_S are known for the particular irregularity. From the ionospheric data from Inverness, assuming the irregularity to be spherical, the maximum ray deviation would be 6½°. Thus, the first effect of the irregularity would be apparent when it was 18 km from the direct line of sight. This distance can also be calculated from the measured velocity. The first effects occurred 11 min before the central passage (maximum depth of envelope). For a speed of 16 m/sec this corresponds to a distance of 10·5 km. Thus, the predicted distance is of the same order of magnitude as that observed. The artificial assumption of a discontinuous change in electron density would result in the predicted value for the distance being larger than that for any real case where the electron density will change less abruptly.

From the simple picture portrayed in Fig. 4(a) it is readily seen that the rate of change of path difference is given by dv/R, where d and R are the distances shown in Fig. 4(a) and v is the velocity of the ridge. Considering the ridge shown in Fig. 3, the maximum denoted by the number 2 occurred 7½ min after the central passage. For a velocity of 16 m/sec this gives a value of d of 7·2 km. The range

to the 100 km level, R, was 160 km. These values indicate a fluctuation rate of 11·5 maxima per minute. The observed fluctuation rate was 0·4 maxima per minute and therefore does not support the simple theory. A more detailed investigation of the factors influencing the fluctuation rate is necessary before a final appraisal of the basic mechanism can be made.

9. Conclusions

The radio-star ridge effects have been shown to be correlated much more closely with ionospheric irregularities in the E region than the F region. A convergent-lens mechanism is inadequate to explain the appearance of ridges, but a divergent-lens mechanism explains the main features qualitatively. This suggestion is partially supported quantitatively by the measurement of a ridge velocity by the three-spaced-receiver technique, but a closer investigation of the factors influencing the fluctuation rate must be made before a final decision is possible.

Acknowledgements—This work was carried out at the Jodrell Bank Experimental Station under the direction of Professor A. C. B. Lovell, and was made possible by financial assistance from the Department of Scientific and Industrial Research; the author is indebted to the Department for the award of a maintenance grant from October 1952 to September 1955. The three receiver-observations and the reduction of the ridge velocity were carried out by Mr. R. W. Vice, to whom the author wishes to express his gratitude.

VOL. 11 1957

References

Bolton J. G., Slee O. B., and Stanley G. J.	1953	*Aust. J. Phys.* **6,** 434.
Hanbury Brown R. and Hazard C.	1951	*Mon. Not. R. Astr. Soc.* **111,** 576.
Little C. G.	1951	*Mon. Not. R. Astr. Soc.* **111,** 289.
Little C. G. and Maxwell A.	1951	*Phil. Mag.* **42,** 267.
Maxwell A. and Dagg M.	1954	*Phil. Mag.* **45,** 551.
Ryle M. and Hewish A.	1950	*Mon. Not. R. Astr. Soc.* **110,** 381.
Smith F. G., Little C. G., and Lovell A. C. B.	1950	*Nature, Lond.* **165,** 422.
Wild J. P. and Roberts J. A.	1956	*J. Atmos. Terr. Phys.* **8,** 55.

RESEARCH NOTE

Ionospheric indices of solar activity

(*Received* 16 *August* 1957)

FROM time to time, indices of solar activity based on ionospheric critical frequencies have been proposed by several writers. APPLETON and NAISMITH (1939) used the "character figure" $f^4/\cos\chi$ for the E and $F1$ layers, to estimate the change in the intensity of the solar ionizing radiation over the sunspot cycle, while WALDMEIER (1944) employed the analogous expression $f^3/\cos\chi$ to measure the intensity of radiation responsible for ionizing region E. ALLEN (1946, 1948) proposed a "relative critical frequency" ${}_Rf$, defined as the ratio of the observed monthly mean critical frequency of a layer to that at the same station, time, and season, extrapolated to zero sunspots. The mean value of this index for ten stations was calculated for the E, $F1$, and $F2$ layers, and the intensity of ionizing radiation was taken as $({}_Rf)^n$ where n had the value 4 for the E and $F1$ layers, and 2 for the $F2$ layer.

Several ionospheric indices have been based exclusively on $F2$ layer critical frequencies. Thus PHILLIPS (1947, 1948) defined an "ionospheric sunspot number" derived from values of f_0F2 for the stations Washington, Huancayo, and Watheroo, and recently MINNIS (1955) has developed an index I_{F2} which is also based on $fF2$ values from three stations (Slough, Huancayo, and Watheroo). MINNIS rejected the possibility of using an $F1$ layer parameter principally because the critical frequency of this layer cannot be measured accurately in the winter. He selected $fF2$ in preference to fE because the percentage error in the measurement of fE is larger than that for $fF2$, and also the sensitivity of the E-layer to changing solar activity is considerably smaller than that of the $F2$-layer.

In the course of some recent studies of small perturbations in the E-layer, we have been impressed with the degree of agreement often found between measurements of fE at different ionospheric stations, and the purpose of this note is to call attention again to the great value of a "character figure" of the simple type originally introduced by APPLETON and NAISMITH, derived from accurate measurements of fE at one or two stations. Indeed, at certain times there is an almost one-to-one correspondence between the *daily* variations of fE and sunspot number R, and a study of the variations in the monthly mean character figure shows that these follow sunspot number very closely, and that it is probably a very sensitive index of the ionizing radiation.

Considering conditions near noon, and neglecting the influence of ionization transport, the intensity S_∞ of the ionizing radiation outside the atmosphere is given by the expression

$$S_\infty = K(\alpha H)\,\frac{f^n}{\cos\chi}$$

where K is a constant, α is the effective recombination coefficient, H is the scale height of the ionized constituent, and the index n depends on the effective processes of electron dissipation. In practice, it is found that the seasonal variation of noon values of fE satisfies this general expression, but that the value of n is a function of latitude (BEYNON and BROWN, 1956). We may therefore conclude that, provided there are no marked variations

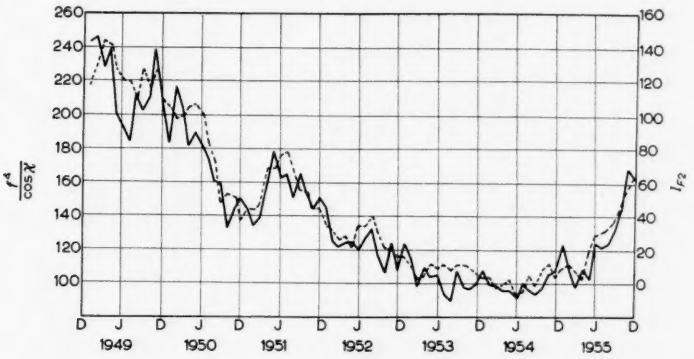

Fig. 1. Variation of the monthly mean E-region character figure and index I_{F2} (after MINNIS) over the period 1949–1955. Full line curve: $(fE^4/\cos\chi)$ for Lindau; broken curve: I_{F2}.

VOL. 11 1957

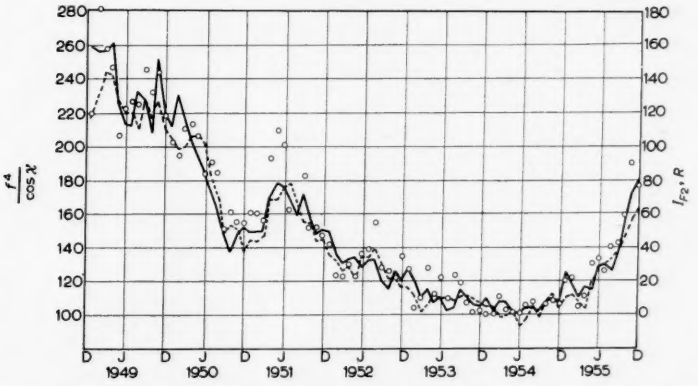

Fig. 2. Variation of the mean E-region character figure $(fE^4/\cos\chi)$ for Lindau and Slough (full-line curve), index I_{F2} (broken curve), and relative sunspot number R (points) over the period 1949–1955.

in the product αH at a station, the character figure $f^n/\cos\chi$ may be used as an index of the ionizing intensity. The appropriate value of the exponent n must be determined from a study of the seasonal variations of the relevant critical frequency, and not from the diurnal variations (which invariably give the value $n = 3$ for the E-layer, as used by WALDMEIER (1944)).

We may illustrate these points by reference to fE data from the two European stations

Lindau and Slough. For both Slough and Lindau the seasonal variation of noon values of fE gives a value of n very near to 4·0. Data are published from Lindau for half-hourly intervals, and fE is given to the nearest 0·05 Mc/s, instead of to the nearest 0·1 Mc/s as is the case for most observatories. Fig. 1 shows the monthly character figure $fE^4/\cos\chi$ based on noon values of fE at Lindau for the period 1949–1955. On the same graph we show the index I_{F2} as published by MINNIS. It will be seen that, in general, there is very good agreement between the two indices. In fact, the correlation coefficient between them over this seven-year period is 0·97.

In Fig. 2 we show the mean character figure for Lindau and Slough, sunspot number R, and I_{F2} for the same period 1949–1955. Over this period the correlation coefficient between the mean character figure and R is 0·96, and between the index I_{F2} and R it is 0·97. Clearly, in comparing them with sunspot number, there is nothing to choose between the E-layer character figure and I_{F2}.

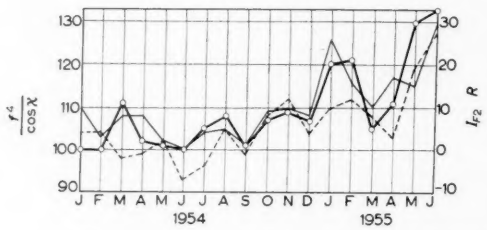

Fig. 3. Variation of mean E-region character figure ($fE^4/\cos\chi$) for Lindau and Slough (full-line thin curve), index I_{F2} (broken curve), and relative sunspot number R (full-line heavy curve) over the period January 1954–June 1955.

Finally, in Fig. 3 we show, on an enlarged scale, the three indices for the period near sunspot minimum. It will be seen that over this period there is little doubt that the simple character figure index follows the sunspot number variation more closely than does I_{F2}.

Now the evaluation of indices such as ${}_Rf$ and I_{F2} involve analyses for several stations, necessitating considerable computation. Moreover, both PHILLIPS and MINNIS mention the effects of disturbance on the values of $fF2$, and special precautions have been taken in the evaluation of I_{F2} to reduce to negligible proportions the effects of ionospheric disturbance on its magnitude. In the calculation of ${}_Rf$ the extrapolation of data to zero sunspot number must be done with care. A detailed examination of the variations in fE, for a constant solar zenith angle, and sunspot number R indicates that over an extended range of R the relationship between these quantities is certainly not linear.

It is clear that the simple E-layer character figure, even when based on only one temperate latitude station, and without any special steps to deal with the effects of disturbance, appears to be a valuable index of solar activity. With improved accuracy in the measurement of fE, some form of index of this kind might prove to be the most reliable ionospheric index of solar activity.

The work described was carried out as part of the programme of the Radio Research Board, and this note is published by permission of the Director of Radio Research of the Department of Scientific and Industrial Research.

W. J. G. BEYNON
G. M. BROWN

University College of Swansea

References

Allen C. W.	1946	*Terr. Magn. Atmos. Elect.* **51,** 1;
	1948	*Terr. Magn. Atmos. Elect.* **53,** 43.
Appleton E. V. and Naismith R.	1939	*Phil. Mag.* **27,** 147.
Beynon W. J. G. and Brown G. M.	1956	*Nature, Lond.* **177,** 583.
Minnis C. M.	1955	*J. Atmos. Terr. Phys.* **7,** 310.
Phillips M. L.	1947	*Terr. Magn. Atmos. Elect.* **52,** 321.
	1948	*Terr. Magn. Atmos. Elect.* **53,** 79.
Waldmeier M.	1944	*Helv. Phys. Acta* **17,** 168.

ANNOUNCEMENT

In order to accommodate the large number of papers now available for publication in the *Journal of Atmospheric and Terrestrial Physics*, the publishers announce that, in future, the Journal will be issued in volumes comprising four issues; these four issues to contain the same number of pages as hitherto contained in the six-issue volumes. It is anticipated that the Journal will be published in three volumes per annum, in monthly issues.

VOL.
11
1957

Journal of Atmospheric and Terrestrial Physics, 1957, Vol. 11, p. 132, Pergamon Press Ltd., London

Indices of geomagnetic activity

of the Observatories HARTLAND (*Ha*), ESKDALEMUIR (*Es*), and LERWICK (*Le*)

June 1957

June 1957

Day	*Ha* *Range for* $K = 9 : 500\gamma$		*Es* *Range for* $K = 9 : 750\gamma$		*Le* *Range for* $K = 9 : 1000\gamma$		*Day*
	K-Indices	*Sum*	*K-Indices*	*Sum*	*K-Indices*	*Sum*	
1	0122 3321	14	0012 3311	11	0111 3311	11	1
2	1210 1222	11	1221 2222	14	1212 1212	12	2
3	2324 4454	28	2324 4454	28	1323 4455	27	3
4	4543 3444	31	4433 3444	29	5533 4456	35	4
5	5433 3434	29	4323 3444	27	6422 3446	31	5
6	4533 3344	29	4433 3334	27	5543 3333	29	6
7	4222 2213	18	4112 1113	14	4412 0112	15	7
8	3212 3322	18	3210 2100	9	3222 2122	16	8
9	1231 2232	16	0000 2121	6	1121 2221	12	9
10	1122 2212	13	0000 0212	5	1011 1112	8	10
11	1202 1111	9	1111 2211	10	1222 1111	11	11
12	2230 3322	17	2111 3322	15	2121 3321	15	12
13	1123 2333	18	1123 2333	18	1123 1223	15	13
14	2223 3232	19	1212 3232	16	2112 3332	17	14
15	3432 3532	25	3322 3532	23	3322 4533	25	15
16	2022 3322	16	1112 3212	13	2112 2212	13	16
17	3443 4323	26	2333 4323	23	2332 4223	21	17
18	4533 4333	28	4432 4333	26	5442 3235	28	18
19	4433 4423	27	4433 4423	27	5533 5433	31	19
20	3332 3442	24	3331 2432	21	4331 2333	22	20
21	2322 3443	23	2232 2443	22	3332 2343	23	21
22	3234 4222	22	2224 4322	21	3124 4323	22	22
23	2223 3332	20	2212 3232	17	2112 3232	16	23
24	4343 3332	25	4333 3322	23	5332 2222	21	24
25	4334 4555	33	4335 4554	33	5434 4544	33	25
26	4555 5545	38	4555 5545	38	6765 6655	46	26
27	3233 5234	25	3233 4334	25	3233 3323	22	27
28	3343 4431	25	3343 4432	26	2333 4332	23	28
29	1121 3222	14	1112 3322	15	1112 2111	10	29
30	2556 6767	44	2546 7779	47	3545 7788	47	30

Journal of Atmospheric and Terrestrial Physics, 1957, Vol. 11, pp. 133 to 138. Pergamon Press Ltd.. London

The origin of the ionospheric irregularities responsible for radio-star scintillations and spread-*F*—I

Review of existing theories

M. Dagg*
Jodrell Bank Experimental Station, University of Manchester

(*Received* 18 *July* 1957)

Abstract—The present state of knowledge about the irregularities responsible for radio-star scintillations is summarized, and the existing theories of the origin of these irregularities are discussed. All of the suggestions are shown to be inadequate to explain the observed features of scintillations and spread *F*. It is shown that any ionizing agent from outside the earth's atmosphere is unlikely to be responsible for the ionospheric irregularities that cause radio-star scintillations, and that the mechanism for their production must be sought in the terrestrial atmosphere.

VOL. 11 1957

1. Introduction

Radio-star scintillations have been shown to be due to phase changes in the incoming radiation as it traverses irregularities in the electron density in the *F*-region of the ionosphere (Little, 1951; Hewish, 1952a). Several theories have been put forward since 1950 to account for the occurrence of such inhomogeneities in the ionosphere. The earliest suggestions were principally concerned with the explanation of the most obvious feature of radio-star scintillations, the diurnal variation, and therefore it is not unexpected that these theories have been found to be inadequate as more information has become available about scintillations and the associated geophysical phenomena.

The predominant characteristics of radio-star scintillations are as follows:—

(1) Scintillations are most frequently observed at night but not every night (Hewish, 1952b; Dagg, 1957a).

(2) There is a marked correlation between the occurrence of scintillations and spread *F*-echoes (Ryle and Hewish, 1950; Little and Maxwell, 1951). They show similar diurnal variations (Dagg, 1957a).

(3) There is no hour to hour correlation of scintillation amplitude with magnetic activity, but there is a correlation over an extended period (Dagg, 1957a); sometimes the correlation is good in detail (Dagg, 1957b).

(4) An increase in occurrence of scintillations with latitude is found in temperate to high latitudes (Hewish, 1952b; Little, 1954).

(5) Scintillations and spread-*F* are observed near the magnetic equator (Wright, Koster, and Skinner, 1956).

The ionospheric irregularities themselves have lateral dimensions of 3–4 km and a marked elongation along the lines of magnetic force (Spencer, 1955). They occur above the height of the maximum electron density of the *F*-region, probably at about 400 km (Hewish, 1952b; Dagg, Maxwell, and Vice, 1957). Their

* Now at the East African Agriculture and Forestry Research Organization, Kenya.

motion is probably due to the interaction of the earth's magnetic field with an electric potential field transferred to the F-region from the dynamo region (Martyn, 1955; Dagg, 1957b).

The various theories that have been put forward to account for these irregularities are discussed in paragraphs 2–6 against this background of information.

2. Accretion Theory

Ryle and Hewish (1950) suggested that interstellar matter attracted by the sun's gravitational field might act as an extra ionizing agent as it fell on to the dark side of the earth. The velocity of the falling particles (mainly hydrogen) combined with the earth's orbital velocity should give an onset of fluctuations at 2020 hr, a maximum of occurrence at 0220 hr, and a cut-off at 0820 hr, which is in approximate agreement with the observed diurnal variation. This suggestion has been criticized on the following grounds (see for example Maxwell (1954)).

(1) Incoming hydrogen atoms would have a maximum energy of only 14 eV, which would be insufficient to ionize the constituents of the upper atmosphere (Ginzburg, 1952). Helium atoms (57 eV) would be very scarce.

(2) It is difficult to see why scintillations should not occur every night, as the interstellar gas, presumably, is incident on the earth every night.

(3) No valid mechanism has been suggested which would produce patches of ionization of the dimensions of a few kilometres.

(4) Scintillations occur well outside the prescribed limits of 2020 hr, and 0820 hr and sometimes even at mid-day.

(5) The theory does not explain the correlations with magnetic disturbances.

3. Evaporation Theory

Investigations on the counterglow by Russian workers (reported by Ryle, 1956) have led them to suggest that it is due to the outermost layers of the atmosphere streaming from the earth away from the sun. Ryle (1956) has therefore suggested that the irregularities in ionization in the high atmosphere may be caused by deficiencies of ionization due to this "evaporation" of the outer atmosphere. The ionized particles would tend to stream away along the lines of magnetic force in accordance with the observed shape of the irregularities.

The evaporation mechanism would account for the night time occurrence of scintillations, but it is difficult to see why it should not cause scintillations every night. Furthermore, the theory presents no obvious explanation of the occurrence of daytime fluctuations which become increasingly frequent at high latitudes (Hartz, 1955). A fundamental difficulty is raised by the observations of scintillations at the equator as charged particles would be unable to escape from the atmosphere because of the earth's magnetic field. The evaporation theory appears incapable of meeting these objections, especially the latter one.

4. Low Latitude Aurorae

Peterson *et al.* (1955) suggested that the irregularities causing spread-F and radio-star scintillations are due to extra ionization produced by incoming protons which have the characteristics of auroral particles, but enter the earth's atmosphere

at much lower latitudes. The principal experimental evidence in support is as follows.

(1) Radar echoes have been observed at frequencies below 30 Mc/s which are consistent with reflections in the F- and E-regions from ionized columns aligned with the magnetic lines of force.

(2) Echoes fade rapidly, apparently discontinuously from pulse to pulse, as if due to intermittent trails of high ionization caused by incoming protons or bunches of protons.

(3) The echoes occur mainly at night with a maximum occurrence at about 0200 hr.

(4) No correlation of echo activity with magnetic disturbance was found.

(5) No hourly or daily correlation of echo activity with spread-F was found, although it is claimed that a monthly correlation exists.

There are several experimental points in favour of this theory. There is a ready explanation for the elongation of the irregularities. The theory could explain why scintillations are not seen every night as some variable solar activity could account for the presence or absence of particles. Furthermore the increase of occurrence of scintillations with increasing latitude could be explained by the constraining influence of the earth's magnetic field in directing the charged particles towards the polar regions. The diurnal variation presents some difficulty, but it may be explained by proscribing a trajectory determined by the velocity of the charged particles and the earth's magnetic field, which causes the protons to enter the atmosphere on the dark side of the earth. It is well known that the time of maximum occurrence of visual and radar aurorae is about 2100 hr (Gerson, 1955) and these are caused by the entry of charged particles from the sun in the atmosphere.

VOL. 11 1957

However, the observation of radio-star scintillations at the geomagnetic equator raises a fundamental difficulty. Here the lines of magnetic force are horizontal and any incoming charged particles with energies approaching those of auroral particles would be deflected to higher latitudes. Such particles would be unable to enter the atmosphere and produce ionization at the equator. It might be suggested that a neutral component in the particle stream was responsible for the equatorial scintillations, but if this were the case, assuming the particles came from the sun, the maximum of occurrence would be expected at mid-day, which is contrary to observation.

The evidence presented by Peterson *et al.* appears to show conclusively that ionization by "low-latitude auroral" particles does occur, but the observation of equatorial scintillations implies that this ionization is not a major factor in causing radio-star scintillations, although they may make some contribution in high latitudes.

5. Turbulence in the F-Region

An obvious source of inhomogeneities in a moving fluid is the development of turbulent flow and eddies. The possibility that the ionospheric irregularities in the upper F-region are the outcome of a turbulent wind motion has been discussed by Maxwell (1954). He estimated that turbulent wind-motion at a height of

400 km was to be expected and that the microscale of the turbulent eddies was of the same order of size as the irregularities responsible for scintillations. Three suggestions were made to explain why the turbulent flow occurred by night but not during the day.

(1) A large temperature gradient could suppress turbulence during the day, while a fall in the temperature gradient at night could allow non-laminar flow to develop.

(2) An increase in the mean velocity of the wind from day to night could cause turbulence. There is some experimental evidence to support this suggestion.

(3) The night-time contraction of the ionosphere may lead to a decrease in kinematic viscosity.

One or all of these effects might be critical. Maxwell also pointed out that observations with spaced receivers suggested that the irregularities formed and decayed as they moved, with a decay time constant consistent with the postulate of a turbulent origin.

This theory has many attractive features, to which might be added the comments of experienced observers that spread-*F* echoes appear to arise from scattering centres in turbulent motion (Booker and Wells, 1938). However, the theory requires that there is a motion of the whole atmosphere at a height of 300–400 km and that the measured velocities of drift of the ionization give a measure of the drift of the air as a whole. This requirement raises serious difficulties as follows:—

(a) The irregularities have been found to move with very high velocities, sometimes as high as 2000 m/s (Maxwell and Dagg, 1954). Even assuming a temperature of 3000°K and complete dissociation of the atmospheric constituents at a height of 400 km, the velocity of sound in the region is still only 1700 m/s (a more realistic figure would be 1000 m/s). Thus the measured velocity of the ionization is in excess of the velocity of sound in the region, and it is difficult to imagine the whole air moving at such speeds.

(b) A close correlation has been shown to exist between the drift speed and changes in the earth's magnetic field. It is difficult to understand how changes in the magnetic field could influence the motion of neutral air in the *F*-region except in so far as it may be moved by the movement of the ionized constituents. The correlation could be explained if the seat of the current system producing the magnetic changes lay in the region of the ionosphere in which the motions are measured. However, there is strong theoretical and experimental evidence that the current system is located at a height of 120–140 km and not in the *F*-region (Baker and Martyn, 1953). Thus the difficulty of explaining the correlation of drift velocity with magnetic changes remains.

(c) Theoretically, Martyn (1953) has shown that ionized material driven by east-west winds in the *F*-region would be subject to such strong electromagnetic damping that effectively the ionization would be insensible to the movement of the E.W. component of the neutral air. Thus even if the wind is turbulent in the *F*-region it would not affect the distribution of ionization there.

It would appear, therefore, that despite many favourable aspects the suggestion that the irregularities which cause radio-star scintillations are due to turbulent winds in the *F*-region cannot be upheld.

6. Convective Turbulence in the Upper F-Region

Gersham and Ginzburg (1955) have suggested that the ionospheric irregularities causing radio-star scintillations are due to convective turbulence above the height of maximum ionization in the F-region. They assume that there is a temperature maximum at this height and in the region above they suggest that the lapse rate is high enough to allow convective turbulence cells to develop. The cell dimensions are calculated to be about 40 km which they consider to be reasonably near to the value of a few kilometres that is observed.

They show that the damping effect of the earth's magnetic field on the development of turbulent cells in an ionized medium will be small, since the gyromagnetic frequency is much higher than the collisional frequency.

However, the magnetic effect which they have considered is not the critical effect which must be taken into account. The authors show that the magnetic field will prevent the motion of the ionized gas, but that this will not effect the movement of the neutral molecules, but this conclusion also demonstrates that any turbulent motion of the neutral gas will not cause irregularities in the electron density.

It would be possible for neutral turbulent cells to form irregularities in the density of the gas, which might then be ionized by a steady ionizing radiation. This process might produce irregularities in electron density, but not those which cause radio-star scintillations, since the ionizing radiation is absent at night when scintillations are most frequently observed.

VOL. 11 1957

Conclusions

A fundamental objection has been raised against all theories ascribing the origin of the ionospheric irregularities responsible for radio-star scintillations to incoming or outgoing charged particles. Neutral particles from the sun cannot give rise to a maximum occurrence of scintillations at night, nor can neutral particles from elsewhere cause the day-time scintillations which are sometimes observed, even if they should have sufficient energy to ionize the atmospheric constituents. The only other source of ionization external to the earth is high energy radiation, but it is improbable that any radiation, that has so far escaped detection, could cause ionization in patches with a night-time maximum of occurrence.

It seems therefore that the mechanism for the production of the ionospheric irregularities must exist within the terrestrial atmosphere. Of the various possibilities it has been shown that a turbulent wind in the F-region, will not produce irregularities in the electron density of the region. The motion of the ionization in the F-region is probably due to the interaction of the earth's magnetic field and an electric potential field communicated to the F-region from the dynamo region. It is suggested therefore that the mechanism responsible for the F-region ionospheric irregularities may be sought in the dynamo region. This suggestion is developed in a companion paper.

Acknowledgements—The work described in this paper was carried out at the Jodrell Bank Experimental Station of the University of Manchester and the

author wishes to thank Prof. A. C. B. Lovell for his interest in the investigation. The author is grateful to the Department of Scientific and Industrial Research for the award of a maintenance grant from October 1952 to September 1955.

References

Baker W. G. and Martyn D. F.	1953	*Phil. Trans. Roy. Soc.* A **246,** 281.
Booker H. G. and Wells H. W.	1938	*Terr. Mag.* **43,** 249.
Dagg M.	1957(a)	*J. Atmosph. Terr. Phys.* **10,** 204.
Dagg M.	1957(b)	*J. Atmosph. Terr. Phys.* **10,** 194.
Dagg M., Maxwell A., and Vice R. W.	1957	In preparation.
Gersham B. N. and Ginzburg V. L.	1955	*Dokl. Akad. Nauk SSSR* **100,** 647.
Gerson N. C.	1955	*Proc. Phys. Soc.* B **68,** 408.
Ginzburg V. L.	1952	*Dokl. Akad. Nauk SSSR* **84,** 245.
Hartz T. R.	1955	*Canad. J. Phys.* **33,** 476.
Hewish A.	1952a	*Proc. Roy. Soc.* A **209,** 81.
Hewish A.	1952b	*Proc. Roy. Soc.* A **214,** 494.
Little C. G.	1951	*Mon. Not. R. Astr. Soc.* **111,** 289.
Little C. G.	1954	*Proc. Inst. Radio Engrs.* **42,** 1700.
Little C. G. and Maxwell A.	1951	*Phil. Mag.* **42,** 267.
Martyn D. F.	1953	*Phil. Trans. R. Soc.* A **246,** 306.
Martyn D. F.	1955	*Conf. on Physics of the Ionosphere* p. 163. Physical Society, London
Maxwell A.	1954	*Phil. Mag.* **45,** 1247.
Maxwell A. and Dagg M.	1954	*Phil. Mag.* **45,** 551.
Peterson A. M., Villard O. G. Leadabrand R. L. and Gallagher P. B.	1955	*J. Geophys. Res.* **60,** 497.
Ryle M.	1956	*Nature, Lond.* **177,** 307.
Ryle M. and Hewish A.	1950	*Mon. Not. R. Astr. Soc.* **110,** 381.
Spencer M.	1955	*Proc. Phys. Soc.* B **68,** 493.
Wright R. W., Koster J. R. and Skinner N. J.	1956	*J. Atmosph. Terr. Phys.* **8,** 240.

Journal of Atmospheric and Terrestrial Physics, 1957, Vol. 11, pp. 139 to 150. Pergamon Press Ltd., London

The origin of the ionospheric irregularities responsible for radio-star scintillations and spread-*F*—II

Turbulent motion in the dynamo region

M. Dagg*
Jodrell Bank Experimental Station, University of Manchester

(*Received* 18 *July* 1957)

Abstract—A theory is presented which attributes the occurrence of ionospheric irregularities in the *F*-region to turbulent wind motion in the dynamo region at a height of 110–150 km. The resulting turbulent component of the electric potential field produced is communicated to the *F*-region, as suggested by Martyn (1955), where magneto-electric forces then cause the ionization to form eddies. It is suggested that the absence of daytime scintillations is due to the inhibition of turbulent flow by large temperature gradients during the day. The theory is then compared in detail with observations and shown to be capable of explaining all the major features of radio-star scintillations, together with such diverse results as the long-term correlation of scintillation amplitude with magnetic activity and the variation in the occurrence of spread-*F* and scintillations at different parts of the earth over the sun-spot cycle.

VOL. 11 1957

1. Introduction

In a companion paper (Dagg, 1957a) the existing theories of the origin of the ionospheric irregularities responsible for radio-star scintillations were reviewed and shown to be unsatisfactory. A conclusion was reached that the mechanism involved in the production of these irregularities must be sought in the terrestrial atmosphere. However, it was shown that the most probable origin, a turbulent wind in the *F*-region, will not produce irregularities in the electron density in the *F*-region.

An alternative mechanism is suggested in paragraph 2. This is subjected to a detailed comparison with the observational data in paragraphs 3–8, and shown to be capable of accounting for all the major features of radio-star scintillations.

2. Mechanism for Production of *F*-Region Ionospheric Irregularities by Turbulent Winds in the Dynamo Region

The motion of the ionization in the *F*-region is probably due to the interaction of the earth's magnetic field with an electric potential field communicated to the *F*-region from the dynamo region (Martyn, 1955; Dagg, 1957b). This electric field can be communicated throughout the ionosphere because the conductivity along lines of magnetic force is very much greater than in any other direction and the lines of force are essentially equipotentials. The electric potential field is generated by a wind system at a height of about 130 km in accordance with the well-known dynamo theory of the variations of the earth's magnetic field (Baker and Martyn, 1953; Baker, 1953).

If the wind at this level is turbulent, the irregular turbulent component of velocity will introduce a turbulent component into the electric field distribution set up by the mean wind. Further, if the coupling between the dynamo and *F*-regions is close—and experimentally this appears to be so (Dagg, 1957b)—the turbulent

* Now at East African Agriculture and Forestry Research Organization, Kenya.

component in the field will be transferred to the F-region. There, the turbulent field will interact with the magnetic field and a turbulent component of velocity will be introduced into the motion of the ionization, thus causing patches or eddies to form. It is suggested that these variations in electron density are responsible for the scintillation of radio stars and spread-F echoes.

A primary consideration must be whether the variation in electron density produced by such a turbulent motion will be sufficient to cause radio-star scintillations. It can be readily shown that to introduce a phase difference of π in an irregularity 5 km in thickness, at a frequency of 80 Mc/s, when the critical frequency of the surrounding region is 5 Mc/s, the variation in electron density relative to the surroundings must be about 15 per cent. These conditions may be taken as extreme, since 5 km is probably a minimum thickness for any irregularity, and the phase change considered is π, whereas scintillations will be produced by considerably less drastic changes (Little, 1951). Nevertheless it is clear that electron density changes of about 10 per cent may be required to explain the most intense fading observed.

The variable wind component measured at a height of about 90 km by observing the drift of meteor trails required pressure variations of at least 10 per cent (Greenhow and Neufeld, 1955). Thus if the turbulent wind component in the dynamo region is comparable with that at a height of 90 km, it may be expected to produce variations in the electron density in the F-region that are adequate to account for radio-star scintillations. Electron density variations of this order would certainly account for spread F-echoes.

Assuming that the proposed turbulent mechanism is adequate to cause the required electron density changes, then it is necessary to consider how the scintillations will depend on other factors in the dynamo region.

(1) The occurrence of scintillations will depend on whether the dynamo wind is turbulent, i.e. whether the atmospheric conditions are conducive to non-laminar flow.

(2) In lower atmospheric flow it has been found that the turbulent velocity increases with the mean velocity (Scrase, 1930). Therefore it would be expected on the proposed theory that the amplitude of the radio-star scintillations should be proportional to the mean velocity of the dynamo wind.

(3) The magnitude of the electric field produced in the dynamo region by a given wind velocity depends on the electrical conductivity of the region. Therefore the amplitude of the scintillations should be proportional to the conductivity of the dynamo region.

3. Turbulence in the Dynamo Region

The height of the dynamo region in temperate latitudes is believed to lie between 110–150 km (Baker and Martyn, 1953). It is of interest to compare this with the results of Greenhow and Neufeld (1956), who find a steady phase variation with height for the atmospheric tidal winds over the range 80–105 km. If their results are extrapolated to greater heights the correct phase for the magnetic variations is obtained at a height of 135 km and for the purpose of the succeeding discussion, the height of the dynamo region will be taken as 135 km. The possibility of turbulent flow in this region is now considered.

The Reynolds' and Richardson's numbers are the conventional criteria for turbulent flow, and an estimate of their values in this region will first be made.

The Reynolds' number R_e is defined as

$$R_e = \frac{vl_0}{\zeta}$$

where v = total velocity difference over a depth l_0

ζ = kinematic viscosity.

It is difficult to assign a value to l_0 in a free atmosphere where there are no distinct boundaries. The approximate depth of eddies observed by GREENHOW and NEUFELD (private communication) at a height of 90 km is 7 km and the root mean square velocity they obtained is 25 m/s. Using these values for l_0 and v at 90 km where $\zeta \sim 10^4$ cm^2 sec^{-1}, $R_e = 1{\cdot}8 \times 10^4$. Using the same values for l_0 and v at 135 km where $\zeta \sim 4 \times 10^6$, $R_e = 400$. The critical value for the Reynolds' number in a free atmosphere is not known, but experiments with jet streams (ANDRADE, 1939) suggest a figure of about 30. Thus, in both regions, the Reynolds' number criterion suggests that the motion would be turbulent. However, little weight can be attached to this conclusion because of the uncertainties in assigning significant values to l_0 and v.

VOL. 11 1957

The Richardson's number R_i is a non-dimensional criterion that is based on the energy balance in turbulent motion. It is defined by

$$R_i = \frac{g\left(\frac{d\bar{T}}{dz} + \Gamma\right)}{T\left(\frac{d\bar{u}}{dz}\right)^2}$$

where g = gravitational acceleration.

T = temperature in °K.

Γ = adiabatic lapse rate.

$\frac{d\bar{u}}{dz}$ = vertical gradient of mean wind velocity.

At 90 km

$$\frac{d\bar{u}}{dz} \sim 1 \text{ m/sec/km}$$

$$\Gamma \sim 1{\cdot}4 \times 10^{-2} \text{ °K/cm}$$

$$T = 220\text{°K}$$

$$\frac{dT}{dz} = 1\text{°/km}$$

The mean wind gradient is that obtained by GREENHOW and NEUFELD (1956) and the temperature gradient is taken from the Rocket Panel (1952) temperature distribution (assuming the correction applied for dissociation of O_2 and N_2 to be correct). The resulting value of R_i is 700: the value is much the same at a height of 135 km. The general rule in the lower atmosphere states that if $R_i < 1$ turbulence increases and if $R_i > 1$ turbulence is suppressed. On this consideration

therefore, turbulence in the *E*-region should be strongly damped or inhibited completely.

However, large variable components of velocity are measured in the *E*-region (Briggs and Spencer, 1954) and Greenhow and Neufeld (private communication) have demonstrated that large flat eddies occur at a height of 90 km. The dimensions of these eddies—about 50 km in a horizontal direction and about 7 km in height—suggest that vertical motions in the *E* region are indeed inhibited, but that at a height of 90 km the temperature gradient of 1° km^{-1} is not sufficient to prevent turbulent flow completely and small vertical movements may take place at the edges of the eddies. The presence of an irregular ionospheric screen at 110 km suggests that turbulent motion is still possible there, although the temperature gradient has increased to 1·6° km^{-1} (Rocket Panel, 1952).

In the dynamo region, at a height of 135–140 km, the temperature gradient has increased still further to 2·7° km^{-1} and its inhibiting effects on turbulent flow, already evident at 90km, might be expected to be greater still, even sufficient to stop turbulent motion altogether. (This point will be considered again in paragraph 4.)

In conclusion, simple consideration of convection and buoyancy in the atmosphere would suggest that turbulence would not be expected above a height of 80 km, where the temperature gradient is positive; however, large turbulent components of motion are found experimentally at heights of 90–110 km, and therefore it is not improbable that turbulent flow may be possible in the dynamo region.

4. The Explanation of the Diurnal Characteristics of Radio-star Scintillations

(a) *Variation in temperature gradient.* The most prominent feature of radio-star scintillations is the tendency to occur only at night. It is suggested that turbulence in the dynamo region is present in general only during the hours of darkness and that non-laminar flow is inhibited during the day, probably because of the large positive temperature gradient. The occurrence of turbulent motion at night causing scintillations would therefore be due to a reduction of the temperature gradient caused by the cooling of the *F*-region after sunset.

In a consideration of the heat balance in the *F*-region of the ionosphere, Bates (1951) came to the conclusion that at sunset, on removal of the source of heating, the temperature of the *F*-region will fall considerably, principally by conduction down the temperature gradient although radiative loss by atomic oxygen (O, $^3P_1$–$^3P_2$) may also be important. Martyn and Pulley (1936) and Lowman (1955) came to the conclusion that the temperature of the *F* region would fall 400°K from 1200°K at a height of 250–300 km in the first 2½ hr after sunset. Thus it is clear that the temperature gradient at a height of 135 km would be expected to decrease at night as suggested in Fig. 1.

(b) *Diurnal variation of magnetic activity.* Once the primary condition for turbulence is fulfilled, the secondary effects of mean wind velocity and electrical conductivity may influence the amplitude of the observed fluctuations (paragraph 2). It is suggested that variations in these parameters are responsible for the diurnal variation in the occurrence or amplitude of scintillations. The annual average diurnal variations are shown in Fig. 2 (from Dagg, 1957c).

It might be expected that the temperature gradient would be least just before dawn, and that this should be the time of maximum occurrence of scintillations. However, the degree of magnetic disturbance shows a very marked fall from 22 to 08 hr. Moreover, the electric potential field system for the S_q variation has maxima at noon and midnight, and would also fall from 00 to 06 hr. These

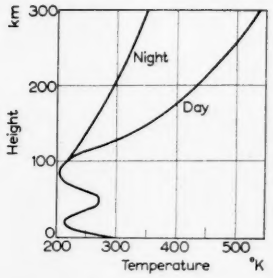

FIG. 1. Variation of atmospheric temperature with height. The daytime distribution is that proposed by the Rocket Panel (1952).

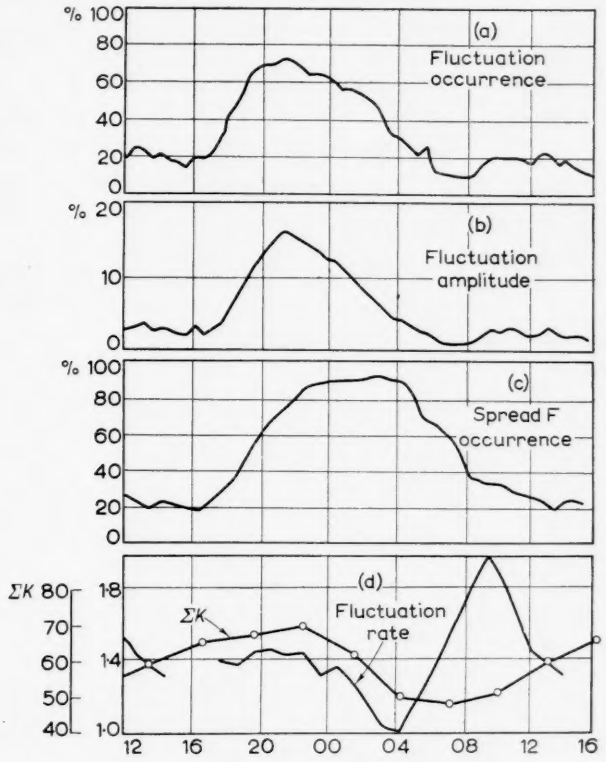

FIG. 2. Yearly average diurnal variations of radio-star scintillations (August 1954 to July 1955). (*a*) fluctuation occurrence, (b) fluctuation amplitude; (c) occurrence of spread-*F* at Inverness; (d) fluctuation rate compared with summation of magnetic *K* indices (ΣK).

magnetic variations are caused by changes in either the wind velocity or the conductivity in the dynamo region, both of which will affect the amplitude of scintillations. Therefore it is suggested that the marked fall in scintillation amplitude from 22 to 08 hr is associated with the secondary magnetic effects.

(c) *Scintillations at the time of the solar eclipse on* 30 *June* 1954. Radio-star scintillations were observed at the time of the solar eclipse, 30 June 1954 (DAGG, 1956). There was about a 20 per cent chance that these effects were merely coincidental, but on the present theory the observed occurrence of scintillations is readily explicable. The simulation of night-time conditions caused a marked drop in the

$F2$ critical frequency, and therefore the fall in temperature gradient may also have been considerable; sufficient, it is suggested, to allow turbulence to develop in the dynamo region.

(d) *Scintillations during aurorae.* Scintillations are often seen during the day if great magnetic storms, accompanying aurorae, occur. Several mechanisms could account for this observation. The wind speed or conductivity, or both, could increase to such an extent that turbulent flow resulted. Alternatively, the effective depth of the dynamo region might be increased considerably during large storms, and therefore include regions where the wind is normally turbulent during the day.

5. The Explanation of the Diurnal Variation of Spread-F

A comparison of the diurnal variations of radio-star scintillations and spread-F is shown in Fig. 2. It is suggested that the ionospheric irregularities responsible for both phenomena are produced by the same mechanism. The time of maximum occurrence of scintillations is about 4 hr before the peak of occurrence of spread-F. However, it has been shown that blanketing by the F-region could influence the observations of spread-F echoes, so that spread-F would show a peak in diurnal occurrence several hours later than that for scintillations (Dagg, 1957c). A further observational point may be added here. Booker and Wells (1938) concluded that the irregularities causing spread-F have dimensions of the order of 25 m. It is a well-known feature of the theory of turbulent motion that a hierarchy of eddies is formed in which the energy is fed into large eddies and transferred down the scale until it is finally dissipated by viscous forces in the smallest eddies. Consequently, eddies of different dimensions might be expected from the theory of a turbulent origin.

In this connection, the description by Berkner, Wells and Seaton (1939) of the ionospheric effects in the $F2$-region associated with magnetic disturbances is of interest. At the commencement of the storm, 23 hr, they obtained distinct extra reflections from the $F2$-region with different penetration frequencies and at a slightly greater height. These they ascribe to clouds of electrons with dimensions considerably larger than the wave-length used. No scattered echoes (spread-F) were observed. An hour later f_0F2 had decreased and spread echoes were also present. As the storm progressed the spread echoes eventually masked everything else.

This description of the course of events is compatible with a turbulent mechanism for the production of the ionospheric irregularities.

6. The Correlation between Magnetic Disturbance and Scintillation Amplitude

If the magnetic variations are caused by electric field systems in the dynamo region and electron density variations in the F-region are proportional to the mean wind and electrical conductivity in the dynamo region, then the amplitude of the radio-star scintillations should be proportional to the geomagnetic changes. It has been pointed out by Hewish (1952) that there is no one-to-one correlation between fluctuation amplitude and K index and the results presented in Fig. 3 (from Dagg,

1957c) bear out this conclusion. However, in the monthly mean diurnal variations the scintillation amplitude and degree of magnetic activity show a similar decrease after 22 hr. Furthermore there is occasionally very high correlation between magnetic disturbances and scintillation amplitude (Dagg, 1957b).

It was pointed out in paragraph 2 that the influence of the electric potential field system on the amplitude of the scintillations was a secondary effect, and that the primary condition for observing scintillations was that the dynamo winds be turbulent. The suggested explanation for the appearance of Fig. 3 is that on

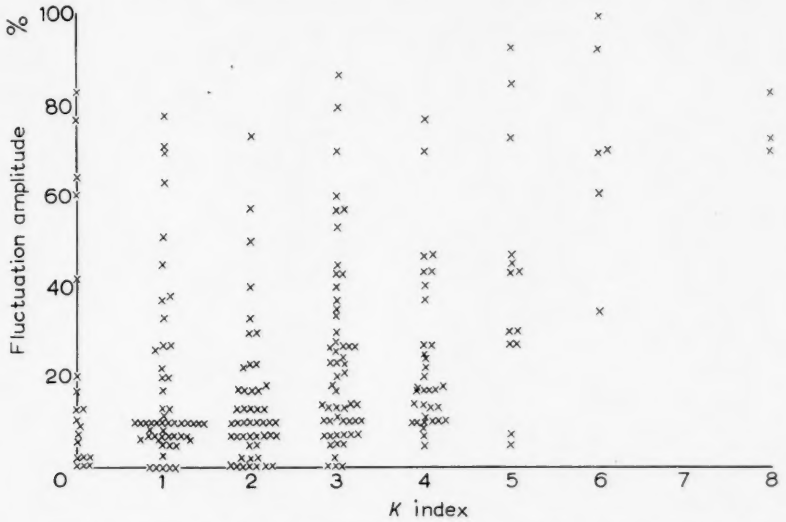

Fig. 3. Comparison of radio-star scintillation amplitude with the magnetic K index.

any one night, with a given turbulent component of velocity, governed by atmospheric parameters such as the temperature gradient, the amplitude would increase with increasing magnetic change. However, the zero point, the amplitude at $K = 0$, may be at any value from 0 to 100 per cent, depending on the conditions for turbulent flow. Thus a diagram plotted as in Fig. 3 might be expected to give a very wide scatter and no one-to-one correlation, but an average of each three hour period over a month would reveal the secondary effect that the dynamo field system has on the amplitude of the scintillations.

7. Scintillations and Spread-F at the Magnetic Equator

The occurrence of scintillations and spread-F at the magnetic equator are probably associated with the large electric potential field variations which are necessary to produce the abnormally large S_q magnetic variation at the equator. Relatively small turbulent components in the wind system would therefore cause scintillations. Furthermore, Baker and Martyn (1953) estimate that the height of the dynamo region near the equator is about 100 km. The temperature gradient at this height is considerably less than that at 135 km and therefore turbulence is more probable.

VOL. 11 1957

8. A Consideration of the Seasonal Variations in Radio-star Scintillations

The critical frequency of the $F2$-region shows a very marked seasonal variation. Since the only effective heating agent in the F-region is photo-ionization by solar radiation the temperature of the F-region will vary in a similar way. If the temperature of the F-region is a dominant controlling factor in the occurrence of radio-star scintillations, as postulated, then it would be expected that scintillations should also show a seasonal variation. However, several other factors influencing scintillations also vary during the year. Some comments on the seasonal influence of these factors, on the basis of the proposed theory of the origin of the irregularities, are given below.

A preliminary comment is necessary. The presentation of radio-star scintillation results in terms of monthly mean diurnal variations (Hewish, 1952; Dagg, 1957c) somewhat confuses their interpretation on a seasonal basis because of two factors: very small scintillations are indistinguishable from receiver noise and the scintillation amplitude varies greatly from night to night. It can be seen therefore that on a night with scintillations of large amplitude the onset of scintillations will appear to be much earlier than on a night with scintillations of small amplitude, simply because in the former case, the scintillations reach the limit of observation earlier. Thus it is difficult to separate a seasonal variation in time of onset of scintillations from a seasonal variation in amplitude. The two effects are therefore considered together.

(1) *The maximum temperature of the F-region* is higher in summer than in winter. The time taken for the temperature gradient to fall to a critical value for turbulent flow in the dynamo region will be less in winter than in summer. Scintillations should, therefore, commence earlier in the night in winter than in summer.

(2) *The density of ionization in the F2-region* is greater in summer than winter; therefore, any fractional variations introduced into the electron density will cause a greater phase change in extra-terrestrial radio waves in summer than in winter and the amplitude of scintillations should be greater in summer than in winter.

(3) *The density of ionization in the dynamo region* is greater in summer than winter. Therefore, for similar winds, the turbulent component of electric potential field produced is greater in summer than winter because of the increase in conductivity. Thus, radio-star scintillations should be of greater amplitude in summer than winter.

(4) *Motion of the radio source: latitude effect.* Cassiopeia is at lower culmination at night in winter and in transit at night in summer. The critical frequency and therefore the maximum temperature of the $F2$-region decreases with increasing latitude in temperate latitudes. Thus scintillations should commence earlier in winter than in summer.

(5) *Magnetic activity.* The amplitude of scintillations depends to a certain extent on the degree of magnetic activity. The seasonal variation in magnetic activity would therefore exert an influence on the occurrence of scintillations.

The observations of radio-star scintillations from August 1954 to July 1955 (Dagg, 1957c) show that any night-time seasonal variation in the time of occurrence must have been small to have escaped detection. On a qualitative basis it is clear

that the absence of a night-time seasonal variation is not incompatible with the suggested theory, for effects (2) and (3) could balance out effects (1) and (4). Quantitatively, the relative importance of the above factors is difficult to assess, but a discussion of the scintillations during the sunspot cycle, when most of the parameters vary, will be informative. Before considering this, two further points are of interest.

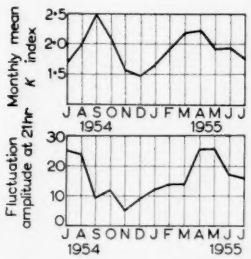

FIG. 4. Seasonal variation of fluctuation amplitude (2100 hr) and magnetic activity.

In 1954–1955 a seasonal effect was observed in *daytime* scintillations: they were more frequently observed in summer daytime than winter daytime (DAGG, 1957c). Cassiopeia is at lower culmination during the summer day, but is in transit during the winter day. In this case effects (2), (3), and (4) all act in the same direction and it appears that they are stronger than (1).

The seasonal effect associated with magnetic activity, effect (5), was examined by comparing the monthly mean amplitude of scintillations at 2100 hr with the monthly mean K index. The annual variation (August 1954 to July 1955) is shown in Fig. 4. It is clear that over an extended period, such as a year, the degree of magnetic disturbance will exercise a considerable control over the amplitude of radio-star scintillations.

9. A Consideration of the Sun-spot Cycle Variations of Radio-star Scintillations and Spread-F

Fig. 5 shows the variation of spread-F (hours per month), the annual magnetic character figure, c_i, the monthly mean $F2$-critical frequency at midnight, and the relative sun-spot numbers over the years 1947 to 1955. The ionospheric information was taken from the published figures of the radio-research station, Slough, and the sun-spot numbers from the Quarterly Bulletin on Solar Activity (Zurich). The magnetic character figure c_i is an international figure measuring the degree of disturbance of the earth's magnetic field. The values were taken from published figures by the International Association of Geomagnetism and Aeronomy. The radio-star scintillation results were taken from two sources. The points for 1949, 1950, and 1951 labelled "L" were obtained by LITTLE* and the points for 1950, 1951, 1954, and 1955 labelled "H" were obtained from HEWISH.† LITTLE's results refer to the months of September and August and are expressed in terms of frequency

* Ph.D thesis (University of Manchester, 1951).

† The author is grateful to Dr. A. HEWISH for supplying these results prior to publication.

VOL. 11 1957

of occurrence. Hewish's results are for the month of April and are expressed in terms of scintillation amplitude.

Fig. 5 shows clearly that from 1947 to 1955, at least, spread-F at Slough does not follow the sun-spot cycle but is more closely associated with the magnetic character figure, c_i.* The scintillation results are unfortunately not extensive

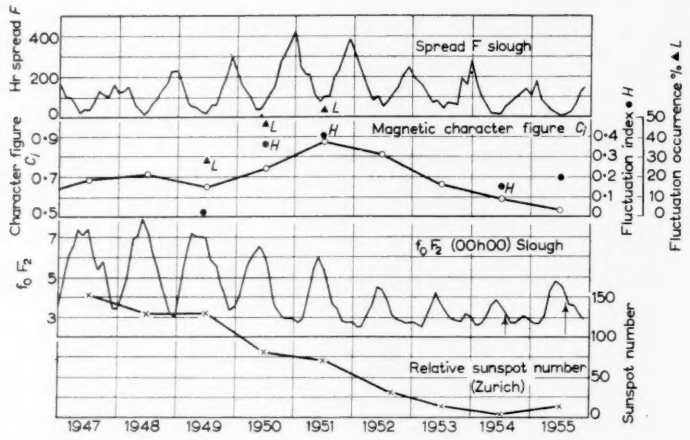

Fig. 5. Sunspot cycle variations. (a) total number of hours of spread-F per month, (b) annual magnetic character figure, c_i, with some radio-star scintillation results (see text); (c) monthly mean value of $F2$-region critical frequency at 0000 hr (Slough); (d) relative sunspot number (Zurich).

enough for it to be possible to make a conclusive statement, but they show a rise in frequency of occurrence over 1949–1951, corresponding to spread-F, and Hewish's results show that the fluctuation amplitude in 1954 and 1955 was certainly much lower than in 1950 and 1951.

(a) *Sunspot cycle variation in diurnal occurrence of scintillations.* The critical frequency of the $F2$-region at midnight follows the sun-spot cycle closely. Assuming that the maximum temperature of the F-region varies in some way with f_0F2 over the sunspot cycle, then the time taken for the temperature gradient in the dynamo region to fall to some critical value at a certain season of the year will be greater at sunspot maximum than at the same season at sunspot minimum. For instance, in June 1950 the monthly mean value of f_0F2 (0000 hr) at Slough was about 6·5 Mc/s whereas in June 1955 the corresponding value was about 4·8 Mc/s. On the present theory therefore the time of maximum occurrence of scintillations should occur much later at night near sunspot maximum (1950) than near sunspot minimum (1955). This is found to be the case; Hewish (1952) found that the time of maximum occurrence of scintillation in June 1950 was about 01 hr, whereas in June 1955 the corresponding time was about 22 hr (Dagg, 1957c).

Furthermore, it is of interest that the sunspot cycle variation in f_0F2 (0000 hr) is much more marked in summer values than in the winter values: the summer-winter difference is about 3·2 Mc/s in 1950 whereas it is only about 2·0 Mc/s in 1955.

* Maxwell, Ph.D thesis (University of Manchester, 1953) arrived at this conclusion.

No significant seasonal variation in time of maximum occurrence was found in 1955 but some variation might be apparent in observations made near sunspot maximum. HEWISH's (1952) scintillation results for 1950 show that the time of maximum occurrence in winter was much earlier than in summer (January 21 hr, JUNE 01 hr). This result would be expected if the summer F-region temperature was much higher than that in winter.

The above argument has neglected the correspondence of scintillation amplitude with magnetic activity but it is clear from Figs. 4 and 5 that the factors causing magnetic disturbances are also of considerable importance in determining the amplitude of radio-star scintillations over long periods.

(b) *Sunspot cycle variation of spread-F.* The seasonal variation in occurrence of spread F is probably due principally to a blanketing effect by the F-region as originally suggested by BOOKER and WELLS (1938). This effect should also manifest itself over the sunspot cycle. However, the occurrence of spread-F at Slough does not show a clear inverse relation with f_0F2 over the sun-spot cycle; it shows a correlation with magnetic activity. It has been shown that this correlation is to be expected, if the irregularities causing spread-F are due to turbulent winds in the dynamo region.

At Hawaii, REBER (1954a) found that the occurrence of spread-F showed a clear inverse correlation with f_0F2. It is of interest to note that the magnetic latitude of Hawaii is 40° where the disturbance daily magnetic variation, S_D, is near its minimum value. Here, it is suggested, therefore, that the blanketing effect of the F-region is greater than the small magnetic effect. However, REBER's (1954b) analysis for Washington, magnetic latitude +50°, shows a similar spread-F variation to that described for Slough (magnetic latitude +54°). At these places the S_D magnetic variation is much greater than at Hawaii.

VOL. 11 1957

CONCLUSIONS

A theory of the origin of the ionospheric irregularities responsible for radio-star scintillation has been presented in paragraph 2 as an atmospheric system capable of producing irregularities in the F-region, without being restricted by the low collisional frequency in that region. It attributes the occurrence of these irregularities to turbulent winds in the dynamo region. With few additional complications it has been successful in explaining the diurnal variations of scintillations, their correlation with geomagnetic variations and such diverse observations as the variation of the time of maximum occurrence of scintillations over the sun-spot cycle and the differences between spread-F observations in Hawaii and Washington. To the present, the theory has proved compatible with observation; further scintillation, ionospheric and magnetic observations in the International Geophysical Year will provide excellent material for it to be assessed more rigorously.

Acknowledgements—The work described in this paper was carried out at the Jodrell Bank Experimental Station of the University of Manchester (Director, Prof. A. C. B. LOVELL). The author is indebted to Dr. J. S. GREENHOW, Mr. E. L. NEUFELD, and Mr. R. W. VICE for many helpful and stimulating discussions. The

author is also grateful to the Department of Scientific and Industrial Research for the award of a Maintenance Grant from October 1952 to September 1955.

REFERENCES

ANDRADE E. N. DA C	1939	*Proc. Phys. Soc.* **51,** 784.
BAKER W. G.	1953	*Phil. Trans. Roy. Soc.* A **246,** 295.
BAKER W. G. and MARTYN D. F.	1953	*Phil. Trans. Roy. Soc.* A **246,** 281.
BATES D. R.	1951	*Proc. Phys. Soc.* B **64,** 805.
BERKNER L. V., WELLS H. W. and SEATON S. L.	1939	*Terr. Mag.* **44,** 283.
BOOKER H. G. and WELLS H. W.	1938	*Terr. Mag.* **43,** 249.
BRIGGS B. H. and SPENCER M.	1954	*Rep. Progr. Phys.* **17,** 245.
DAGG M.	1957(a)	*J. Atmosph. Terr. Phys.* To be published; this issue.
DAGG M.	1957(b)	*J. Atmosph. Terr. Phys.* **10,** 194.
DAGG M.	1957(c)	*J. Atmosph. Terr. Phys.* **10,** 204.
DAGG M.	1956	*Jodrell Bank Annals* **1,** 99.
GREENHOW J. S. and NEUFELD E. L.	1955	*Phil. Mag.* **46,** 549.
GREENHOW J. S. and NEUFELD E. L.	1956	*Phil. Mag.* **1,** 1.
HEWISH A.	1952	*Proc. Roy. Soc.* A **214,** 494.
LITTLE C. G.	1951	*Mon. Not. R. Astr. Soc.* **111,** 289.
LOWMAN A. N.	1955	*J. Geophys. Res.* **60,** 421.
MARTYN D. F.	1955	*Conf. on Physics of the Ionosphere* p. 163. Physical Society, London.
MARTYN D. F. and PULLEY O.	1936	*Proc. Roy. Soc.* A **154,** 455.
REBER G.	1954(a)	*J. Geophys. Res.* **59,** 257.
REBER G.	1954(b)	*J. Geophys. Res.* **59,** 445.
RYLE M. and HEWISH A.	1950	*Mon. Not. R. Astr. Soc.* **110,** 381.
SCRASE F. J.	1930	*Met. Office, Geophysical Memoir* No. 54.

Journal of Atmospheric and Terrestrial Physics, 1957, Vol. 11, pp. 151 to 162. Pergamon Press Ltd., London

Calculation of group indices and group heights at low frequencies*

J. J. Gibbons and B. Ramachandra Rao
Ionosphere Research Laboratory, The Pennsylvania State University, University Park, Pennsylvania

(*Received* 8 *June* 1957)

Abstract—A formula is derived from which the group index for normal incidence, including collision effects, can be easily computed as a function of μ and χ for frequencies below one megacycle. A set of curves can then be prepared from which the group height to be expected from a given electron density profile can be quickly determined by graphical methods.

VOL. 11 1957

1. Introduction

At megacycle frequencies the effect of collisions is neglected in computing group delays since the term ν/ω appearing in the Appleton–Hartree equation is small compared to unity. But for frequencies in the range of hundreds of kilocycles, and with the regions important to transmission and reflection lying considerably lower than for the higher frequencies, the collisions may have important effects. For example, in the collision free case the group index would become infinite at the reflection level, whereas the present work will show that for reasonable electron density profiles, 75 kc/sec and 150 kc/sec group indices have maximum values of only 4 or 5 around the reflection level. The object of this paper is to give a method which, once a few curves have been plotted for a given operating frequency, can be used to determine in about 10 min the group height, collision effects included, for any given electron density profile, $N(z)$.

Starting in the same manner as Davids and Schrag (1951), we assume a transmitted Gaussian pulse

$$f(t) = Ae^{-\left(\frac{t}{T}\right)^2} e^{j\omega_0 t} \tag{1}$$

where ω_0 is the centre frequency of the pulse, and T the time for the envelope to drop to $1/e$ of its maximum value A.

The Fourier transform of $f(t)$ is

$$\frac{AT}{\sqrt{2}} e^{-\frac{T^2}{4}(\omega-\omega_0)^2} \tag{2}$$

and thus

$$f(t) = \frac{AT}{2\sqrt{\pi}} \int_{-\infty}^{+\infty} e^{-\left[\frac{T(\omega-\omega_0)}{2}\right]^2 + j\omega t} d\omega \tag{3}$$

Then for a complex reflection coefficient $R(\omega)e^{-j\phi(\omega)}$ the returned pulse will be

$$F(t) = \frac{AT}{2\sqrt{\pi}} \int_{-\infty}^{+\infty} R(\omega) e^{-j\phi(\omega)} e^{-\left[\frac{T(\omega-\omega_0)}{2}\right]^2 + j\omega t} d\omega \tag{4}$$

* The research reported in this paper was supported by the Geophysics Research Directorate of the Air Force Cambridge Research Center, Air Research and Development Command, under Contract AF19(604)–1304. One of the authors, B. R., was supported under the India Wheat Loan Agreement.

We now assume $R(\omega)$ and $\phi(\omega)$ across the band of frequencies contributing significantly to the pulse have the linear form

$$R(\omega) = R_0[1 + p(\omega - \omega_0)] \tag{5}$$

$$\phi(\omega) = \phi_0 + q(\omega - \omega_0) \tag{6}$$

The received signal then integrates to

$$F(t) = e^{-j\phi_0} A T R_0 e^{j\omega_0 t}\left[1 + \frac{2jp(t-q)}{T^2}\right] e^{-\left(\frac{t-q}{T}\right)^2} \tag{7}$$

If p were zero, i.e. constant absorption for all frequencies in the pulse, the received pulse would have the same shape as the transmitted pulse, but the maximum would be delayed by a time q over the time for the phase wave of centre frequency ω_0 to traverse the path. Since the total phase optical path is $2\int \mu\, dz$, we have

$$\phi(\omega) = 2\int \mu\, dz\, \frac{2\pi}{\lambda_0} \tag{8}$$

then,

$$q = \left(\frac{d\phi}{d\omega}\right) = 2\int \frac{\partial \mu}{\partial \omega} \cdot \frac{2\pi}{\lambda_0} = \frac{2}{C}\int f \frac{\partial \mu}{\partial f}\, dz \tag{9}$$

and setting $qc/2$ equal to the additional virtual one way path due to group delay, we obtain that the virtual group height is

$$h' = \int \left(\mu + f\frac{\partial \mu}{\partial f}\right) dz \tag{10}$$

We designate $\mu' = \mu + f\dfrac{\partial \mu}{\partial f}$ as the group index.

When $p \neq 0$, that is, when the absorption does vary linearly with frequency, and when $2p^2/T^2 \leq 1$, the pulse maximum is still delayed by the same time q: the pulse broadens and is no longer purely Gaussian. When $2p^2/T^2 > 1$ secondary maxima appear, but this condition would correspond to very unlikely values of $dR/d\omega$ in our work. The presence of a rate of change of absorption across the principal frequencies of the pulse will then not affect the group height if it is measured at the pulse maximum, but could do so when the group height is determined by differentiating the leading edge.

An important question yet remaining is how to estimate the phase path in the neighbourhood of the reflection level. Here μ and χ do not have the simple meaning given to them in ray optics, and apparently a full wave solution would have to be carried out to find the actual phase delay. We can fall back here on a test we fortunately had available in the work of Davids and Schrag (1951). They noted that Nertney's (1951) work on fairly exact wave solutions indicated how to extrapolate the phase integrand in the reflection region. They computed indices for 140, 150, and 160 kc/sec for a certain ionospheric model. From these results we were able to compute directly $d\phi/d\omega$ and found that very good agreement could be obtained by integrating μ' up to the Ny point ($\omega^2 = \omega^2 + \omega\omega_H$), as a

first guess might have indicated. In any case μ' drops very sharply beyond Ny, and any slight uncertainty in the limit of integration produces a negligible effect. The problem now reduces to obtaining the values of $\mu + f\,\partial\mu/\partial f$ in the ranges of N and ν important to the operating frequency.

2. Calculation of Group Indices using Approximate Appleton–Hartree Equation

In the low frequency range graphical methods of obtaining $\partial\mu/\partial f$ from a $\mu - f$ plot constructed from values for μ at the 10 or 20 kc intervals available in tables will fail in the reflection region because of the rapid variation of μ with f. To get accurate values of $\partial\mu/\partial f$ against which to check the approximation methods used later, values of μ were accurately computed from the full Appleton–Hartree formula for pairs of closely neighbouring frequencies.

To arrive at a practicable analytic form for μ', one starts by differentiating the Appleton–Hartree expression with respect to f. In the usual notation (Mitra, 1953) this expression may be written as

$$(\mu - j\chi)^2 = 1 + \frac{1}{\alpha + j\beta - \gamma_L[\delta \pm \sqrt{1 + \delta^2}]} \tag{11}$$

where

$$\delta = \frac{{\gamma_T}^2}{2\gamma_L(1 + \alpha + j\beta)} = \frac{y}{\sigma} \cdot \frac{\alpha}{1 + \alpha + j\beta}$$

$$\sigma = \frac{2\cos\theta}{\sin^2\theta}; \qquad \alpha = -\frac{\omega^2}{{\omega_0}^2}$$

$$\beta = \frac{\omega\nu}{{\omega_0}^2}; \qquad {\omega_0}^2 = \frac{4\pi Ne^2}{m}$$

With a view to simplifying the calculation of μ values without sacrificing accuracy the relation (11) is written as

$$(\mu - j\chi)^2 = 1 + \frac{1}{\alpha + j\beta - \gamma_L[\delta \pm (1 + \tfrac{1}{2}\delta^2)]} \tag{12}$$

where a first order approximation is made for the root term, as δ^2 is found to be normally very small for the range of values of N and ν encountered in the low frequency work. The general polarization term from magneto-ionic theory given by

$$R = -\frac{j}{\gamma_L}\left[-\frac{{\gamma_T}^2}{2(1 + \alpha + j\beta)} \pm \sqrt{\frac{{\gamma_T}^4}{4(1 + \alpha + j\beta)^2} + {\gamma_L}^2}\right] \tag{13}$$

can be written as

$$R = r + js = j[1 + \delta + \tfrac{1}{2}\delta^2] \tag{14}$$

for the case of ordinary ray, after making a similar approximation for the root term. Equating real and imaginary terms in (14) one can write

$$r = \beta\varepsilon[1 + \varepsilon(1 - \alpha')] \tag{15}$$

and

$$s = 1 + \varepsilon(1 - \alpha') + \tfrac{1}{2}\varepsilon^2[(1 - \alpha')^2 - \beta^2] \tag{16}$$

VOL. 11 1957

where

$$\alpha' = -\alpha = \frac{\omega^2}{{\omega_0}^2}$$

and

$$\varepsilon = \frac{y}{\sigma} \cdot \frac{\alpha'}{(1 - \alpha')^2 + \beta^2}$$

Using again the negative sign for the ordinary ray which is the main reflected ray for these frequencies and separating real and imaginary terms in relation (12) we obtain

$$\mu^2 - \chi^2 = 1 - \frac{A}{A^2 + B^2} = C = 1 - \tau \tag{17}$$

$$2\mu\chi = \frac{B}{A^2 + B^2} = D \tag{18}$$

where

$$A = \alpha' + \gamma_L s \tag{19}$$

and

$$B = \beta + \gamma_L r \tag{20}$$

To test the validity of this relation for using it for μ' computations, the values of μ and χ are calculated for a frequency of 150 kc, for an electron density of 200–3000 and collision frequency range of 10^5 to 10^7. It is discovered that the values of μ agree very well with those computed by using the general formula (11).

It is interesting to note from relations (15) and (16) that r is proportional to ν and s is independent of ν for the low collision range where β^2 is negligible compared to $(1 - \alpha')^2$. For the same collision range it can be also shown from relations (19) and (20) that B is proportional to ν while A is independent of ν. In this collision range B^2 is usually very small compared to A^2, so that from relations (17) and (18) it can be shown that μ is independent, of ν, and χ is proportional to ν.

Having tested the validity of this relation over a wide range of N and ν, group index values are now computed for a wave frequency of 150 kc using relations (17) to (18) for computing values of μ at 149 and 151 kc/sec. Table 1 gives the values of μ' thus calculated for various values of electron density and collision frequency in the ranges of 500–3000 electrons/cm^3 and 10^5 to 10^6 per sec respectively. An increase of collision frequency is found to decrease the group index invariably and this effect is found to be particularly prominent for high values of N near the reflection level as can be clearly seen from the data presented in this table.

An interesting empirical relation is established by plotting values μ'/μ against $1/\mu^2 + \chi^2$. It was at first observed that for each value of electron density and different values of collision frequency these points lie on a straight line. The constants of these straight lines are then found to be the same for different values of N in the range of 1000–3000 electrons/cm^3. Thus, we are led to the interesting discovery of a linear relationship between μ'/μ and $1/\mu^2 + \chi^2$ for a collision frequency range of 10^5 to 10^6 sec^{-1} and an electron density range of 1000–3000

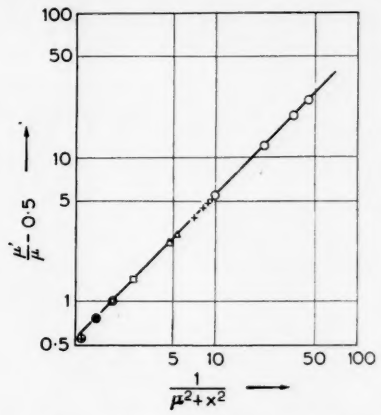

Fig. 1. μ'/μ as a function of $1/(\mu^2 + \chi^2)$ for 150 kc/sec.
○ $N = 3000$ □ $N = 2000$
+ $N = 2750$ ⊙ $N = 1500$
△ $N = 2500$ ● $N = 1000$
⊕ $N = 500$

VOL. 11 1957

electrons/cm³. For a wave frequency of 150 kc/sec the equation for this straight line is given by

$$\frac{\mu'}{\mu} = 0{\cdot}5 + \frac{0{\cdot}57}{\mu + \chi^2} \tag{21}$$

Fig. (1) shows a log plot of $\mu'/\mu - 0{\cdot}5$ versus $1/\mu^2 + \chi^2$ to illustrate graphically this remarkable linear relationship. It is interesting to note that for the case of non-ionized medium relation (21) reduces to give a value of $\mu' = 1{\cdot}07$ which is sufficiently close to unity. Actually, however, relation (21) is valid up to a lower limit of $N = 1000$. For values of N below this value the points fall on a different straight line having lower slope and intercept, so that ultimately, when the electron density is very low, the sum of the constants of this straight line approach

Table 1. Values of μ' computed by using numerical computation and by formula

ν sec^{-1} / N Elec/cm³	10^5		2×10^5		4×10^5		10^6	
	N.C.	By F.	N.C.	By F.	N.C.	By F.	N.C.	By F.
3000	3·843	3·821	3·216	3·233	2·392	2·409	1·540	1·562
2750	1·914	1·913	1·890	1·897	1·880	1·890	1·581	1·592
2500	1·514	1·514					1·420	1·426
2000	1·232	1·233					1·214	1·218
1500	1·128	1·128					1·119	1·124
1000	1·085	1·084					1·071	1·083

unity. This interesting relationship between μ', μ, and χ led to a theoretical study with a view to obtaining an analytical expression for μ'/μ in terms of $1/\mu^2 + \chi^2$. This investigation is presented in the following section.

3. Derivation of an Expression for μ' as a Function of μ and χ, and Construction of Group Index Curves

Starting from the approximate Appleton–Hartree equation (12) which has been shown to be valid for a wide range of N and ν, we can now evaluate $\partial\mu/\partial f$ analytically as follows. Differentiating (17) and (18) we get

$$2\mu \frac{\partial \mu}{\partial f} - 2\chi \frac{\partial \chi}{\partial f} = \frac{\partial C}{\partial f} \tag{22}$$

and

$$2\chi \frac{\partial \mu}{\partial f} + 2\mu \frac{\partial \chi}{\partial f} = \frac{\partial D}{\partial f} \tag{23}$$

Eliminating $\partial\chi/\partial f$ and substituting for $\partial\mu/\partial f$ from relation (10) we have

$$2(\mu^2 + \chi^2)(\mu' - \mu) = \mu f \frac{\partial C}{\partial f} + \chi f \frac{\partial D}{\partial f} \tag{24}$$

Substituting the values for C and D,

$$\frac{\partial C}{\partial f} = \frac{1}{(A^2 + B^2)^2}\left[(A^2 - B^2)\frac{\partial A}{\partial f} + 2AB\frac{\partial B}{\partial f}\right] \tag{25}$$

and

$$\frac{\partial D}{\partial f} = \frac{1}{(A^2 - B^2)^2}\left[(A^2 - B^2)\frac{\partial B}{\partial f} - 2AB\frac{\partial A}{\partial f}\right] \tag{26}$$

Relation (24) now reduces to

$$2(\mu^2 + \chi^2)(\mu' - \mu) = \frac{1}{(A^2 + B^2)^2}\left\{[\mu(A^2 - B^2) - 2AB \,.\, \chi] f \frac{\partial A}{\partial f} + [2AB \,.\, \mu + \chi(A^2 - B^2)] f \frac{\partial B}{\partial f}\right\} \tag{27}$$

We now evaluate $\partial A/\partial f$ and $\partial B/\partial f$ using relations (19) and (20) as follows

$$f\frac{\partial A}{\partial f} = A + \left(\alpha' + \gamma_L f \frac{\partial s}{\partial f}\right) \tag{28}$$

and

$$f\frac{\partial B}{\partial f} = B + \gamma_L + \frac{\partial r}{\partial f} \tag{29}$$

The substitution of these values of $f\partial A/\partial f$ and $f\partial B/\partial f$ in relation (27) is done in two stages in order to avoid writing lengthy expressions. The contribution K' to the right hand side in (27) by substituting first terms A and B from relations (28) and (29) is given by

$$K' = \frac{\mu A - \chi B}{(A^2 + B^2)} \tag{30}$$

Using relations (17) and (18) this reduces to

$$K' = \mu(1 - \mu^2 - \chi^2)$$

Substituting the remaining terms from the equations for $f\partial A/\partial f$ and $f\partial B/\partial f$ in right-hand side of relation (27) we get the contribution K'' due to these given by

$$K'' = \frac{\mu}{(A^2 + B^2)^2}\left\{\left[(A^2 - B^2) - \frac{\chi}{\mu} \cdot 2AB\right]\left(\alpha' + \gamma_L f \frac{\partial s}{\partial f}\right)\right.$$
$$\left. + \left[2AB + \frac{\chi}{\mu}(A^2 - B^2)\right]\gamma_L f \frac{\partial r}{\partial f}\right\} \quad (31)$$

The right-hand side in this relation can be regarded as a sum of k_1 and k_2 which are given by the relations

$$k_1 = \frac{\mu A^2}{(A^2 + B^2)^2}\left[1 - \frac{B^2}{A^2} - 2\frac{\chi}{\mu} \cdot \frac{B}{A}\right]\alpha' \quad (32)$$
$$= \mu\tau^2\alpha' - \mu\tau^2 \frac{B}{A}\left(\frac{B}{A} + 2 \cdot \frac{\chi}{\mu}\right)\alpha'$$
$$= \mu\tau^2\alpha' - 4\mu\chi^2\alpha'$$

VOL. 11 1957

Since

$$\frac{B}{A} + 2\frac{\chi}{\mu} \simeq 2 \cdot \frac{\chi}{\mu}\frac{1}{\tau}$$

when χ^2 is small compared to unity and

$$K_2 = \mu\tau^2\gamma_L + \frac{\partial s}{\partial f} + \mu\tau^2\gamma_L\left[\left(\frac{2B}{A} + \frac{\chi}{\mu}\right)f\frac{\partial r}{\partial f} - \frac{4\chi^2}{\tau^2}f\frac{\partial s}{\partial f}\right] \quad (33)$$

neglecting the $(\chi/\mu)(B^2/A^2)$ term which is usually very small.

Differentiating relation (16) we obtain

$$f\frac{\partial s}{\partial f} = \frac{\varepsilon(1 + \alpha')}{(1 + \alpha')^2 + \beta^2}\{[1 + \varepsilon(1 - \alpha')][(1 - \alpha')^2 - \beta^2] - 2\beta^2\varepsilon(1 - \alpha')\}$$
$$= (1 + \alpha')\frac{r}{\beta} - \frac{2\beta(1 + \alpha')(2r - \beta\varepsilon)}{(1 - \alpha')^2 + \beta^2} \quad (34)$$

Substituting this value for only the first term in relation (33), which is the significant term, we have

$$K_2 = \mu\tau^2\gamma_L(1 + \alpha')\frac{r}{\beta} + \mu\tau^2\gamma_L\left\{\left(\frac{2B}{A} + \frac{\chi}{\mu}\right)f\frac{\partial r}{\partial f} - \frac{2\beta(1 + \alpha')(2r - \beta\varepsilon)}{(1 - \alpha')^2 + \beta^2}\right\}$$
$$- 4\mu\chi^2\gamma_L f\frac{\partial s}{\partial f} \quad (35)$$

Combining relations (32) and (35) we obtain the value of K''. Substituting the value of $K' + K''$ for the right hand side in equation (27) and dividing by

$2\mu(\mu^2 + \chi^2)$ we can write the final relation as

$$\frac{\mu'}{\mu} = 0{\cdot}5 + \frac{1}{\mu^2 + \chi^2}\left\{0{\cdot}5 + \frac{\tau^2}{2}\left[\alpha' + (1 + \alpha')P_H \cos\frac{r}{v}\right] - 2\chi^2\left(\alpha' + \gamma_L f\frac{\partial s}{\partial f}\right) + \frac{\tau^2}{2}\gamma_L\left[\left(\frac{2B}{A} + \frac{\chi}{\mu}\right)\right]\right\} \quad (36)$$

It is shown by numerical computations that this equation can be approximated as

$$\frac{\mu'}{\mu} = 0{\cdot}5 + \frac{1}{\mu^2 + \chi^2}\left\{0{\cdot}5 + \frac{\tau^2}{2}\left[\alpha' + (1 + \alpha')P_H \cos\theta\frac{r}{v}\right]\right\} \quad (37)$$

leaving out the last terms in (36) whose contribution is found to be negligible. This final relation between μ'/μ and $1/\mu^2 + \chi^2$ is found to be in a very convenient and useful form for the rapid and accurate computation of μ' values using the known values of μ and χ.

Relation (37) shows that μ'/μ is a linear function of $1/\mu^2 + \chi^2$ for any fixed value of N or α' for which r/v and τ are independent of v. The intercept of this relation which is 0·5 is the same for all values of N and v satisfying the conditions for obtaining relation (37). It is interesting to note that the gradients of this linear relation are found to be very nearly the same for different values of electron density in the range of 1000–3000 electrons/cm^3. The reason for the gradient being fairly constant is partly that the major contribution to the gradient is due to the first figure 0·5 within brackets in relation (33), the changes in the variable term whose value is of the order of 0·07 being too small to affect the value of the gradient. However, it may be noted that for low values of N, say below 100 electrons/cm^3 the gradient begins to decrease significantly. For waves of 150 kc/sec, calculations have shown that for electron densities above 1000 electrons/cm^3 and collision frequency below 10^6 sec^{-1}, μ'/μ is a linear function of $1/\mu^2 + \chi^2$ with a gradient 0·575 which agrees well with the value in relation (21). The relation (37) is also valid for other frequencies below the gyro-frequency as well, and it can be seen that it is only the gradient of the linear relation that varies for different frequencies while the intercept remains the same, namely 0·5 for all. These gradients are calculated for several spot frequencies in the range of 55–500 kc for high values of N and low v and the values are presented in Table 2.

It will be seen that the gradients are higher for high frequencies and tend to approach a value near to 0·5 as the frequency is decreased. It appears from this that the gradient does not vary widely for different values of μ at low frequencies as it is already near to 0·5 which is the lowest limit, while for high frequencies there is a likelihood of a greater change in the values of the gradient for different values of μ. Relation (37) can be reduced to the simple form

$$\frac{\mu'}{\mu} = 0{\cdot}5 + \frac{1}{\mu^2 + \chi^2}\left[0{\cdot}5 + \frac{\tau^2\alpha'}{2}\right] \quad (38)$$

when the effect of the magnetic field is neglected. If in addition the effect of

Table 2. Computed values of gradients for different frequencies

Frequency (kc)	Gradient
55	0·547
70	0·551
80	0·554
100	0·560
125	0·569
150	0·575
200	0·588
300	0·615
500	0·657

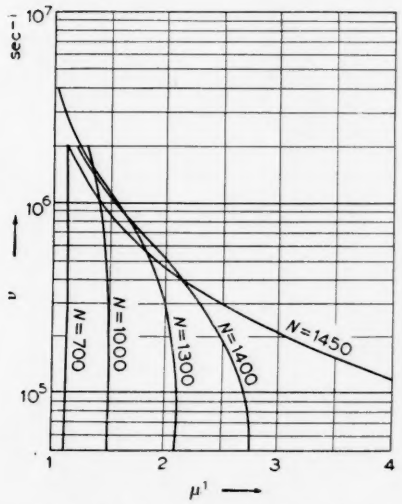

Fig. 2. Group indices at 75 kc as a function of ν for various values of N.

collisions is disregarded we will have $\chi = 0$ and $\mu^2 = 1 - 1/\alpha'$ so that their relation reduces to the form

$$\mu\mu' = 1$$

which is the well-known expression for the non-magnetic and non-collision case.

To test the validity of the relation (37) the values of μ' for 150 kc are calculated by this simple method with a view to compare them with the accurate values already presented in Table 1 obtained by the method obtained in Section 4. A comparison of the values of μ presented in the Table 1 obtained by both methods shows that over most of the range the agreement is excellent. Even in the region of high N and ν where the agreement is expected to be least the values do not differ by more than 1 per cent. The values of μ' obtained by using the formula (37) are calculated taking into account the slight variations of the gradient for

VOL. 11 1957

different values of N so as to get more exact values. It is interesting to note that the values obtained by the formula are always just slightly higher than those obtained by the laborious but more accurate method given in Section 2. This agrees

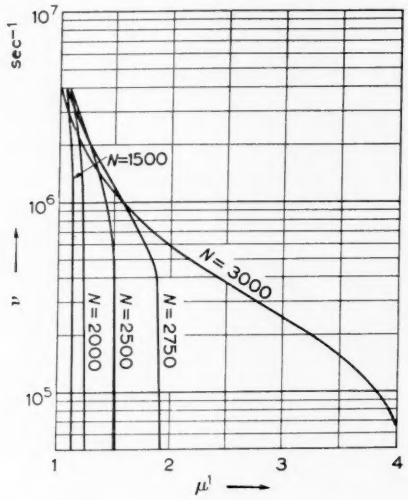

Fig. 3. Group indices at 150 kc as a function of ν for various values of N.

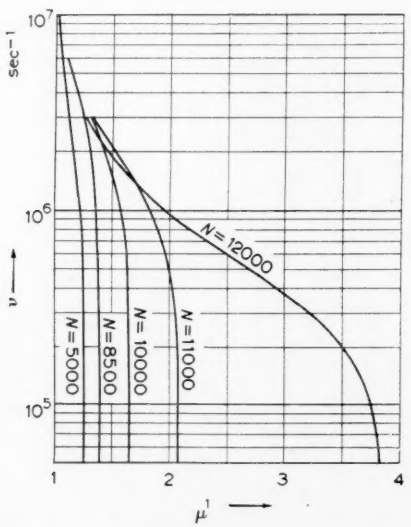

Fig. 4. Group indices at 500 kc as a function of ν for various values of N.

well with the fact that the last terms in relation (36) which have been neglected, are found to give a small negative correction term when evaluated numerically.

Using the formulas derived above group indices as functions of N and ν were

computed for 75, 150, and 500 kc/sec (Figs. 2, 3, and 4). The collision frequencies used correspond to the height range of the E- and D-regions. A study of the graphs reveals the following features:

(1) An increase of collision frequency decreases the value of μ' by an amount dependent on ν, N, and f.

(2) The effect of collision frequency on μ' is greatest for high values of N. The effect is very great at Ny, the reflection level, for which the curves approach infinity as ν decreases.

(3) At the reflection level the value of μ' is only of the order of 4 or 5, unlike the non-collision case, in which it becomes infinite.

(4) A characteristic feature of the μ' curves is that for values of N below Ny the μ' remain constant up to a certain ν value and then begin to decrease as ν is further increased. The constant value corresponds to the non-collision value of μ'. This implies that the collision frequency ν affects the group index for a given N appreciably only when ν exceeds a certain limiting value.

(5) A curious feature of the $\mu' - \nu$ curves is the overlapping at high collisions. This becomes understandable when we examine the curves of μ' plotted against N for $\nu = 10^6$ and for $\nu = 10^5$. The value of μ' reaches a maximum at a value of N less than Ny and the value of N at maximum μ' is lower the higher the collision frequency. Hence the order of variation of μ' with N may be reversed as the collision frequency increases.

VOL. 11 1957

4. Application to some Ionospheric Models

To use the μ' curves to determine the group height for a given N model one has only to read off the heights at which N has the values given on the set of μ' curves. Where this height (or collision frequency) intersects the constant N curve one reads directly below the value of μ' at that height for the model. Then a plot of six or eight points is made to give a curve of μ' against z, the height. The area between this curve and the line $\mu' = 1$, to Ny, gives directly the difference between the observed group height and the real height of the Ny level.

The $N - \nu$ model used by Davids and Schrag (1951) and their tables of μ and χ for 140, 150, 160 kc/sec can be used as an example for the method given above. We should, however, note what we believe to be two errors in that paper. The model designated as 0·55 mc/sec critical is actually about 190 kc/sec critical, and the value of $d\phi/d\omega$ is incorrect.

To obtain the contributions of $d\phi/d\omega$ due to dispersion effects alone, we should determine the areas between the 140 and 150 kc/sec μ curves, and between the 150 and 160 kc/sec μ curves. These areas are 0·625 and 0·755 km respectively. Since they are about the same, the rate of change of phase path per kc/sec can be taken as the average, 0·0690 km/kc/sec. Then,

$$\left(\frac{d\phi}{d\omega}\right)_{\text{dispersion}} = 2 \times 0{\cdot}0690 \cdot \frac{2\pi}{\lambda_0} \cdot \frac{1}{2\pi df} = 69\ \mu\text{sec}$$

Dividing by two and multiplying by the velocity light we obtain 10·35 km excess group path to be added to the phase height, $\int \mu\, dz$. This gives the group height as 112·7 km, whereas the real height of Ny is 107·5 km, leaving an excess of group height over real height of 5·2 km.

When the μ' curves given in the preceding section are used to integrate $\int \mu' \, dz$ up to the Ny point, the group delay is 5·0 km, in agreement with that given just above. We use this as an indication that no wave solution correction is necessary if we integrate μ' up to Ny.

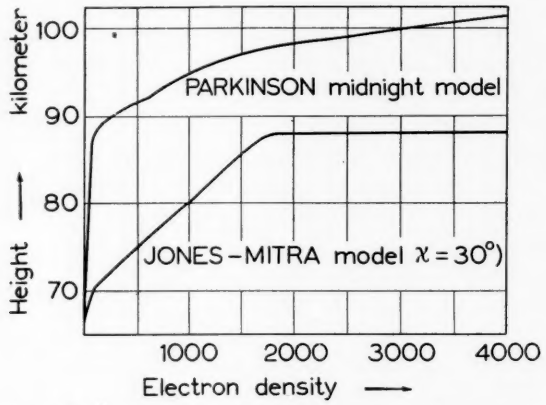

Fig. 5. Ionospheric models used for group height computations.

Two examples will show the effect of collisions on group height computations for 75 kc/sec. In Fig. 5 are given two proposed electron density profiles, one due to Parkinson (1955) for equinox midnight, the other from Jones (1955) and Mitra (1955) for zenith angle 30°. Using the Nicolet (1953) ν values, the group delay for the midnight model is 2·5 km; without collisions it would have been 3·4 km. For the $\chi = 30°$ model the group delay is 1·0 km; without collisions it would have been 6·2 km. The reason for the large difference in the last case is the high collision frequency at and below the Ny level.

References

Davids N. and Schrag R. L.	1951	*J. Atmos. Terr. Phys.* **2,** 355.
Gibbons J. J. and Nertney R. J.	1951	*J. Geophys. Res.* **56,** 355.
Jones R. E.	1955	*J. Atmosph. Terr. Phys.* **6,** 1.
Mitra S. K.	1952	*The Upper Atmosphere.* The Royal Asiatic Society of Bengal.
Mitra A. P.	1955	*J. Atmosph. Terr. Phys.* **5,** 28.
Nicolet M.	1953	*J. Atmosph. Terr. Phys.* **3,** 200.
Parkinson R. W.	1955	*J. Atmosph. Terr. Phys.* **7,** 203.
Ross C. and Fluke C. S.	1953	*Magneto-Ionic Calculations.* WADC Technical Report 53–96.

Journal of Atmospheric and Terrestrial Physics, 1957, Vol. 11, pp. 163 to 176. Pergamon Press Ltd., London

A critical discussion about special ionospheric characteristics

RUDOLF EYFRIG*

(*Received* 3 *August* 1956)

Abstract—A series of examples prove that the present measurements of the characteristic ($M3000$) $F2$ have an unambiguous relation with change of the solar activity, but only for limited regions on the earth. M values as reported at present by different stations are partly insufficient and even too contradictory to justify a worldwide examination.

The importance of accuracy of both height and MUF measurements has been specially stressed, because of the geophysical year. Complete results, in view of the geophysical meaning of the relation between ($M3000$)$F2$ and solar activity, will be published elsewhere.

INTRODUCTION AND RESULTS OF EARLIER EXPERIMENTS

($M3000$)$F2$-factor, the transmission-factor of $F2$-layer for a distance of 3000 km, is determined by the following proportion:

$$\frac{F2 - 3000 - \text{MUF}}{f_0\, F2} = (M\ 3000)F2 \quad \text{(characterized by } M \text{ hereafter)}$$

It is well connected with the layer's height—indeed, with the layer's maximum. M decreases in proportion to the growth of the layer's height and increases when the latter decreases. The characteristic $hpF2$ may also be related to M. The result will then be a curve like a hyperbola (compare Fig. 4 of BIBL *et al.*, 1951). Now, to make a statement for forecasting purposes it will be useful to write this factor in its dependence to solar activity, following the example given by GALLET and RAWER(1950) about the electron density of $F2$ layer, i.e. for the value Q:

$$Q = \frac{1}{24} \sum_{t=0}^{t=23} \overline{f_0^2}$$

($\bar{f}_0$ being a month's median at a given time). The author has followed the variation of M at given hours (1200 and 0000 LMT) for a series of stations (EYFRIG, 1951). He concluded that a rectilinear relation exists between twelve months' sliding mean of the relative sunspot number and that of the M factor. THEISSEN (1955) has lately developed a method by which the M factor can be computed for every hour by aid of charts. He used M factors reported by the different stations. In one of his sketches, THEISSEN concludes the possibility of establishing a world-forecast of these factors (see his paper, Fig. 6). Desirable as this attempt may be, doubts arise if the material on hand is suitable to the case in question.

RESEARCH PURPOSE

It is the meaning of this endeavour to collect all available M values and to accomplish former researches. For further details see EYFRIG (1951).

* During the writing of this publication the author was with the former Service de Prévision Ionosphérique Militaire (France).

VOL. 11 1957

STATIONS USED

Contrary to EYFRIG (1951), stations with series of only a few years have also been used.

Table 1. Stations and periods of data used in the statistics

Station	φ	λ	I	
Adak	51·9 N	183·4	63·0 N	XII 1951–IV 1954
Anchorage	61·2 N	210·1	73·0 N	IX 1951–IV 1954
Baguio	16·4 N	120·6	18·0 N	X 1952–IV 1954
Baker Lake	64·3 N	264·0	86·5 N	VIII 1951–IV 1954
Bâton Rouge	30·5 N	268·8	62·0 N	VII 1946–II 1953
Brisbane	27·5 S	153·0	57·0 S	XII 1944–IV 1954
Canberra	35·3 S	149·0	65·5 S	VII 1947–IV 1954
Casablanca	33·6 N	352·4	49·0 N	II 1952–IV 1954
Christchurch	43·6 S	172·7	68·0 S	I 1947–IV 1954
Churchill	58·8 N	265·8	83·5 N	VIII 1946–I 1948 (a.)
				VIII 1951–IV 1954
De Bilt	52·1 N	5·2	65·5 N	IV 1949–IV 1954
Freiburg	48·1 N	7·8	64·0 N	VIII 1948–IV 1954
Huancayo	12·0 S	284·8	2·5 N	VII 1944–IV 1954
Inverness	57·4 N	355·8	71·0 N	II 1948–IV 1954
Johannesburg	26·1 S	28·0	61·0 S	X 1947–IV 1954
Kiruna	67·8 N	20·5	76·0 N	X 1952–IV 1954
Leyte	11·0 N	125·0	8·0 N	II 1946–II 1948
Lindau	51·4 N	10·1	66·5 N	XII 1950–IV 1954
Maui	20·8 N	203·5	38·0 N	VIII 1946–IV 1954
				(night I 1948–IV 1954)
Narsarssuak	61·2 N	314·6	77·5 N	V 1951–IV 1954
Nha-Trang	12·2 N	109·2	7·0 N	XI 1951–IV 1954
Okinawa	26·3 N	127·8	38·0 N	I 1947–IX 1948 (a.)
				II 1951–IV 1954
Oslo	59·6 N	11·1	72·0 N	X 1949–IV 1954
Ottawa	45·4 N	284·3	76·0 N	III 1946–IV 1948 (a.)
				VIII 1951–IV 1954
Palmyra	5·9 N	197·9	12·0 N	V 1947–V 1949
Panama Canal	9·4 N	280·1	39·0 N	XII 1951–IV 1954
Poitiers	46·6 N	358·0	62·0 N	VIII 1950–IV 1954
				(night V 1952–IV 1954)
Reykjavik	64·1 N	338·3	76·0 N	IX 1944–I 1945 (a.)
				VI 1950–IV 1954
San Francisco	37·4 N	237·8	62·0 N	V 1946–IV 1954
San Juan	18·5 N	292·8	52·5 N	III 1946–IV 1954
Slough	51·5 N	359·4	67·0 N	I 1946–V 1954
Taipeh	25·0 N	121·3	34·0 N	VIII 1950–IV 1954
				(night VI 1950–IV 1954)
Trinidad	10·6 N	298·8	42·0 N	VII 1946–XII 1950
Tromsoe	69·4 N	18·6	76·5 N	VI 1950–IV 1954
Washington	38·7 N	282·9	71·0 N	VI 1944–V 1954
Watheroo	30·3 S	115·9	64·0 S	VI 1946–IV 1954
White Sands	32·3 N	253·5	60·5 N	VI 1947–IV 1954

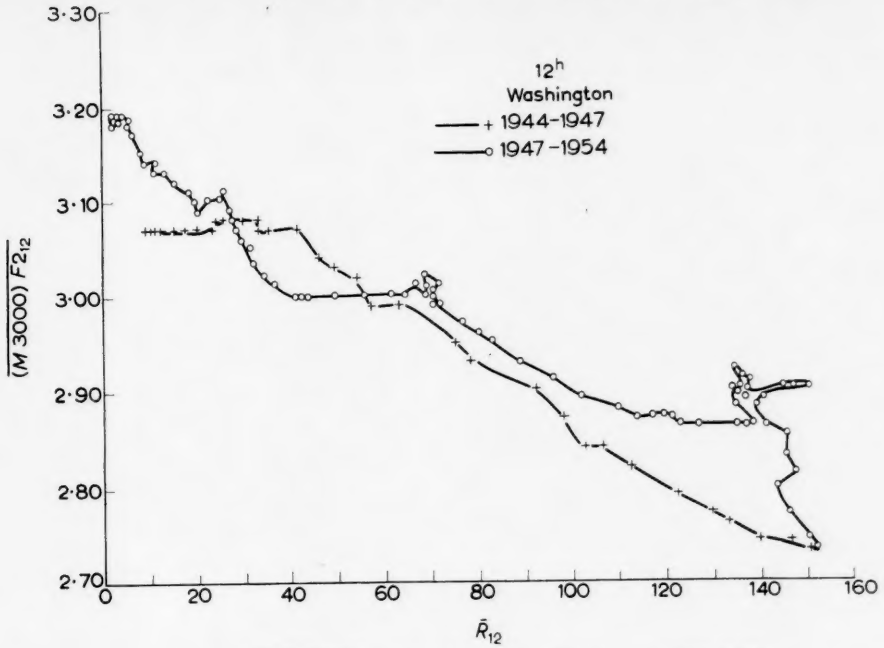

Fig. 1. $\overline{(M3000)F2}_{12}$ in function of $\bar{R}_{12}$, Washington, 1200 LMT.

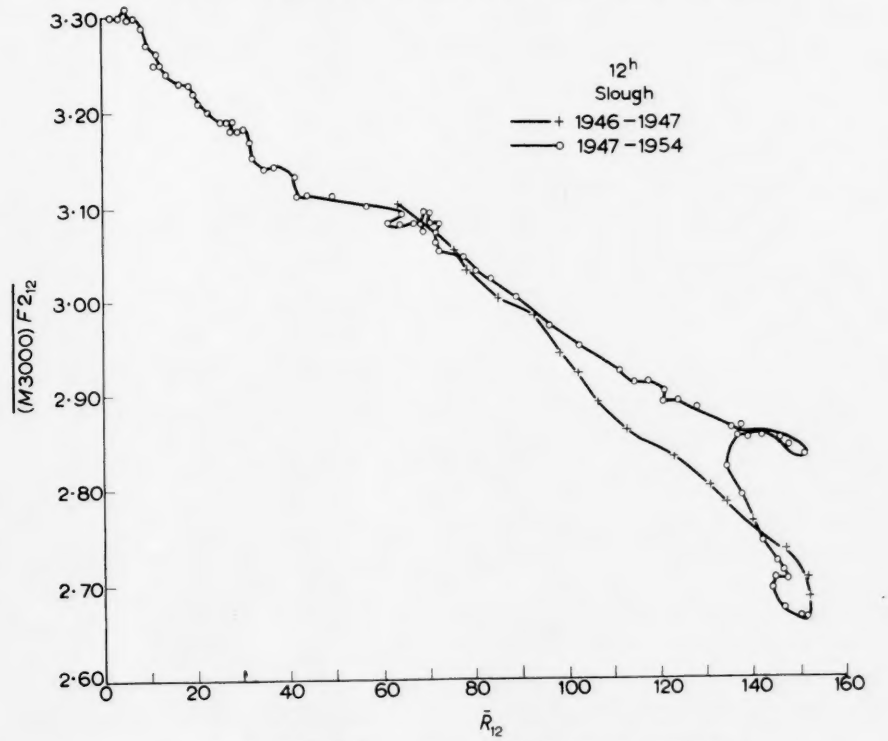

Fig. 2. $\overline{(M3000)F2}_{12}$ in function of $\bar{R}_{12}$, Slough, 1200 LMT.

VOL. 11 1957

RESULTS

The correlation lines formerly calculated for increasing activity for a number of stations are also valid for decreasing solar activity. First, let us mention the Washington station's results (Fig. 1). Preciseness and clearness of the measurements are most satisfactory.

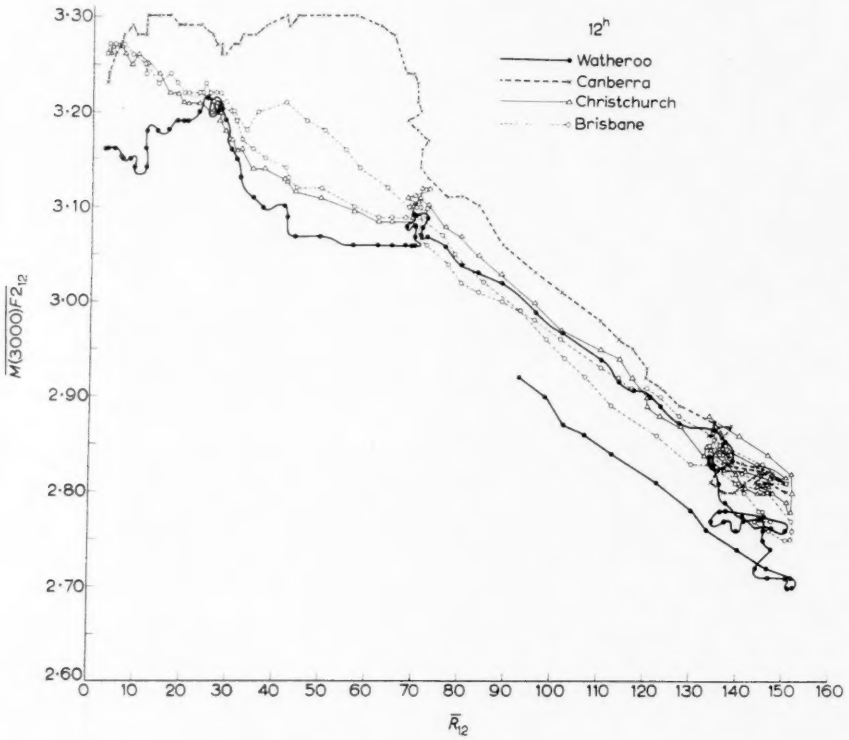

Fig. 3. $\overline{(M3000)F2}_{12}$ in function of $\bar{R}_{12}$, Australia, 1200 LMT.

The slight fluctuations of the curve will certainly be real. Special attention must be given to the accumulation of values near $\bar{R} = 70$ as well as to the dispersion during the second maximum of solar activity. It is easy to perceive that the maximum (May 1947 $\bar{R} = 151{\cdot}9$) represents the chief maximum of the cycle and that the second one is in fact only a secondary maximum (September 1948 $\bar{R} = 150{\cdot}5$). The first one is therefore the "real maximum" and not, as one now and again proposes, the centre between both maxima. This is further demonstrated by results given by Slough (Fig. 2). Although British stations have another method for calculating M values, the results in middle latitudes can be compared with those reached, thanks to the American method (SMITH).

It would be to wearisome to describe the results of each station separately; therefore, may I be allowed to group up results according to the regions?

VOL. 11 1957

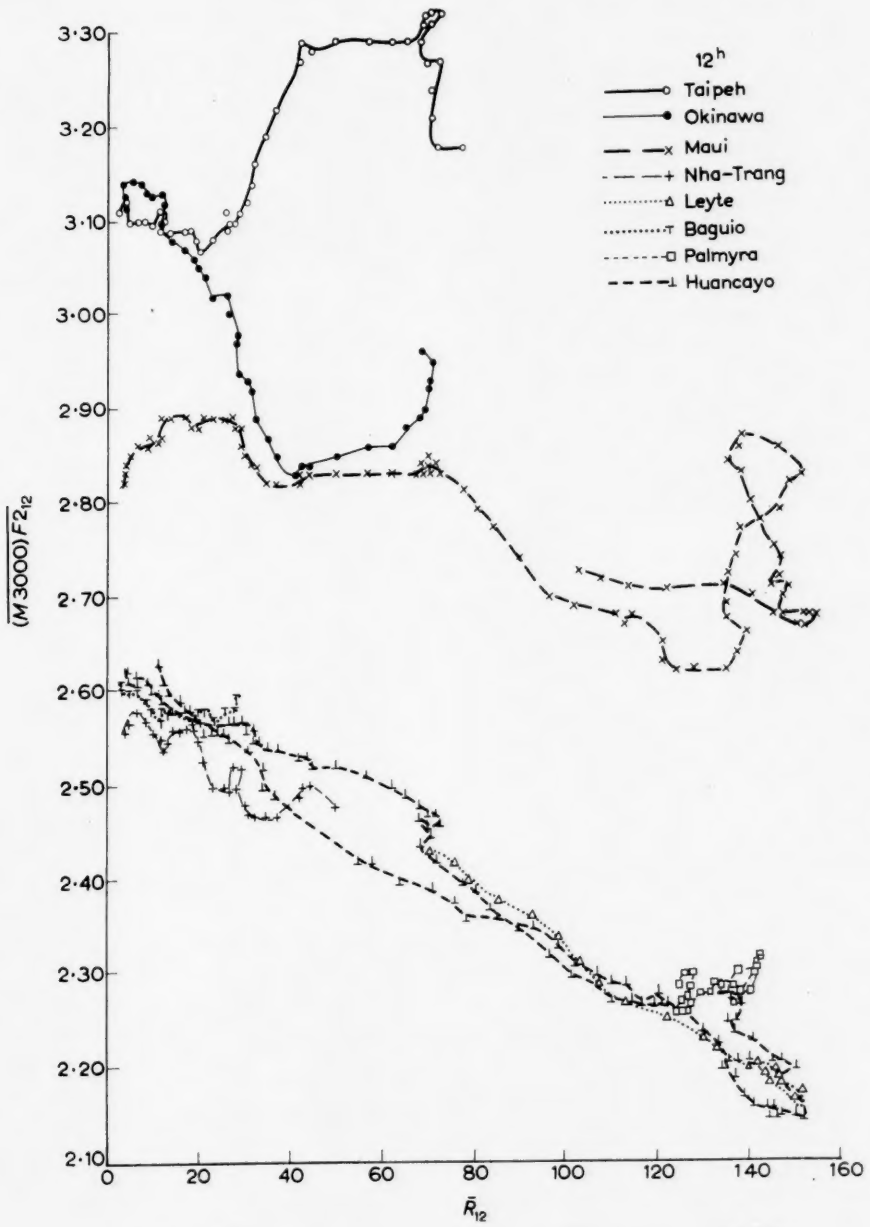

Fig. 4. $\overline{(M3000)F2}_{12}$ in function of $\bar{R}_{12}$, East Indian region, 1200 LMT.

(a) *Australia* (Fig. 3)

Results from Christchurch are presented only for decreasing solar activity. There is a linear relation, but a loop appears at $\bar{R} = 70$. Brisbane has good linearity, both by increasing and decreasing solar activity. Both Canberra and Watheroo show from $\bar{R} = 30$ to $\bar{R} = 70$ rather strange deviations. Values at $\bar{R} = 70$ for Canberra increase rapidly, whereas they slightly decrease at first for Watheroo just to increase again. These deviations cannot be easily understood.

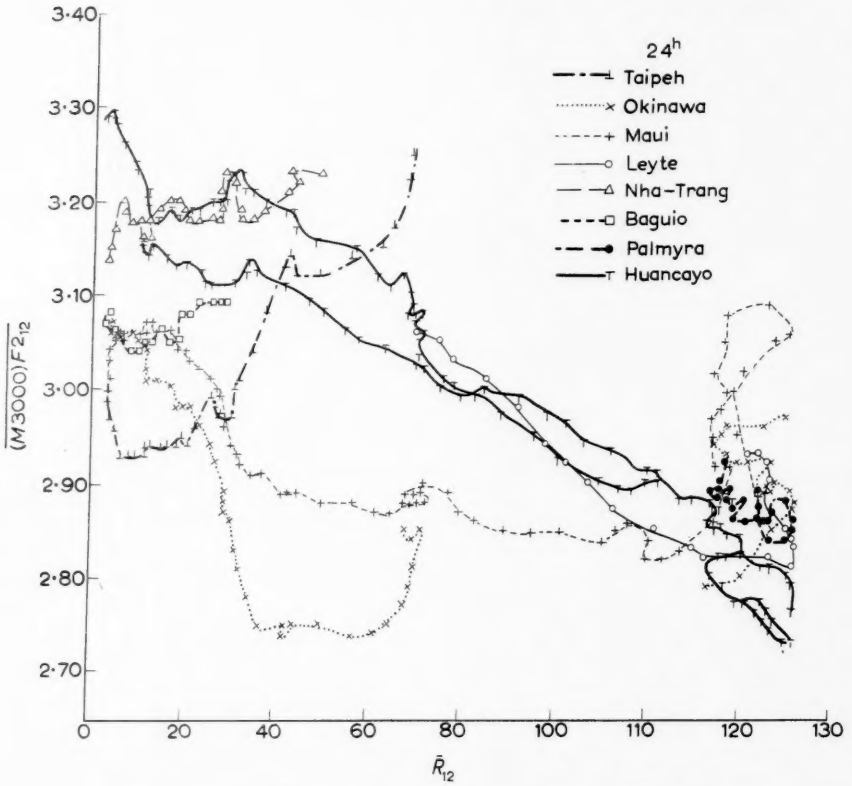

Fig. 5. $\overline{(M3000)F2}_{12}$ in function of $\bar{R}_{12}$, East Indian region, 0000 LMT.

They are not comprehensible either geographically or geomagnetically. One might be led to presume that mistakes have made their way into the readings of height values (respectively MUF values), if one did not know for certain that all stations here mentioned publish otherwise uncommonly precise ionospheric data. However, in the case of Canberra for instance, the error amounts to about 8 per cent. Apart from these deviations, observations in the Australian region remain without contradiction between different stations. Making restrictions for Canberra, the results of all other stations can be used for forecasting purposes.

(b) *Philippine Islands and East Indian region* (Figs. 4 and 5)

It is evident that the curves shown for this district (one cannot speak about straight lines) do not show an unequivocal M-value variation with solar activity. Only one station in the entire region (Leyte) shows a quasi-linear M variation in dependence from the relative number of sunspots. All other stations show curves

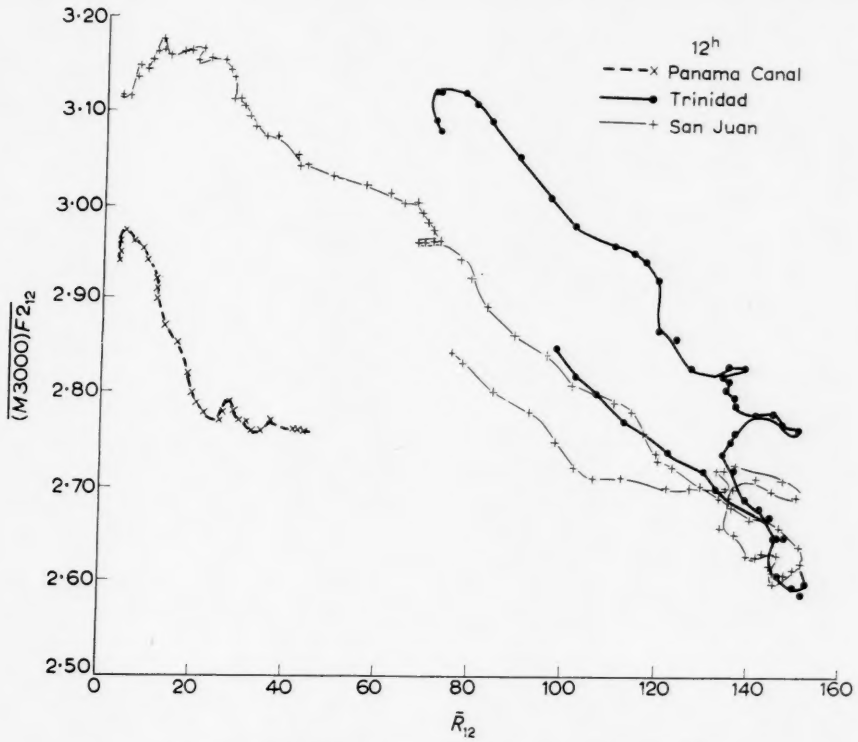

Fig. 6. $\overline{(M3000)F2}_{12}$ in function of $\bar{R}_{12}$, Antilles, 1200 LMT.

which are, let us say, very curious. Taipeh and Okinawa give most strange results. Although only 600 km distant one from the other, they have completely different M values. 90 km height differences for the $F2$-layer maximum correspond to these M differences. Supposing these values to be real, one must conclude that the $F2$-layer lies very inclined in this region. Also the values published by all the other stations in this region are very difficult to explain. It is especially striking that there should be the same M values for Maui at both maximum and minimum solar activity and at $\bar{R} = 100$ on the contrary low values. It seems impossible to predict M factors as an unambiguous function of solar activity with such basic data. One may be tempted to think that perhaps the linear relation exists only for certain latitudes. But for Huancayo, on the other hand, a variation was found to correspond perfectly to that of Brisbane. The results of this station are therefore also indicated in Figs. 4 and 5.

VOL. 11 1957

(c) *Antilles* (Fig. 6)

The results of three stations have been examined for this region: San Juan shows an excellent linearity with noon values; M values do not differ much either by increasing or decreasing solar activity. Trinidad, with its M series, which was ended in June 1951, shows important differences between M factors

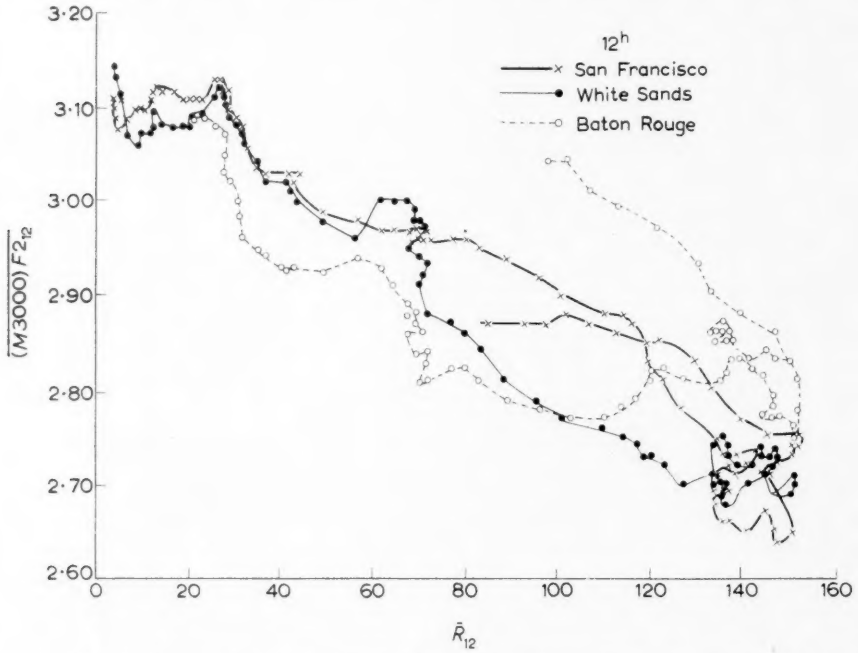

Fig. 7. $\overline{(M3000)F2}_{12}$ in function of $\bar{R}_{12}$, Southern North American region, 1200 LMT.

by sunspot increase and decrease. The Panama Canal (successor station) starts with much lower M values and rests also at $\bar{R} = 0$ much lower than the Trinidad M series would lead one to expect it is an incomprehensible fact that two neighbouring stations situated close to each other both geographically and geomagnetically should show such differences. By the way, when such regional differences

	φ	I	Distance
Panama Canal	9·4 N	39 N	1900 km
Trinidad	10·6 N	40 N	

really do exist, it would mean that a worldwide forecast would be most problematic. On the other hand, both height scale and reading exactness influences the M values. The CCIR standard, which is still mostly applied, provides a 10 km height-precision; this corresponds to nearly 3 per cent. About half the error of the height should appear for the MUF. Frequency-scale errors may also appear. We suppose that the median error of the readings is of the order of 3–5 per cent. But when the height-marks themselves are not correct, a large systematic error must

exist. We fear that at some stations for which we have found extraordinary results such influences may have occurred.

(d) *Southern North American region*

Fig. 7 shows M-factor daily variation for three stations in the south of the U.S.A. The variation is not so well balanced as is for instance the case with curves

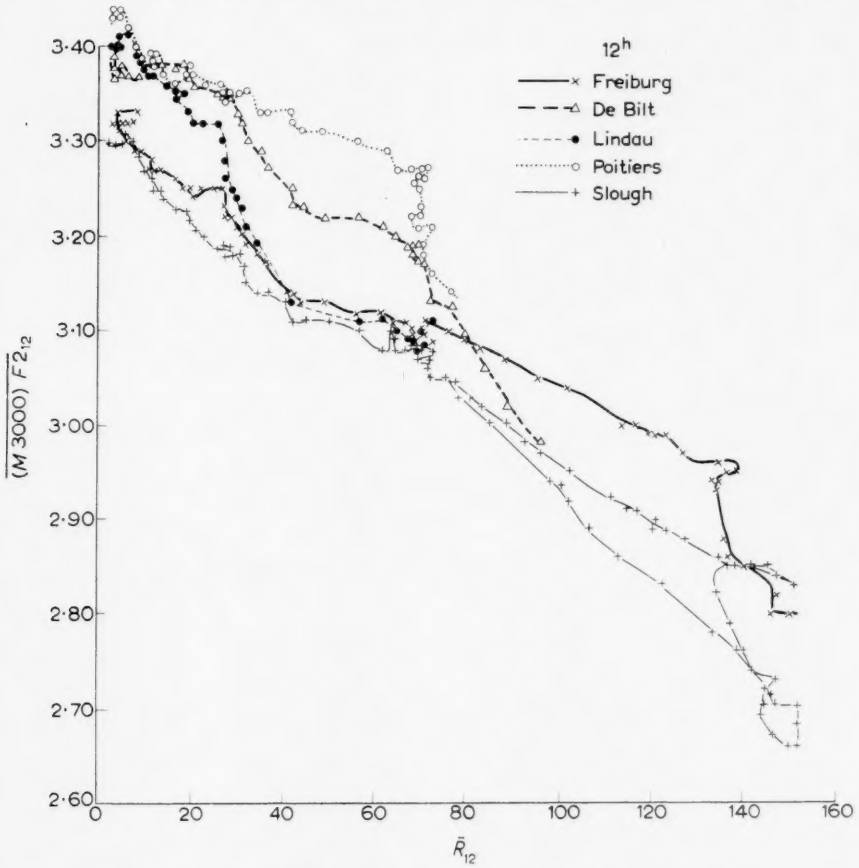

Fig. 8. $\overline{(M3000)F2}_{12}$ in function of $\bar{R}_{12}$, Central Europe, 1200 LMT.

of Australian stations. However, there is a clear variation with the number of sunspots. Only at Bâton Rouge quite a remarkable difference exists between M factors observed during increase and decrease of the sunspot-cycle.

(e) *Central Europe and North African region*

The M-factor variation at European stations (see Figs. 8 and 9), is less reliable than we first supposed. We must insert here that M results were omitted for Swiss (Schwarzenburg) and French stations (Domont), the series of observations being so short. Inverness, Slough, Lindau, and Freiburg are very close together. On the

VOL. 11 1957

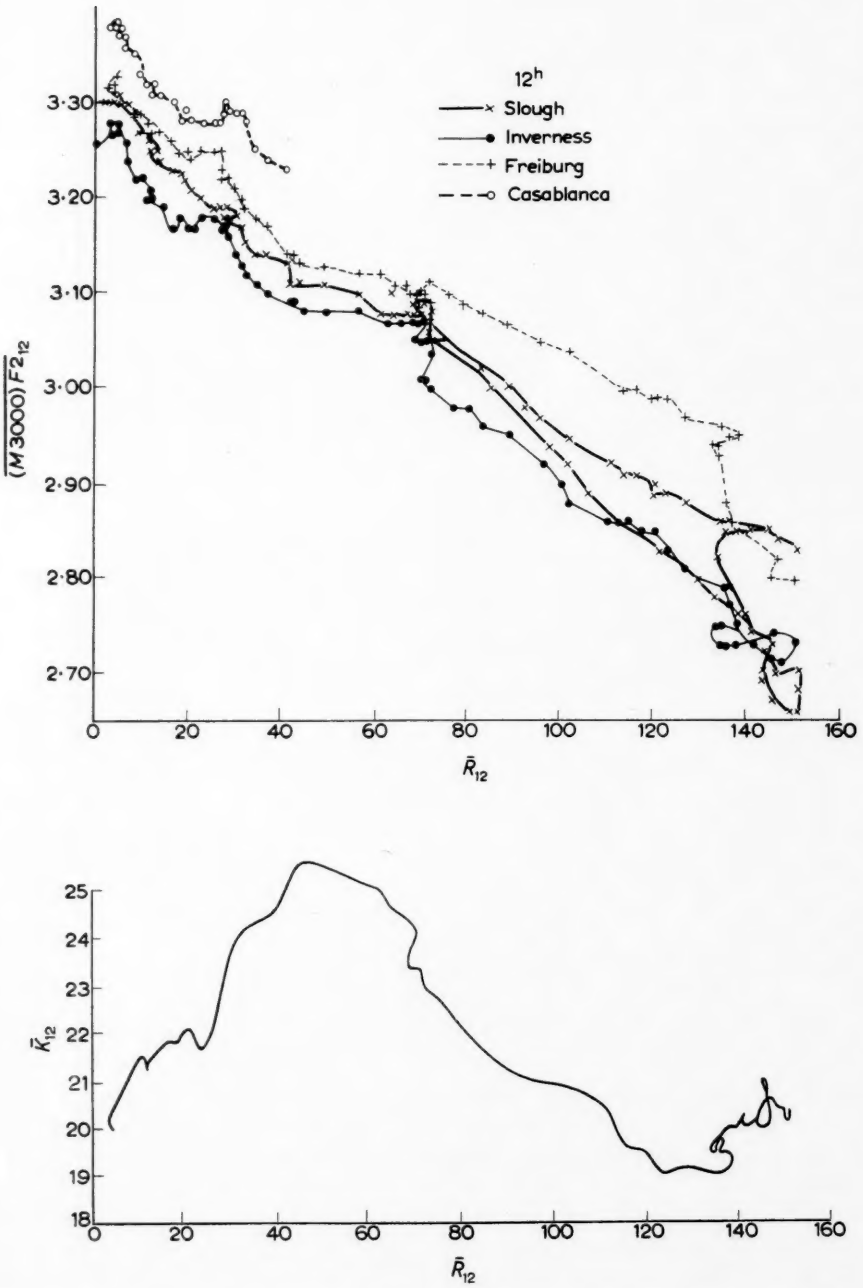

Fig. 9. $\overline{(M3000)F2}_{12}$ in function of $\bar{R}_{12}$, European stations and Casablanca, 1200 LMT.

other hand, M-factors measured at De Bilt, and those measured at Poitiers even more so, are considerably higher, especially at numbers of solar spots between $\bar{R} = 0$ up to 70. Further, M-values measured at Casablanca are just as great as the De Bilt ones. A clear performance will be gained by comparing the values of:

Station	φ	J
Casablanca	33·6 N	49
Freiburg	48·1 N	64
Slough	51·5 N	67
Inverness	57·5 N	71

i.e. decreasing M values by increasing geographical latitude (Fig. 9). Further, we think it important that, in the range of $\bar{R} = 70$ to 40, all curves are nearly parallel to the abscissa. Such a perfect conformity cannot be accidental. We think we have an explanation for this; a strong increase of the magnetic character figures was observed at the time in question. Now, it has already been shown by NETZER in 1939 (NETZER, 1940), that a strong relation exists between the layer-height of the $F2$ layer and magnetic 3-hr-range indices K (BARTEL's index), such that we must write $\bar{M} = f(\bar{R}, \bar{K})$. For this reason in Fig. 9 we also give the 12 months running mean of BARTEL's monthly K value. We recognize indeed, a relation between our M and BARTEL's K indices. It is thus to be feared that the M factors will be more disturbed in polar regions. The effects of the variation of magnetic activity can already be seen in Europe. We refer here once more to Fig. 4 (Huancayo): here an *increase* of M-factor is noticeable, similar to the one which has been observed in the critical frequencies of $F2$ layer at the time of increased K indices.

(f) *North Europe–Greenland region* (Fig. 10)

While Inverness still shows a perfectly clear variation of the $\bar{M}$ factor with $\bar{R}$, we miss this for the Oslo results, and especially the Greenland station, Narsarssuak, gives a most strange M factor variation.

(g) *Canadian region* (Fig. 11)

A dependence of M factor from R, in the Canadian stations, is hardly perceptible. The influence of the K indices is so strong in the results of these stations that the *linear relation* which we have found in other regions of the world is not visible. There can be no doubt as to the correctness of the observations. It is not probable that five stations at once should make the same errors. These results are, unfortunately, inadequate for forecasting purposes. The consequence would be that, for high latitudes, the M factor could only be approximately forecasted when only the relative sunspot number is known. This, because a forecast of magnetic activity does not yet exist and also because the data is not sufficient for this purpose.

Last, but not least, we wish to mention the variation of one more station which, thanks to its geographical position and its good results, gives a very satisfying relation; this is Johannesburg, South Africa (Fig. 12).

VOL. 11 1957

DISCUSSION

The question is: Which is the actual precision of MUF values? International instructions on the subject seem to be sufficiently precise as to exclude difficulties in MUF readings. But still these instructions do not seem to be always sufficiently observed, while, so far, statistics of the height of the $F2$ layer have only very seldom been executed; for instance, APPLETON (1950).

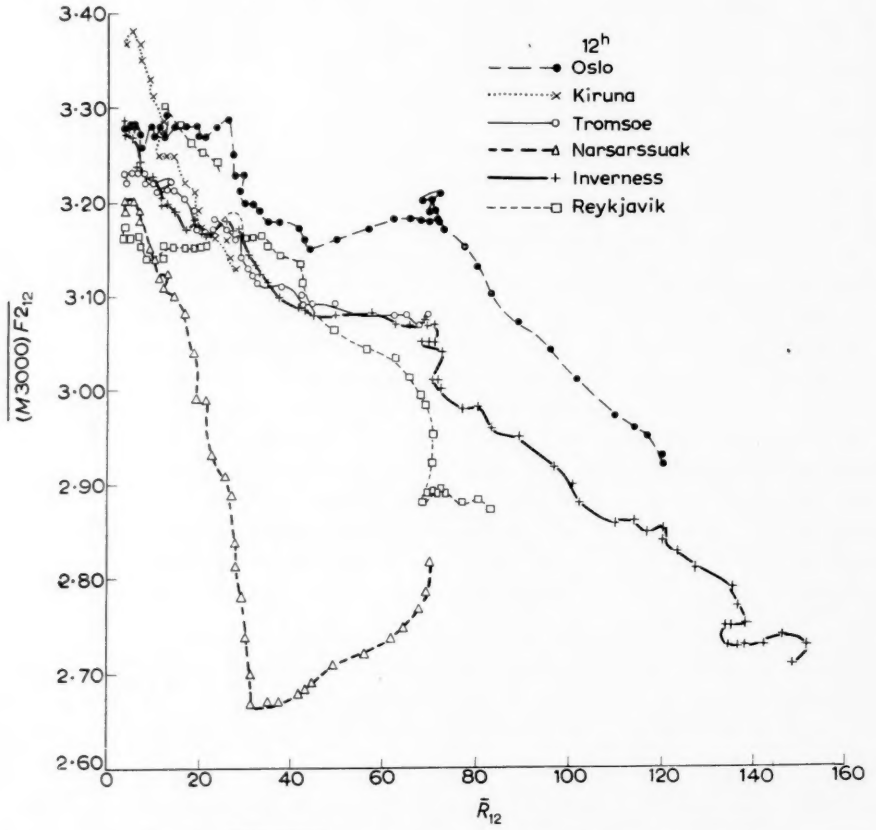

Fig. 10. $\overline{(M3000)F2}_{12}$ in function of $\bar{R}_{12}$, North Europe, 1200 LMT.

Washington, Slough, Huancayo, Brisbane, Christchurch, and Johannesburg are the "good old" stations which seem to have reduced frequency and height-reading errors to a minimum, thanks to their permanent watchfulness; these stations give strictly linear relation between $\bar{R}$ and $\bar{M}$.

Still, the fact must not be overlooked that exact height statements just with regard to geomagnetic tidal effects are urgently needed. In view of the Geophysical Year 1957/58, stations may be informed to avoid errors in height measurements. This means, of course, that high claims will be made not only upon the apparatus and its construction, but also upon the staffs attending the *ionosonde* and the evaluation of the ionograms.

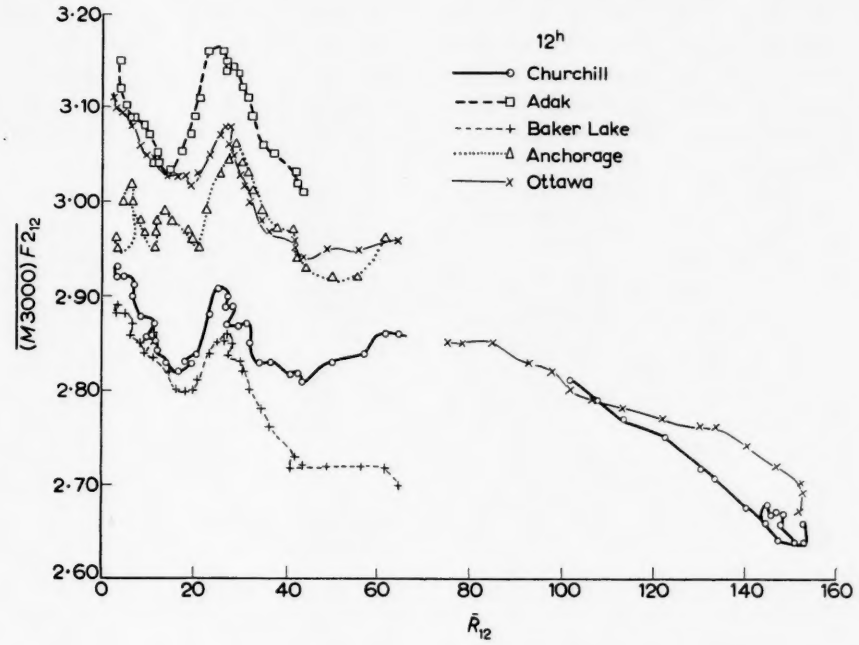

Fig. 11. $\overline{(M3000)F2}_{12}$ in function of $\bar{R}_{12}$, Canadian region, 1200 LMT.

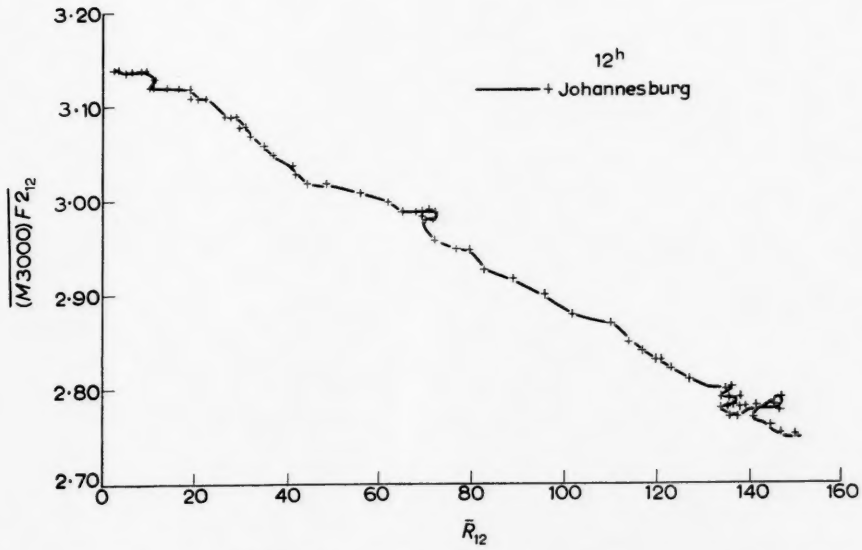

Fig. 12. $\overline{(M3000)F2}_{12}$ in function of $\bar{R}_{12}$, Johannesburg, 1200 LMT.

VOL. 11 1957

If the above-mentioned discrepancies should be real, one would have to admit the existence of strong "local anomalies" for certain regions. The said "anomalies" may be of interest from a geophysical point of view, but very difficult to handle for forecast purposes. Anyway, Theissen's globular way of considering the subject must not lead one to take his basic data for granted. On the other hand, if the linear relation between $\bar{M}$ and $\bar{R}$ is verified, it would offer a good medium for controlling the accuracy of the height scales.

REFERENCES

BIBL K., RAWER K. and THEISSEN E.	1951	Le rôle de l'occultation dans la propagation des ondes décamétriques. *SPIM*-R11 (Décembre).
GALLET R. and RAWER K.	1950	*Ann. Geophys.* **6,** 104.
EYFRIG R.	1951	*Z. Angew. Physik* **3,** 96.
THEISSEN E.	1955	*J. Atmosph. Terr. Phys.* **6,** 243.
NETZER Th.	1940	*Hochfrequenztechn. Elektroakustik* **55,** 86.
APPLETON E. V.	1950	*J. Atmosph. Terr. Phys.* **1,** 106.

Journal of Atmospheric and Terrestrial Physics, 1957, Vol. 11, pp. 177 to 186. Pergamon Press Ltd., London

The movements of sporadic-*E* layer clouds

G. L. Goodwin*
Physics Department, University of Adelaide, Australia.

(*Received* 17 *July* 1957)

Abstract—An account is given of some measurements of the magnitude of the drift velocity of isolated sporadic-*E* clouds, using a C.W. technique. The method involves determining the rate of change of phase path of a wave reflected at almost vertical incidence, by measuring the rate of fading of the received signal due to interference between the reflected and ground waves. A method using two spaced loop-aerials is suggested for determining the direction of drift.

Some experimental evidence is described indicating that the angular spread of scatter from E_s clouds is larger at night than during the day.

VOL. 11 1957

1. Introduction

Various methods have been employed for studying the horizontal drifts of irregularities in the *E*-layer of the ionosphere. Ferrell (1948) and Gerson (1950) studied the movements of E_s clouds over large areas by combining the observations from many widely scattered observers on the times and places of enhanced transmissions by way of the sporadic-*E* layer. More recently, observations have been made by Clark and Peterson (1956) who used backscatter techniques. These observations were concerned with the drifts of large sheets of ionization some hundreds of kilometres in extent. Mitra (1949), Krautkrämer (1950) and others have used a method in which signals from a pulse transmitter were received at three or more closely spaced receiving points after reflection from the *E*-layer. B. R. Rao and E. B. Rao (1954) employed a modification of this method using C. W. instead of pulse transmissions. In both the pulse and C.W. versions of this method the measurements refer to the movement of small irregularities which only affect the amplitude of the received signals for a matter of seconds.

Findlay (1953) studied changes in the phase path of waves reflected from isolated clouds of E_s ionization (extending some hundreds of metres in the horizontal plane) and estimated the magnitudes of the horizontal drift velocities. The results of some experiments similar to those of Findlay are described in the present paper. Whereas Findlay used pulse transmissions (2·4 Mc/s) at vertical incidence during the day-time, the present experiments employed C.W. transmissions (1·55 Mc/s) at almost vertical incidence, and were made at night.

2. Principle of the Method

The method used for calculating the magnitudes of the drift velocities is similar to that described by Findlay (1953). Considering Fig. 1, let the transmitter and receiver be at T and R respectively, and suppose an E_s cloud (C) moves in the direction QC with a uniform velocity v. Let Q be the perpendicular from O (midpoint of TR) to the line QC.† Suppose that the cloud passes Q at zero time, and

* Now at Physics Department, University College of Swansea, U.K.
† It is noted that OQ is not necessarily in the vertical direction OZ.

is at C at time t. In practice the distance TR is small enough to justify assuming that $TC + CR = 2\,OC = P$, say.

If $2\,OQ = P_o$ (the minimum value of P) then

$$P^2 = P_o^2 + 4v^2t^2$$

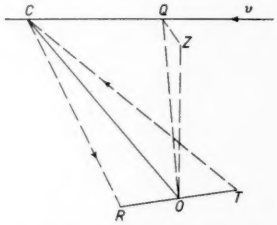

Fig. 1. Path of E_s cloud, velocity v.

If $P = P_o + \Delta P$, where ΔP is the change in phase path P as the E_s cloud moves from Q to C, then

$$2P_o\Delta P + (\Delta P)^2 = 4v^2t^2$$

$$\text{i.e.} \quad \Delta P(2P_o + \Delta P) = 4v^2t^2 \qquad (1)$$

ΔP, P_o and t may be found experimentally, and hence the magnitude of v may be estimated.

The magnitude of v may be found from the slope of the straight line graph obtained by plotting $\Delta P(1 + \Delta P/2P_o)$ against t^2.

3. Apparatus

The apparatus used in these experiments was primarily designed for measurements on the self-demodulation of radio waves (Aitchison and Goodwin, 1955) but as described below it could also be used without modification to study ionospheric drifts.

Essentially, the equipment consisted of a 5 kW, 1·55 Mc/s transmitter located some 5·6 km from the receiver. For most of the time the transmitter radiated C.W. signals amplitude-modulated at 400 c/s, but in each measurement, for a short period, pulse-modulated signals were transmitted. The receiving equipment included an Eddystone "680" receiver with a vacuum-tube voltmeter and wave-analyser connected to its final I.F. stage for the purpose of measuring variations in the radio frequency and audio frequency levels respectively. Signals were received on a tuned loop-aerial which was adjusted so that the amplitude of the received ground-wave only slightly exceeded that of the sky-wave signal. In this way maximum amplitude changes in the resultant signal occurred during changes in phase path of the sky-wave signal.

In the above arrangement with just a single loop-aerial, only the magnitudes of ionospheric drift velocities could be measured. It should be possible to measure both the magnitude and direction if two loop-aerials are employed. This possibility is discussed in paragraph 8.3.

4. Experimental Methods

It will be assumed that possible small differences between phase path, group path and actual path can be neglected. This assumption is probably well justified for reflections from sporadic-E ionization for which only a very small fraction of the total path occurs in the E_s layer itself.

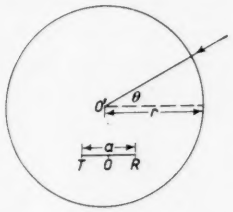

Fig. 2. Arrangement for reception at ground level. The "cone of reception" contains both T and R. (The scale is exaggerated.)

4.1 *Estimation of ΔP, t and P_o*

ΔP is the number of wavelengths change in P, and was measured by counting the number of amplitude fading cycles through which the received carrier level varied per minute. The time $t = 0$ was taken to occur in the 1 min interval for which ΔP was a minimum (approximately zero), when P was also a minimum.

The magnitude of the group path P' was measured by transmitting a pulse-modulated signal for 3 min at 15 min intervals, the audio output of the receiver being displayed on a cathode-ray screen. As stated above, the magnitudes of phase path P and group path P' were assumed to be equal. P_o could then be found, since $P_o = P - \Delta P$.

4.2 *Estimation of virtual height*

Due to the fact that reflections from a cloud can occur even when it is not immediately overhead, there is some uncertainty in estimating the virtual height of reflection. The approximate magnitude of this uncertainty can be estimated in the following manner. In Fig. 2, O' represents the point on the ground vertically below a sporadic-E cloud. The transmitter and receiver were at T and R respectively, but since the distance TR was small, it will first be assumed that the transmitter and receiver were both situated at O. From a discussion in paragraph 6.2 on scattering from E_s clouds, it would follow that a signal reflected from the cloud was only received if the half-angle of the cone of reception was less than 26·6°, so that the corresponding distance OO' was less than r (about 54 km). Clearly, the correct value of group path length would lie between P_o' and P_o' cos 26·6° (= 0·89 P_o'), where P_o' corresponds to the minimum value of $2OC$, in Fig. 1. It follows that $0{\cdot}95P_o'/2$ would represent virtual height (which may be assumed to equal half the group height) to an accuracy of ± 6 per cent.

Considering that O was the midpoint of the finite distance TR, and that an E_s cloud was at point C indicated in Fig. 1, the distance d', actually measured with pulse-modulated signals, was given by:

$$d' = TC + CR - TR = TC + CR - 5{\cdot}6 \text{ km}$$

VOL. 11 1957

where TR is 5·6 km. Since TR was small compared with $TC + CR$, the distance OC was approximately:

$$P'/2 = (TC + CR)/2 = d'/2 + 2{\cdot}8 \text{ km}$$

Thus,
$$P_o'/2 = d'/2 + 2{\cdot}8 - \Delta P/2 \text{ km}$$

where $\Delta P/2$ and $\Delta P'/2$ were assumed to be equal.

It would follow that virtual height could be taken as $0{\cdot}95(d'/2 + 2{\cdot}8 - \Delta P/2)$ km, with an accuracy of ± 6 per cent. In practice, the accuracy would be somewhat less than this, due to the usual errors incurred in measuring d'.

4.3 *The approach or recession of an E_s cloud*

In order to ascertain whether an E_s cloud was approaching or receding, it was necessary to determine whether the phase path P was decreasing or increasing. This was done by adjusting the crystal filter of the receiver to reject the upper sideband of a received signal, thus producing single-sideband reception. It was then possible to decide whether an E_s cloud was travelling towards or away from TR by noting whether the audio level in the receiver led or lagged behind the carrier level during the "cycles" of fading.

It was often unnecessary to use this procedure because the change in P followed a similar pattern for each cloud. When an E_s reflection was first observed, the rate of change of P decreased steadily with time until the rate of change of P became zero, after which the rate steadily increased again until the echo disappeared. The rates of change of P taken at equal times before and after zero time were always about the same in magnitude. The fact that this type of fading and the period of time over which reflections were obtained were similar to those observed by Findlay (1953) strongly suggests that similar E_s clouds were being studied in both sets of experiments.

5. Experimental Results

Measurements of drift velocities were made on twelve nights during the months of May and July, 1954. Table 1 summarizes the results obtained and includes the magnitude of the velocity of each E_s cloud, the corresponding time of closest approach (i.e. "zero" time) and the virtual reflection height. The mean observed drift velocity of 65 ± 22 m/sec is in good agreement with the results of Findlay (1953) and Clark and Peterson (1956).

6. Scattering from E_s Clouds

In this section it is shown that the magnitude of the scattering of radio waves (1·55 Mc/s) from E_s clouds at night is greater than the scattering expected during the day-time.

6.1 *Scattering during day-time*

From the work of Briggs and Phillips (1950) at 2·4 Mc/s and that of Phillips (1954) at 863 kc/s it may be concluded that during day-time conditions the angular spread of a single-hop E-layer reflection would tend to increase roughly inversely proportional to frequency. The assumption will be made that the same dependence

would hold for E_s clouds with dimensions appreciably greater than the wavelength of the reflected wave. FINDLAY's (1953) results indicate that the amplitude of a

Table 1. Data from observations of sporadic-*E* clouds

Date	Local "zero" time	Velocity (m/sec)	t_1 (min)	t_2	virtual height (km)	$2r$ (km) for virtual height 108 km
12/5/54	02·32½	88	12	13	103	197
	03·00	80	14·5	20·5	103	250
15/5/54	02·12½	108	12	18	110	271
19/5/54	00·55	34	3*	26	95	96
	01·07	28	3*	30	95	90
	03·42	64	7·5*	23·5	131	140
	04·22	68	8(+)	15*	130	111
21/5/54	00·42	79	6	9	113	97
	01·21	52	6*	15	130	77
	01·30	59	1*	15	134	65
26/5/54	02·52½	73	6	10·5	120	93
28/5/54	04·02	27	13	13	90	72
14/7/54	00·50½	74	3·5*	6·5	117	58
	00·57	93	3*	5	117	59
15/7/54	00·45½	34	?	6·5	92	?
	02·01½	65	4·5	12·5	92	111
	02·34	61	1·5	7	107	45
21/7/54	00·33	75	5	8	91	99
	00·54	79	8	9	91	136
22/7/54	01·29	69	8	10	83	138
	03·24	73	3	4	105	45
28/7/54	01·00	84	6	6	125	74
29/7/54	00·44	61	10	11	130	91
	02·52	29	10	11	92	61
Mean values		65 ± 22			108	108

* Indicates that these values may possibly be too small, due to the appearance of two clouds almost at the same time

t_1 and t_2 are defined in paragraph 8.1.

wave reflected from an average E_s cloud falls from maximum to zero value at an angle of about 8·2° for a frequency of 2·4 Mc/s; that is, an average E_s cloud would only be observed at 2·4 Mc/s if the transmitter and receiver lay within a vertical

VOL. 11 1957

cone with a half-angle of 8·2°, and apex at the cloud. Such a cone may be regarded as the "cone of reception" of an average E_s cloud, as far as observation by reflected waves is concerned.

The reasoning leading to this estimate of 8·2° is as follows: in his data, Findlay grouped together those E_s clouds which had approximately equal velocities and found that, for each group, the mean velocity v_m, say, and mean period of observation t_m were such that the product $v_m \,.\, t_m$ had the same value (20·4 km) for all groups; that is, the average distance a_m travelled by an E_s cloud while it could be observed was constant. Hence, if the cone of reception of an average E_s cloud intersected the ground in a circular area of diameter $2r$, then both transmitter and receiver would need to lie within this circular area before the cloud could be detected. On the assumption that Findlay ignored E_s clouds with duration times less than one minute, and that the average velocity was about 80 m/sec, then the minimum distance travelled by an average cloud which could be recorded was approximately 5 km. Furthermore, if it is assumed that Findlay's values are typical of a random distribution of directions, then

$$a_m = \int_0^{\chi} 2r \cos\theta \, d\theta \Big/ \int_0^{\chi} d\theta = 1{\cdot}41r$$

where θ is the angle shown in Fig. 2 and $\chi = \cos^{-1}(5/2r)$.

Inserting the expected value of 20·4 km for a_m, the expression then gives $2r = 29$ km, which corresponds to a half-angle of 8·2° for the cone of reception. (Findlay mentioned a value of 6° for the half-angle, on the assumption that $2r = 20{\cdot}4$ km). This applies to the frequency 2·4 Mc/s. Assuming an inverse frequency law, it would thus be expected that at 1·55 Mc/s the frequency used in the present experiments, the half-angle would be 12·8° during the day-time.

6.2 *Scattering at night*

Night-time observations of reflections from the E_s layer were made by Briggs and Phillips (1950) at a frequency of 2·4 Mc/s. The results of these workers indicated a value of 5–7° for the angular spread of a reflected wave, which may be compared with their value of 5° observed during the day-time for E-layer reflections. These results suggested that scattering was slightly greater at night. This view was supported by the work of Phillips (1954) who showed that at a frequency of 863 kc/s the angular spread of reflected waves tended to increase above the day-time value after 21·00 L.M.T. and continued to increase at least until 23·00 L.M.T. The mean angle of spread observed by Phillips for the time interval 22·00–23·00 was about 40 per cent greater than for the interval 18·00 to 21·00 corresponding to day-time conditions.

The scattering observed at night in the present experiments at a frequency of 1·55 Mc/s refers to the months of May and July (i.e. local winter at Adelaide). The mean value of $2r$ was 108 km corresponding to a half-angle of the cone of reception of 26·6°. This is much greater than 12·8°, the value expected in the day-time, and it may be safely concluded that the scattering is considerably greater at night than in the day-time.

7. Overall Rise in Reflection Level

7.1 *Two reflections received simultaneously*

When two reflections, one from the E_s layer and another from some higher level, together with a strong ground-wave were received, most of the fading in the resultant carrier level occurred between the ground-wave and the stronger

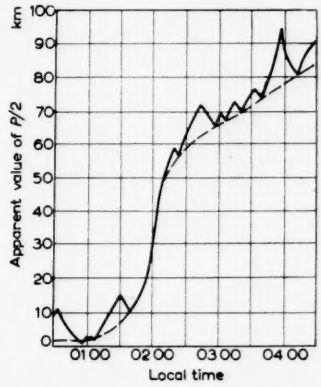

Fig. 3. "Apparent" rise in reflection level during the night of 19 May 1954, with irregularities due to E_s clouds. (The full line is through points at 3 min intervals.)

VOL. 11 1957

reflection. By following the procedure described in paragraph 4.3 it was possible to decide whether each observed fading cycle represented an increase or decrease in the length of phase path P of the relevant reflected wave. It was, of course, impossible to record all fading cycles for both reflected waves, but a rough indication could be obtained of the change in $P/2$ with time, regardless of reflection level.

On all twelve nights of the present observations, an overall increase in $P/2$ similar to that shown in Fig. 3, always occurred after approximately 01·00 L.M.T. Fig. 3 shows the resulting curve for 19 May 1954, and it will be seen that a rapid increase of about 40 km in $P/2$ took place between 01·40 and 02·07. Superimposed upon the overall increase were irregular changes which could be attributed to the passage of E_s clouds since they were shown by pulse-modulated transmissions to coincide with strong single-hop E-layer reflections. The trough of each irregularity contained the instant of closest approach of an E_s cloud, when the phase path of the wave reflected from it was momentarily constant in length. In the corresponding 3 min interval, the changes observed in P were due, almost entirely, to the higher reflected wave. By interpolating between values of ΔP known to apply to the higher reflection, the overall increase in $P/2$ during the interval 01·00 to 04·30 L.M.T. on 19 May 1954 was estimated at 130 km. Since observations on the group height of the F-layer, carried out during the same interval, showed a steady increase from 220 to 250 km, it seems likely that the large increase in $P/2$ could best be explained in terms of multiple reflections from the F-layer.

It should be added that the fading effects observed here involving two reflected waves cannot be explained in terms of fading between the components of a magneto-ionically split wave. At a frequency of 1·55 Mc/s which is close to the local gyro-frequency, absorption is expected to make the amplitude of the extraordinary (E)

component negligibly small compared with the ordinary (O) component, because k_E/k_O is of the order of 1000 at Adelaide for a deviating E-region where k_E and k_O are the absorption coefficients for the two components.

7.2 *Errors in velocities of E_s clouds*

Errors in estimating $\Delta P/2$ for reflections from E_s clouds could occur if allowance was not made for simultaneous reflections from the higher level. For that reason the velocities of E_s clouds were calculated only when the amplitude of the E_s-reflected wave was more than three times that of the higher reflected wave, or when there was apparently negligible movement of the higher reflection level. The increase in phase path of the higher reflected wave was also allowed for in all calculations.

8. A Possible Method for Finding Directions of Motion of E_s Clouds

8.1 *Direction angle θ*

Consider a transmitter (T) and receiver (R) separated by a distance a, indicated in Fig. 2. A signal radiated from T will be received at R after reflection from an E_s cloud only if T and R lie within the cone of reception of the cloud, which is assumed to intersect the ground in a circle with centre at O' and radius r. O is the midpoint of TR.

Clearly, the time during which signals radiated from T will be received after reflection from the cloud will depend on the direction of motion of the cloud with respect to TR. The time will be a minimum if the cloud is moving in the direction of the line TR, and a maximum for movement at right angles to this direction. Consider now the general case of the cloud moving at an angle θ to the direction of TR. The total time during which reflections will be received from the cloud will depend not only on the direction of motion, but also on the distance of closest approach to the line TR. The total time will be given by $(t_1 + t_2)$ where t_1 and t_2 represent the two unequal time intervals from the first appearance of the cloud to its closest approach, and from its closest approach to final disappearance, and we define t_1 as the smaller interval and t_2 as the larger.

It can be shown from geometrical considerations that for a cloud moving with velocity v,

$$vt_1 = \{r^2 - (r\cos\phi + a\sin\theta)^2\}^{1/2} - (a/2)\cos\theta \tag{2}$$

If $0 < \theta < \phi$, or $(\pi - \phi) < 0 < \pi$, then

$$vt_2 = \{r^2 - (r\cos\phi - a\sin\theta)^2\}^{1/2} - (a/2)\cos\theta \tag{3}$$

or, if $\phi < \theta < (\pi - \phi)$, then

$$vt_2 = \{r^2 - (r\cos\phi + a\sin\theta)^2\}^{1/2} + (a/2)\cos\theta \tag{4}$$

where $$\phi = \cos^{-1}\left\{\frac{1}{r}(d - (a/2)\sin\theta)\right\} \tag{5}$$

and d is the distance of nearest approach, which is assumed to be the minimum value of OO'. This assumption generally involved a negligibly small error in the

present experiments since OO' was much greater than TR for all except a very few clouds. The direction angle θ may be found from equation (2) and equation (3) or (4).

8.2 *Calculation of* θ

Instead of calculating θ for each E_s cloud, a more satisfactory estimate may be made by averaging the data over many clouds, and substituting in the equations of paragraph 8.1. For this purpose it may be assumed from considerations in paragraph 6.1 that while being observed, the average distance travelled by an E_s cloud is $1{\cdot}41r$. By using the data from Table 1, the mean value of θ for eleven clouds observed in July, was $25 \pm 20°$. In the present results, with manual recording of the fading cycles, t_1 and t_2 were only measured to within an accuracy of $\pm 0{\cdot}5$ min, and no accurate estimates of the direction of motion of the clouds could be made. However, if the fading cycles are recorded photographically or with a pen recorder it should be possible to deduce accurately the direction of drift of the E_s clouds.

8.3 *A proposed method for finding directions unambiguously*

When θ has been determined, the direction of motion of an E_s cloud still has four possible values, and may be at an angle of θ, $(\pi + \theta)$, $-\theta$ or $(\pi - \theta)$ to the direction of TR. In order to find the direction of motion explicitly, a third variable must be known besides t_1 and t_2. It is suggested that instead of using only one loop-aerial as in the present experiments, two spaced loop-aerials could be used, the distance between the aerials being at an optimum angle of $\pi/4$ to TR. The third variable would be the time displacement between the fading patterns of the resultant carrier levels, C_1 and C_2, received at the two loop-aerials and amplified in two receivers, where C_1 and C_2 are each the resultant of the reflected wave and the ground-wave. At 1·55 Mc/s satisfactory results would probably be obtained with photographic or pen recordings if the loop-aerials were 100–150 m apart, while at higher frequencies the required separation would be proportionately smaller.

The above procedure would have the advantage of requiring only two spaced loop-aerials at one receiving station. If three spaced loop-aerials were used, then directions of motion could be found directly by measuring the time displacements between three resultant carrier levels, C_1, C_2, and C_3, and it would not then be necessary to consider the equations given in paragraph 8.1. The method described in this paper should be particularly useful on occasions when many E_s clouds may be expected, such as during periods of increased meteor activity.

Acknowledgements—Thanks are extended to Professor L. G. H. Huxley for his keen interest and supervision in the work, to Dr. G. J. Aitchison who operated the transmitter on the twelve nights of observation, and to the Australian Radio Research Board for financial assistance in purchasing equipment. The author also thanks Dr. W. J. G. Beynon of the University College, Swansea, for valuable advice regarding the presentation of the paper. The author was assisted by a Research Grant from the University of Adelaide, and by a scholarship from the Radio Research Board of Australia.

VOL. 11 1957

References

Aitchison G. J. and Goodwin G. L.	1955	*Nuovo Cim.* **1,** 4, 722.
Briggs B. H. and Phillips G. J.	1950	*Proc. Phys. Soc.* B **63,** 907.
Clark C. and Peterson A. M.	1956	*Nature, Lond.* **178,** 486.
Ferrell O. P.	1948	*Proc. Inst. Radio Engrs., N.Y.* **36,** 879.
Findlay J.W.	1953	*J. Atmosph. Terr. Phys.* **3,** 73.
Gerson N. C.	1950	*Nature, Lond.* **166,** 316.
Krautkrämer J.	1950	*Arch. Elect. Übertr.* **4,** 133.
Mitra S. N.	1949	*Proc. Inst. Elect. Engrs.* **3,** 96, 441.
Phillips G. J.	1954	Report of Physical Society Conference (Cambridge), p. 174.
Rao B. R. and Rao E. B.	1954	*J. Sci. Industr. Res.* A **13,** 462.

Journal of Atmospheric and Terrestrial Physics, 1957, Vol. 11, pp. 187 to 191. Pergamon Press Ltd., London

Diurnal absorption in the *D*-region

J. W. Warwick and H. Zirin
High Altitude Observatory, University of Colorado,
Boulder, Colorado

(*Received* 29 *June* 1957)

Abstract—We have analysed the diurnal variation of cosmic noise at a frequency of 18 Mc/s. From these records we derive the electron density as a function of local time and height in the *D*-region. We also derive a one-parameter, exponential approximation to the vertical distribution of the ionizable constituent, nitric oxide. The electron density curves fit those derived in different ways by other groups. We predict that the recombination coefficient, within the *D*-region, is either constant, or increases with height.

1. Introduction

Since December, 1955, Lee (1957) has operated an SCNA (sudden cosmic noise absorption) recorder in Boulder. The equipment continuously records the flux of cosmic noise, at 18 Mc/s, received by a low-gain antenna whose main lobe is directed vertically upward. The antenna consists of two half-wave dipoles, separated by one half-wave at 18 Mc, and mounted 1/10-wave above a ground plane. The beam width between the half-power points amounts to about 90°. The receiver consists of a modified surplus high-frequency ARR-7. The output time-constant circuits operate very rapidly in the downwards direction, but respond slowly to an increase in receiver level. These circuits, together with a swept-frequency local oscillator, permit the receiver to record only interference-free channels.

VOL. 11 1957

The records obtained since January, 1956, show not only the sidereal variation of cosmic noise impinging on the ionosphere from outside, but also diurnal absorption of the radio waves, and sudden variations (SCNA's) that characteristically occur during solar flares. Although the latter records are of great interest to us, and will be the subject of later reports, we shall concern ourselves here with the analysis of the diurnal absorption only. Furthermore, we restrict ourselves to the analysis of records obtained in late June, 1956. Although many useful records have been taken at other times during the year, this interval is of particular interest to us because of a very well-observed solar flare, that occurred in conjunction with an SCNA on 24 June 1956.

Our technique for determining the absorption is identical to that of Mitra and Shain (1953). We assume that the night-time records of cosmic noise are free of absorption. The difference between sidereal and local time changes by 12 hr in six months. Therefore, the night-time records during December represent absorption-free levels comparable with daytime observations during June. We find that the absorption observed in June at dawn is zero, within the precision of calibration.

The points labelled x in Fig. 1, at the end of the report, present the observations of diurnal absorption, averaged for nine days from 19 June 1956 to 27 June 1956, inclusive. Individual curves, for each day, reproduce the shape of the average curve with very little variation. Our results should be compared with those of

Mitra and Shain, Fig. 8(b). These authors believe that maximum absorption occurs a few minutes after local noon. Our records, suggest, if anything, an asymmetry in the opposite sense. We do not feel that a delay found in this way is significant.

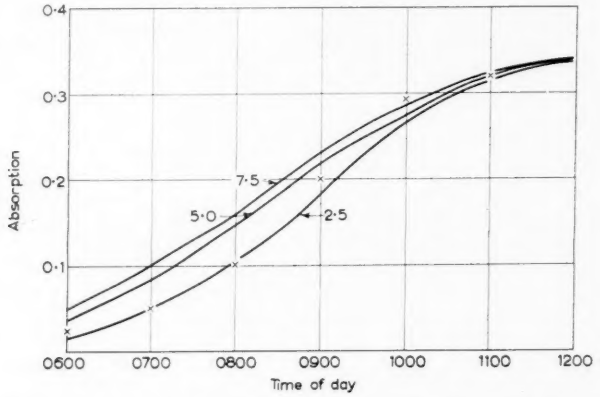

Fig. 1. Observed and predicted diurnal absorption as a function of local time. × observed data. Curves labelled with nitric oxide scale heights in kilometers.

2. Assumptions and Basic Analysis

The absorption data do not allow us to separate *D*-region absorption from absorption produced in the other layers of the ionosphere. However, Mitra and Shain show that the *F*-layer makes only a small, and virtually constant, contribution to the total absorption. The diurnal variation in our absorption records therefore allows us to study the *D*-layer by itself.

We shall assume that Lyman-alpha creates the normal *D*-region. This assumption is consistent with the conclusions of Friedman (1954). Nicolet (1945) and Bates (1954) suggest that Lyman-alpha produces the *D*-region electrons by photo-ionization of nitric oxide (NO). Since nitric oxide is a minor constituent of the *D*-region, the absorption of Lyman-alpha is produced by the normal atmospheric constituents, mainly O_2, a result consistent with rocket observations (Friedman, 1954). However, the nitric oxide is only weakly ionized (unlike a Chapman region). These assumptions enable us to compute, to within a constant, the Lyman-alpha flux at each level in the *D*-region.

3. Analysis of Diurnal Absorption Curves

Equilibrium between photo-ionization and two-body recombination determines the ionization in the *D*-region. In the general case, when these two mechanisms are not in balance, we write

$$\frac{dN}{dt} = q - \alpha N^2 \tag{1}$$

where N is the electron density, q is the rate of production of electrons by Lyman-alpha ionization, and α is the recombination coefficient. The possibility of removal of electrons by electron attachment does not alter the form of the equation. In

the present case, the absorption varies slowly through the day. Therefore, neglecting the time derivative of the electron density, we have

$$q = \alpha N^2 \tag{2}$$

The rapid recovery of the ionosphere, with respect to flare effects, suggests that this assumption is valid, except, perhaps, for the first hour after dawn. Since 18 Mc/s is high in comparison with both the collisional and gyro frequencies, we can write the power absorption in nepers along an average path within our antenna beam,

$$A = \sec\bar{\theta}\,\frac{4\pi e^2}{mc}\,\frac{1}{\omega^2}\int N\omega_c\,dh = \sec\bar{\theta}\,\frac{4\pi e^2}{mc}\,\frac{\sigma}{\omega^2}\sqrt{\frac{8k}{\pi m}}\,\frac{1}{\bar{\mu}m_H}\int N\rho\sqrt{T}\,dh \tag{3}$$

Here, ω is the circular frequency of the wave, ω_c is the collisional frequency, and σ is the collisional cross-section for electrons against atmospheric particles. We assume (Mitra, 1952) that $\sigma = 7 \times 10^{-16}$ cm^2. $\bar{\mu}$ is the mean molecular weight through this region of the ionosphere; we take the value 28·966 from Whipple (1954). $\bar{\theta}$ represents the average angle that the ray path of the cosmic noise within our antenna beam makes to the vertical; we assume that $\bar{\theta} = 30°$. Inserting numerical values in equation (3), and the relation (2) for N, we find that

$$\begin{aligned} A &= 8{\cdot}89 \times 10^{-5}\int N\rho\sqrt{T}\,dh \\ &= 8{\cdot}89 \times 10^{-5}\int\frac{\sqrt{q(t)}}{\alpha}\,\rho\sqrt{T}\,dh \end{aligned} \tag{4}$$

We may write

$$q = B\Phi(h)Ce^{-p(h)\sec\chi} \tag{5}$$

where $B\Phi(h)$ represents the vertical distribution of NO, C is the product of the probability of photo-ionization (per unit incident flux) and the Lyman-alpha flux outside the atmosphere, and $p(h)$ is the optical depth in Lyman-alpha measured from the top of the atmosphere down to height h. χ is the zenith distance of the sun. Since zenith distance is a function of time only, we write equation (4) in the form

$$A(\chi) = 8{\cdot}89 \times 10^{-5}\sqrt{\frac{BC}{\alpha}}\int\Phi(h)e^{-\frac{1}{2}p(h)\sec\chi}\rho\sqrt{T}\,dh \tag{6}$$

where we have also assumed that α is independent of height. This basic assumption will be discussed below. All quantities, except for $\Phi(h)$, are known. We take ρ and T from Whipple's table (1954).

We fitted $\sqrt{\Phi(h)}$ with both quadratic and exponential functions of height. Of these two forms, only the exponential,

$$\Phi(h) = \exp\left(-\frac{h - 64\text{ km}}{H}\right) \tag{7}$$

gave a satisfactory fit to the observations. In Fig. 1, along with the observed values of the absorption, we show the predicted variation of the absorption during the day for scale heights 2·5, 5·0, and 7·5 km. Note that the smaller values fit the observed

VOL. 11 1957

points far better than the values found with the normal atmospheric scale height, but that this conclusion rests primarily on absorption measures for the early hours of daylight, from 06.00 to 10.00. We conclude that $H = 2{\cdot}5$ km.

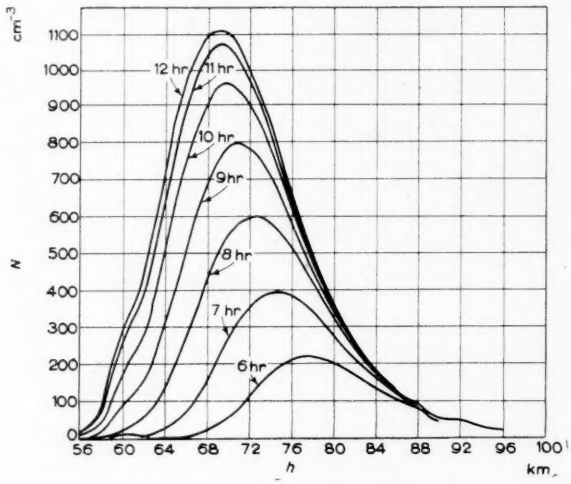

Fig. 2. Electron density as a function of height and local time.

The absolute value of the electron density, $N(h)$, is set by the condition that it fit the observed absorption at noon. This condition determines the constant $\sqrt{\frac{\overline{BC}}{\alpha}} = 14{,}641$ cm^{-3}. This enables us to use equations (2) and (5) to compute $N(h)$. Fig. 2 exhibits the electron density profile as a function of height at several times during the day.

4. Discussion

In order to interpret $\Phi(h)$ as the distribution in height of NO, we must assume that the recombination coefficient is constant with height. Although the question is not definitely settled, Mitra and Jones (1954) suggest that the recombination coefficient decreases nearly exponentially with height. If we assume that the ionizable particles also decrease exponentially with height, we can regard our solution for the height-dependence, $\Phi(h)$, as a determination of the height-dependence of n/α, where n is the nitric oxide density. Therefore the derived value, $H = 2{\cdot}5$ km, is really the scale height of n/α. Nicolet states that the vertical distribution of NO should be given by the normal atmospheric density gradient through the D-region. In this event, $H_{NO} = 7$ km. If H_α is the scale height for the recombination coefficient, we can then set $\frac{1}{H_{NO}} - \frac{1}{H_\alpha} = \frac{1}{2{\cdot}5}$. Then, H_α would be about $-2{\cdot}5$ km. In fact, any scale height for NO, $H_{NO} > 2{\cdot}5$ km, will lead to a negative scale height for the recombination coefficient. Therefore, barring the unlikely event that the recombination coefficient increases upwards, 2·5 km is the maximum NO scale height that is consistent with our observations. This implies that α is independent of height within the D-region. This conclusion may be

consistent with the individual points plotted by MITRA and JONES (1954), even though the overall trend of their values of α is obviously downward. Their observations were taken at different heights, and by widely different methods; their results hardly specify the detailed variation of α over short intervals in height, say, within the *D*-region.

The question remains as to why the scale height for nitric oxide is much smaller than the scale height predicted by NICOLET on apparently valid physical grounds. Nicolet notes that the lifetime of a NO molecule is of the order of six months in the *D*-region. Over such a long interval, dynamical mixing effects present in the normal atmosphere would establish a NO gradient essentially identical to the normal atmospheric gradient. If the lifetime of a NO molecule were much shorter than six months (which might be the case if the computed cross-sections for equilibrium formation of NO are greatly in error), then the scale height of NO would be given by its dissociative equilibrium. Since the NO is formed by the interaction of several atmospheric constituents, its scale height would then be much less than the normal atmospheric scale height.

This work was supported by the Air Force Cambridge Research Center, Electronics Research Directorate, through Contract AF 19(604)–1491.

VOL. 11 1957

REFERENCES

BATES D. R. 1954 *The Earth as a Planet* p. 614. The University of Chicago Press, Chicago.

FRIEDMAN H. 1954 *Report of the Commission for the Study of Solar-Terrestrial Relations* p. 64. J. and R. Sennac, Paris.

LEE R. H. 1957 *Electronics* **30,** 162.

NICOLET M. 1945 *Mem. Roy. Met. Inst.* **19,** 1.

NICOLET M. 1953 *Aeronomical Problems of Nitrogen Oxides* Scientific Report No. 52, Ionosphere Research Laboratory, State College, Pennsylvania; published under AMC Contract AF 19(122)–44.

MITRA S. K. 1952 *The Upper Atmosphere* (2nd Ed.) p. 258. The Asiatic Society, Calcutta.

MITRA A. P. and JONES R. E. 1954 *Trans. Inst. Radio. Engrs., N.Y.* **2,** 99.

MITRA A. P. and SHAIN C. A. 1953 *J. Atmosph. Terr. Phys.* **4,** 204.

WHIPPLE F. L. 1954 *The Earth as a Planet* p. 500. The University of Chicago Press, Chicago.

Journal of Atmospheric and Terrestrial Physics, 1957, Vol. 11, pp. 192 to 199. Pergamon Press, Ltd., London

Measurements of the absolute intensity of the aurora and night airglow in the 0·9–2·0 μ region

A. W. Harrison and A. Vallance Jones*
University of Saskatchewan, Saskatoon

(*Received* 3 *June* 1957)

Abstract—Absolute intensity measurements have been made at Saskatoon of the bands of $\Delta v = 2$ and $\Delta v = 3$ sequences of the OH vibration-rotation bands of the night airglow. The relative intensities are in reasonable agreement with the calculations of Heaps and Herzberg (1952). The rate of production of OH molecules excited to the ninth vibrational level was estimated from the intensity of the 4,2 band to be 15×10^{11} molecules/cm^2 column sec. Spectra of the aurora in the 0·9 μ–2·0 μ region have been obtained with a spectrometer employing a PbS cell detector. The spectra show several new bands of the Meinel N_2^+ system and a strong emission at 1·04 μ to which both the 0,0 $1PG$ N_2 band and the ^2P–^2D NI doublet probably contribute. Absolute intensity measurements of the infra-red auroral bands are in reasonable agreement with estimates based on extrapolations from bands at shorter wavelengths.

Introduction

Measurements of the absolute intensity of night airglow and auroral emissions provide data which are required for the discussion of excitation processes responsible for the radiation. For the OH bands (which are predominant in the infra-red night airglow spectrum) the relative intensities have been calculated by Heaps and Herzberg (1952). Measurements of the absolute intensities of these bands in the 1·0–2·0 μ region make possible a test of these predictions for the intensities of the $\Delta v = 3$ and $\Delta v = 2$ sequences of OH bands as well as giving data for a more accurate estimate of the absolute intensity of the unexplored $\Delta v = 1$ sequence beyond 3·0 μ.

A number of investigations have been made of the night airglow spectrum between 0·9 and 1·1 μ (Kron, 1950; Meinel, 1950; Krassovsky, 1955; Dufay, 1957). Auroral spectra in the 0·9–1·1 μ region have been obtained by Bagariaçki and Fedorova (1955) with the help of a spectrograph equipped with a CsO–Ag image converter.

Absolute intensity measurements of features of the visible auroral spectrum have been made recently by a number of investigators (Hunten, 1955; Omholt, 1954; Ashburn, 1955). The absolute intensity of the OH bands in the photographic infra-red region has been estimated by Heaps and Herzberg (1952) from the results of Meinel (1950). Measurements of the integrated intensity in the region between 1·0 and 3·0 μ made with the help of a PbS cell and a wide band filter have been reported by Osherovich and Rodionov (1954).

In this paper further observations of the night airglow spectrum at Saskatoon between 1·0 and 2·0 μ are reported. The spectral brightness of the emission has

* The research reported in this paper has been sponsored by the Geophysics research Directorate of the Air Force Cambridge Research Center, Air Research and Development Command, under Contract AF 19(604)–1831.

been obtained in absolute units as a function of wavelength for spectral slits widths of 100 and 200 Å. Measurements of bands of the infra-red auroral spectrum have also been made, including some not previously observed.

2. Instrumentation

The spectrometer which uses a PbS cell detector has been described by Gush and Vallance Jones (1955). A Corning 7–56 filter was used to eliminate higher spectral orders. The absolute intensity measurements were made by calibrating a secondary standard low-brightness source against a black body. The calibration of the low-brightness source was carried out with the spectrometer by following a procedure similar to that adopted by Shepherd (1954). The black-body source employed was a cavity maintained at temperatures ranging from 250 to 350°C. It is estimated that the intensity calibration should be accurate to within 10 per cent. The standard low-brightness source was used to make intensity calibrations of the spectrometer at frequent intervals during the course of each night on which auroral or night airglow spectra were obtained.

3. Night Airglow Spectrum

The night airglow spectrum, obtained with a spectral slit width of 100 Å, from 1·1 to 2·0 μ is shown in Fig. 1. In this figure the ordinates represent differential brightness (i.e. brightness/unit wavelength) referred to the zenith expressed in rayleighs/micron.* A spectrum obtained with a spectral slit width of 200 Å is reproduced in Fig. 2. The ordinate of the latter spectrum is differential brightness, expressed in units of W/cm^2 steradian micron. These units were chosen to make this spectrum directly comparable with the results of Osherovich and Rodionov (1954). Figs. 1 and 2 were obtained by averaging a large number of spectra obtained at a zenith angle of 80°; the intensities have been referred to the zenith by multiplying by cos 80°.

The absolute intensity of the OH emission is subject to fluctuations during the course of the night and from night to night. Fig. 6 shows the results of measurements of the intensity of the emission, at a wavelength of 1·68 μ, during the course of a year. These measurements were made 2 hr after sunset on nights which were apparently very clear. Although no systematic seasonal variation appears to be evident, it is of interest to note the magnitude of the fluctuations.

These results may be compared with the measurements made by Osherovich and Rodionov (1954), who made a measurement of the total radiation between 1·0 and 3·0 μ. The comparison was made by weighting the results from Fig. 2 by the sensitivity curve of the photometer used by Osherovich and Rodionov. An approximate integration between 1·0 and 2·0 μ then yielded a value of $3{\cdot}4 \times 10^{-2}$ erg/cm^2 steradian sec. This value is consequently the result which one would expect to obtain with Osherovich and Rodionov's apparatus, if it were exposed to radiation having the spectral composition of Fig. 2. This value should be multiplied by a small factor to take account of the additional bands between 2·0 μ and 3·0 μ to which their apparatus was sensitive. Since Osherovich and Rodionov actually

* The brightness in rayleighs (Hunten, Roach, and Chamberlain, 1956) equals $4\pi B$, where B is the angular surface brightness of the emitting layer in units of 10^6 photons/cm^2 steradian sec.

VOL. 11 1957

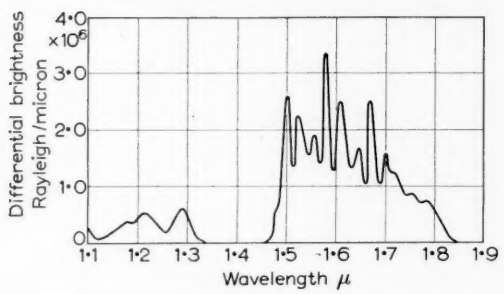

Fig. 1. Night airglow spectrum from 1·1 to 2·0 μ obtained with a spectral slit width of 100 Å. Differential brightness measured in rayleigh/micron referred to the zenith.

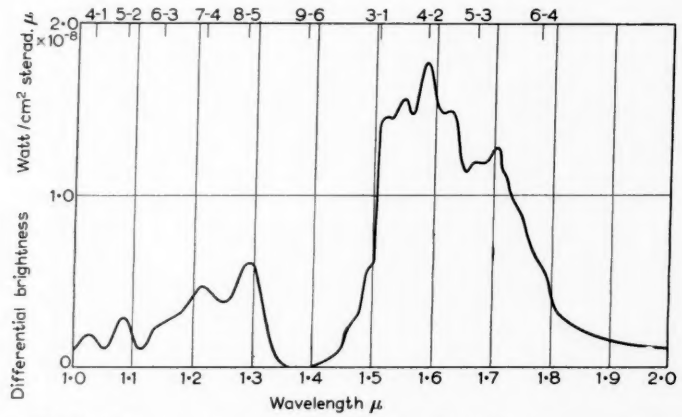

Fig. 2. Night airglow spectrum from 1·0 to 2·0 μ obtained with a spectral slit width of 200 Å. Differential brightness measured in W/cm² steradian micron referred to the zenith.

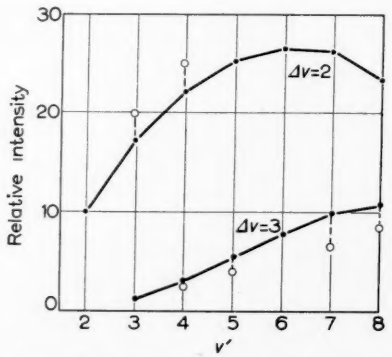

Fig. 3. Predicted and observed relative intensities of $\Delta v = 2$ and $\Delta v = 3$ sequences of OH bands. Solid curve: Intensities calculated by Heaps and Herzberg (1952); Circles: Measured relative intensities ○ observed, — ● — calculated.

obtained a value of $5{\cdot}0 \times 10^{-2}$ erg/cm^2 steradian sec it is seen that there is satisfactory agreement between the two sets of measurements, especially in view of the nightly fluctuations of intensity noted above.

Another interesting comparison is that which may be made with the predicted calculated intensities of HEAPS and HERZBERG (1952). Their calculation was made on the assumption that the OH molecules are all formed in the ninth vibrational level of the ground electronic state; a linear variation of the dipole moment of the OH molecule with internuclear distance was also assumed. Fig. 3 shows the calculated and observed relative intensities of some $\Delta v = 2$ and $\Delta v = 3$ bands of OH derived from Fig. 2. The OH bands measured are fairly free from atmospheric absorption.

Fig. 3 shows a very satisfactory agreement between predicted and observed intensities in view of the approximations involved in the theory and the uncertainties introduced into the experimental results by the difficulty of correcting for atmospheric absorptions. It is noteworthy that the tendency found by HEAPS and HERZBERG for the $\Delta v = 4$ sequence to be stronger than calculated relative to the $\Delta v = 5$ sequence is also found to be maintained here in the relation between the $\Delta v = 2$ and $\Delta v = 3$ sequences.

Finally, another estimate of the population rate of the ninth vibrational level may be made from the measured intensity of the 4,2 band. The emission rate for this band which is almost unaffected by atmospheric absorption was estimated to be 175 kR (kilorayleigh) by comparing the peak intensity of the band from Fig. 1 with the area under a synthetic spectrum of the same band for a temperature of 260°K. The production rate of excited OH molecules in the ninth vibrational level was then estimated by the same method as that employed by HEAPS and HERZBERG who applied the procedure to an estimate of the intensity of the 4,0 band. The result obtained from the 4,2 band is 15×10^{11} molecules/cm^2 column sec compared to the value of $8{\cdot}3 \times 10^{11}$ molecules/cm^2 column sec derived by HERZBERG.

ROACH (1956) has recently given an estimate of the intensity of the OH bands based on the filter photometer measurements of ROACH, PETTIT, and WILLIAMS (1950) and the theoretical calculations of SHKLOVSKY (1956). His value for the 4,2 band is 20 kR compared to our value of 175 kR. This difference may be a latitude effect or may arise from an accumulation of errors in the indirect method by which ROACH's estimate was made.

4. AURORAL SPECTRUM

A composite spectrum of the aurora in the 0·9–1·2 μ region is shown in Fig. 4. The spectral slit width was 100 Å. These spectra were obtained from the brighter outbursts of aurora using a one-minute scanning time. Since such bright outbursts are very transitory it was not possible to record all the features during a single scan. Fig. 4 was obtained, therefore, by averaging a large number of spectra which showed individual bands strongly. Consequently it is unlikely that this spectrum represents correctly the instantaneous relative intensities. It is possible that other weak features are present beyond 1·1 μ. Fig. 5 is a reproduction of a microphotometer tracing of a photographic spectrum obtained on a Kodak

VOL. 11 1957

1Z(3) plate using the 5 in. Schmidt spectrograph at Saskatoon. This spectrum covers the wavelength range between 1·0 and 1·1 μ with an estimated spectral slit width of 10 Å. It was obtained during the strong auroral display of 19/20 January 1955.

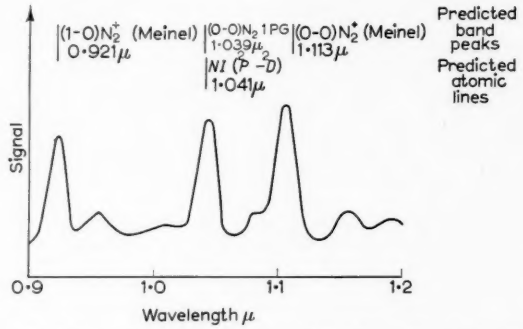

Fig. 4. Composite infra-red auroral spectrum 0·9–1·2 μ. Spectral slit width 100 Å.

Suggested identifications of the emission features are indicated in Fig. 4.

The identity of the 1·04 μ feature is somewhat uncertain because, as is shown in Fig. 5, both the 0,0 first positive group $(1PG)N_2$ band and the forbidden ^2P–^2D *NI* doublet lie close to this wavelength. The narrowness of the emission feature

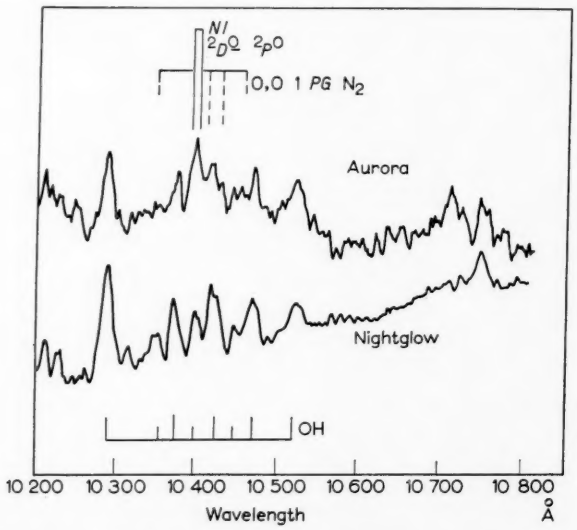

Fig. 5. Microphotometer tracing of photographic spectrum of aurora and night airglow in the region of 1·0 μ.

at this wavelength in Fig. 5 supports the identification with the *NI* doublet for the photographic spectrum. On the other hand, arguments in section 5 based on the absolute intensity of the band suggest that the emission of the 0,0 $1PG$ N_2 band should be easily observed by the spectrometer. It is possible that the

strongest feature in this region averaged over the time of a photographic exposure is the *NI* doublet but that the 0,0 1*PG* N_2 becomes more intense for short periods especially for type B red aurora. The spectrometer would then detect the N_2 band. Evidence that the 1*PG* bands do behave in this way has been obtained by HUNTEN (1955). Image-converter spectra of aurora obtained by BAGARIAÇKI and FEDOROVA (1955) also show a narrow emission at 1·04 μ which is interpreted by them as being due to the *NI* doublet. Their results should be comparable with the photographic spectrum since they required a two-night exposure to record the spectrum.

Table 1. Calculated intensities of N_2^+ (Meinel) bands

v' \ v''	0	1	2	3
0	λ11109 Å 282	14648 256		
1	9190 162	11486 <1	15237 124	
2		9475 42	11889 21	15873 21
3			9780 27	12324 21

VOL. 11 1957

The remaining emission features of Fig. 4 can be satisfactorily interpreted as bands of the Meinel N_2^+ system. In Table 1 are set out calculated intensities of the most intense bands of the system in the 0·9–2·0 μ region.

These intensities were calculated from a consideration of the intensities of the

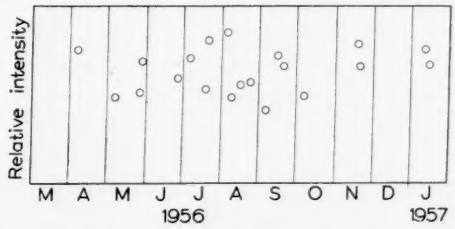

Fig. 6. Variations in the brightness of the night airglow spectrum at 1·68 μ from March 1956 to January 1957.

bands in the visible region (MEINEL, 1951) and *p*-values published by FRASER, JARMAIN and NICHOLLS (1954); they were corrected roughly for absorption by water vapour from the data of GEBBIE *et al.* (1951). It may be seen that the observed spectrum agrees well with the qualitative predictions of Table 1. In particular, the 0,0 band at 1·11 μ is undoubtedly present. The failure of BAGARIAÇKI and FEDOROVA to observe this band must have been due to the decreased sensitivity of their apparatus at this wavelength.

5. Absolute Intensities of Auroral Emissions

The absolute intensities of the auroral emissions were measured by comparison with the standard low-brightness source. The maximum absolute intensities recorded are set out in Table 2. As pointed out in Section 4, the intensity of the aurora fluctuates so quickly that little significance can be attached to the relative intensities.

Table 2. Absolute intensities of auroral emissions in 0·9–2·0 μ region

Emission feature	Type of aurora	Maximum brightness (kR)
0·92 μ N_2^+ (1,0)	RA, 20° elevation, north intensity 2–3	440
1·105 μ N_2^+ (0,0)	RA, intensity 3	364
1·04 μ N_2 and/or NI	RA, intensity 2–3 20° elevation, north	410

These intensities may be used as a check on the identifications by comparing them with values predicted on the basis of intensity measurements of bands in the visible region of the spectrum by Hunten (1955). The intensity of the v', v'' vibrational band, $I(v', v'')$ is given by the expression,

$$I(v', v'') = kN(v') \, . \, p(v', v'') \tag{1}$$

where k is a constant for a particular band system, $p(v', v'')$ is the relative vibrational transition probability for the band, and $N(v')$ is the population of molecules in the vth vibrational level of the upper electronic state.

For the 1 *PG* N_2 system $I(3,0)$ was observed by Hunten to be 250 kR in a very bright type B red aurora. $I(0,0)$ would then be given by the relation,

$$I(0,0) = I(3,0) \, N(0) \, . \, p(0,0)/N(3) \, . \, p(3,0) \tag{2}$$

The value of $p(0,0)/p(3,0)$* may be calculated from the table of Jarmain and Nicholls (1951) to be about 7. $N(0)/N(3)$ may be estimated by extrapolating the population ratios obtained by application of equation (1) to the intensity measurements of Hunten and of Meinel (1951); a value of 29 is thus obtained for this ratio. Consequently the predicted intensity of the 0,0 1 *PG* band should be $250 \times 29 \times 7$ kR. The value in Table 2 is 410 kR. Thus the observed emission was weaker by a factor of 125 than should have been observed from the intense type B aurora studied by Hunten. The intensity in Table 2 is therefore consistent with the emission to be expected from aurora of intensity II or even III, if it is remembered that the aurora observed by Hunten was a type B red aurora in which the 1 *PG* bands were probably enhanced.

For the Meinel N_2^+ bands similar calculations can be made using the relation analogous to equation (2), since the intensity of the 4,0 band was also measured by Hunten. The ratio $p(0,0)/p(4,0)$ is in this case about 16 (Fraser, Jarmain and Nicholls, 1956) while extrapolation of Meinel's results for the $\Delta v = 2$ sequence gives $N(0)/N(4)$ to be about 30. The measured intensity for the 4,0 band

* The p-values used were calculated assuming a constant value for the electronic transition moment.

was 26 kR, so that the corresponding intensity of the 0,0 band should be $26 \times 30 \times 16$ kR. This is 34 times the value in Table 2. This factor is also consistent with the estimates of the intensities of the aurorae studied by HUNTEN and ourselves. Further support is provided, therefore, for the identification of the 1·105 μ emission with the 0,0 band of the MEINEL N_2^+ system.

REFERENCES

ASHBURN E. V.	1955	*J. Atmosph. Terr. Phys.* **6,** 57.
BAGARIAÇKI B. A. and FEDOROVA N. I.	1955	*Dokl. Akad. Nauk, SSSR.* **103,** 1009.
DUFAY M.	1957	*C. R. Acad. Sci., Paris* **245,** 364.
FRASER P. A., JARMAIN W. R. and NICHOLLS R. W.	1954	*Astrophys. J.* **119,** 286.
GEBBIE H. A., HARDING W. R., HILSUM C., PRYCE A. W. and RUBERTS V.	1951	*Proc. Roy. Soc.* A **206,** 87.
GUSH H. P. and VALLANCE JONES A.	1955	*J. Atmosph. Terr. Phys.* **7,** 285.
HEAPS H. S. and HERZBERG G.	1952	*Z. Phys.* **133,** 48.
HUNTEN D. M.	1955	*J. Atmosph. Terr. Phys.* **7,** 141.
HUNTEN D. M., ROACH F. E. and CHAMBERLAIN J. W.	1956	*J. Atmosph. Terr. Phys.* 8, 345.
JARMAIN W. R. and NICHOLLS R. W.	1954	*Canad. J. Phys.* **32,** 201.
KRASSOVSKY V. I.	1955	*The Airglow and the Aurorae* p. 87. Pergamon Press, London.
KRON G. E.	1950	*Pub. Astron. Soc. Pac.* **62,** 264.
MEINEL A. B.	1950	*Astrophys. J.* **111,** 555; **112,** 120.
MEINEL A. B.	1951	*Astrophys. J.* **114,** 431.
OMHOLT A.	1954	*J. Atmosph. Terr. Phys.* **5,** 243.
OSHEROVICH A. L. and RODIONOV S. F.	1954	*Dokl. Akad. Nauk* **96,** 1159.
ROACH F. E., PETTIT H. and WILLIAMS D. R.	1950	*J. Geophys. Res.* **55,** 183.
ROACH F. E.	1956	*I.G.Y. Instruction Manual, Aurora and Airglow* p. 76. Pergamon Press London.
SHEPHERD G. G.	1954	*Scientific Report No. AR–16* Contract AF19(122)–152 University of Saskatchewan.
SHKLOVSKY I. S.	1956	*Liège Conference on Molecular Spectra.*

VOL. 11 1957

Journal of Atmospheric and Terrestrial Physics, 1957, Vol. 11, pp. 200 to 208. Pergamon Press Ltd., London

Atmospheric helium

D. R. Bates and M. R. C. McDowell*
Department of Applied Mathematics, The Queen's University of Belfast

(*Received* 4 *September* 1957)

Abstract—Calculations are carried out on the escape of helium, using a less crude model of the thermosphere than did earlier workers. Low rates are obtained. It is found that He^4 atoms could not escape as rapidly, as they are apparently being released from the crust, unless the temperature at the base of the exosphere were higher than seems possible from consideration of the heat balance in the thermosphere or seems consistent with the number of He^3 atoms present. The hypothesis that escape occurs during occasional brief intervals of enhanced solar emission is found to be difficult to accept. A solution to the basic problem does not appear to be provided by invoking aurorae, solar gas or interplanetary dust. The validity of the customary assumption that atmospheric helium is in equilibrium is queried.

1. Introduction

Theoretical studies (Spitzer, 1949; Bates, 1951, 1956) reveal that it is unlikely that the heating action of solar ultra-violet or X-radiation maintains any considerable temperature gradient in the region beyond the F layers or any considerable temperature difference between these layers (which are thought to be at not above 1000°K) and the base of the exosphere. The problem of explaining the observed abundance of atmospheric helium immediately presents itself in an acute form. After briefly summarizing current views on the sources of the two isotopes we shall consider variants of the thermal escape hypothesis of Stoney (1898) assuming that radiation is responsible for the heating. Finally we shall discuss whether significant escape of helium is likely to result from matter incident on the atmosphere.

2. Sources

He^4 *isotope*. The task of estimating the rate of release of radiogenic helium from the crust is very complex, and it would be unwise to assume that all relevant factors have yet been appreciated and properly taken into account. However it is generally agreed that the number of He^4 atoms that have been released exceeds the number now present, which Glückauf (1946) finds to be $1{\cdot}1 \times 10^{20}/cm^2$.

As realized by Goldschmidt (1937), Lindemann (1939) and others, occulted helium is freed when rock is weathered. The amount of weathered rock is believed to be at least 200 kg/cm^2 (cf. Wickman, 1954); and the volume of helium associated with surface rocks is probably at least $5 \times 10^{-4}\ \tau\ cm^3/g$, where τ is the age in units of 10^9 years (cf. Damon, 1957). Assuming that sedimentary rock does not retain appreciable helium, it follows that 1×10^5 atoms/cm^2 sec is a lower limit to the rate of entry of He^4 into the atmosphere due to weathering.

Many geologists have recently tended to the view that irrespective of weathering the crust is being continuously degassed (cf. Mayne, 1956). According to Damon (1957) the rate of liberation of He^4 is about 1×10^6 atoms/cm^2 sec; according to Nicolet (1957) it is about 2×10^6 atoms/cm^2 sec; according to Mayne (1957) it is about 5×10^6 atoms/cm^2 sec. Naturally, precision is not claimed.

* Now at Royal Holloway College, University of London.

He^3 *isotope.* The He^3/He^4 ratio is about $1{\cdot}2 \times 10^{-6}$ in air (ALDRICH and NIER, 1948). By considering what are judged to be the principal nuclear reactions involved it has been deduced that this ratio is much smaller in the crust and hence that degassing cannot give a significant contribution to the He^3 content of the atmosphere (MORRISON and PINE, 1955; MAYNE, 1956).

Cosmic rays are generally regarded as responsible for the main contribution. As pointed out by HILL (1941) and LIBBY (1946) they cause nuclear reactions in the atmosphere which have He^3 as an end product. FIREMAN (1953) calculated that the rate of generation is between about 0·7 and about 1·5 atoms/cm² sec. A rather higher rate, 2 atoms/cm² sec, is favoured by KORFF (1956) and NICOLET (1957). This rate is sufficient to yield the total number of free He^3 atoms in two million years.

Seeking a more effective source, BROWN (1955) suggested that the He^3 atoms in the atmosphere originated mainly in the dust accreted by the earth. MAYNE (1956) has argued that the rate of supply from this dust might be as high as 10 atoms/cm² sec, but, as he fully appreciated, the uncertainties are very considerable.

It would be surprising if the major source has been overlooked. However, the possibility cannot be excluded completely.

In the present state of knowledge it would seem best to assume provisionally that the isotope is added to the atmosphere at a rate of about 2 atoms/cm² sec; but to bear in mind that the rate may possibly be greater (though probably not by a large factor).

VOL. 11 1957

3. THERMAL ESCAPE HYPOTHESIS

The most recent mathematical treatment of the escape of a planetary atmosphere by virtue of the thermal agitation is that of SPITZER (1949). Like him we shall suppose that diffusive separation sets in sharply at a certain level (altitude z_D, total particle concentration N_D), but unlike him, we shall not suppose that the atmosphere is isothermal between this level and the base of the exosphere (altitude z_X, total particle concentration N_X). In the first instance we shall ignore the fact that the escape influences the equilibrium distribution of the helium owing to the finiteness of the diffusion coefficient.

We shall denote the thermal diffusion factor by α, the temperature by T, the atomic mass and number density of a particular constituent by the letters n and m followed by the appropriate chemical symbol, and we shall employ the subscripts D and X as above. *Independent* of the $T - z$ variation we have that

$$\frac{n_X(\mathrm{He})}{n_D(\mathrm{He})} = \left(\frac{T_D}{T_X}\right)^{1+\alpha-p} \left(\frac{n_X(\mathrm{O})}{n_D(\mathrm{O})}\right)^p \qquad (1)^*$$

with

$$p = m(\mathrm{He})/m(\mathrm{O}); \qquad (2)$$

and to a sufficient approximation we have further that

$$n_D(\mathrm{O}) = \tfrac{1}{3}N_D, \qquad n_X(\mathrm{O}) = N_X \quad , \qquad (3)$$

$$n_D(\mathrm{He}^4) = 5 \times 10^{-6}N_D, \qquad n_D(\mathrm{He}^3) = 6 \times 10^{-12}N_D. \qquad (4)$$

* We omit the identifying superscript (4 or 3) from He and other symbols when referring to either isotope.

If $H_X(\mathrm{He})$ is the scale height of helium at the base of the exosphere, c is the root mean square velocity there and v_e is the velocity of escape at the surface, then the escape flux of atoms is approximately

$$l = \frac{n_X(\mathrm{He}) c\, Y}{\sqrt{6\pi}} \exp\left[-Y + \frac{z_X}{H_X(\mathrm{He})}\right] \tag{5}$$

with

$$Y = 3v_e^2/2c^2$$

(cf. SPITZER, 1949). Substitution from (1) and (3) yields

$$l = \frac{n_D(\mathrm{He}) c\, Y}{\sqrt{6\pi}} \left(\frac{T_D}{T_X}\right)^{1+\alpha-p} \left(\frac{3N_X}{N_D}\right)^p \exp\left[-Y + \frac{z_X}{H_X(\mathrm{He})}\right]. \tag{6}$$

For comparison it may be recalled that the corresponding formula for SPITZER's rather cruder model of the thermosphere is

$$l = \frac{n_D(\mathrm{He}) c\, Y}{\sqrt{6\pi}} \exp\left[-Y + \frac{z_D}{H_X(\mathrm{He})}\right]. \tag{7}$$

The ratio of the new expression for the escape flux to the old is thus

$$r = \left(\frac{T_D}{T_X}\right)^{1+\alpha-p} \left(\frac{3N_X}{N_D}\right)^p \exp\left[\frac{z_X - z_D}{H_X(\mathrm{He})}\right]. \tag{8}$$

SPITZER did not compute l directly. He computed what purported to be the time τ_e that would be required for the helium present to decrease by the exponential factor if there were no release from the crust. This time is proportional to the ratio B of the amount of helium in the actual atmosphere to the amount in the hypothetical atmosphere, which has an identical exosphere, but which is isothermal throughout. SPITZER took

$$B = \{T_G n_G(\mathrm{He})/T_X n_X(\mathrm{He})\} \exp\left[-z_X/H_X(\mathrm{He})\right], \tag{9}$$

the subscript G indicating the value at ground level. Implicit in this is the incorrect assumption that the scale height of the helium in the lower atmosphere is that corresponding to diffusive equilibrium. Clearly SPITZER's expression for B should be multiplied by $m(\mathrm{He})/\bar{m}_G$, that is by the ratio of the atomic mass of helium to the weighted mean molecular mass of the atmospheric constituents. The effect of the correction to the original B is in the opposite sense to the effect of the refinement introduced in the earlier paragraphs.

In (6) we took α to be 0·4 (cf. GREW and IBBS, 1952), N_X to be $3 \times 10^7/\mathrm{cm}^3$ (cf. SPITZER, 1949), z_X to be 450 km (cf. BATES, 1954), and T_D to be as specified below. The derived value of l is not seriously affected by the uncertainties directly associated with these parameters. However, in addition to being sensitive to T_X it is dependent on N_D, which is not known with assurance to even within an order of magnitude (cf. MANGE, 1957). We therefore computed l as a function of T_X for N_D equal to $10^{10}/\mathrm{cm}^3$, $10^{11}/\mathrm{cm}^3$, $10^{12}/\mathrm{cm}^3$ and $10^{13}/\mathrm{cm}^3$, taking the corresponding values of the related parameter T_D to be 580°K, 370°K, 280°K and 220°K in

accordance with the R-model of the atmosphere compiled by BATES (1954) from rocket data. The results obtained are displayed in Fig. 1.

We now turn to the back-action of the escape on itself. From formulae developed by MANGE (1955) it is immediately apparent that if there is an outward helium atom flow, l', the concentration at the base of the exosphere is approximately

$$n'_X(\mathrm{He}) = n_X(\mathrm{He})\{1 - Al'\}, \tag{10}$$

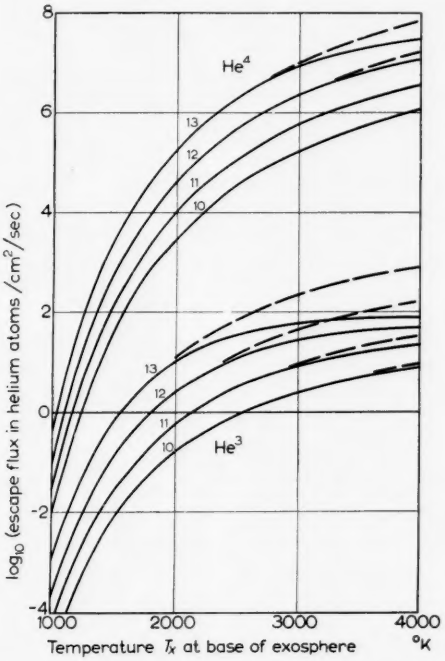

FIG. 1. The broken (·····) curves give log l and the full (———) curves give log l', where l and l' are helium escape fluxes, the former obtained ignoring the finiteness of the diffusion coefficient, and the latter obtained taking account of the finiteness of this coefficient. The upper set refers to He^4 and the lower set refers to He^3. The value of $\log_{10} N_D$ is shown on each curve, N_D being the number of air atoms and molecules per cm^3 at the level at which diffusive separation is assumed to begin.

where $n_X(\mathrm{He})$ is as given by (1) and where

$$A = \bar{H}_D/n_D(\mathrm{He})\mathscr{D}_D q, \tag{11}$$

with

$$q = 1 - \frac{m(\mathrm{He})}{\bar{m}_D} - \tfrac{1}{2}\beta - \alpha\beta \tag{12}$$

in which $\mathscr{D}_D$ is the diffusion coefficient at the level indicated, β is the derivative of the mean scale height with respect to the altitude (which derivative is assumed to be constant), and the other symbols are as already defined.

Noting that

$$\mathscr{D}_D N_D T_G^{\frac{1}{2}} = \mathscr{D}_G N_G T_D^{\frac{1}{2}} \tag{13}$$

VOL. 11 1957

(11) becomes

$$A = \bar{H}_D T_G^{\frac{1}{2}} / \mathscr{D}_G n_G(\mathrm{He}) T_D^{\frac{1}{2}} q \tag{14}$$

$$\simeq \begin{cases} 1{\cdot}2 \times 10^{-9} T_D^{\frac{1}{2}} & \text{for} \quad \mathrm{He}^4 \\ 8 \times 10^{-4} T_D^{\frac{1}{2}} & \text{for} \quad \mathrm{He}^3. \end{cases} \tag{15}$$

From (10) it is seen that the escape flux is not l of (6) but is

$$l' = l/(1 + Al). \tag{16}$$

Clearly l' is not markedly less than l unless Al is appreciable compared with unity, that is (cf. (15)) unless l exceeds about 10^7 atoms/cm^2 sec in the He^4 case and about 10 atoms/cm^2 sec in the He^3 case.

Inspection of Fig. (1) shows that even if the number density, N_D, at the level at which diffusive separation sets in were as great as 10^{13}/cm^3, the temperature, T_X, at the base of the exosphere would have to be about 1900°K to let l'(He^4) equal 1×10^5 atoms/cm^2 sec (which is lower than the estimates of the He^4 release flux due to degassing of the crust); and shows that with the same N_D the values of T_X for l'(He^4) to be 1×10^6 atoms/cm^2 sec and 5×10^6 atoms/cm^2 sec are 2300°K and 2800°K respectively. These temperatures are higher than the thermal escape hypothesis was at one time judged to demand; and in view of the value of N_D to which they correspond they must be regarded as lower limits. There seems little doubt that they cannot be maintained by the heating action of ultra-violet and X-radiation from the sun (cf. Bates, 1956).

Another discordant feature is that if the atmospheric parameters were as seemingly required, l'(He^3) would exceed the estimated He^3 generation rate (2 atoms/cm^2 sec): thus the values of l'(He^3) are 7, 30 and 50 atoms/cm^2 sec in the three illustrative cases just considered (l'(He^4) : 1×10^5, 1×10^6 and 5×10^6 atoms/cm^2 sec).

One of our aims is to stress the extent of the difficulties associated with the attempts that have been made to account for the apparent escape. We shall concentrate our attention on the escape of He^4 since this is what occasions the more extreme postulates regarding the temperature of the upper atmosphere and since the escape of He^3 is not in itself so informative. While the present paper was being prepared an important paper by Nicolet (1957) was published, in which detailed consideration was given to the ratio of the two escape fluxes. In harmony with our results, Nicolet concludes that there is no *steady* temperature T_X at which the escape of He^4 is rapid enough and yet the escape of He^3 is not too rapid. This conclusion might be invalidated if it should prove that the rate of release of He^4 has been seriously overestimated or that the rate of generation of He^3 has been seriously underestimated.

Spitzer (1949) has tentatively suggested that the He^4 escape occurs during brief intervals when the solar emission is exceptionally intense in the short-wavelength part of the spectrum. This general picture is widely regarded as plausible. In order to favour it we shall suppose that (i) the heating is world-wide instead of being confined to the sunlit hemisphere; (ii) the brief intervals concerned occur

throughout the sunspot cycle and cover 5 per cent of the time rather than 2 per cent as SPITZER contemplated; (iii) the value of N_D is 10^{13}/cm^3 even though sudden temperature changes might be expected to promote mixing; (iv) the outward flow is too transient to affect the altitude distribution of the He^4 atoms (but is not necessarily too transient to affect that of the He^3 atoms). On those suppositions T_X must rise to about 2500°K for the *average* He^4 escape flux to be 1×10^5 atoms/cm^2 sec, must rise to somewhat over 3000°K for it to be 1×10^6 atoms/cm^2 sec and must rise to somewhat over 4000°K for it to be 5×10^6 atoms/cm^2 sec. In each case the corresponding average He^3 escape flux might perhaps be of the magnitude needed to balance the generation (Fig. 1). However, acceptance of even the lowest of the peak temperatures listed is scarcely possible. It requires the photo-ionization invoked to cause the excess heating to be much more rapid than is the normal photo-ionization near the maximum of the sunspot cycle; and this is difficult to credit, since the F layers do not show the expected consequential response during flares or other solar events.

We wish now to draw attention to a possibility which does not seem to have received the consideration it merits.

It is conceivable that the helium in the atmosphere is not in equilibrium, but that instead the current release or generation rate exceeds the current escape flux. Neglecting escape, times of 40, 4 and 0·7 million years would be needed to yield the existing amount of He^4 at steady release rates of 1×10^5, 1×10^6 and 5×10^6 atoms/cm^2 sec respectively; and as already mentioned, a time of 2 million years would be needed to yield the existing amount of He^3 at a steady generation rate of 2 atoms/cm^2 sec. Hence there might be no anomaly if the escape flux a million or so years ago were fast enough to keep the abundance of atmospheric helium several times below the present abundance. It may be recalled (cf. ÖPIK, 1953) that palaeclimatological research indicates that the surface temperature of the earth fluctuated markedly during the past million years, covering the repeated glaciation and inter-glaciations of the Quaternary era and was considerably higher than it now is in the preceding Pliocene era. One interpretation is that there have been appreciable changes in the main solar emission during the period in which we are interested. While nothing can be inferred regarding the short-wavelength emission, the possibility that it was very different in the remote past is at least raised. In the absence of positive supporting evidence the hypothesis is of course purely speculative. Other hypotheses must be sought and examined.

VOL. 11 1957

4. INCOMING PARTICLES

Aurorae. An auroral system 10 km wide, and extending along each of the two 67° lines of latitude, would cover only about one-thousandth of the earth's surface; and the systems which actually occur are of course much less vast. For the main loss of helium to be attributed to heating in aurorae the outward flow near the active zones would clearly have to be very rapid indeed during average displays. Temperatures at least as high as those cited in connection with SPITZER's hypothesis involving exceptional intervals (Section 3) would have to be reached. Spectroscopic studies (cf. PETRIE, 1953; SHEPHERD and HUNTEN, 1955)

give no indication of marked temperature increases in aurorae; and as we shall see such increases would not be expected.

The local rate of gain of thermal energy per gas atom or molecule is

$$g = Q\varepsilon F \tag{17}$$

where Q is the cross-section describing the inelastic collisions suffered by the primary protons, ε is the energy released in each collision and F is the flux in the incident proton stream. At most, Q is about 3×10^{-16} cm^2 and ε about 100 eV. In the case of a moderately brilliant arc (observed by Fan) Chamberlain (1954) estimated F to be 6×10^7 protons/cm^2 sec. Substitution in (17) gives the corresponding value of g to be not more than some 2×10^{-6} eV/sec for this particular aurora. Even should a given volume of air remain in the proton stream of a similar aurora for 20 min, its temperature would be raised by less than 10°K. Now in 20 min the volume would be carried a distance of 12 km by even a 10 m/sec wind; and so it is unlikely to remain in the stream for so long a period. The possibility of a temperature increase of as much as 1000°K would thus seem remote.

In very intense auroras the incident proton flux F exceeds the value adopted above by several orders of magnitude. It might be suggested that such auroras are responsible for the escape. However, even if they occupied as much as 1 per cent of the time, and even if the associated active zones extended over as much as 1 per cent of the earth's surface, unacceptably high escape fluxes would be required. Thus the He^4 escape fluxes to balance He^4 release rates of 1×10^5, 1×10^6 and 5×10^6 atoms/cm^2 sec are 1×10^9, 1×10^{10} and 5×10^{10} atoms/cm^2 sec respectively. It may be noted that even if N_D were as much as 10^{13}/cm^3 and T_X were as much as 5000°K, then then according to (6) $l(He^4)$ would be only 2×10^8 atoms/cm^2 sec.

Solar gas. Chapman (1957) has drawn attention to the possibility that the coronal atmosphere of the sun extends beyond the earth's orbit. He supposes that in the neighbourhood of the earth the number density of protons and electrons is about 1×10^3/cm^3 and the mean kinetic energy per particle is about 30 eV. According to him the earth must act as a sink of heat in this hot solar gas. Herein, he suggests, may lie the explanation of the upward rising temperature of the thermosphere.

From certain relevant sections of the Chapman–Ferraro theory of magnetic storms, Dungey (1955) concluded that a cavity is formed around the earth, and estimated its equatorial radius to be about 9 earth radii. Presumably the solar gas can only enter the atmosphere in the polar regions. Some lateral diffusion across the cavity must indeed occur, but as far as can be judged the effect is negligible.

Instead of attempting to calculate the amount of energy actually given to the atmosphere we shall consider the luminosity that would occur if the amount were sufficient.

A considerable fraction of the energy must be given up in collisional excitation. If helium is to escape, the energy input (averaged over the surface of the globe and the time) must be well in excess of 10^{11} eV/cm^2 sec (cf. Bates, 1956). It is

very doubtful if the solar gas could provide so much energy without making the forbidden red and green lines of oxygen stronger than observed.

NICOLET's conclusion (cf. §3), that the He^3/He^4 ratio cannot be explained if T_X is steady, must be borne in mind. The seemingly necessary sharp peaks in T_X could scarcely result from the action of the solar gas.

Interplanetary dust. KAISER and SEATON (1955) have summarized the observational evidence relating to interplanetary dust. As they recall, information on $n(r)\,dr$, the number density of particles with radius between r and $r + dr$, may be obtained from light-scattering studies and from meteor studies. The former give what is called the L-distribution.

$$n(r)\,dr = 10^{-19} r^{-2}\,dr \qquad (10^{-2} \geqslant r \geqslant 10^{-4}\ \text{cm}) \tag{18}$$

and the latter give what is called the M-distribution

$$n(r)\,dr = 10^{-27{\cdot}7} r^{-4}\,dr \qquad (0{\cdot}5 \geqslant r \geqslant 5 \times 10^{-3}\ \text{cm}). \tag{19}$$

Taking the specific gravity of the particles to be 4 and the geocentric velocity to be 40 km/sec, KAISER and SEATON (1955) estimated the energy flux into the atmosphere from the L-distribution (which is clearly greater than that from the M-distribution) to be $1{\cdot}6 \times 10^9$ eV/cm² sec. This is much too small to support the temperature gradient that is required if the base of the exosphere is to be at a high enough temperature for the escape of helium (cf. BATES, 1956); and furthermore, the main energy imput takes place at too low an altitude to be effective. Interplanetary dust must be unimportant in the present connection.

VOL. 11 1957

REFERENCES

ALDRICH L. T. and NIER A. O.	1948	*Phys. Rev.* **74,** 1590.
BATES D. R.	1951	*Proc. Phys. Soc.* B **64,** 805.
BATES D. R.	1954	*Rocket Exploration of the Upper Atmosphere* (Edited by R. L. F. BOYD and M. J. SEATON) p. 347. Pergamon Press, London.
BATES D. R.	1956	*Proc. Roy. Soc.* **A 236,** 206.
BROWN H.	1955	See MORRISON and PINE, 1955.
CHAMBERLAIN J. W.	1954	*Astrophys. J.* **120,** 360.
CHAPMAN S.	1957	*Smithsonian Contributions to Astrophysics* **2,** No. 1.
DAMON P. E.	1957	*Geochim. et Cosmochim. Acta* **11,** 200.
DUNGEY J. W.	1955	*The Physics of the Ionosphere* p. 229. The Physical Society, London.
FIREMAN E. L.	1953	*Phys. Rev.* **91,** 922.
GLÜCKAUF E.	1946	*Proc. Roy. Soc.* A **185,** 98.
GOLDSCHMIDT V. M.	1937	*Skrifter Norske Videns. Akad.* No. 4.
GREW K. E. and IBBS T. L.	1952	*Thermal Diffusion in Gases* p. 129. Cambridge University Press.
HILL R. D.	1941	*Phys. Rev.* **59,** 103.
KAISER T. R. and SEATON M. J.	1955	*Mem. Soc. Sci. Liége* (Fourth Series) **15,** 48.
KORFF S. A.	1956	*Ann. N.Y. Acad. Sci.* **67,** 35.
LIBBY W. F.	1946	*Phys. Rev.* **69,** 671.

Lindemann F. A.	1939	*Quart. J. Roy. Met. Soc.* **45,** 330.
Mange P.	1955	*Ann. Geophys.* **11,** 153.
Mange P.	1957	*J. Geophys. Res.* **62,** 279.
Mayne K. I.	1956	*Geochim. et Cosmochim. Acta* **9,** 174.
Mayne K. I.	1957	*Geochim. et Cosmochim. Acta* **11,** 201.
Morrison P. and Pine J.	1955	*Ann. N.Y. Acad. Sci.* **62,** 69.
Nicolet M.	1957	*Ann. Geophys.* **13,** 1.
Öpik E. J.	1953	*J. Glaciology* **2,** 213. Contributions from Armagh Observatory No. 9.
Petrie W.	1953	*J. Atmosph. Terr. Phys.* **4,** 5.
Shepherd G. G. and Hunten D. M.	1955	*J. Atmosph. Terr. Phys.* **6,** 328.
Spitzer L.	1949	*The Atmospheres of the Earth and Planets* (Edited by G. P. Kuiper) p. 213. University of Chicago Press.
Stoney G. J.	1898	*Proc. Roy. Dublin Soc.* **8,** 701.
Wickman F. E.	1954	*Geochim. et Cosmochim. Acta* **5,** 97.

Journal of Atmospheric and Terrestrial Physics, 1957, Vol. 11, pp. 209 to 222. Pergamon Press Ltd., London

Relation between virtual and actual heights in the ionosphere

G. A. M. KING
Geophysical Observatory, Christchurch, New Zealand

(*Received* 3 *June* 1957)

Abstract—There are two general methods of deducing the "true" heights from the virtual height–frequency curve.

Aspects of the comparison method treated are choice of model, effect of the earth's magnetic field, the meaning of total electron content, and the use of hp and $M3000$ as height indicators.

The integral method is discussed from the viewpoints of the derived curve and the step-by-step procedure. There is a brief treatment of the nominal accuracy of reduction, sections on the importance of the earth's magnetic field and on "valleys" between layers, and a discussion of factors affecting the actual accuracy of analysis.

There are five current research projects at Christchurch based on true height analysis.

The bibliography is divided up according to subject, and there are notes on the references.

VOL.
11
1957

1. INTRODUCTION

SINCE the middle of 1954, we have been using electron distributions obtained from routine h'–f recordings by a method described in earlier notes (KING, 1954, 1956).

There is much in the literature to suggest that the techniques, limitations, and results of "true height" analysis are not generally appreciated. The purpose of this paper is to set down our experiences in the field, in the hope that more workers will be encouraged to use h–N curves.

Naturally, our work has been based on our own method of reduction, which has proved to have many valuable features: it follows that the tone of this paper is partial. We fully realize, though, that other methods have excellent points, and may be more suitable to the needs of some workers.

The references have been separated into sections, and are accompanied by short notes. The list is by no means complete.

2. THE PROBLEM

Given $h'(f)$, we want $N(h)$.

At the reflection point of the ordinary ray, N is related immediately to f.

$$N = 1{\cdot}24 \times 10^4 \, . f^2 \tag{1}$$

where f is in Mc/s.

A convenient measure of N is, then, f_N, defined by putting $f = f_N$ in this equation. It is sufficient if we can find the relation between f_N and h.

h is connected with h' by an integral equation:

$$h'(f) = \int_{h(0)}^{h(f)} \mu'(f, f_N) \, . \, dh(f_N) \tag{2}$$

μ' is the group refractive index.

This integral equation has been tackled in two ways:

(1) *Comparison method.* A layer shape is assumed, and theoretical h'–f curves

are drawn; these are compared with the experimental record, which is assigned parameters accordingly.

(2) *Integral method.* Equation (2) is inverted to give h as the integral of a virtual height function; the integration is carried out by standard graphical or numerical methods.

Both will be discussed in the following sections.

3. Comparison Method

We shall not consider here the techniques of using the comparison method, for they have been well described in the literature (see references).

Let us first look at the choice of a theoretical model of electron distribution in the $F2$-layer, from which the comparison h'–f curves will be drawn. The easiest to try is a power law,

$$(N_{\max} - N) = a \,.\, (h_{\max} - h)^n, \tag{3}$$

or

$$\log (N_{\max} - N) = \log a + n \log (h_{\max} - h). \tag{4}$$

Several Christchurch ionograms have been analysed (see later), and n has been determined from the graph of log $(N_{\max} - N)$–log $(h_{\max} - h)$. It is necessary, of course, to fix $h_{\max}$ by fitting to the h,N curve a "nose" of the power law matching the curve; this was done by successive approximations.

Values of n are given in Table 1.

Table 1

	0200 10.2.45	0200 22.4.45	0200 19.6.45	0200 20.8.45	0200 28.10.45	0200 9.12.45	1308 1.5.56	1300 26.1.54	1330 1.2.54
	1·7	1·6	1·5	1·7	1·7	1·6	1·2	2·0	1·4
Effect of earths magnetic field neglected			1·7				1·3	3·2	2·3
With 64 km valley between E and F							1·3		
With 43½ km valley between $F1$ and $F2$									2·0

Departures from the power law are surprisingly small; however, the agreement is due partly to the fitting of $h_{\max}$, and, even on the best records, n could be out by 5 per cent.

The first six examples are night F-layers; a suitable model for them is a power law with index 5/3.

Now, it is commonly supposed that the distribution of the night F-layer is well fitted by a parabola, and indeed, Booker and Seaton (1938) curves, assuming a

parabolic model, and neglecting the earth's magnetic field, do match these records. There are two reasons:

(1) The comparison method is not sensitive to systematic departures from the theoretical model.

(2) Neglect of the earth's magnetic field raises the index in the power law.

Both factors assume greater importance when daytime records are being treated; then also, we meet the problem of allowing for possible valleys between layers. The common neglect of the magnetic field emphasizes the division into layers, making it appear that the gradient, dh/dN, continuously increases within a layer; actual electron distributions often have decreasing gradients, and are usually almost monotonic up to the maximum of $F2$. The last three examples in Table 1 illustrate these points; clearly, it is unwise to expect much of the comparison method in summer, when both $F1$ and $F2$ are present.

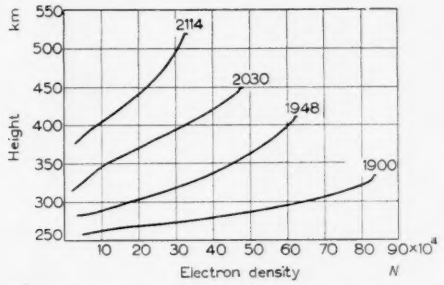

Fig. 1. Electron distributions from four records taken during a night-time ionospheric storm on 19 March 1950. (Christchurch).

The purpose of the discussion so far has been to show that we should be unwilling to expect the ionized layers to have a particular form, for the comparison method will only too readily provide support for it—it lacks discrimination. In the past parabolic and Chapman models have been proposed for physical reasons, and many rash conclusions have been drawn; nowadays, a more critical attitude prevails.

The most satisfactory application of the comparison method is that advocated by RATCLIFFE (1951)—to estimate the electron content below the maximum of the layer. However, it is important to include the effect of the earth's magnetic field, for its neglect can give rise to spurious temporal changes—e.g. the division of the F region into $F1$ and $F2$ is most pronounced at the middle of the day, and neglect of the field causes an additional diurnal variation.

We should be quite clear, too, about the meaning of the electron content. The maximum of a layer is not fixed; indeed, the whole shape is continually altering, so that we cannot say definitely that what is visible at one time corresponds to what was visible a little earlier. By day, the changes are mostly associated with "travelling disturbances," while, at night, vertical motions of the whole layer are accompanied by slight changes in shape. For illustration, however, we shall look at a night-time storm, where the changes are more obvious. Fig. 1 shows four N–h curves derived from records taken on 19 March 1950. The maximum density

VOL. 11 1957

at 1948 is only three-quarters that at 1900, but the visible content is 1·3 times as great. The change in shape is also apparent in the other two curves (2030 and 21·14).

Certainly, it is often convenient to think of the layer as a whole, but it does not always behave as a whole—we must be prepared to use many parameters to describe it.

A measure deserving special mention is hp (BOOKER and SEATON, 1938): it is the virtual height at 0·834 of the critical frequency of the layer, and is intended to give the height of maximum density; it is based on a parabolic model, neglecting the magnetic field, and supposing that there is no retardation from lower layers. On calm nights, the true height of the maximum can be estimated from hp by multiplying the apparent thickness by a factor which allows for the first two assumptions. But hp should not be used at all in the daytime, when it gives completely misleading values. This fact does not seem to have been sufficiently appreciated by many workers.

An illustration of the behaviour of hp has been given in an earlier paper from this observatory (Fig. 5 of KING and CUMMACK, 1956).

The transmission factor, $M3000$, has been proposed also as a measure of the height of the $F2$-layer (SHAPLEY, 1956). It suffers from the same defects as hp, being quite unreliable by day.

4. INTEGRAL METHOD

A useful concept for handling the integral method is the "derived curve".

We are given $h'(f)$, the virtual height as a function of frequency. It is possible to express it as a function of a variable, $k(f)$, so that the true height corresponding to a chosen upper limit of f is proportional to the area under the $h'(k)$ curve. $h'(k)$ is the derived curve; if we follow through the inversion of the integral equation relating h' to h, the idea will follow naturally.

Repeating equation (2):

$$h'(f) = \int_0^{h(f)} \mu'\,(f, f_N)\,.\,(dh\, f_N) \tag{5}$$

To find h corresponding to f_r, multiply both sides of this equation by $dk(f_r, f)/df$, a function of f yet to be determined, and integrate with respect to f.

$$\int_{k(0)}^{k(f_r)} h'\,.\,dk = \int_{k(0)}^{k(f_r)} \int_0^{h(f)} \mu'\,.\,dh\,.\,dk \tag{6}$$

Provided $h(f_N)$ and $k(f)$ are single valued functions, we can reverse the order of integration on the right-hand side.

$$\int_{k(0)}^{k(f_r)} h'\,.\,dk = \int_0^{h(f_r)} \int_{k(f_N)}^{k(f_r)} \mu'\,dk\,.\,dh \quad \text{(note limits)} \tag{7}$$

If we can find a function, $k(f_r, f)$, such that

$$\int_{k(f_N)}^{k(f_r)} \mu'\,.\,dk = K(f_r) \propto f_N \tag{8}$$

Then

$$\int_{k(0)}^{k(f_r)} h' \,.\, dk = \int_0^{h(f_r)} K(f_r) \,.\, dh(f_N) = K \,.\, h(f_r)$$

or

$$h(f_r) = \frac{1}{K} \cdot \int_{k(0)}^{k(f_r)} h' \,.\, dk \tag{9}$$

Of course, the form of k depends on the form of μ' (equation 8). A simple case arises when the earth's magnetic field is neglected; for then,

$$\mu' = \sec \,.\, \sin^{-1}\frac{f_N}{f} \tag{10}$$

$$k = \sin^{-1}\frac{f}{f_r} \tag{11}$$

$$K = \frac{\pi}{2} \quad \text{(in this case } \not< f_r\text{)} \tag{12}$$

and

$$h = \frac{2}{\pi}\int_0^{\pi/2} h' \,.\, d \sin^{-1}\frac{f}{f_r} \tag{13}$$

h is proportional to the area under the derived curve.

This result has been given by several workers (see references).

In a more useful case, the refractive index obeys the Appleton-Hartree equation (omitting collisional effects), and unfortunately there is no analytical form for k. However, we can still carry out the above operations numerically, using tables of μ'.

Techniques for integrating the derived curve will be discussed in the next section.

Now let us look at a step-by-step analysis.

We write equation (2) as the sum of a number of steps in a function $\phi(f_N)$.

$$h'(f) = \sum \int_{\triangle\phi(f_N)} \mu' \cdot \frac{dh}{d\phi(f_N)} \,.\, d\phi(f_N) \tag{14}$$

If, over each step, the gradient, $dh/d\phi$ is sensibly constant, it can be put outside the integral sign.

$$h' = \sum \frac{dh}{d\phi} \cdot \int_{\triangle\phi} \mu' \,.\, d\phi = \sum D \,.\, a \tag{15}$$

in which the integral portion, a, is independent of h; it is the product of the step width and the mean value of μ' over the step.

Using tables of a, we can build up the layer step by step from the bottom.

The analysis can be put in the form of the previous approach by solving the set of simultaneous equations,

$$h_j' = \sum a_{ji} \,.\, D_j \tag{16}$$

giving

$$D_j = \sum b_{ji} \,.\, h_i' \tag{17}$$

$$\begin{aligned} h_j &= \sum D_i \\ &= \sum c_{ji} \,.\, h_i' \end{aligned} \tag{18}$$

VOL. 11 1957

which is equivalent to integrating the derived curve by summing, with unequal weights, ordinates spaced according to $\phi(f)$.

So far, we have not defined $\phi(f_N)$. Any continuous function will do, but, at Christchurch, we use $\log \phi(f_N)$ for several practical reasons—the recordings have a logarithmic frequency scale; the values of a_{ji} change only slowly with j at fixed $j - i$, permitting a labour-saving plan of work for a desk calculator; the tables of a, including the earth's magnetic field, can be readily compiled, using only a good set of mathematical tables: the relative accuracy is the same at all frequencies.

5. Integrating the Derived Curve

In the previous section, we found that the true height is proportional to the area under a derived curve, $h'(k)$.

It is possible to graph the derived curve, and find its area with a planimeter or by counting squares, but the labour is too much for routine work; besides, the problem of including the earth's magnetic field must be solved before we can plot the curve.

It is more practical to sum ordinates, for they can be picked off directly from the $h'(f)$ record. This is the basis of the popular method due to Kelso (1952); a measure of the true height, h_j, is the average value of ordinates, h'_i, at frequencies,

$$f_i = f_j \cdot \sin\left(\frac{2i - 1}{2i} \cdot \frac{\pi}{2}\right) \tag{19}$$

The magnetic field has been neglected; obviously, to include it, we need only shift the ordinates on the $h'(f)$ record so that k is the function appropriate to the refractive index with the field. I understand (private communication) that Dr. Shinn* has done this.

The great advantage of Kelso's method is the speed of operation, due to giving the ordinates equal weights. But this also brings about the greatest drawback. For each ordinate represents an interval of frequency, narrow near f_j, and getting wider as we move back. The appropriate value of h' is some form of weighted mean over the interval; yet there can be large variations of h' in the interval, especially if the critical point of a lower layer is included. Accuracy is not good.

It is not satisfactory merely to increase the number of ordinates, because of crowding near f_j. It is better to put them closer together at the low frequency end and use a system of weighting factors.

$$h_j = \sum W_{ji} \cdot h'_i \tag{20}$$

Let us suppose that the ordinates are distributed at equal steps in a function, $P(f)$; we will try to find the best P. Obviously, if we are to treat all frequencies alike, it is such that each weight factor depends only on the number of steps in P from f_i. That is,

$$W_{ji} = W(j - i) \tag{21}$$

On comparing equations (18) and (20), we see that equation (21) is equivalent to

$$a_{ji} = a(j - i) \tag{22}$$

* Address: Marconi Research Laboratories, Great Baddow, Chelmsford, Essex, England.

where, as earlier,

$$a_{ji} = \int_{\phi_{i-1}}^{\phi_i} \mu'(f_i, f_N) \cdot d\phi(f_N) \tag{23}$$

Now, approximately, the refractive index is of the form,

$$\mu' = \mu'(\log f - \log f_N) \tag{24}$$

(This is strictly true if the magnetic field is neglected)
So that

$$a_{ji} = a(\log f_j = \log f_i) \tag{25}$$

and

$$P(f) = \log f \tag{26}$$

If all frequencies are to be treated alike, the sampling ordinates must be spaced according to $\log f$.

Notice, though, that to go from equation (21) to equation (22) we needed to have h'_j as one of the ordinates. This is equivalent to choosing the form of $h(f_N)$ so that we can apply an integration formula. Had we chosen a form for $h'(f)$ or $h'(k)$, P would only have approximated to a logarithmic function. It is worth mentioning that KELSO fitted a polynomial to $h'(f)$, while WRIGHT, KNECHT and DAVIES (1956) advocate fitting a polynomial to $h'(k)$; by mischance, the table of frequency spacings with their text is not correct.

It is debatable whether we should treat all frequencies alike, for the h' (measured from the bottom of the trace) at the low frequency end are small, and they generally increase with frequency; however, the matter cannot be settled on a general basis, the best sampling depending on the shape of the $h'(f)$ record.

A practical illustration of the substance of this section has already been given (KING, 1954); it compares reductions by KELSO's method using eight and ten ordinates with one based on equal intervals of $\log f$.

The maximum of a layer presents a difficulty, and there is an interesting device to overcome it—fitting a "nose" to the electron distribution.

Suppose that the sampling ordinates are at values of $\log f = \ldots, 0{\cdot}39, 0{\cdot}41, 0{\cdot}43, 0{\cdot}44, 0{\cdot}45$, and that the $F2$ critical frequency occurs at $\log f = 0{\cdot}457$. Then, we fit a power law "nose" passing through $h_{0{\cdot}44}$ and $h_{0{\cdot}45}$, and having a vertical tangent at $\log f = 0{\cdot}457$. This is done by using, instead of $a_{0{\cdot}45,0{\cdot}45}$, a factor $a'_{0{\cdot}45,0{\cdot}45}$, which allows for the curvature of $h(\log f_N)$; a' is calculated using refractive indices at intervals of 0·001 in $\log f/f_N$ ($h_{0{\cdot}457} - h_{0{\cdot}45}$) is determined by a geometrical factor from ($h_{0{\cdot}45} - h_{0{\cdot}44}$). For routine work at Christchurch, we fit a parabolic "nose", but we also have tables of factors, a', for a 5/3 power law, and it is not a difficult matter to run out a special "nose".

6. The Refractive Index

For all reductions made at Christchurch, we use refractive indices based on the Appleton-Hartree equation, neglecting collisions. The two principal assumptions, geometrical optics and neglect of collisions, seem to be satisfactory for our purposes, although there are indications that both will need a closer look when we

VOL. 11 1957

start reducing records from our newly established station in the Antarctic; it may be that the Appleton-Hartree equation is not good enough when propagation is almost along the magnetic field.

Now, it is a common practice to neglect the effects of the magnetic field, presumably because it is thought that at the higher frequencies it does not matter, and that, anyway, the shapes of the layers are not greatly altered but only the thicknesses. These are dangerous assumptions to make.

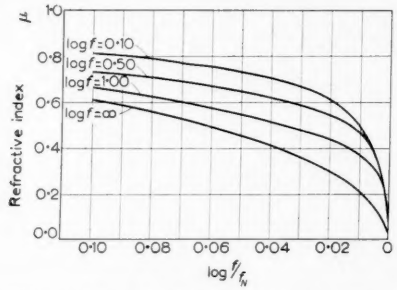

Fig. 2. Phase refractive index as a function of $\log f/f_N$, for four values of $\log f$. ($f_H = 1{\cdot}475$ Mc/s, $\theta = 21°53'$)

Fig. 2 shown how the phase refractive index, μ, varies with $\log f/f_N$ for different values of $\log f$ (gyro-frequency is 1·475 Mc/s, $\log f_H = 0{\cdot}169$, $\theta = 21° 53'$). The group refractive index is given by,

$$\mu' = \frac{d}{df} \cdot (\mu f) = \mu + \frac{1}{2{\cdot}303} \cdot \frac{d\mu}{d \log f} \tag{27}$$

Over the range illustrated, most important for producing retardation, the major term is the second—the gradient of this graph (putting $d \log f \doteqdot -d \log f_N$).

Obviously, there is as much difference between the no-field ($\log f = \infty$) and the 10 Mc/s curves as between the 10 Mc/s and 1·26 Mc/s curves.

The same fact is strongly brought out by the table of factors used in a step-by-step reduction (see equation 16).

Table of factors, a_{jj}, for log spacing

Without field	09·35	3·93	3·05	2·60	2·31	2·12	1·97
Log f = 1·0, log f_N =	1·00	0·99	0·98	0·97	0·96	0·95	0·94	0·93
With field	16·39	3·04	2·36	2·10	1·94	1·81	1·72	
Log f = 0·5, log f_N =	0·50	0·49	0·48	0·47	0·46	0·45	0·44	0·43
With field	20·33	4·11	2·51	1·99	1·79	1·66	1·54	
Log f = 0·1, log f_N =	0·10	0·09	0·08	0·07	0·06	0·05	0·94	0·03
With field	21·78	5·61	3·21	2·31	1·90	1·67	1·53	

Notice that the field does not change all the factors in the same ratio (nor even in the same direction); consequently, neglect of the field produced a differently

shaped $h(f_N)$—not merely a scaled one. This is most marked when there is a sharp $F1$ critical point, as is shown in Fig. 3—reductions of a moderately stormy sequence of records in summer.

Generally speaking, neglect of the field leads to inaccurate ideas on the variations of layer shapes through the day, with season, and with disturbance.

Again, it may be thought that the field is important only at medium and high latitudes. However, we include it for work on records from our low-latitude station at Rarotonga, for the difference there is still significant; anyway, it is just as easy once the refractive indices have been calculated—not too great a task, and well worth while.

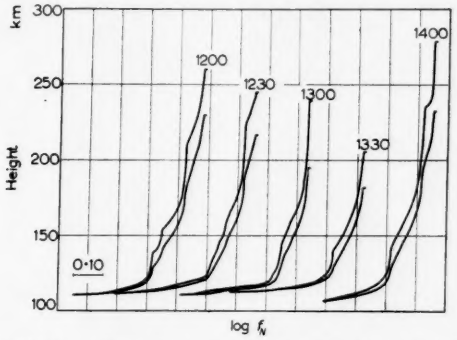

Fig. 3. Electron distributions from five records taken during a daytime ionospheric storm on 20 January 1954. (Christchurch). In each case, the upper curve shows a reduction neglecting the magnetic field, while in the lower curve, it is included.

VOL. 11 1957

7. Valleys Between Layers

The E-layer critical frequency is nearly always marked by an infinite virtual height, and, in summer, the $F1$ critical frequency often is. It is likely, then, that $h(f_N)$ is not single valued, and the integral method, giving a reduction which is single valued, will only indicate the lowest heights of the possible range for the upper layer.

Manning (1949) and Piggott (1954) have discussed the problem for the no-field case, and have shown that there is a wide region in which the $h(N)$ curve of the upper layer can lie.

Naturally, results including the magnetic field are similar; it turns out that the range of possible heights is even wider, although the highest distributions are incredible.

As the two previous workers have done, we can study the effects of inserting different shaped valleys. It is handy to note, in passing, that the step-by-step method of analysis is particularly well suited to this problem, using, if necessary, the modulus of D instead of D (see equation 15).

$$h = \sum |D| \tag{28}$$

$$h' = \sum a \,.\, |D| \tag{29}$$

Fig. 4 shows the normal reduction of a record (1204, 1 May 1956) taken to part way up the F layers, together with reductions including valleys of different

widths—the widest is 67 km. This record was chosen because the next in the series, at 1208, is practically identical, except that the virtual height does not become infinite at f_0E. It is fair to assume from this that the distribution at 1204 has only the slightest depression above the maximum of E, even though the h–f trace cannot tell us more closely than indicated by the wide limits in the figure.

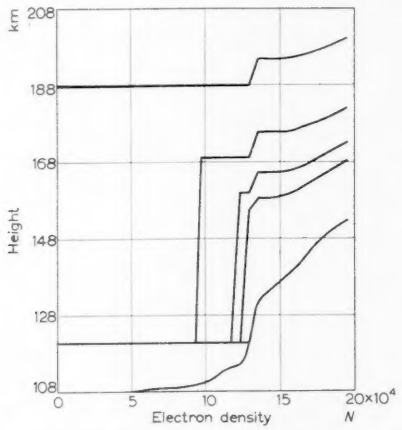

Fig. 4. Electron distributions from the record 1204, 1 May 1956. Almost rectangular valleys of different widths and minimum densities are portrayed in the different curves.

There are five physical facts suggesting that, regularly the density falls off only a little between E and F:

(1) Results of rocket flights (SEDDON, PICKAR and JACKSON, 1954).
(2) The cusp at f_0E is not always infinite.
(3) Slight distortion of the ionization causes an $E2$ layer to appear.
(4) The progress of a travelling disturbance from F to E indicates a considerable density in the valley.
(5) The appearance of a Z echo between f_zE and f_0E indicates a considerable density in the valley (LANDMARK and LIED, 1957).

Thus, we are left in a most unsatisfactory position; we feel that a direct reduction without a valley will be close to the actual distribution, yet we cannot be sure of it—it is always possible that there may be a valley.

Work at Christchurch ignores the valley.

8. ACCURACY OF ANALYSIS

On a normal clean recording, we can carry out a reduction to give a measure of the height of reflection within 2 km. But this does not mean that we know the true height to this accuracy, for many factors can affect the interpretation of the recording; a list of them is quite formidable.

(a) *Instrumental*

1. Resolution of the recording system.
2. Delay in the receiver (LYON and MOORAT, 1956).

(b) *Non-instrumental*

(1) Pulse distortion in the ionosphere (RYDBECK, 1942).
(2) Valleys between layers.
(3) Oblique paths.
(4) Retardation in D.
(5) Absorption in D.
(6) Broadcast interference.
(7) Blanketing by E_s.
(8) Obscuring of E trace by E_s, and F trace by a multiple of E_s and extraordinary of F.
(9) Spread echoes.

The instrumental factors can be controlled. It is not difficult to get better resolution than 2 km in the cathode ray tube and photographs system; incidently, if this has been achieved, there is little point in using an expanded height scale.

Delay in the receiver is very important. Some improvement may be possible with a system of recording at the peak of the echo, using a shaped transmitter pulse. Such may also help with the first of the non-instrumental factors.

The question of valleys has already been considered.

VOL. 11 1957

Next in importance is the fact that the path of the normal component of the exploring ray is not always vertical. Mainly because of travelling disturbances, there are practically always gradients of ion density, and, when the phase refractive index is nearly zero, these can cause large changes in the virtual height; the generation of an $F1$ cusp ($F1$ otherwise being absent), rapid changes about the E-layer cusp, and the formation of sequential E_s are familiar examples of this. As with the valleys, we cannot properly assess the importance of oblique paths. An excellent discussion is given by MUNRO and HEISLER (1956).

Retardation in the D layer affects mainly the value of the minimum height; the error is considerably reduced by the time we get to F. If this retardation be assumed responsible for the departure of E from the Chapman form (it may not be, of course), it would amount to several kilometres.

Absorption of the lower part of the trace by day, and broadcast interference at night both also affect the value of the minimum height. Except in winter, the absorption is not usually serious, but broadcast interference is a major factor; it can put a ten kilometre error in the heights of a night-time layer only fifty kilometres thick. It was for this reason that all the night F records given in Table 1 were taken at 0200 when the interference is least.

The last three non-instrumental factors are familiar to all workers. To gather some idea of their importance, consider a series that we reduced to provide background for a study of the F region; it is of the records at 08, 10, 12, 14, 16 and 18 hr for every day of June, 1954. Of the 180 records, 138 were reduced; reasons for not doing the other 42 were:

Obscured or blanketed by E_s	27 records
Absorption of the E region	8 records
Equipment failure	4 records
Spread echoes	3 records

This is a good set. Normally, E_s would spoil more, and night-time records are often lost through spread F. Absorption does not usually spoil many, while equipment failure is in the lap of the gods.

For a large part of our work, we can select clean records of the desired type; however, work on storms is often complicated by the presence of E_s and spread echoes.

9. APPLICATIONS OF "TRUE HEIGHT" ANALYSIS AT CHRISTCHURCH

The use of h–N curves has clarified greatly our ideas on the shapes and the variations of the ionized regions; ionospheric research has reached the stage where they are indispensable.

The major projects based on them at Christchurch are:

(1) Graphs of electron distributions at 03, 09, 12, 15, 21 and 24 hr on one calm day of each month; two and a half years have been done up to the present time.
(2) Theory of the F region
(3) Comparison of the ionosphere at Rarotonga and Hawaii.
(4) Study of nocturnal storms.
(5) Study of daytime storms.

Like most stations, we are hampered by lack of computing staff. Work on these projects is done by three physicists, with part-time assistance from a member of the technical staff. However, in less than three years, about five hundred records have been reduced, without taking up too much of our time. The process certainly is tedious, but it amply repays the work put into it.

Acknowledgements—This paper is the result of experience in the use of N–h curves in work by Mr. C. H. CUMMACK, Mrs. R. MASON, and myself. The interest of other members of the staff and of the Superintendent, Mr. J. W. BEAGLEY, is gratefully acknowledged.

REFERENCES

Comparison methods

BOOKER H. G. and SEATON S. L. 1938 *Phys. Rev.* **57,** 87.
Parabolic function, no magnetic field, application to more than one layer, use of hp, deficiency of h' as a measure of the height of an upper layer.

RATCLIFFE J. A. 1951 *J. Geophys. Res.* **56,** 463.

BEYNON W. J. G. and THOMAS J. O. 1956 *J. Atmosph. Terr. Phys.* **9,** 184.
Extend work of BOOKER and SEATON. The first pays particular attention to obtaining the total electron count using parabolic, linear, and inverse parabolic functions.

PIERCE J. A. 1947 *Phys. Rev.* **71,** 698.

GUHA U. C. 1949 *J. Geophys. Res.* **54,** 355.
Chapman function, no magnetic field.

SHINN D. H. 1953 *J. Atmosph. Terr. Phys.* **4,** 240.

MARIANI F. 1953 *Ann. Geofis.* **6,** 21.

ARGENCE E. and MAYOT M. 1953 *J. Geophys. Res.* **58,** 147.

ARGENCE E and MAYOT M. 1953 *Ibid.* **58,** 493.

BECKER W. 1956 *Arch. Elek. Ubert.* **10,** 207.
Five papers extending comparison methods to include the magnetic field.

APPLETON E. V. and BEYNON W. J. G. 1940 *Proc. Phys. Soc.* **52,** 518.
Parameters of parabolic layer from plot of h' against $f/2fc \ln (1 + f/f_c)(1 - f/f_c)$ near critical frequency.

Cox J. W. *Air Ministry Report TR/432.*
Analyses error in Appleton-Beynon method, due to layer shape and position of fc.
Shapley A. H. 1956 *First Report of Special Committee on World-Wide Ionospheric Soundings* Section III. 1. (4).
Recommends the use of $M3000$ as a height measure.
Shimazaki T. 1955 *J. Radio Res. Lab.* **2,** 85.
Gives a linear relation between hp and $M3000$.
Shinn D. H. and Whale H. A. 1952 *J. Atmosph. Terr. Phys.* **2,** 85.
Part I—calculation of refractive indices including the magnetic field. Part II—effect of neglecting field on methods of Booker and Seaton, and Appleton and Beynon.
King G. A. M. and Cummack C. H. 1956 *Ibid.* **8,** 270.
Fig. 5 shows how hp is misleading by day.

Integral methods
De Groot W. 1930 *Phil. Mag.* **10,** 521.
Pekeris C. L. 1940 *Terr. Mag.* **45,** 385.
Manning L. A. 1947 *Proc. Inst. Radio Engrs.* **35,** 1203.
Rydbeck O. E. H. 1942 *Trans. Chalmers Tech. Hogsk.* No. 3;
1940 *Phil. Mag.* **30,** 282.
Inversion of the integral equation for no-field case, and examples of reductions. Rydeck's papers show transformation of the X trace for vertical field to a form where a no-field analysis applies.
Whale H. A. 1951 *J. Atmosph. Terr. Phys.* **1,** 244.
Modification of the derived curve to include the magnetic field and simultaneous integration using a differential analyser. Mathematical technique is faulty, but the method is workable.
Nakata Y. 1946 *Rep. Jap. Res. Radio Wave Propagation* Vol. I. Ref. 29E.
Integration of the derived curve by spaced ordinates. References is not sufficiently detailed to make clear the method.
Kelso J. M. 1952 *J. Geophys. Res.* **57,** 357.
Kelso J. M. 1957 *J. Atmosph. Terr. Phys.* **5,** 11.
1957 *J. Atmosph. Terr. Phys.* **10,** 101.
The first gives a simple method of sampling the $h'f$ record to integrate the derived curve. The other two extend it to include the magnetic field by methods of successive approximations—they are too tedious for general use.
Budden K. G. 1954 *Proc. Conf. Ion. Phys. (Cambridge)* p. 332.
Step-by-step process set out to give h directly—especially suitable for an automatic computer.
Jackson J. E. 1956 *J. Geophys. Res.* **61,** 107.
Step-by-step process using graphs of the integral of refractive index.
King G. A. M. 1954 *J. Atmosph. Terr. Phys.* **5,** 245;
1956 *J. Atmosph. Terr. Phys.* **8,** 184.
Step-by-step process, the basis of the present paper. The second describes calculation of the refractive indices.

Miscellaneous
Grawart G. and Larsen H. 1954 *Z. Angew. Phys.* **6,** 736.
Becker W. 1955 *Arch. Elek. Ubert.* **9,** 277.
Saha A. K. 1956 *Indian J. Phys.* **30,** 464.
Wright J. W., Knecht R. W., and Davies K. *I.G.Y. Manual on Vertical Sounding* Section 3.9.
Four survey articles.
Manning L. A. 1949 *Proc. Inst. Radio Engrs.* **37,** 599.
Piggott W. R. 1954 *J. Atmosph. Terr. Phys.* **5,** 201.
Discussions on valleys between layers.

VOL. 11 1957

LYON A. J. and MOORAT A. J. G. 1956 *J. Atmosph. Terr. Phys.* **8,** 309.
Height errors due to receiver delay.

SEDDON J. C., PICKAR A. D., and JACKSON J. E. 1954 *J. Geophys. Res.* **59,** 513.
Rocket measurement of electron density.

APPLETON E. V. 1932 *Proc. Inst. Radio. Engrs.* **7,** 260.
Deduces Appleton-Hartree equation.

MUNRO G. H. and HEISLER L. H. 1956 *Aust. J. Phys.* **9,** 343.
Effect of travelling disturbances on $h'f$ records.

Journal of Atmospheric and Terrestrial Physics, 1957, Vol. 11, pp. 223 to 236. Pergamon Press Ltd., London

The waveforms of atmospherics and the propagation of very low frequency radio waves

J. Chapman*
Cavendish Laboratory, Cambridge

(*Received* 11 *July*, 1957)

Abstract—Experimental observations upon atmospherics by several techniques are described. It is shown, in particular, that the results obtained for waveforms and for frequency spectra can be interrelated. The frequency spectrum of the electromagnetic disturbance at the source—the lightning discharge—is considered, and evidence is presented indicating appreciable differences, in this respect, between individual flashes. The interpretation of the results, on the basis of wave-guide theory applied to the space between the earth and the lower ionosphere, is considered; this approach is entirely successful qualitatively, but quantitatively the agreement is less satisfactory.

VOL. 11 1957

1. Introduction

This paper describes recent work on atmospherics, carried out at the Cavendish Laboratory, Cambridge, designed to integrate the many different experimental and theoretical approaches in this field into a consistent whole. Several workers have observed the waveforms of atmospherics using conventional wideband receiver technique. Typical of this school is the work of Appleton and Chapman (1937), Rivault (1945) and Caton and Pierce (1952), their objects being to relate the appearance of the waveforms to source effects in the lightning discharge, and to effects in the path of propagation. Bowe (1951), Chapman and Matthews (1953) and Chapman and Macario (1956), on the other hand, have presented results in which sharply tuned receivers were used. This work enabled the propagation of individual frequencies in the spectrum of an atmospheric to be studied.

Theoretical work has been concentrated on the characteristics of the propagation path. Watson (1919) first used the concept of the ionosphere and the concentric earth as forming the two surfaces of a waveguide, in order to study long wave propagation, and Budden (1951) made the first systematic attempt to explain the propagation of atmospherics by this method; this approach has also been adopted by Schumann (1954), Wait and Howe (1957) and others.

In the present work, the three methods of approach outlined above have been used to complement each other. Only waveforms generated by the return-stroke of a lightning discharge to earth are considered in this account.

2. Experimental Techniques

The waveforms were recorded on an apparatus which was essentially that described by Caton and Pierce (1952), with modifications carried out to make it completely automatic in operation. The aerial and amplifying system gave a faithful reproduction of frequencies in the range 0·1–30 kc/s. Atmospherics

* Now with Courtauld's Ltd., Coventry.

were displayed upon a 10 msec cathode ray tube raster consisting of three parallel lines of approximately 3·3 msec duration each. An amplitude operated trigger selected the waveforms to be recorded, a typical example being given in Fig. 1.

Also illustrated is the record of the same waveform as displayed on the tuned receiver apparatus. This equipment, which has been described by BOWE (1951), was used simultaneously with the waveform apparatus. It incorporated five receiving channels, tuned to frequencies of 0·65, 3·5, 10, 18 and 27 kc/s, with their outputs displayed on five separate oscilloscopes. The record for each frequency consisted essentially of a free oscillation decaying with a time constant governed by the bandwidth of the receiver; the initial amplitude of this decay envelope gave a measure of the frequency content of the atmospheric at the frequency of the receiver. This quantity will be denoted by $A(f)_n$, n referring to the particular frequency concerned. Several hundred atmospherics originating from distances between 0 and 3000 km were simultaneously studied with both equipments.

BOWE only considered in detail frequencies of 10 kc/s and less, 10 kc/s being adopted as the reference frequency. In order to maintain the continuity of the geophysical record, one channel was tuned to this frequency throughout the present work. The other frequencies used were selected for the following reasons: 27 kc/s was chosen as being the frequency used by narrow sector recorders for the location of thunderstorms (LUGEON, 1939); it was hoped that propagation data obtained on this frequency would have an immediate bearing upon the working of these instruments, while at the same time providing data on the effect of precursors, the disturbances associated with the stepped leader preceding a return-stroke, on the spectra of the main atmospherics. Eighteen kc/s was chosen to bridge the gap in the spectrum between 10 and 27 kc/s, it being sufficiently close to the radio transmitter GBR on 16 kc/s for the work done with GBR by BRACEWELL, BUDDEN, RATCLIFFE, STRAKER and WEEKES (1951) to be relevant, and yet far enough to avoid interference effects. The two lower frequencies were chosen, as they lie on either side of the attenuation maximum observed by BOWE (1951) at about 2 kc/s; furthermore, the lowest frequency approaches those involved in the "slow-tail" of atmospherics (WATSON-WATT, HERD and LUTKIN, 1937).

Besides the waveform and tuned-receiver equipments, continuous records were made simultaneously on magnetic tape and, later, photographically, with fairly low time resolution, in order to relate the triggered records to preceding and succeeding events such as precursors or long, slow field changes. Other apparatus made a link with the Sferics organization of the British Meteorological Office (OCKENDEN, 1947); this organization immeasurably enhanced the value of the work by locating the sources of the recorded atmospherics, and the author gratefully acknowledges his indebtedness to the Director of the Meteorological Office and his staff for their co-operation.

3. RELATIONSHIPS BETWEEN WAVEFORMS AND THEIR FREQUENCY SPECTRA

The first step in the analysis of the results was to classify the waveform records in terms of their appearance, as done by many previous workers (RIVAULT, 1945; CATON and PIERCE, 1952); this classification is dealt with in Section 4. Maps were

prepared showing the places and times of origin of the many hundreds of waveforms collected. Details of this work have been published elsewhere (CHAPMAN and PIERCE, 1957); however, the salient point which emerged was that the classification, which had been adopted purely on the basis of appearance, was obviously linked with the distance, time, and geographical position of origin of the individual waveform types. This was in agreement with the findings of LUTKIN (1939), CATON and PIERCE (1952) and HORNER and CLARKE (1955).

Logically, the next step was to check whether the tuned receiver results showed a similar systematic behaviour. These results were expressed as the ratios of the responses of a pair of receivers, with the 10 kc/s receiver being used as one of the pair in all instances. Thus, for a given waveform, four quantities were obtained, these being $A(f)_n/A(f)_{10}$, where n took the values 0·65, 3·5, 18 and 27 kc/s. This method of presentation was adopted in order to minimize the spread in results due to variations between the amplitudes of individual lightning discharges. The assumption was made, on general considerations, that amplitude changes, without variations in the frequency spectrum of a discharge, were more probable than frequency spectrum changes with the amplitude remaining constant. That this assumption was reasonable has been shown to be justified by the regular nature of the results obtained. The ratios were plotted on maps similar to those utilized for the waveforms, and it was obvious that their distributions showed the same type of systematic behaviour.

VOL. 11 1957

The next step was to relate individual waveforms to their frequency spectra. Selected waveforms were analysed by the Beevers-Lipson strip technique, and the types of frequency spectra thus obtained were shown to be typical by confirmatory averaging carried out on the tuned receiver data for all examples of each type of waveform. It was found that each waveform type had its own characteristic type of frequency-amplitude spectrum, as had indeed been expected. Thus, the waveform classification based upon appearance alone had been linked with the objective tuned-receiver method, enabling precision to be given to the hitherto subjective methods of classification.

4. WAVEFORM CLASSIFICATIONS

Many former workers have classified waveforms, but all previous attempts have, however, used subjective methods and failed to deal comprehensively with the variations in source, temporal and propagation influences; it is considered that the present classification is an improvement, both in the former (the check by the objective tuned-receiver technique) and the latter respects. The relation of the present work to previous systems can readily be recognized.

The classification finally adopted is illustrated diagrammatically in Fig. 2; a waveform of a given type is governed primarily by whether it has been propagated under day or night conditions, and by the distance that it has travelled to the observing point. The geographical source of origin is also an important parameter (CHAPMAN and PIERCE, 1957), but in the classification, for convenience, this can be considered as covered by a modification of the distance effect. Fig. 3 illustrates records of some of the types in the classification.

When observations are made, by day, close to the point of origin of the waveforms, at least six types are observed (Fig. 3), referred to as 1+, 2+, 3+, and 1−, 2−, 3− in the classification. It is apparent that the last three are "mirror images" of the first three respectively, presumably being initiated from charge

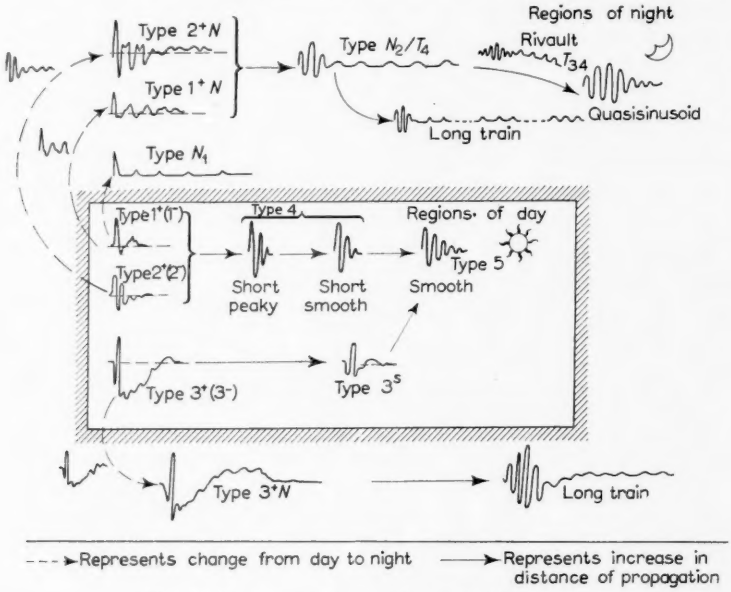

Fig. 2. Diagrammatic waveform classification.

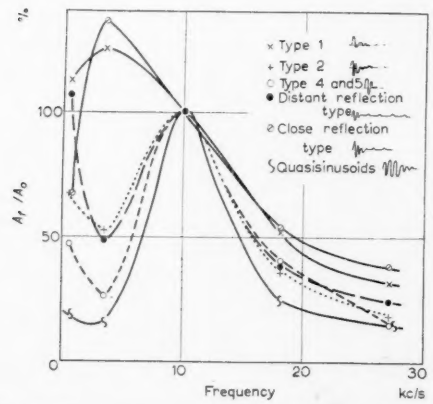

Fig. 4. Frequency spectra for selected waveform types.

centres of opposite sign. The salient distinctions between types 1, 2 and 3, + or −, are the presence of a sharp peak in 1, the presence of a sharp peak and a slow-tail in 3, and the absence of sharp peaks but the presence of a small slow-tail in 2. As the distance r increases, both types 1 and 2 merge into type 4 for

VOL.
11
1957

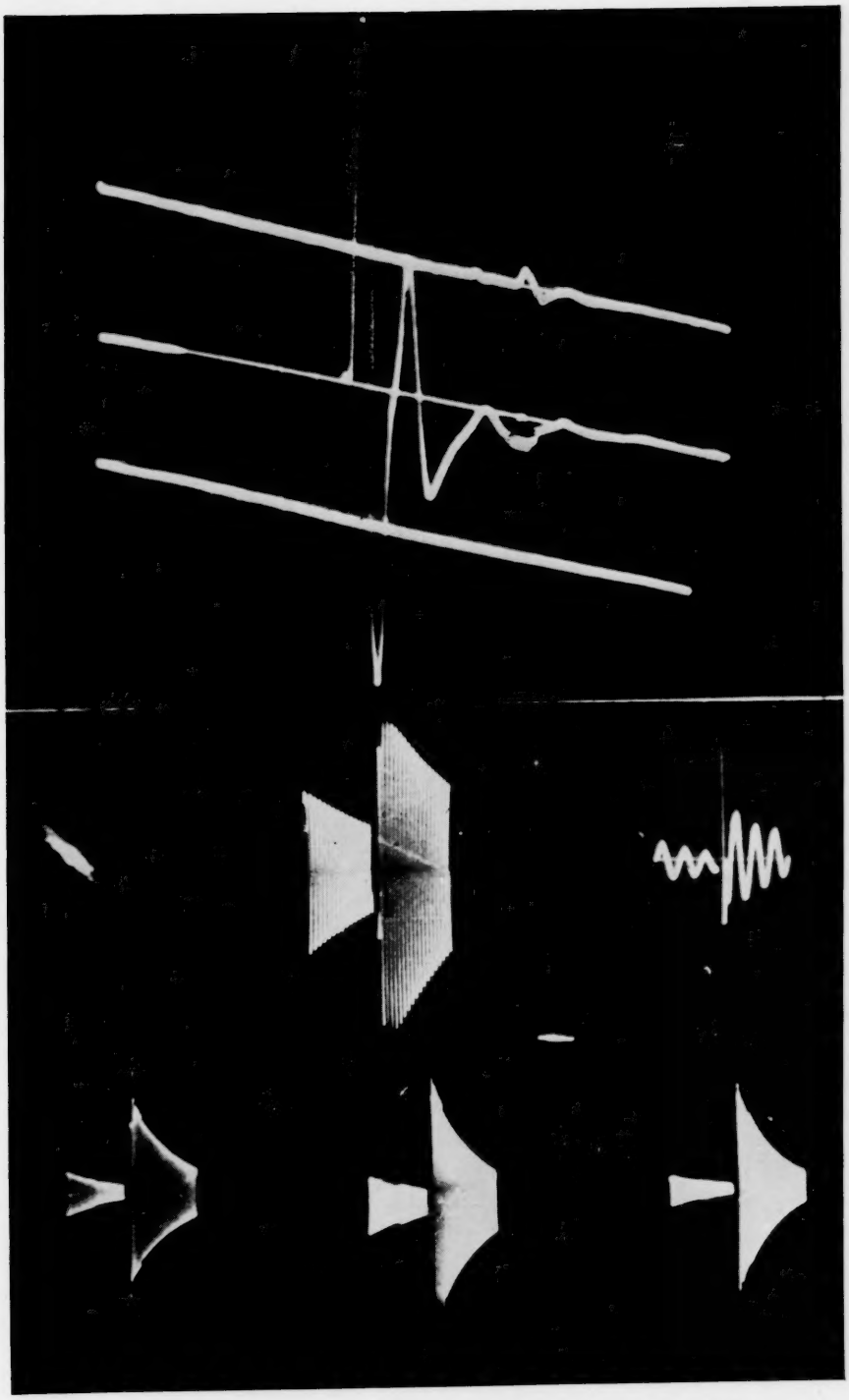

Fig. 1. Waveform record and the corresponding tuned-receiver record

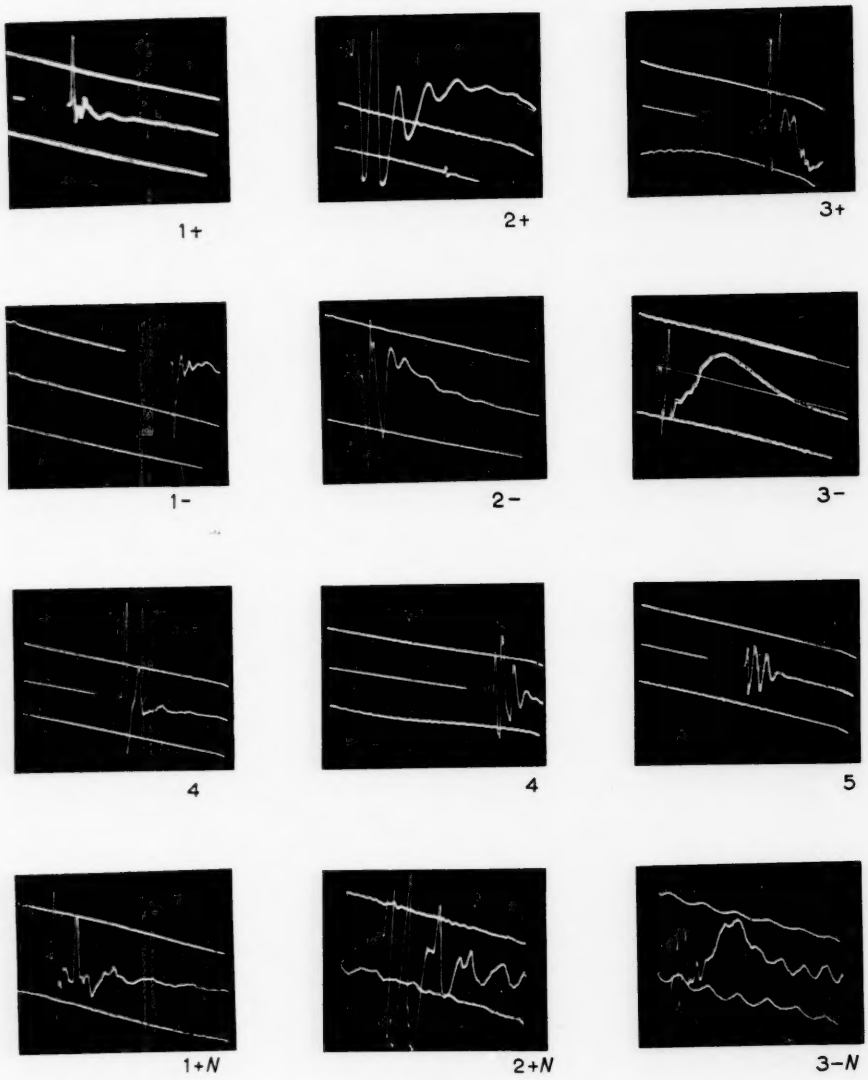

Fig. 3. Types of waveforms recorded

$r \approx 500$ km; type 4 then becomes increasingly smooth until for $r > 2000$ km it is replaced by type 5. Type 3 also develops with distance into 5, but without the intervention of 4.

At night the fundamental types are modified and extended by strong successive reflections from the ionosphere. There is again, however, an increasing smoothing of the waveforms with distance.

Now that the types of waveform have been defined, we may consider their frequency-amplitude spectra. Fig. 4 shows the spectra of selected types normalized to 10 kc/s for comparison, and it gives some precision to the statement that waveform shape and frequency content are interrelated. The curves were derived by the averaging of results from tuned receiver records. It is established (BOWE, 1951; CHAPMAN and MACARIO, 1956) that the propagation of atmospherics involves a frequency-selective attenuation in which there is a maximum of attenuation at about 2 kc/s and a minimum at 10 kc/s; below 2 kc/s propagation improves with decreasing frequency, while, above 10 kc/s, the higher the frequency the greater is the attenuation. It is apparent in the figure that this differential attenuation has been most pronounced for the quasisinusoidal atmospherics; this result is indeed to be expected, since quasisinusoidal waveforms are of very distant origin.

5. Source Effects

VOL. 11 1957

It is of interest to enquire into evidence suggesting the existence of the three different types of lightning discharge as indicated by the close waveform data. Indirect supporting data were given by the tuned-receiver work, in which it was found that the scatter in ratio amplitudes became very great when discharges were observed from very close ranges. This scatter is smoothed out by propagation, but at very close distances it clearly indicates considerable variation from discharge to discharge.

It appears that type 3 waveforms may have their origin in flashes in which a prolonged low current occurs after the return-stroke. Evidence for the existence of such currents is given by studies of "hot lightning" (BELLASCHI, 1939), and the presence occasionally of a pronounced slow electrostatic field-change immediately following a return-stroke. Several workers (APPLETON and CHAPMAN, 1937; WATSON-WATT *et al.*, 1937) have suggested that this slow field change is responsible for the "slow-tail," and observations by PIERCE (1955) show that the frequency of occurrence of this kind of field-change is consistent with the observed frequency of type 3 waveforms; the good propagation characteristics of very low frequencies (CHAPMAN and MACARIO, 1956) account for their observation from great distances.

Fig. 4 shows that we must seek the distinction between types 1 and 2 in discharges producing markedly different amplitude-frequency spectra at frequencies above 1 kc/s. This suggests that the two types are caused by differences in the rate of increase of the initial current in the discharge rather than by differences in continuing low currents at the end. That such differences do exist has been suggested by PIERCE (1955) from observations of the rapid electrostatic field changes corresponding to return-strokes. The optical spectra of lightning discharges also show much variation (DUFAY and TCHENG, 1949), but the most convincing evidence for the existence of at least two source types comes from the

widely different expressions for the current time variations in the return-stroke given respectively by NORINDER (1951, 1952) on the basis of flashes to open country and by BRUCE and GOLDE (1941) for, predominantly, discharges to prominent objects. The two different source spectra, deduced from the two current-time curves and using SCHONLAND's (1956) data for the rate of ascent of the return-stroke, are given in Fig. 5, which also shows in the middle curve the frequency-selective reduction in amplitude over a 200 km path by day. The lower curve shows the resulting spectra of the two waveforms 200 km, from the source obtained by combining the upper and middle graphs. It may be noted that these spectra are broadly similar to those of types 1 and 2, with a minimum at about 1 to 2 kc/s present in one case but absent in the other. A brief examination of these spectra would have suggested that type 2 had been subjected to much more

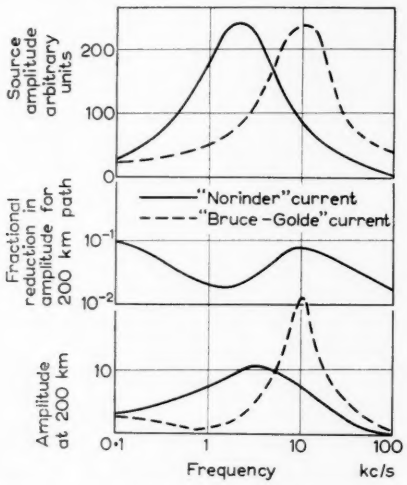

Fig. 5. Relationship between source spectra, propagation characteristics, and types 1 and 2 waveforms.

of the frequency dependent attenuation than had type 1, and so had originated at a greater distance, but the above work explains why in fact the two types are observed from similar distances.

It seems from all available evidence that two extreme types of return-stroke occur, with probable intermediate forms also existing, depending upon the rate of rise of the initial current. Also, either type may be followed by a continuing current giving a slow-tail which will produce, in the extreme case, type 3 waveforms. In fact, close type 3 waveforms might possibly be split into two types according to the character of the high-frequency part, but the evidence is insufficient for this to be done.

6. EXAMINATION OF DATA BY WAVEGUIDE THEORY

A detailed examination of the experimental information obtained was made using the theory of BUDDEN (1951). In this approach, propagation is considered

as being in a waveguide formed by the earth and a sharply-bounded ionosphere for which two parameters, h the height and p_r ($= 4\pi Ne^2/\varepsilon_0 mv$), where $N=$ number of electrons per unit volume of the ionosphere, e = charge on the electron, ε_0 = electric permittivity of free space, m = mass of the electron, v = number of collisions (per unit time per electron) are important. The electromagnetic field in any of the waveguide modes that are involved may be thought of as being composed of two component planewaves, having their wave normals inclined to the vertical at a complex angle θ; the value of θ is characteristic of a particular mode. BUDDEN shows the signal strength in a single mode, at a distance r measured horizontally from the transmitting discharge to be proportional to

$$r^{-1/2}(\sin\theta)^{1/2} \exp\{-ipr(\sin\theta)/c\}$$

where p is the angular wave frequency, and c is the velocity of light. This expression is approximate and is only valid for values of r greater than two wavelengths.

If we denote the real and imaginary parts of $\sin\theta$ by R and I, and put $k = -2\pi/\lambda$, where λ is the wavelength in free space, then the above expression may be rewritten,

$$r^{-1/2}(\sin\theta)^{1/2} \exp(-Ikr) \exp(-ikrR)$$

The quantity $\exp(-ikrR)$ gives the phase, and the remaining quantity is proportional to the amplitude, in the particular mode defined by θ, at distance r. θ depends on the parameters h and p_r, and, by assuming certain values for these, it was possible to compute values of amplitude and phase for given frequencies in any required mode. The EDSAC calculating machine of the University Mathematical Laboratory was used for this work, and reference should be made to the original work by BUDDEN (1951) for further details of the method.

In practice it is found that, for reasonable values of the parameters h and p_r, only the modes -2, -1, 0 and $+1$ are sufficiently unattenuated to be of importance; furthermore, the properties of modes -1 and 0, and of -2 and $+1$ are very similar This latter fact is fortunate, since there are now doubts as to whether negative order modes are indeed excited; these doubts, however, because of the virtual identity of the two pairs of modes, do not vitally affect the procedure that was applied.

The experimental observations may be compared with theory by three different approaches. We might define an "average waveform" for different areas and times from the maps which were prepared showing the origins of different types of waveform. Then an "average spectrum" for each area could be defined and used with the theory. In practice, this technique proved complicated and it was found best to adopt the other two approaches and present the tuned-receiver results in terms of the variation with distance, either of the response on one frequency, or of the ratio of the outputs on two frequencies. The latter method was preferred, since a certain amount of the scatter due to the source variations was thus eliminated, but both methods were used.

The process of comparing the observations with theory was complicated owing to the need to use EDSAC, and so only a small portion of the data was fully tested, namely those for 10 and 18 kc/s. Reasonable values of h and p_r

VOL. 11 1957

were assumed for calculating the amplitude and phase change for each of these frequencies, in each of the four important modes, over a range of distances. For each frequency, at each distance, the four amplitudes were then added vectorially and the amplitude-distance relationships were thus obtained. Either these or the ratio of the 18 and 10 kc/s curves could be compared directly with experiment. The values of h and p_r were then progressively modified, and further curves calculated, until a final satisfactory fit was obtained between theory and experiment.

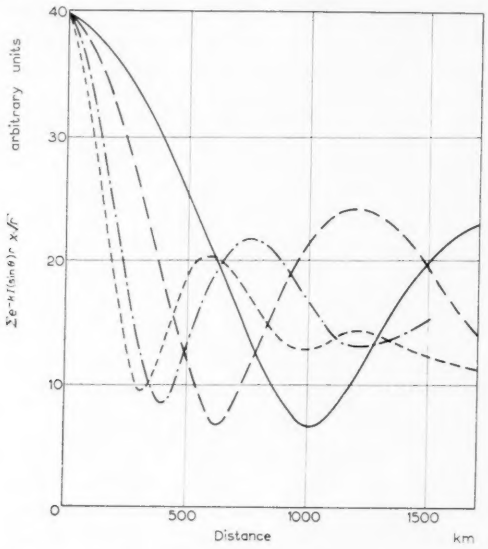

Fig. 6. Theoretical amplitude–distance curves. (The factor $r^{-1/2}$ is incorporated in the curves).
– – – – 10 kc/s
— – — 12·5 kc/s
—— —— 18 kc/s
———— 27 kc/s
$\beta = 10, u_{18\text{kc/s}} = 2{\cdot}644$
Vertical ordinate is proportional to (received amplitude) $\times$ (distance) $\frac{1}{2}$

Typical amplitude–distance curves are shown in Fig. 6. The quantities β and u referred to in the figure are subsidiary parameters given by the equations:

$$\beta = hp_r/c \quad \text{and} \quad u = p/p_r.$$

where c is the velocity of light. Fig. 7 illustrates preliminary and final theoretical fits to the experimental data for summer day runs in 1953.

Some of the tuned-receiver data are presented in Figs. 8 and 9; these curves were constructed by block-averaging data at 50 km intervals. Some of the fluctuations at the extreme ranges of the curves correspond to inadequacies in the data, but the majority of the points on the curves represent an average of from ten to twenty observations, and most of the oscillations therefore appear to be significant. Beyond a few hundred kilometres, the curves may all be likened to slowly falling exponentials, and it seems probable that only one waveguide mode is then important for their interpretation. At closer ranges, at least two, and probably more

modes, are required for a full explanation. The obvious danger of extrapolating data obtained from distant sources back to zero distance, in order to obtain information concerning the source spectrum of the discharge, is shown by the symbols on the zero-distance axis. These show where the ratio curves intersect the axis if they are extrapolated back as simple exponential curves. The spectra obtained by this method are markedly different from those obtained by extrapolating to zero the fully detailed curves as here presented.

In Fig. 7 the preliminary theoretical fit corresponds to the very reasonable values of the parameters, $h = 69$ km, and $N/v = 135 \times 10^{-7}$ cm^{-3} sec; at 69 km,

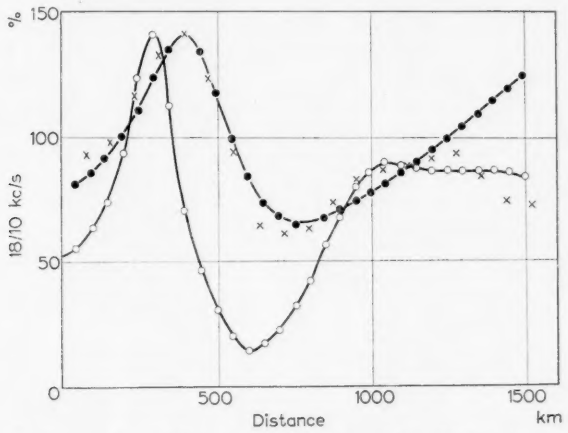

Fig. 7. Comparison of theory and experiment for 18/10 kc/s ratio curves.
Summer day runs 1953.
×—× Experiment
○—○ Preliminary theoretical
Fit $\beta = 10$; $u_{18\text{kc/s}} = 2{\cdot}644$
●—● Final theoretical
Fit $\beta = 2$; $u_{18\text{kc/s}} = 16{\cdot}9$

N may be estimated as 135–400 cm^{-3}, and v as 10^7–3×10^7 sec^{-1}. The final theoretical curve of Fig. 7 gave the best fit, but the ionospheric parameters associated with the indicated values of β and u are, particularly for daytime, far more unreal. Even with this curve, the agreement between theory and experiment is not striking owing to the divergence beyond 1000 km, but it must be remembered that the display of the experimental results in terms of ratios eliminates a factor of $r^{-1/2}$ (r being the distance) in the amplitude–distance relationship, and thus emphasizes the oscillations due to the presence of more than one mode. If comparison is restricted to a single frequency, and the factor $r^{-1/2}$ is therefore included, the agreement, as shown in Fig. 10, is apparently much more convincing. The experimental observations in this figure were made at night, while the theoretical results given are for the values of the ionospheric parameters $h = 90$ km and $N/v = 21 \times 10^{-7}$ cm^{-3} sec.

Although, quantitatively, agreement between the Budden theory and experiment is not entirely satisfactory, qualitatively the theory is entirely in accord with the experimental results. Fig. 11 shows two theoretical curves calculated for

VOL. 11 1957

constant values of h and variable values of p_r; it is apparent that the consequent changes in β and u merely alter the amplitude of the initial maximum. However, the theoretical curves of Fig. 12 show that if β is kept constant, h and p_r both being

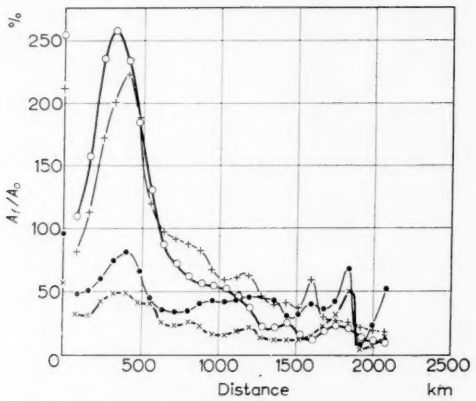

Fig. 8. Results of tuned receiver experiments expressed in ratio curves.
Summer day runs 1953.
+—+ 0·65/10 kc/s
○—○ 3·5/10 kc/s
●—● 18/10 kc/s
×—× 27/10 kc/s
The points on zero-distance axis show points at which hypothetical exponential curves intersect it.

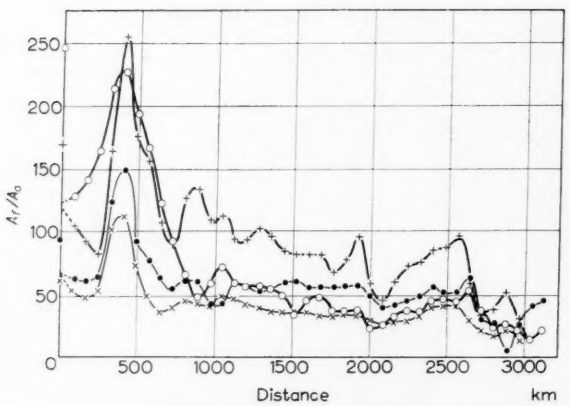

Fig. 9. Results of tuned receiver experiments expressed in ratio curves.
Summer night runs 1954.
+—+ 0·65/10 kc/s
○—○ 0·35/10 kc/s
●—● 18/10 kc/s
×—× 27/10 kc/s
The points on zero-distance axis show points at which exponential curves intersect it.

varied, then increasing values of h displace the initial maximum to greater values at greater distances than for the daytime curves. Figs. 13 and 14 show experimental ratio curves for 3·5 and 10 kc/s for day and night, the results obtained

from eastern and western sources being displayed separately. The major peaks obviously occur for greater distances at night-time, demonstrating the validity of the distance. In other words, changes in p_r vary the size but not the position of the peak, and a change in h is necessary to alter its position. Thus, at night,

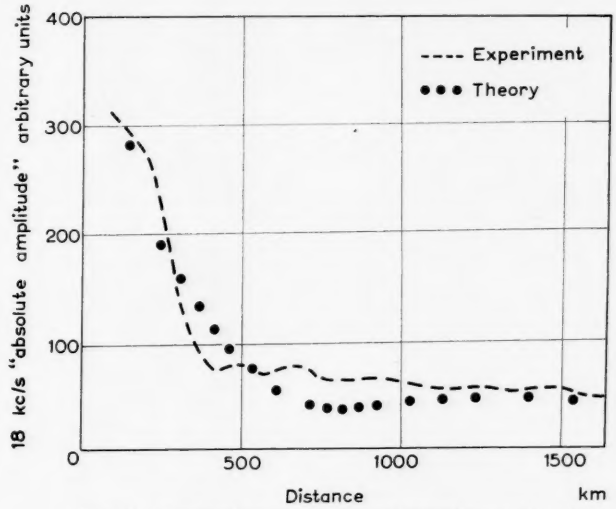

Fig. 10. Comparison of theory and experiment at 18 kc/s. Summer night runs 1954.

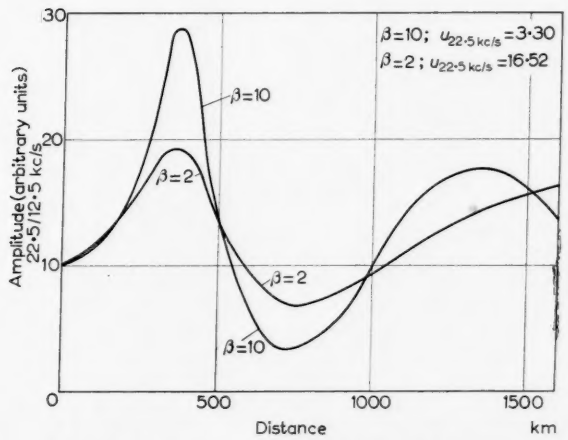

Fig. 11. Effect of changing β and u while h remains fixed.

we would expect the corresponding peaks on the experimental curves to occur of the theory. More detailed comparison between theory and experiment shows that changes between day and night are interpreted as an increase in h associated with a comparatively small decrease in p_r.

VOL. 11 1957

The curves of Figs. 13 and 14 introduce another feature of the results, namely, the marked difference between the curves constructed for eastern and western origins. This is to be expected from the observed differences in the distribution

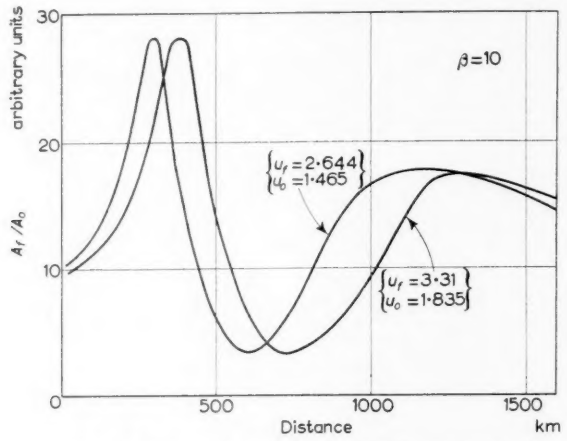

Fig. 12. Effect of changing u while β remains fixed.
(Again for frequencies of 22·5 and 12·5 kc/s.)

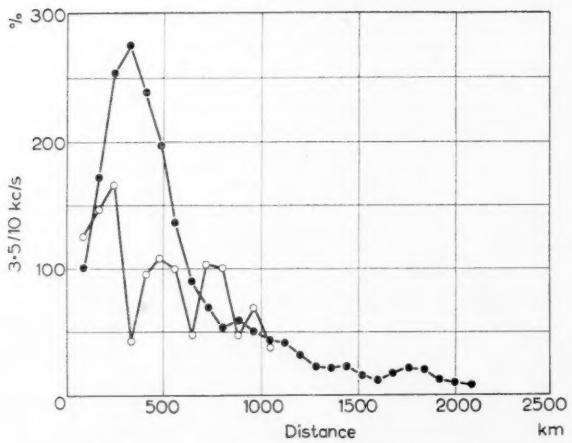

Fig. 13. Ratio curves for 3·5/10 kc/s. Summer day runs.
Eastern and western sources separated.
○ Western sources. ● Eastern sources.

of waveforms for different geographical sources (CHAPMAN and PIERCE, 1957). Comparison with the Budden theory indicates that an explanation of the differences may be obtained by assuming that the values of the parameters h and p_r to be used for east to west propagation are different from those for west to east propagation. However, a more likely explanation becomes apparent when we observe

that, for the British Isles, waveforms arriving from the west have travelled over a predominantly sea path, while those from the east have travelled mainly over land. TREMELLEN (1950) has shown that differences in propagation over land and sea do exist, and WAIT and HOWE (1957) have recently shown that these

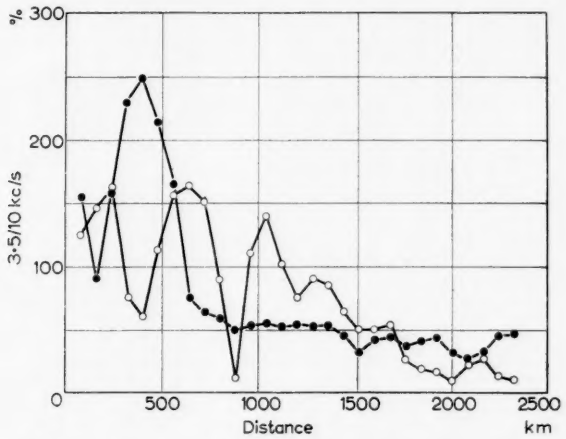

Fig. 14. Ratio curves for 3·5/10 kc/s. Summer night runs.
Eastern and western sources separated.
○ Western sources ● Eastern sources.

VOL. 11 1957

differences may be theoretically explained by considerations of the differences in conductivity of land and sea surfaces.

7. CONCLUSIONS

The interrelation of atmospheric waveform types and frequency spectra has been shown, and it has been indicated how there are systematic differences for both, dependent upon the time and the geographical position of origin of the atmospherics. It has been demonstrated that at least three different source spectra exist, and a new and comprehensive classification of waveforms based upon these, upon waveform observations and upon frequency-spectra data has been presented. The general problem of the propagation of atmospherics has been considered from both the point of view of waveform studies and of frequency spectra. Although both approaches are related, the latter has been preferred, as the main features of the experimental results were then explicable qualitatively in terms of the Budden waveguide theory. Quantitatively, the agreement shown between theory and experiment is less satisfactory. This may reflect inadequacies caused by insufficient data, or, more likely, by the scatter in amplitude or location errors of atmospherics. Alternatively, the theory, in which a sharply-bounded ionosphere and a perfectly conducting earth are assumed, may not be adequate for a full quantitative comparison with experiment. Observed differences in the geographical distributions of waveforms have been indicated; these have an explanation in the differences in propagation over land and sea paths.

Acknowledgements—The author wishes to thank the Department of Scientific and Industrial Research for the tenure of an award enabling this work to be completed. In addition, his grateful thanks are due to Dr. E. T. PIERCE for invaluable helpful discussions and suggestions throughout this work, and to Mr. R. V. E. BRUNDISH for help with the preparation of prints and diagrams.

REFERENCES

APPLETON E. V. and CHAPMAN F. W.	1937	*Proc. Roy. Soc.* A **158,** 1.
BELLASCHI P. L.	1939	*Elect. Engng.* **58,** 466.
BOWE P. W. A.	1951	*Phil. Mag.* **42,** 121.
BRACEWELL R. N., BUDDEN K. G., RATCLIFFE J. A., STRAKER T. W. and WEEKES K.	1951	*Proc. Inst. Elec. Engng.* Part III, **98,** 221.
BRUCE C. E. R. and GOLDE R. H.	1941	*J. Inst. Elec. Engng.* **88**(2), 487.
BUDDEN K. G.	1951	*Phil. Mag.* **42,** 1.
CATON P. G. F. and PIERCE E. T.	1952	*Phil. Mag.* **43,** 393.
CHAPMAN F. W. and MACARIO R. C. V.	1956	*Nature, Lond.* **177,** 930.
CHAPMAN F. W. and MATTHEWS W. D.	1953	*Nature, Lond.* **172,** 495.
CHAPMAN J. and PIERCE E. T.	1957	*Symposium on Propagation of V. L. F. Radio Waves* Paper No. 2, Boulder Colorado.
DUFAY J. and TCHENG MAO-LIN	1949	*Ann. Geophys.* **5,** 137.
HORNER F. and CLARKE C.	1955	*J. Atmosph. Terr. Phys.* **7,** 1.
LUGEON J.	1939	*Annales de la Station Centrale Suisse de Meteorologie,* No. 10.
LUTKIN F. E.	1939	*Proc. Roy. Soc.* A **171,** 285.
NORINDER H.	1951	*International Council of Scientific Unions, Joint Commision on Radio-Meteorology* p. 17.
NORINDER H.	1952	*Ark. Geofys.* **1,** 543.
OCKENDEN C. V.	1947	*Met. Mag.* **76,** 78.
PIERCE E. T.	1955	*Quart. J. R. Met. Soc.* **81,** 211.
RIVAULT R.	1945	*Notes Prel. du L. N. R.* No. 65.
SCHONLAND B. F. J.	1956	*Handbuch der Physik* **XXII,** 576.
SCHUMANN W. O.	1954	*Z. Angew. Phys.* **6,** 35.
TREMELLEN K. W.	1950	*Marconi Rev.* **13,** 153.
WAIT J. R. and HOWE H. H.	1957	*Proc. Inst. Radio. Engrs., N.Y.* **45,** 95.
WATSON G. N.	1919	*Proc. Roy. Soc.* A **95,** 546.
WATSON-WATT R. A., HERD J. F. and LUTKIN F. E.	1937	*Proc. Roy. Soc.* A **162,** 267.

Journal of Atmospheric and Terrestrial Physics, 1957, Vol. 11, pp. 237 to 254. Pergamon Press Ltd., London

Radio reflections from aurorae—III
The association with geomagnetic phenomena

K. BULLOUGH,* T. W. DAVIDSON,† T. R. KAISER‡ and C. D. WATKINS§

(*Received* 18 *April* 1957)

Abstract—This paper presents a further study of the radio-echo observations of auroral ionization, made on a frequency of 72 Mc/s between June 1949 and October 1953, described in a previous paper of this series (BULLOUGH and KAISER, 1955). The data are compared with geomagnetic observations made at Eskdalemuir during the same period.

A good correlation is found between the daily frequency distribution of the radio echoes and the mean daily variation in magnetic disturbance. The change from a positive to negative bay type of disturbance tends to occur between 2100 and 2200 hr local time and coincides with a minimum in the frequency of echo occurrence. This minimum separates the diffuse echoes (from westward-moving ionization) of the evening sequence and the discrete echoes (from eastward-moving ionization) of the morning sequence.

There exists a close correspondence between the occurrence of radio echoes and features in the magnetic disturbance. In a number of cases there appears to be a displacement in time between echo components and peaks in the magnetograms; it is suggested that this corresponds to the time of transit of the ionization between the reflecting region and the magnetic meridian through Eskdalemuir (some 10° in magnetic longitude to the west). The probability of occurrence of 72 Mc/s echoes during a positive disturbance is approximately double that for a negative one, being 50 per cent for $\Delta H > 100\,\gamma$ and $\Delta H < -200\,\gamma$.

The results and conclusions appear in several respects to conflict with the Chapman–Ferraro–Martyn theory of magnetic storms and aurorae.

VOL. 11 1957

1. INTRODUCTION

PAPER II of this series (BULLOUGH and KAISER, 1955; see also KAISER and BULLOUGH, 1955) described a series of radio echo observations of E-region auroral ionization made at the Jodrell Bank Experimental Station between June 1949 and October 1953. In the present communication, these radio-echo data are compared with the magnetic disturbances recorded at Eskdalemuir during the same period.

The equipment operated on 72 Mc/s and employed an aerial with a low-elevation pencil-beam directed 50° to the west of the magnetic meridian. Its characteristics are described briefly in II. The location of the region from which echoes were obtained is shown in Fig. 2 of II; its mean geomagnetic co-ordinates are 59·5° N, 76° E, while those of Eskdalemuir are 58·5° N, 83° E, and of Jodrell Bank 56° N, 83° E.

2. DAILY VARIATION OF RADIO-ECHO CHARACTERISTICS AND MAGNETIC DISTURBANCE

In this part of the analysis it proved convenient to study the disturbance, ΔV, in the vertical magnetic component at Eskdalemuir, since its fluctuations tended to be smoother than those in ΔH, while exhibiting a similar pattern of variation.

* Expéditions Polaires Françaises.
† Ferranti Ltd., Wythenshawe.
‡ Physics Department, University of Sheffield.
§ Jodrell Bank Experimental Station, University of Manchester.

The mean disturbance is referred to a quiet-day reference level, tending to be that of the undisturbed period centred on 1000–1100 hr UT; the resultant uncertainty in the zero of ΔV is $\pm 10\ \gamma$.

Previous analysis (see II) has revealed a well-defined daily variation in the frequency of occurrence and of the motion of auroral ionization. These are compared, in Figs. 1 and 2, with the corresponding mean daily variation of the magnetic disturbance at Eskdalemuir. The frequency shows a marked dip at about 2100 hr UT which divides what have been defined in II as the evening (before 2100 hr) and morning (after 2100 hr) echo sequences. The motion of the ionized regions, as has been shown in II, follows a parallel of magnetic latitude and is predominantly westward and eastward during the evening and morning sequences respectively. The two curves given for ΔV refer to those days on which echoes were observed during the evening and morning sequences respectively; the fact that echoes were sometimes observed before 2100 hr but not after, and vice versa, accounts for the failure of the two curves to meet exactly near 2100 hr.

Figs. 1 and 2 show the close relation between the daily variations of the echo characteristics and the magnetic disturbance. The diffuse evening echoes are associated with a westward movement of ionization and magnetic disturbances of the positive bay type, while during morning echoes, which have pronounced discrete structure, the motion is eastward and the magnetic disturbance is negative. The minimum in the frequency of echo occurrence coincides with the reversals both in direction of motion and in ΔV which occur between 2100 and 2200 hr UT. There is, in fact, a displacement of approximately 30 min in local time between the location of the reflecting ionization and Eskdalemuir such that in UT the mean variation of magnetic disturbance might be expected to precede that of the radio echoes. A displacement of this order is indeed suggested in Figs. 1 and 2.

Chapman (see Chapman and Bartels, 1940) has made a statistical analysis of worldwide observations of magnetic storms, from which he derived an idealized upper atmospheric current system. Vestine (1938) has studied the deviations from this model in some detail and has found a total variation of 4 hr in local time phase of the S_D variation along a parallel of geographic latitude, which can be attributed to the eccentricity of the earth's dipole field. This local time phase is earliest and latest at geographic longitudes 0–10° E and 180–190° E respectively.*

Chapman's peak current curve, adjusted to the longitude of Eskdalemuir, is also given in Fig. 2. It is in good agreement with the mean daily variation in ΔV except in two respects: the time separation between the peaks in ΔV (8–9 hr) is significantly less than indicated by the model and there is a striking lack of magnetic disturbance between 0900 hr and 1200 hr. A similar discrepancy has been noted at Saskatoon (Meek, 1954). The present analysis refers, of course, to fairly intense magnetic disturbances. However, an analysis by Vestine *et al.* (1947) has not revealed any essential change in character, apart from a southward penetration, from the moderate storms studied by Chapman; also, according to Chapman and

* A corresponding variation in local time phase of the daily variation in radio-echo occurrence has been shown by Kaiser (1956); the observations of Dyce (see Booker *et al.*, 1955), made at geographic longitude 76° W, show a bimodal distribution with a minimum at 2400 hr local time compared with 2100 hr for the Jodrell Bank results.

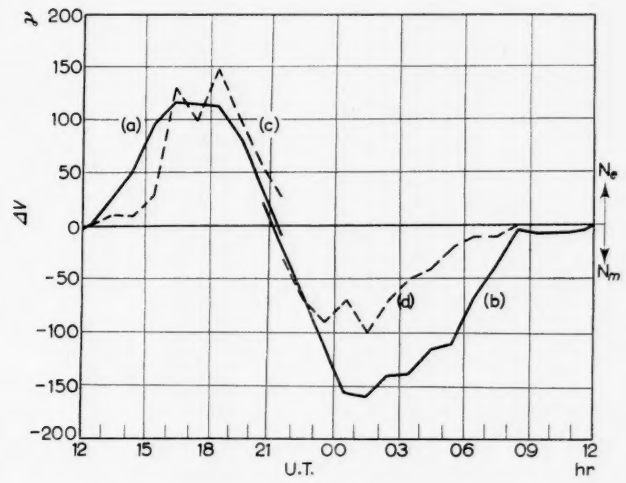

Fig. 1.
(a) ΔV for days when echoes occurred before 2100 hr UT.
(b) ΔV for days when echoes occurred after 2100 hr UT.
(c) and (d) Relative frequencies of occurrence of echoes during the evening sequence (N_e) and morning sequence (N_m) respectively.

VOL.
11
1957

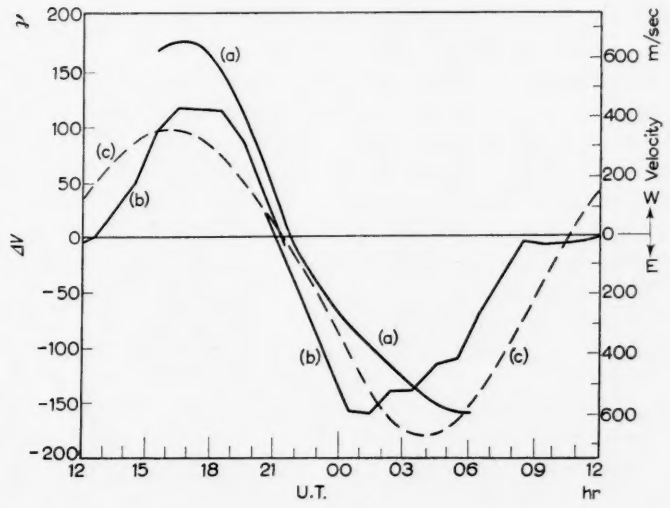

Fig. 2.
(a) Daily variation in the velocity of auroral ionization.
(b) ΔV (as in Fig. 1).
(c) Peak current (arbitrary scale).

Bartels (1940), the average characteristics of a magnetic storm do not vary greatly in type over a wide range in intensity of the D field. The daily variation in the velocity of the ionization appears to have a better correlation with the idealized current system (the velocity curve is missing, due to absence of echoes, during the quiet period centred on 1000–1100 hr UT). The above effects show that the statistical variation in the magnetic disturbance is related both to the velocity and to the intensity of the ionization, the low value of the latter, during the morning daylight hours, being associated with the quiet period in magnetic disturbance.

While the morning maximum in magnetic disturbances (and in peak current) is significantly larger than the evening one, there is no evidence for a similar asymmetry in the daily variation in velocity and occurrence of ionization (in fact, the reverse applies in the latter case). If the observed velocity is related to the velocity of effective net transport of charge, then this may imply a widening of the conducting region during the morning echo sequence.

The velocities of the ionized regions are often greatly in excess of the velocity of sound in the E region (and of E-region wind velocities derived from the drifts of meteor trails); they therefore represent a travelling disturbance rather than a real mass motion. It is clear, nevertheless, that there is an effective net transport of negative charge in the direction of motion of the ionization.

3. Radio-echo and Geomagnetic Observations during Individual Aurorae

A comparison, for individual aurorae, of the patterns of the radio echoes with the Eskdalemuir magnetograms for H brought out a quite remarkable correspondence between the occurrence of echoes and peaks in the magnetic disturbance.

The radio observations were transcribed to the same time-scale as the magnetograms (15 mm/hr) and the total range-spread, direction of motion, and echo-type (diffuse or discrete) was recorded for successive 4 min intervals. Some results are presented in Figs. 5–15. The range-spread is plotted upwards for generally westward motion and downwards for eastward (a few exceptional occasions when individual echo components exhibited movements opposite to the general trend are indicated by arrows).

It has been shown (Bullough and Kaiser, I, 1954; II, 1955; Kaiser, 1957) that the ionization during an individual aurora is distributed along an arc which follows a parallel of magnetic latitude and which intersects the aerial beam. Thus, if there is equal *a priori* probability during a given 4 min interval of finding intense blobs of ionization at all points of the arc which lie in the beam, the range-spread gives a representation (on a grossly non-linear scale) of the average echo-amplitude. The maximum possible range-spread equals the intercept on the arc between the zeros in the beam (ignoring effects of side lobes); it varies with the latitude of the arc, and for the present results lies between 350 and 550 km (see II, Fig. 3).

3.1. *The correlation between echo occurrence and the amplitude of the magnetic disturbance*

The results shown in Fig. 3 were obtained from analysis of 26 days (each reckoned from noon till noon) between 14/15 October 1949 and 15/16 October 1953,

the total integrated echo duration, T, being 2274 min. The disturbance amplitude, ΔH, was measured relative to a quiet-day level derived from the 24 hr record containing the storm period and tending to be that of the quiet period centred on 1000–1100 hr UT.

An examination of Fig. 3 reveals the following important feature of the 72 Mc/s echoes:

(i) The intervals during which $|\Delta H| > 50\ \gamma$ account for 92 per cent of the integrated echo duration.

(ii) Although for a given lower limit to $|\Delta H|$, negative disturbances tend to be more frequent than positive ones, the integrated echo duration is greater for positive ΔH. Fig. 3(b) shows that the probability of echo occurrence during a

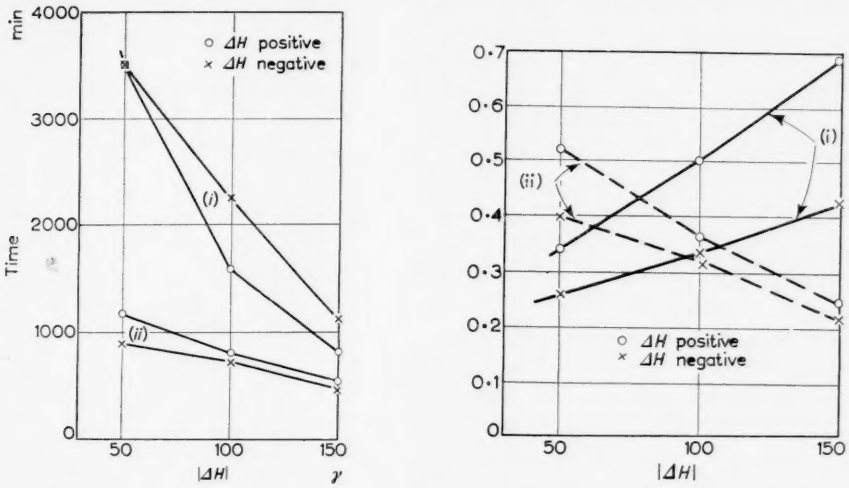

Fig. 3.

(a) (i) Total time T_1 and (ii) integrated echo duration T_2, for $|\Delta H|$ greater than the given value.

(b) (i) T_2/T_1.
(ii) T_2/T ($T = 2274$ min is the total integrated echo duration for the period covered by the analysis).

positive disturbance is approximately double that for a negative one, being 50 per cent for $\Delta H > 100$ and $\Delta H < -200$ respectively. The same tendency is apparent in Fig. 1.

It would therefore appear that for a given value of $|\Delta H|$ the electron density in the auroral ionization is larger during the evening sequence (ΔH positive) than in the morning (ΔH negative). This gives support to the suggestion (KAISER, 1956) that the morning maximum in echo occurrence may become relatively less pronounced at higher radio frequencies.

3.2. *The correlation between individual echoes and peaks in the magnetic disturbance*

For the purpose of analysis, the correlation between individual echoes (or groups of echoes) and peaks in the magnetic disturbance was divided into three categories:

Class α. The radio-echo sequence bore a marked resemblance to the pattern of

VOL. 11 1957

magnetic disturbance and often there was no possible doubt of the association between individual echoes and well-defined disturbance irregularities.

Class β. Peaks of magnetic disturbance occurred during the reception of echoes, but the detailed resemblance between the patterns of the two phenomena was not so marked.

Class γ. Magnetic disturbances of amplitude greater than 100 γ were unaccompanied by echoes.

Class α was most easily recognizable when the magnetic disturbance consisted either of isolated peaks with a relatively quiet background or well-defined peaks superimposed on a general disturbance. These occurred most frequently during the evening sequence. When the magnetic disturbance is more complex, it is normal to observe simultaneously echo components exhibiting a range of velocities; hence, in view of the separation between the reflecting clouds and Eskdalemuir ($\sim$500 km in longitude), only the class β type of correlation can be expected. This is especially so for the discrete echoes during the morning sequence, the components of which, in addition, are often of fairly short duration.

There were only seven occasions (12/13 June 1949; 29/30 June, 22/23 December 1950; 15/16 November 1951; 6/7 March, 5/6 November 1952; 17/18 April 1953) when radio echoes were not accompanied by large ($>100\ \gamma$) magnetic disturbance; however, except for 5/6 November 1952 0113–0213 hr UT, when intense multiple discrete echoes were obtained, the echoes were weak and of short duration.

An analysis, restricted to peaks of magnetic disturbance greater than 100 γ and omitting the great storm of 19/20 August 1950 because of the complexity of the magnetogram, gave fifty-four examples of class α correlations, thirty-nine of class β, and twenty-seven of class γ. Table 1 illustrates the close association between the direction of motion of ionization and the sign of the magnetic disturbance. In only 7 cases out of 93 was there an exception to the rule that westward and eastward motion of ionization are associated with positive and negative magnetic peaks in ΔH respectively; these could well have been accidental coincidences (particularly

Table 1. Analysis of the number of cases of classes α and β correlation in terms of the motion of the ionization for positive and negative magnetic disturbances. The columns "S" refer to stationary echoes (not necessarily to stationary ionization—see below)

Class	Direction of motion						Total
	ΔH positive			ΔH negative			
	W	E	S	W	E	S	
α	13	1	15	6	16	3	54
β	9	0	2	0	26	2	39
Total	22	1	17	6	42	5	93

Table 2. Number of cases of the various classes of correlation as a function of magnetic disturbance

$\lvert\Delta H\rvert$ (in γ)	Class of correlation					
	ΔH positive			ΔH negative		
	α	β	γ	α	β	γ
50–100	1	—	2	1	—	—
100–150	9	4	2	1	3	6
150–200	7	—	2	8	6	1
200–250	3	—	1	6	3	2
250–300	2	5	1	9	3	4
300–350	4	2	1	2	5	4
350–400	—	—	—	1	4	1
400–450	—	—	—	—	1	—
450–500	2	—	1	—	—	—
500–550	—	—	—	—	2	—
550–600	—	—	—	—	1	—
600–650	—	—	—	—	—	—
650–700	—	—	—	1	—	—

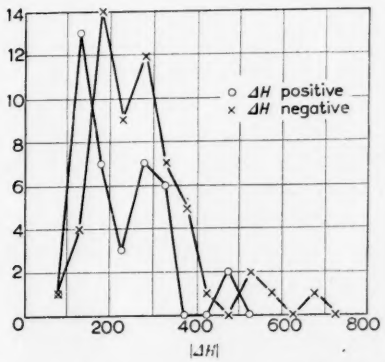

Fig. 4. Frequency of occurrence of class α and class β correlations as a function of magnetic disturbance.

VOL. 11 1957

in view of the displacement in longitude between the reflecting region and Eskdalemuir).

Table 2 and Fig. 4 illustrate the distribution of the various classes of correlation with amplitude of magnetic disturbance. These again show that there is a strong probability of obtaining radio echoes when the magnetic disturbance exceeds 150 γ, also that the occurrence of echoes requires rather larger values of $|\Delta H|$ for negative than for positive disturbances.

Figs. 5–15. The upper curve in each figure represents H at Eskdalemuir. Below appears the range-spread and the type of echo received during successive 4 min intervals. The former is plotted upwards for westward- and downwards for eastward-moving ionization.

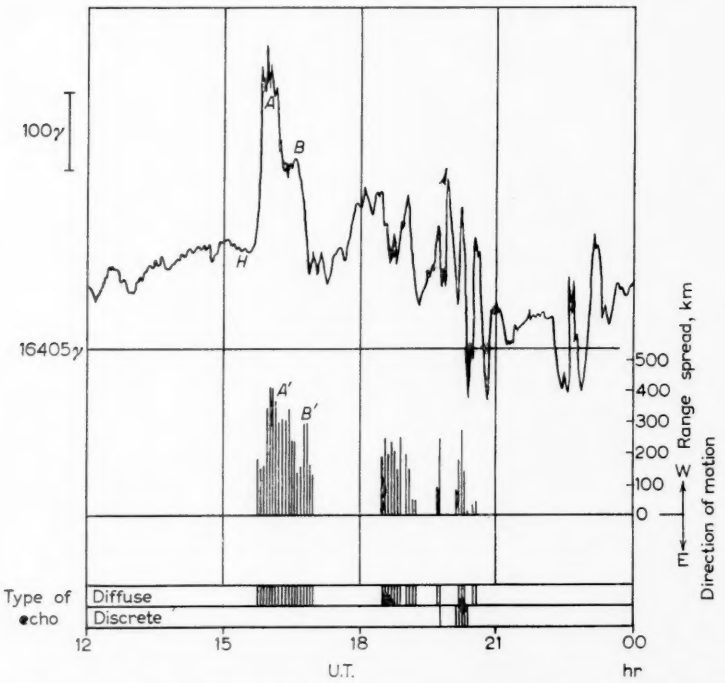

Fig. 5. 14 October 1949. The group of echoes between 1500 and 1800 hr were stationary diffuse, but are shown as corresponding to westward motion (see text).

4. Discussion

A superficial inspection of the magnetograms and echo patterns of Figs. 5–15 shows the close correspondence between the passage overhead (in or near the E region) of ionized clouds capable of reflecting 72 Mc/s radio waves and simultaneous magnetic disturbances—positive and negative for westward- and eastward-moving clouds respectively.* This correspondence is emphasized by the analysis given in Sections 3.1 and 3.2.

In a number of cases, particularly during the evening, it is possible to detect time displacements between isolated features in the magnetograms and groups of

* A similar excellent correlation between magnetic disturbance and scintillations of the Cassiopeia radio source has been found by Dagg (1957).

echoes. These correspond to the time of transit of the ionization between the reflecting region and the meridian of Eskdalemuir (a distance of 500–600 km). During the morning sequence, it is common to observe eastward-moving irregularities with a fairly wide spread of velocities; the corresponding magnetograms have a complex structure and it is not generally possible to identify with certainty time displacements between disturbance peaks and groups of echoes.

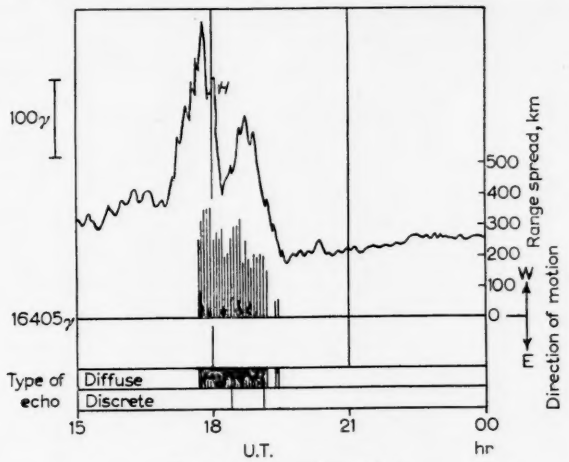

Fig. 6. 1 November 1949.

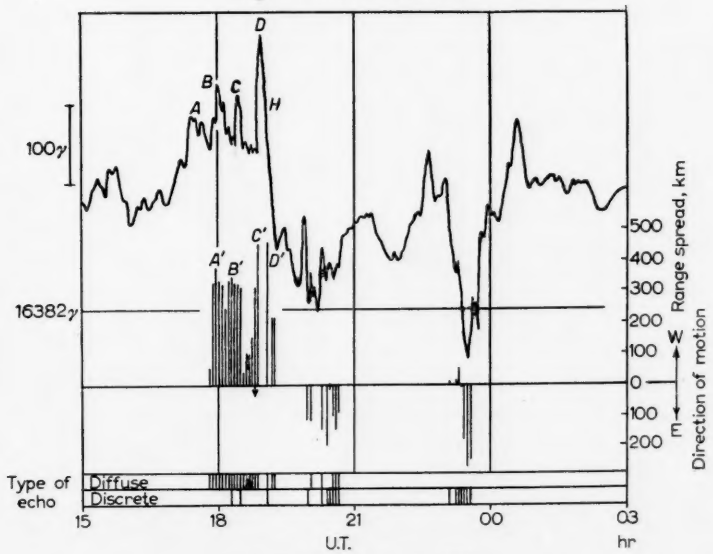

Fig. 7. 28/29 October 1950.

The following gives a description of some of the outstanding features, which are discernable in Figs. 5–15:

Fig. 15. This shows, for a single occasion, the complete daily trend in magnetic disturbance and echo characteristics. The echo observations commenced at 1550 hr,

VOL. 11 1957

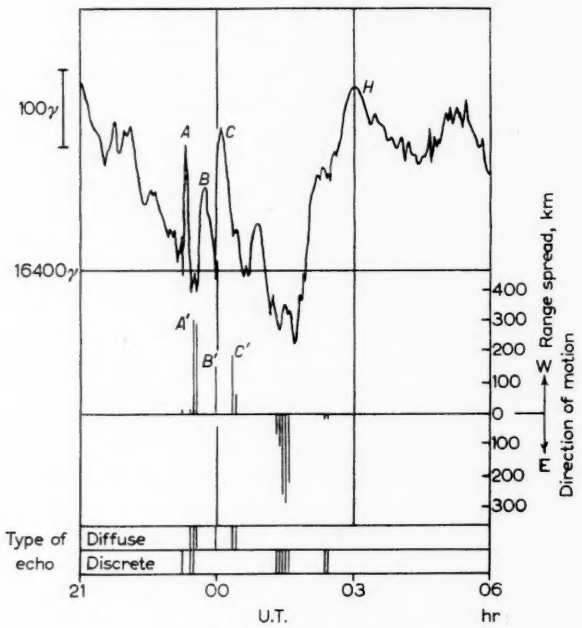

Fig. 8. 7/8 August 1950.

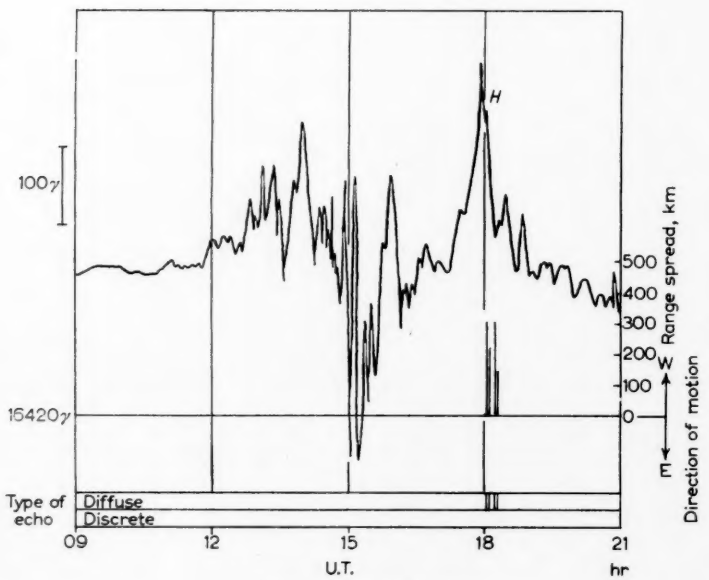

Fig. 9. 21 April 1952.

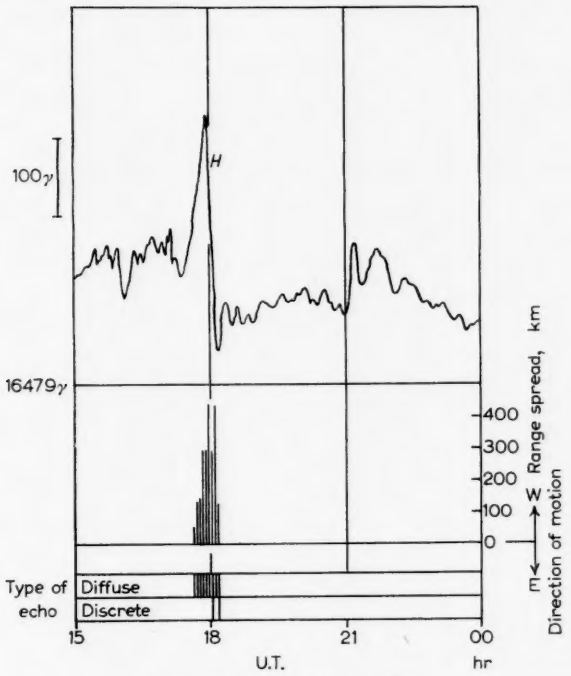

Fig. 10. 15 October 1953.

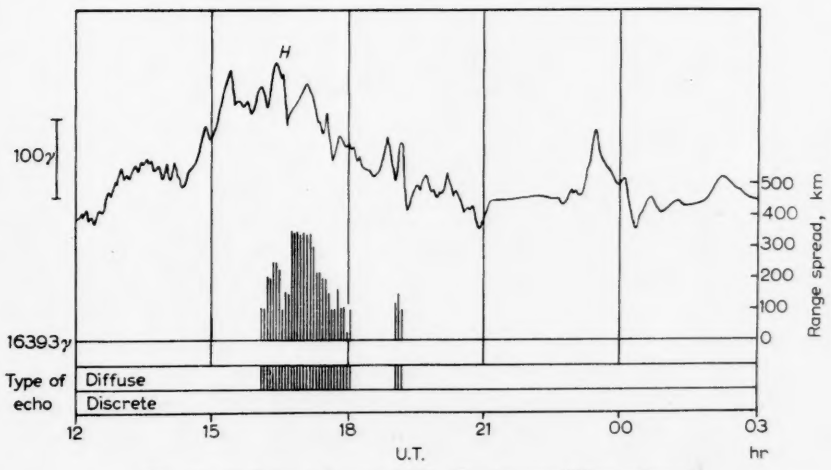

Fig. 11. 31 July, 1 August 1951. (Stationary diffuse echoes.)

VOL. 11 1957

when westward-moving ionization, giving diffuse echoes, accompanied a positive bay. The echoes faded out from 1845 till 2200 hr, while the magnetic disturbance reversed in sign. Subsequently, the ionization moved eastwards, giving discrete echoes, and persisted for the duration of the negative disturbance. Time displacements are not easily discernable due to the complexity both of the echo pattern and the magnetogram.

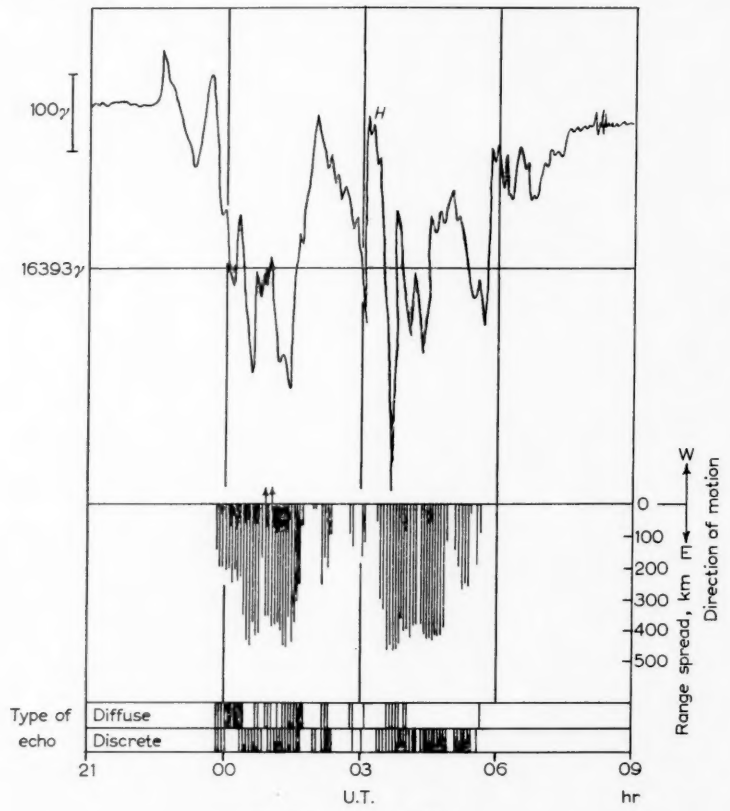

Fig. 12. 1/2 July 1951.

Figs. 9 *and* 10. Isolated positive bays are associated with echoes from westward-moving ionization. The echo maxima occur after the peak in H and the time displacements correspond to velocities of westward motion of about 500 m/sec (Fig. 9) and 900 m/sec (Fig. 10); the observed velocities were 300–500 and 550–850 m/sec respectively.

Fig. 8. The echo groups A', B', C' appear to follow about 15 min after the peaks A, B, C in H. The velocity of westward motion estimated from this delay ($\sim$750 m/sec) is somewhat less than that determined from the increasing range of the echoes ($>$1000 m/sec).

Fig. 7. The first group of echoes corresponds to a broad positive bay with several subsidiary maxima, A, B, C, D, while the echo pattern appears to have

VOL. 11 1957

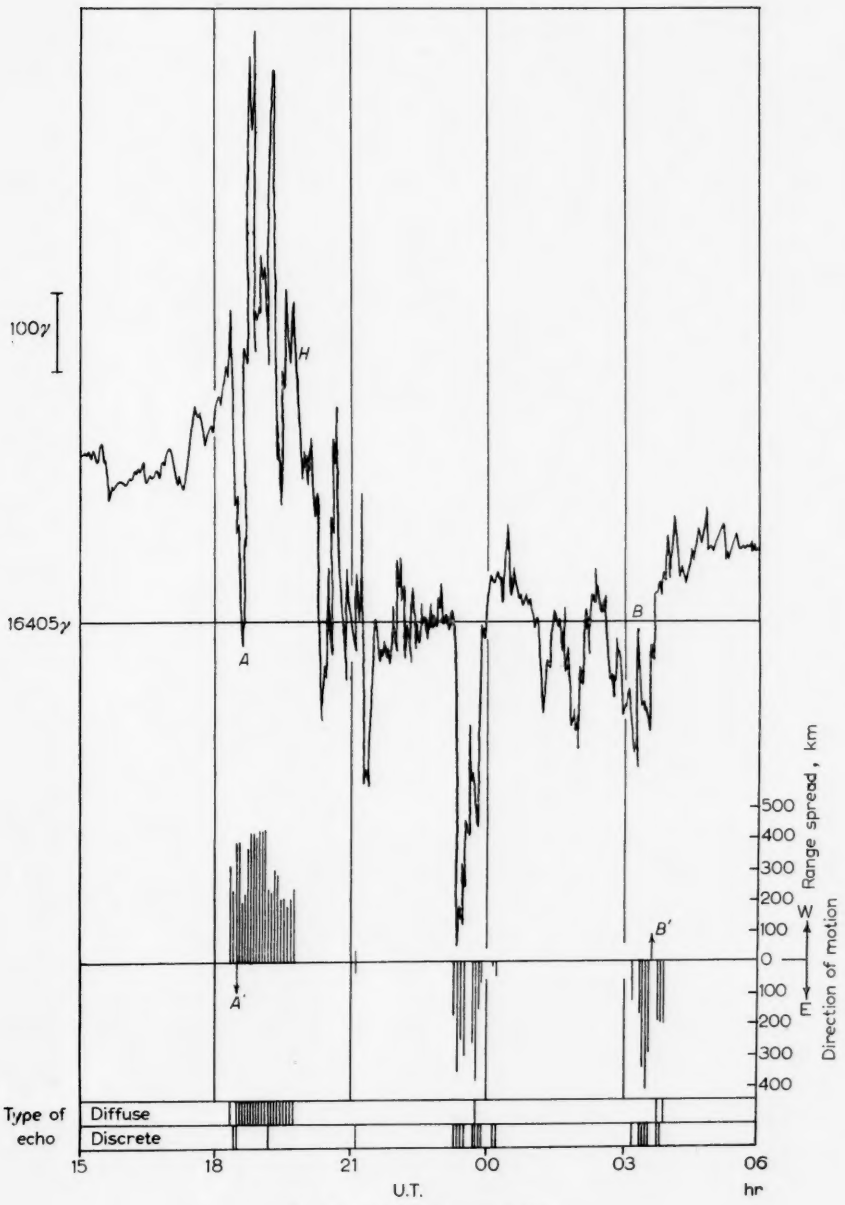

Fig. 13. 20/21 February 1950.

corresponding maxima A', B', C', D'. A', B' and C' occur some 20 min after the peaks in H, suggesting westward motion of velocity 500 m/sec, while D' occurs only 10 min after D, corresponding to a velocity of about 1 km/sec. It is interesting

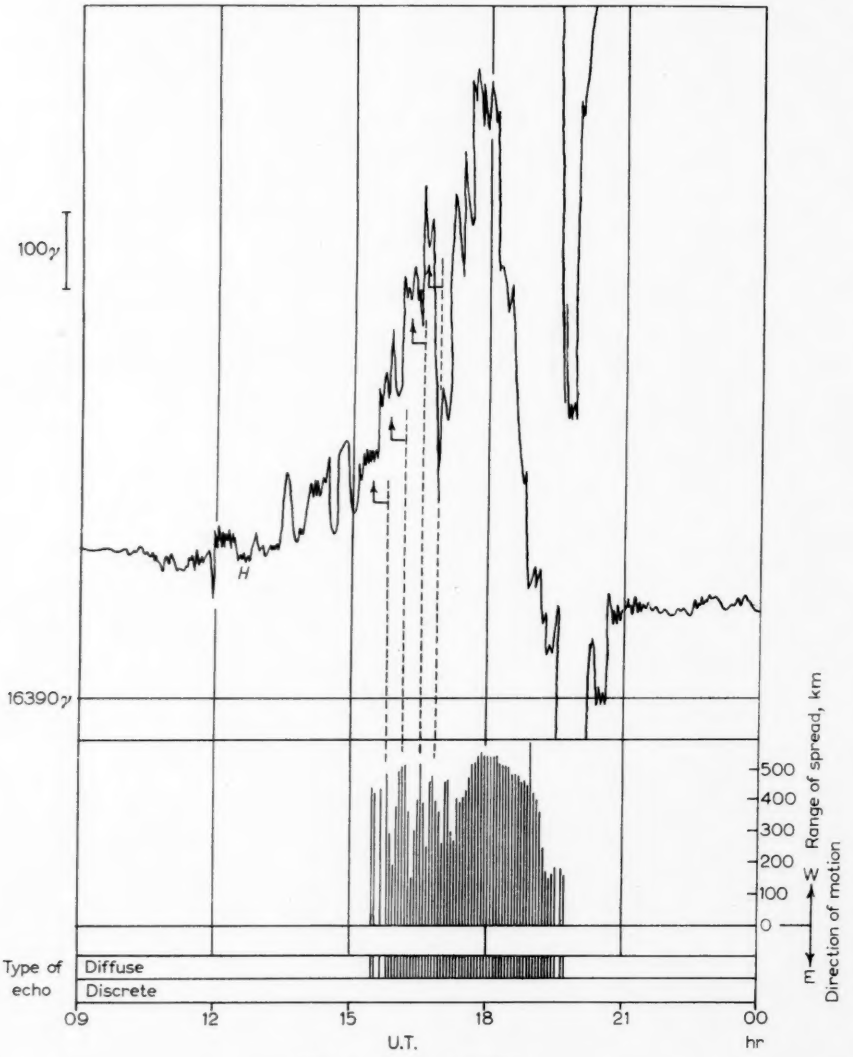

Fig. 14. 28 October 1951.

to note that the measured velocities were 500–600 m/sec for the echoes A', B', C', and 1200 m/sec for D'.

Fig. 14. Moving diffuse echoes passed through the centre of the aerial beam at the times indicated by the vertical broken lines. These were approximately 20 min after the subsidiary maxima in H indicated by the arrows. The westward velocity

(500 m/sec) estimated from this time displacement agrees with that determined from the rate of increase in range of the moving echoes.

Fig. 13. This occasion was an exceptional one, since well-defined echoes at A' and B' (see II, Figs. 17(a) and 17(b) exhibited directions of motion opposite to the prevailing trend. There appears to be little doubt of the association of A' with

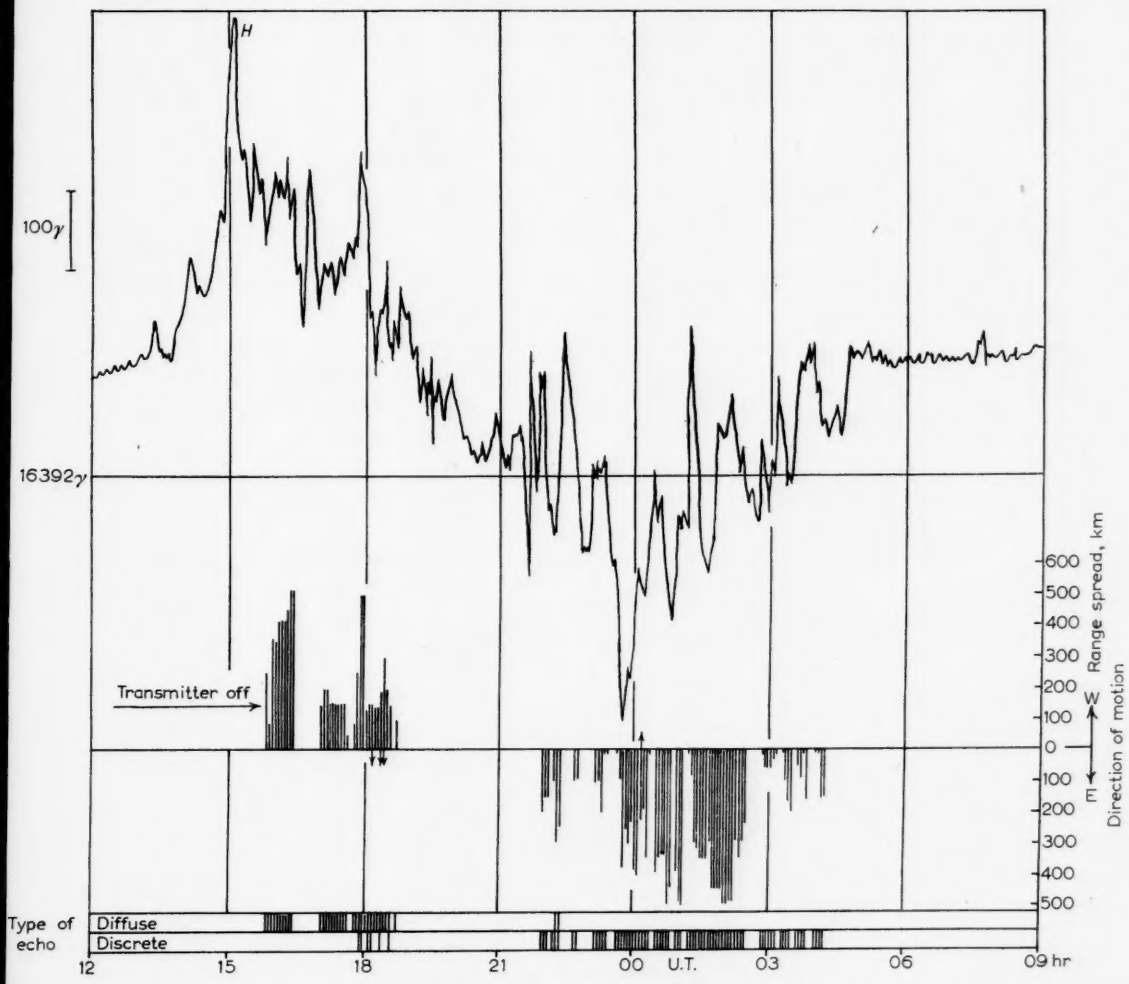

Fig. 15. 25/26 September 1951.

the pronounced negative peak A in H, which follows 7 min after the echo. The eastward velocity determined from the time displacement (1200 m/sec) agrees well with that obtained from the rate of decrease in range of the echo. The anomalous westward moving feature, B', follows about 18 min after the peak B in H. The association here is far from definite; however, the velocity deduced from the time-difference agrees with that measured directly (~500 m/sec).

VOL. 11 1957

Figs. 5 and 11. The echo group between 1500 hr and 1800 hr in Fig. 5 and all the echoes in Fig. 11 were of the stationary diffuse kind. In the former case, the structure of the echoes shows some similarity with the magnetic bay with a delay of about 15 min, suggesting that the ionization had a westward motion of about 500 m/sec, i.e. of the order normally found at the time of day.

On the basis of the foregoing, we can summarize the main features of the magnetic disturbances accompanying radio echoes as follows.

Stationary diffuse echoes (see II, Fig. 2(a)) occur in the evening and are accompanied by fairly smooth, long-enduring, positive bay disturbances (Figs. 5 and 11). We interpret these (see II) as originating in a distribution of blobs of ionization distributed along a parallel of magnetic latitude and extending through the whole aerial beam. Thus the stationary pattern does not imply stationary ionization, but only that it has a large east–west extension. In a number of cases, the lower range limit increased with time at the end of the echo, corresponding to the eastern limit of the ionization moving through the aerial beam—i.e. the ionization shared the westward motion normally observed in the evening.

Moving diffuse echoes (see II, Fig. 2(b)) arise when the east–west extension of the intense ionization is somewhat less than the intercept of the aerial beam with the magnetic parallel on which it is moving. They are observed in the evening, have westward motion, and correspond to positive magnetic disturbances, either isolated (Figs. 6,9,10) or superimposed on the main disturbance (Figs. 7, 8, 14), which have durations comparable with the time of passage of the ionization across the meridian of the magnetic observatory.*

The discrete echoes of the morning sequence are generally of larger amplitude and much shorter individual duration than the diffuse evening echoes. The corresponding magnetograms have the more complex fluctuating character associated with the negative bay type of disturbance.

The implication of the above would appear to be that the magnetic disturbance is associated with spatially localized regions of intense ionization moving horizontally along a magnetic parallel of latitude, and not with a purely time-changing current of worldwide extent. It suggests that, while the ionized clouds must preserve nearly electrical neutrality, there is a net drift of negative charge (presumably of electrons) in the direction of motion of the clouds. Some type of electrical discharge seems the most likely cause. The correlation between radio echoes and the Eskdalemuir magnetograms, obtained some 500 km to the east, shows that the ionized clouds have considerable stability, especially in the evening.

The clouds of ionization we have in mind would have a relatively small cross-section ($<$ a few tens of km, see I) transverse to the arc on which they lie and a much larger dimension of hundreds of km (or more in the case of stationary diffuse echoes such as in Fig. 11) along the arc. While the mean density, n_e, of electrons would be less than the critical density for 72 Mc/s (7×10^7 cm^{-3}), it would fluctuate, creating smaller regions with $n_e > 7 \times 10^7$. In the evening these may be relatively small but large in number (giving diffuse echoes), while in the morning they may be

* Observations, made with a rotating aerial, of auroral ionization during the magnetic storm of 25 February 1956 (Dagg *et al.*, 1957), show an excellent correlation between the times at which localized ionized regions cross the meridian of Eskdalemuir and maxima in the H component.

larger and smaller in number (giving discrete echoes). If we take a transverse cross-section of 100 km^2 for such a cloud and assume that the electrons drift relative to the positive ions with the observed velocity of the cloud (say 500 m/sec), then, neglecting earth currents, a magnetic disturbance of 150 γ would require a mean electron density $\bar{n}_e \sim 10^7$ cm^{-3}, which appears fairly reasonable. During the morning sequence the transverse cross-section of the ionization may tend to be greater than in the evening, hence for a given value of $\bar{n}_e$ the value of $|\Delta H|$ would be larger.

This picture brings into question the idea of a persistent worldwide storm current system, since it would appear that (i) the magnetic disturbances are associated with the transient occurrence of the auroral ionization and take place with respect to the quiet period of the 24 hr record (see Section 3), and (ii) the structure of the moving ionization is reflected in the "irregular" variation of the magnetic field. In this respect the present results lend some weight to the views of NIKOLSKY (1947), who has suggested, on the basis of a study of the irregular disturbance D_i, that the mean regular variations (S_D and D_{st}) are merely statistical results and do not represent persistent field changes. NIKOLSKY also finds that the values of H during the quiet hours of a disturbed day are exactly the same as on the quietest days. In view of this, the magnetic variations studied in the present work would represent the total disturbance.

The above results and conclusions seem in several respects to conflict with the Chapman–Ferraro–Martyn theory of magnetic storms and aurorae (MITRA, 1952; FERRARO, 1955). This derives the S_D and D_{st} systems from an upper atmosphere current and an extra-terrestrial ring current respectively, whereas the present results suggest a common atmospheric origin for the whole disturbance. MARTYN's theory also predicts a drift of ionization from the day to the night hemisphere, while the opposite is actually observed. A further difficulty appears when we try to reconcile the quiet period of several hours (centred on 1000–1100 hr) with the idea of a continuous worldwide current system.

Acknowledgements—The observations described in the paper were carried out at the Jodrell Bank Experimental Station (Director, Prof. A. C. B. LOVELL), and were supported by a grant from the Department of Scientific and Industrial Research. We are especially indebted to the Meteorological Office for generously providing the magnetic information.

VOL. 11 1957

REFERENCES

BOOKER H. G., GARTLEIN C. W. and NICHOLS B.	1955	*J. Geophys. Res.* **60**, 1.
BULLOUGH K. and KAISER T. R.	1954	*J. Atmosph. Terr. Phys.* **5**, 189.
BULLOUGH K. and KAISER T. R.	1955	*J. Atmosph. Terr. Phys.* **6**, 198.
CHAPMAN S. and BARTELS J.	1940	*Geomagnetism* Clarendon Press, Oxford.
DAGG M.	1957	*J. Atmosph. Terr. Phys.* **10**, 194.
DAGG M., VICE R. W. and WATKINS C. D	1957	*Jodrell Bank Annals* In publication.
FERRARO V. C. A.	1955	*Ann. Géophys.* **11**, 166.
KAISER T. R.	1956	*The Airglow and the Aurorae* p. 156. Pergamon Press, London.

Kaiser T. R.	1957	*J. Geophys. Res.* **62,** 297.
Kaiser T. R. and Bullough K.	1955	*Ann. Géophys.* **11,** 279.
Meek J. H.	1954	*J. Geophys. Res.* **59,** 87.
Mitra S. K.	1952	*The Upper Atmosphere* (2nd Ed.). The Asiatic Society, Calcutta.
Nikolsky A. P.	1947	*Terr. Mag.* **52,** 147.
Vestine E. H.	1938	*Terr. Mag.* **43,** 261.
Vestine E. H., Laporte L., Lance I. and Scott W. E.	1947	*Carnegie Inst. Publ.* **580,** 359 Washington, D.C.

Journal of Atmospheric and Terrestrial Physics, 1957, Vol. 11, pp. 255 to 258. Pergamon Press Ltd., London

Curvature-induced error in the analysis of fading records

N. J. RUMSEY
Dominion Physical Laboratory, Department of Scientific and Industrial Research,
Lower Hutt, New Zealand

(*Received* 20 *June* 1957)

Abstract—Curvature of lines of maximum amplitude in a radio field-strength pattern drifting across an array of three receivers can introduce an error into the estimate of the drift velocity, but the error is expected to be large only infrequently. The mean error is smaller for an array of receivers at the corners of an equilateral triangle than for one at the corners of a right-angled triangle.

VOL. 11 1957

WHEN RATCLIFFE (1954) introduced the idea of "lines of maximum amplitude" in the radio field-strength pattern drifting across an array of receivers, he showed in his Fig. 3 that such lines may be curved, but he treated them as straight in his subsequent deduction of the drift vector. In this he seems to have been justified by other investigations. Curvature appears to be negligible in the synthetic field-strength pattern of BRIGGS and PAGE (1954): and time variations of the pattern (BRIGGS, PHILLIPS, and SHINN, 1950; PHILLIPS and SPENCER, 1955) are likely to be much more important. However, on investigating the effect of curvature of lines of maximum amplitude, it was found that under certain conditions this can introduce large errors into the estimated speed and direction of movement of the field strength pattern; also that the maximum and mean errors are smaller for an array of three receivers at the corners of an equilateral triangle than for the more usual array of receivers at the corners of a right-angled isosceles triangle of comparable size. This supports BIBL, HARNISCHMACHER, and RAWER (1954) in their choice of an equilateral array. An outline of this investigation is given below. The notation used will follow RATCLIFFE (1954).

It will be assumed here that the form of the field-strength pattern does not change with time, but that the pattern moves bodily with velocity V. Consider three receivers O, A, and B where $OA = OB = a$ and $A\hat{O}B = 90°$ as shown in Fig. 1. Let ϕ be the angle between the direction of movement of the pattern and the line OA. Let ψ be the angle between the line QOP and the direction of movement of the pattern—where QOP is the tangent at O to the curved line of maximum amplitude $Q'OP'$ at the instant when this passes over O. Let c be the curvature (reciprocal of the radius) of $Q'OP'$. (c is assumed small.) Then, by a slight extension of RATCLIFFE'S analysis we can calculate the time intervals T_x (between the instants at which the line of maximum amplitude passes over O and A) and T_y (between the corresponding instants for O and B).

It is convenient to think of T_x and T_y as the components of a vector. But the forms of the expressions for these quantities immediately suggest that the vector should be considered to be the sum of the following three vectors:

$$T_0 = ((a/V)\cos\phi, (a/V)\sin\phi),$$

which is the vector sought, because it indicates the true speed and direction of the movement;

$$T_\psi = ((a/V) \sin \phi \cot \psi, -(a/V) \cos \phi \cot \psi),$$

which may be called the ψ-error vector. It is always normal to T_0. And

$$T_c = (-\tfrac{1}{2}(a^2/V)c \sin^2 \phi \operatorname{cosec}^3 \psi, -\tfrac{1}{2}(a^2/V)c \cos^2 \phi \operatorname{cosec}^3 \psi),$$

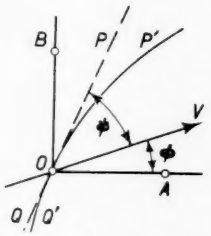

Fig. 1. A curved line of maximum amplitude, $Q'OP'$, passing over the array of receivers at O, A, and B.

which may be called the c-error or curvature-error vector. It may lie at any angle to T_0 depending on the particular value of ϕ.

It is further convenient to resolve T_c into two components, parallel and normal respectively to T_0. The second of these components is, of course, parallel to T_ψ and may be added directly to it This component need not concern us further here, since minor extensions of methods already proposed for dealing with ψ-induced

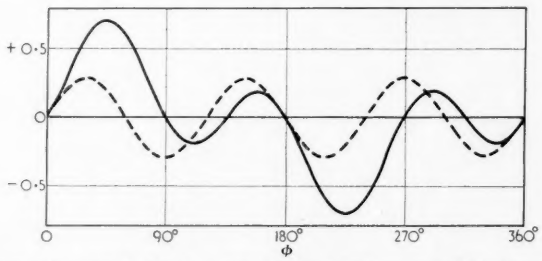

Fig. 2. Full line: $\sin \phi \cos \phi (\sin \phi + \cos \phi)$, the function on which depends the variation of curvature-induced error with direction of movement in the case of the right-angled array. Dashed line: $(\sin 3\phi)/(2\sqrt{3})$, the corresponding function for the equilateral array.

error (PÜTTER, 1954; COURT, 1955; CHAPPELL and HENDERSON, 1956) should be able to deal with this also. However, the component of T_c parallel to T_0 (which will be denoted by T_{c0}) produces an error in the estimate of T_0, and hence of V. In the case we have been considering

$$T_{c0} = -\tfrac{1}{2}(a^2/V)c \sin \phi \cos \phi (\sin \phi + \cos \phi) \operatorname{cosec}^3 \psi.$$

In the case of an equilateral triangular array ($A\hat{O}B = 60°$), the corresponding expression is

$$T_{c0} = -\frac{1}{4\sqrt{3}} (a^2/V)c \sin 3\phi \operatorname{cosec}^3 \psi.$$

In both cases $\operatorname{cosec}^3 \psi$ is a factor. This means that the curvature-induced error tends to be very large when the line of maximum amplitude makes a small angle with the direction of movement. Fortunately, this happens relatively infrequently (BRIGGS and PAGE, 1954). The numerical example worked out below throws light on this.

When a factor $-\frac{1}{2}(a^2/V)c \operatorname{cosec}^3 \psi$ has been removed from each of the two expressions above for T_{c0}, the functions of ϕ remaining behave as shown in Fig. 2. It will be seen that the functions have zeros whenever the direction of movement is along a line joining two of the receivers, and maxima for directions normal to such a line. The most striking features of the figure are the large maxima associated with movement normal to the hypotenuse in the case of the right-angled triangular array. The values at the maxima for the equilateral case are only 41 per cent of these. A fairer idea of the relative merits of the two arrays is given by comparing the mean values of T_{c0} over all values of ϕ. The average magnitude of T_{c0} in the equilateral case is 67 per cent, and the r.m.s. value 58 per cent, of the corresponding quantity for the right-angled case.

We still know too little about the details of radio field strength patterns on the ground to know whether significant curvatures of lines of maximum amplitude are present, or, if so, how frequently. However, in order to gain some idea of the seriousness of the effects investigated here, the following example has been worked out. It is assumed that errors caused by any other effects can be corrected. The direction of movement (ϕ) is assumed to be such as to give T_{c0} its r.m.s. value over all directions. The angle ψ is assumed to have the probability distribution associated with a pattern whose correlogram is circular and Gaussian (LONGUET-HIGGINS, 1957). This is most conveniently given by the expression $p(\cot \psi) = 1/[6(\frac{1}{3} + \cot^2 \psi)^{3/2}]$. The probability of a given curvature, c, of a line of maximum amplitude is assumed to be independent of ψ and ϕ. Then, taking a specific value of $c = 1/(5a)$ as an example, we ask for what fraction of the time that this curvature is present will it cause an error of 10 per cent or larger in the estimate of T_0 (and hence of the speed of movement of the field strength pattern). The answer is 13·4 per cent of the time in the case of the right-angled array, and 7·8 per cent of the time for the equilateral array. Whether the reader considers that this does or does not represent something of significance will depend mainly on his estimate of the frequency with which curvatures at least as large as $1/(5a)$ are likely to occur.

In any case, the investigation shows that the equilateral array has an advantage over the right-angled array if curvatures are present. Because the significant dimension of an array varies with ϕ from $0{\cdot}707a$ to $1{\cdot}414a$ in the right-angled case, while it varies only from $0{\cdot}866a$ to a in the equilateral case, it is clear that the equilateral array also has other advantages in performing the more nearly independently of direction of movement of the field strength pattern. This can be of importance in connection with errors of time interval measurement (treated by BARBER (1957) in an accompanying note), with effects of time variation of the form of the field strength pattern, and with the decrease in correlation between records with increase in separation of receivers normal to the direction of movement of the pattern. A strong case appears to have been built up in favour of the equilateral array

VOL. 11 1957

References

Barber. N. F	1957	*J. Atmosph. Terr. Phys.* **11,** 298.
Bibl K., Harnischmacher E. and Rawer K.	1954	Phys. Soc. Conf. *Phys. of the Ionos.* p. 113.
Briggs B. H. and Page E. S.	1954	*Ibid.* p. 119.
Briggs B. H., Phillips G. J. and Shinn D. H.	1950	*Proc. Phys. Soc.* B **63,** 106.
Chappell D. W. G. and Henderson C. L.	1956	*J. Atmosph. Terr. Phys.* **8,** 163.
Court G. W. G.	1955	*J. Atmosph. Terr. Phys.* **7,** 333.
Longuet-Higgins M. S.	1957	*Proc. Phys. Soc.* B **70,** 559.
Phillips G. J. and Spencer M.	1955	*Proc. Phys. Soc.* B **68,** 481.
Pütter P. St.	1954	Phys. Soc. Conf. *Phys. of the Ionos.* p. 191.
Ratcliffe J. A.	1954	*J. Atmosph. Terr. Phys.* **5,** 173.

Journal of Atmospheric and Terrestrial Physics, 1957, Vol. 11, pp. 259 to 271. Pergamon Press Ltd., London

The electron content of the ionosphere

J. V. Evans
Jodrell Bank Experimental Station, University of Manchester

(*Received* 1 *July* 1957)

Abstract—The investigation of the long period fading of radio echoes from the moon has provided a new technique for the measurement of the total electron content of the ionosphere (Browne *et al.*, 1956). This method is based on the measurement of the rotation of the plane of polarization of the radio waves produced by the magneto-ionic effect in the earth's ionosphere. Some preliminary results (Evans, 1956) indicated that the total electron content is approximately twice that which would be expected on the basis of a simple parabolic layer from $p'f$ data. In this paper a brief account of the technique is given together with a description of the method of analysing the records. The results of observations over a period of one year are then given. The technique is at present severely handicapped by the limited observing time imposed by the fixed (transit) aerial, and in consequence the results for some lunar months are poor. However where good results have been obtained, the ratio between the observed electron content and that in the parabolic model has always been in the region of 2 : 1. There appears to be some evidence that the diurnal variation of the total ionospheric electron content is not completely regular, which is suggestive of tidal effects.

VOL.
11
1957

1. Introduction

Murray and Hargreaves (1954) observed radio echoes reflected from the moon using a horizontally polarized transit aerial at a frequency of 120 Mc/s. They found that the echoes were subject to severe rapid fading which, like Kerr and Shain (1951), they attributed to the effect of the moon's libration. They also found that the mean amplitude of the echoes was subject to slow variations, which were prominent during the daytime but largely absent at night. This suggested an ionospheric origin, and application of the Appleton-Hartree equation for the propagation of radio waves through the ionosphere showed that the plane of polarization of the radio waves will be rotated due to the presence of the earth's magnetic field. A brief account of the relevant features of this magneto-ionic effect is given in the next section.

The extent of the rotation is dependent upon the total electron content along the line of sight to the moon, and Browne *et al.* (1956) suggested that the electron content of the ionosphere might be found by measuring the amount of rotation. A technique was therefore developed in which the amount of rotation could be deduced by comparing the fading on two close spaced frequencies. This experiment required modifications to the equipment which will be briefly described.

Some preliminary results (Evans, 1956) have been published for the months of October and November 1955. Since that time the observations have been continued, and this paper presents the results of this work. So far the technique has been handicapped by the limited observing time imposed by the aerial which restricts observations to within ± 30 min about transit for fourteen days every month. Thus in order to obtain useful results, it has been necessary to assume that the ionosphere behaves similarly from day to day and to anticipate continuity in the fading observed on successive days (transit occurs about an hour later each day). Where,

however, continuity is not observed between two successive days, or where there is little long period fading the results become very uncertain. A new technique for measuring the total electron content is being developed which obviates these difficulties and it is hoped that this new method will shortly be brought into use.

2. The Magneto-Ionic Effect

At a frequency of 120 Mc/s, and for ray directions within 60° of the lines of force of the earth's magnetic field a plane polarized radio wave is propagated through the ionosphere as two circularly polarized waves having different phase velocities. Thus when these circularly polarized waves re-combine the plane wave produced is rotated relative to the original one. For the double path from the earth to the moon, Browne *et al.* (1956) have shown that the total amount of rotation introduced is given by

$$\Omega = \frac{1}{2\pi^2} \cdot \frac{e^3 c}{m^2 f^2} \int_0^R N B \cos\theta \sec\chi \, . \, dh \text{ rotations} \tag{1}$$

where Ω is the number of rotations (2π) of the plane of polarization, f is the frequency of the radio wave, R the range of the moon, θ the angle between the field and the ray, and χ the angle between the ray and the zenith. Browne and Evans (1957) have investigated the amount of rotation likely to be produced in various regions of the earth-moon space. They considered a model of the ionosphere which was based largely on Rocket Panel data, and assumed that the space beyond the ionosphere to the moon had a uniform electron density of 600 electrons cm^{-3}. This figure is perhaps high, though the work of Storey (1953) on atmospheric whistlers and Siedentoph *et al.* (1953) on zodiacal light, suggests that there is an electron density of this order of magnitude at a few earth's radii. It was found on the basis of this model that 97·5 per cent of the rotation will occur in the ionosphere, i.e. below about 500 km height. Now since the function $B \cos\theta \sec\chi$ changes by only ~10 per cent up to 1000 km, the expression (1) may be written as

$$\Omega = \frac{1}{2\pi^2} \cdot \frac{e^3 c}{m^2 f^2} \cdot \overline{B \cos\theta \sec\chi} \int_0^{500} N \, dh \text{ rotations} \tag{2}$$

where $\int_0^{500} N \, dh$ is the electron content of the ionosphere. Since Ω may be several complete rotations (2π radians) use must be made of the relation

$$\Omega \propto \frac{1}{f^2}$$

in order that the number of rotations may be found without ambiguity. The technique developed at Jodrell Bank involves observing the slow fading on two frequencies which are separated by a small amount δf. There will be a difference $\delta\Omega$ in the amounts of rotation on the two frequencies, given by

$$\frac{\delta\Omega}{\Omega} = \frac{2\,\delta f}{f}$$

Now $\delta\Omega$ may be measured by observing the rate at which the fading is taking place, $d\Omega/dt$ (from the times at which the maxima and the minima in the fading occur) and the time separation δt between the curves, say between the same minima on the two frequencies, then

$$\delta\Omega = \frac{d\Omega}{dt} \cdot \delta t \tag{4}$$

This enables Ω to be found from (3) and thence the electron content of the ionosphere from (2).

3. Apparatus

A brief description of the aerial, transmitter and receiver in use at Jodrell Bank has been given (Browne *et al.*, 1956) and it is intended here only to give an account of the modifications which were necessary to enable the equipment to be operated on two close spaced frequences.

In order to achieve the high sensitivity required to detect echoes from the moon, a narrow receiver bandwidth of only 26 c/s is employed. The problem of keeping the receiver and transmitter tuned to the same frequency then arises. This is overcome by deriving the first three local oscillator frequencies in the receiver from the crystal which drives the transmitter. The remaining two oscillator frequencies can be compared with this master crystal by means of Lissajous figures. In this manner a drift in frequency of 1 c/s in the master crystal produces a 1 c/s frequency difference between the transmitter and the receiver, instead of 1200 c/s as would be the case without this compensating system. Since larger frequency drifts are unlikely to occur in the interval of time between the pulse being transmitted and its echo returning, this stability is quite adequate. The final local oscillator frequency may be varied by up to ± 100 c/s to compensate for the Doppler shift in the returned echoes. A diagram of this arrangement is given in Fig. 1.

VOL. 11 1957

It can be seen that the transmitter comprises many frequency multipliers and tuned amplifiers, and hence it cannot be retuned quickly or easily. To work on two frequencies there is no alternative to switching the transmitter off tune by changing the input frequency. This imposes a limit on the amount of frequency shift which can be employed, since the transmitter output falls rapidly as the input frequency is changed. A shift in frequency of 700 kc/s was found to be the most that could be tolerated, as this reduced the output power by 3 dB. A much larger change in frequency would be desirable and it was arranged that the original frequency (120 Mc/s) could be changed by ± 720 kc/s so that a separation of 1·44 Mc/s was obtained.

The frequency of the receiver must be changed in such a manner that the frequency drift compensating property is not altered. This is achieved by changing the first local oscillator frequency by ± 720 kc and arranging that a single crystal is used to provide both the frequency shift for the transmitter and that for the receiver. The general arrangement is shown in Fig. 2.

The first local oscillator in the receiver is amplitude modulated at 720 kc/s. Instead of selecting the desired local oscillator frequency with selective filters, all three frequencies (carrier and sidebands) are applied to the mixer. The mixer is, however, preceded by three selective R.F. amplifiers each of which is tuned to one of the three operating frequencies (119·28, 120·0, and 120·72 Mc/s) and gives at

least 20 dB rejection of the other two. A cascode R.F. head provides a signal input for all three R.F. amplifiers simultaneously, and their outputs are mixed before going to the frequency changer. It is now only necessary to apply H.T. to one of the R.F. amplifiers to select the desired receiver frequency.

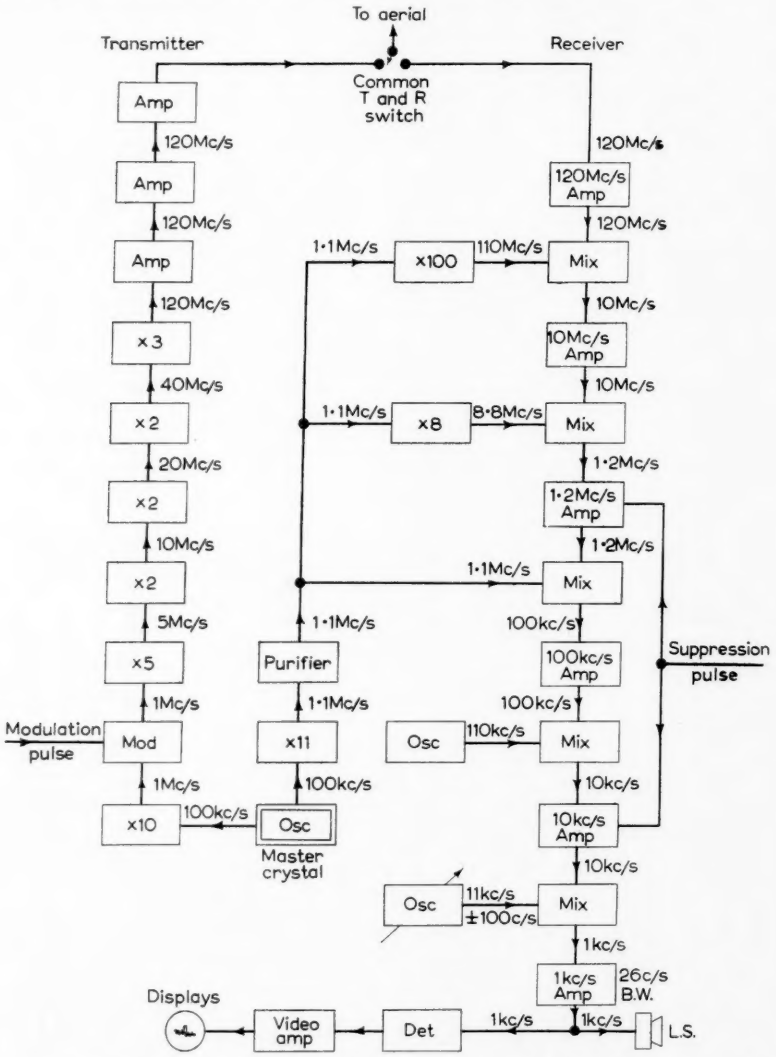

Fig. 1. The frequency control system which is employed in the Jodrell Bank moon radio echo equipment.

A similar system is employed to select the transmitter frequency. It is arranged that the input frequency to the modulated stage (originally 1 Mc/s) can be switched between 994 kc/s, 1000 kc/s, and 1006 kc/s by applying H.T. to a selective amplifier. The operating frequency can now be switched instantly, and though manual

control of the transmitter and receiver frequencies is available, they are normally switched automatically between the two new frequencies (119·28 and 120·72 Mc/s) every 25 pulses by means of a uniselector.

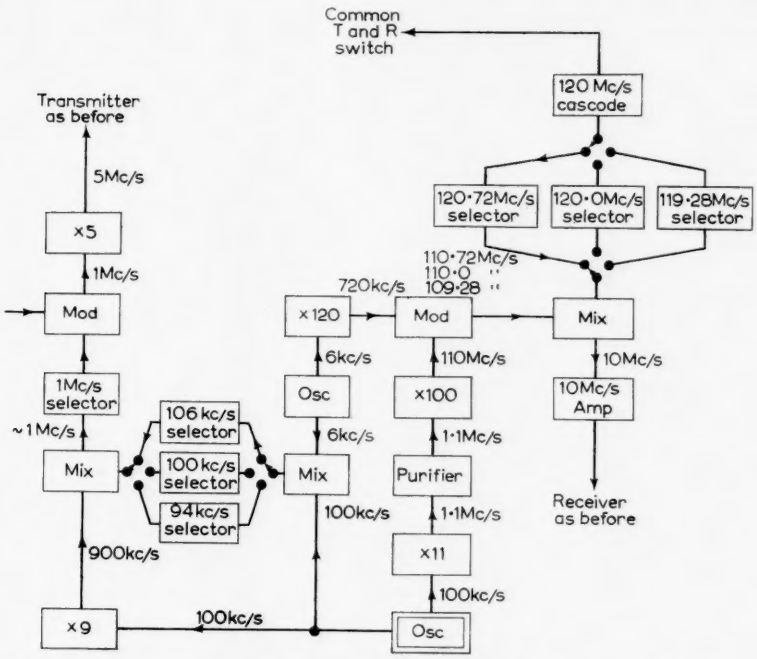

Fig. 2. The modified frequency control system which permits the equipment to be operated on any of three frequencies.

4. Treatment of the Observations

The echoes are photographed on 35 mm film and their amplitudes are read off on an arbitrary scale using a projector. The mean signal to noise ratio for each group of 25 echoes is calculated and plotted against the time of observation. An example of this is given in Fig. 3.

There is an uncertainty in each point of $\pm\frac{1}{5}$ of the observed signal to noise ratio. This is due to the rapid fading of the echoes, whose amplitudes follow a Rayleigh distribution. A larger group than about 25 echoes cannot be taken since this would tend to obscure the long period fading, particularly where this is occurring rapidly. The signal to noise curves therefore are not smooth, but are least uncertain at the minima which should be sharp since the mean amplitude of the echoes is given by

$$E = E_0 |\cos \Omega|$$

It is for this reason that the time separation δt between the curves is generally measured from the separation of the minima, whilst the rate of rotation is measured from the times at which the minima occur. Frequently the fading takes place at such a slow rate that one hour's observation does not produce sufficient information

VOL. 11 1957

to deduce Ω. Such periods are only of use if their signal to noise curves show continuity with the preceding and following days. Even where the fading has been rapid and it is possible to make several independent measurements of Ω from one record, it has been found that due to the rather small frequency separation in use, there remains some uncertainty in the number of rotations measured. For example the fading in Fig. 3 is almost the most rapid that has been observed, and the minima

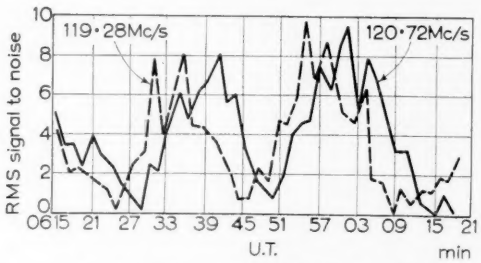

Fig. 3. The observed r.m.s. signal to noise ratio 28 September 1956. The fading is occurring first on the lower frequency and this indicates that the ionospheric electron content is increasing.

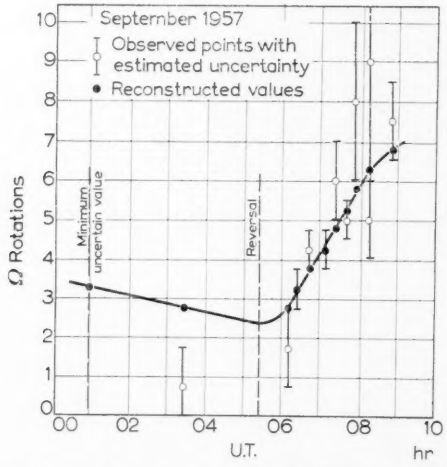

Fig. 4. The observed rotation of the plane of plarization Ω in September 1956. Also plotted is a reconstruction of the variation of Ω against time (full line) derived by the method described in the text.

were found to be $3\frac{3}{4}$, $4\frac{1}{4}$, and $4\frac{3}{4}$ rotations respectively with an uncertainty such that they could all be $\pm\frac{1}{2}$ rotation. This ambiguity can be removed if it is assumed that the ionosphere behaves the same from day to day. Continuity may then be expected between the signal to noise curves, which should join together to form a series providing many measurements of Ω. It is difficult to draw up definite criteria for determining whether the records show continuity or not, and this must be left to the individual observer, who must take into consideration the fact that the elevation of the moon, and thus the line-of-sight through the ionosphere changes from day to day, and also that sunrise might be a few minutes earlier or later. Frequently

however the records overlap by as much as 15 min and it is then not so difficult to decide whether continuity has occurred. Approximately half the records obtained so far show very good continuity, and only on a few occasions has there been a marked change between the fading on one day and the next. Such discontinuities do not appear to be correlated with ionospheric disturbances, and it would appear that the diurnal variation of the total ionospheric electron content is the same from day to day.

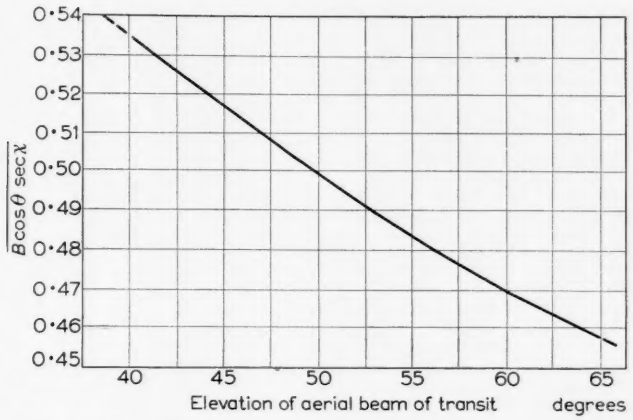

Fig. 5. The mean value of the function $B \cos \theta \sec \chi$ plotted against the elevation of the moon at transit at Jodrell Bank (53° 14′ N, 2° 18′ W).

Where continuity between records has been observed for several days, the values of Ω deduced, together with estimates of their uncertainty are plotted against the time of observation as in Fig. 4. Since each minimum is an exact number of $\pi/2$ radians, and is π radians more or less than the previous minimum, a line can be drawn through the points, which is the variation of Ω against time. This can be converted to electron content against time using equation (2). The mean value of $B \cos \theta \sec \chi$ is given in Fig. 5 as a function of elevation for the position of Jodrell Bank (53°14′ N, 2°18′ W).

5. Results of Observations

Observations have been made at intervals during the year from October 1955 to September 1956 at the following times

October	1 Oct.–14 Oct. 1955
November	26 Oct.–10 Nov. 1955
January	17 Jan.–30 Jan. 1956
February	14 Feb.–27 Feb. 1956
April	8 Apr.–21 Apr. 1956
August	27 July–8 Aug. 1956
September	19 Sep.–1 Oct. 1956

Observations were not made every month, as the analyis of the records of any one fourteen day period takes about a further month to complete. The results of

VOL. 11 1957

the first two periods have been given previously (Evans, 1956) but will be included here for completeness. The results are shown in Fig. 6–13 where the observed electron content n_0 is plotted together with that expected in a simple parabolic layer n_p ($= 16{\cdot}5 \times 10^{-9} (f_0F2)^2 y_m$ electrons) by taking a mean of the Slough critical frequency data for the days of observation.

The periods of observation will now be discussed separately.

October 1955

The observed electron content n_0 is considerably higher than that in the parabolic model n_p, there being a ratio $n_0 : n_p$ of 2 : 1 after sunrise and an even higher ratio before sunrise. This indicates that after sunrise there are three times the number of electrons above the level of the maximum of the *F2* region n_a to the number below n_b, and a higher ratio before sunrise. During the night time no significant ionization takes place, and if recombination decreases rapidly with height, it would be expected that the ratio $n_a : n_b$ will increase above its daytime value, and show a maximum just before dawn. However this does not appear to be the case, since n_b is approximately constant before dawn, while n_0 is decreasing as might be expected. A reason for this apparent anomaly is suggested later (Section 6).

November 1955

The continuity between records before dawn was poor and this period is uncertain. After sunrise the ratio $n_0 : n_p$ was again $\sim$2 : 1.

January 1956

Here a rapid fall in n_0 commenced at about 1600 U.T. and continued until about 1900 U. T. where there was a break in the continuity of the records. Hence from then onwards the results are uncertain. Prior to this $n_0 : n_p$ was $\sim$2 : 1.

February 1956

The continuity this month was somewhat better, though there remains an uncertainty of about $\pm\frac{1}{2}$ rotation throughout. This means that the curve presented could be displaced by $\pm$ 1·9 $\times$ 10^{12} electrons. The ratio $n_0 : n_p$ appears to be somewhat less than 2 : 1 and as in October it is found that n_0 continued to decrease after midnight whilst n_p was almost constant. In both months the height of the layer remained constant, but its semi-thickness y_m showed an almost steady increase.

April 1956

The fading near noon was slow and the results are again uncertain. It is however definite that n_0 reached its maximum at $\sim$1400 U.T. and was decreasing thereafter. At about 1700 U.T. the fading became fairly rapid and from then on the electron content is known to $\pm$1·9 $\times$ 10^{12} electrons (i.e. $\pm\frac{1}{2}$ rotation). The variation of n_0 appears to be more regular than that of n_p.

June 1956

There was little long period fading this month and no reconstruction of the diurnal variation is possible. Instead the few observed points are presented together

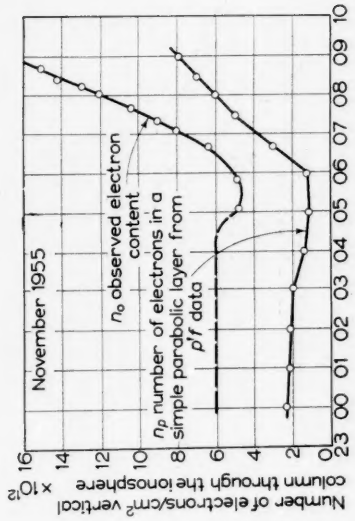
November 1955
n_0 observed electron content
n_p number of electrons in a simple parabolic layer from $p'f$ data
Number of electrons/cm² vertical column through the ionosphere ×10¹²
U.T.

Fig. 7.

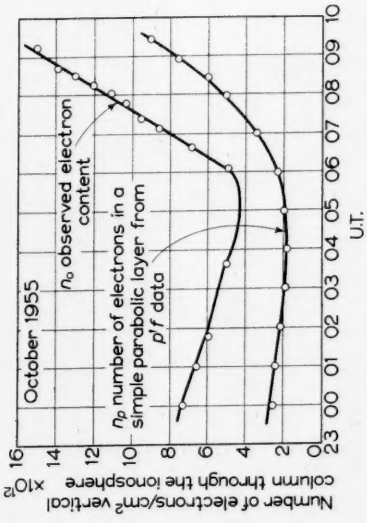
October 1955
n_0 observed electron content
n_p number of electrons in a simple parabolic layer from $p'f$ data
Number of electrons/cm² vertical column through the ionosphere ×10¹²
U.T.

Fig. 6.

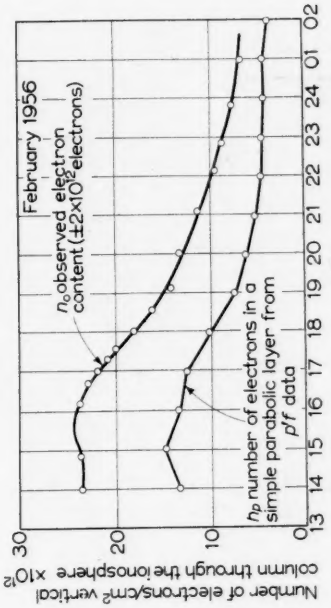
February 1956
n_0 observed electron content (±2×10¹² electrons)
n_p number of electrons in a simple parabolic layer from $p'f$ data
Number of electrons/cm² vertical column through the ionosphere ×10¹²
U.T.

Fig. 9.

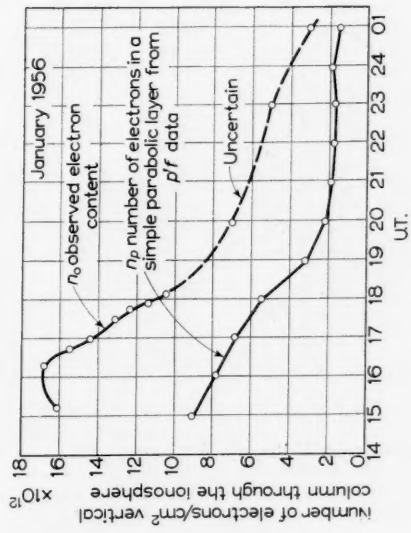
January 1956
n_0 observed electron content
n_p number of electrons in a simple parabolic layer from $p'f$ data
Uncertain
Number of electrons/cm² vertical column through the ionosphere ×10¹²
U.T.

Fig. 8.

Figs. 6–13. The variation with time of the observed electron content n_0. Also shown is the electron content of a simple parabolic layer n_p based on Slough critical frequency data. In general there is a ratio $n_0 : n_p$ of the order 2 : 1.

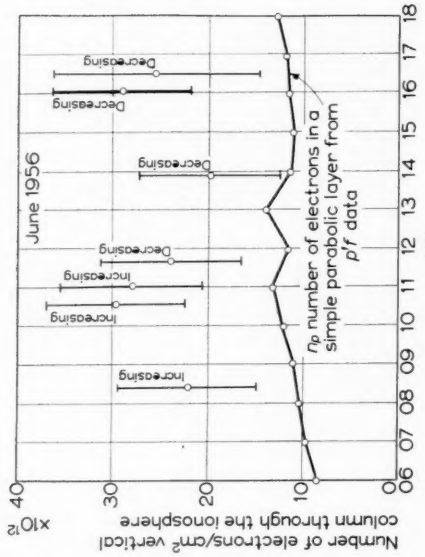

Fig. 11.

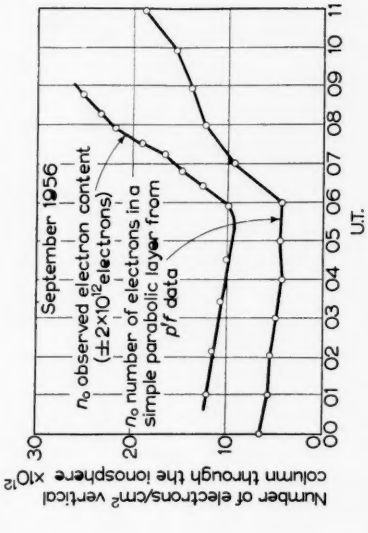
September 1956
n_o observed electron content (±2x10¹² electrons)
n_p number of electrons in a simple parabolic layer from $p'f$ data
Number of electrons/cm² vertical column through the ionosphere x10¹²
U.T.

Fig. 13.

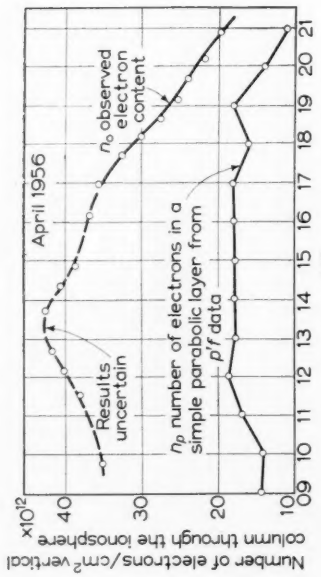
April 1956
Results uncertain
n_o observed electron content
n_p number of electrons in a simple parabolic layer from $p'f$ data
Number of electrons/cm² vertical column through the ionosphere x10¹²
U.T.

Fig. 10.

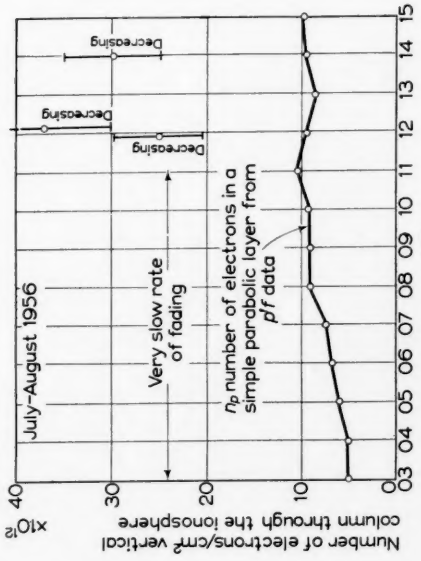
July–August 1956
Very slow rate of fading
Decreasing
Decreasing
Decreasing
n_p number of electrons in a simple parabolic layer from $p'f$ data
Number of electrons/cm² vertical column through the ionosphere x10¹²
U.T.

Fig. 12.

with a note to indicate whether n_0 was increasing or decreasing. Throughout n_0 is considerably greater than n_p and appears to be increasing in the morning and decreasing in the afternoon, with the single exception of a decrease at ~1130 U.T. This suggests that the slight "bite out" in n_p might be real.

August 1956

Here the fading was very slow indeed. This might be expected as the diurnal range of n_p is considerably less in summer than winter due to the long relaxation time of the region. There again appears to be a slight "bite out" in n_p and an observed decrease in n_0 at the same time.

September 1956

This fortnight's observation covered much the same period as October 1955. The curve of n_0 presented, has an uncertainty throughout of $\frac{1}{2}\pm$ rotation—i.e. it could be replaced by one higher or lower by $1{\cdot}9 \times 10^{12}$ electrons, but the agreement between the results obtained on successive days precludes any other solution (c.f. Fig. 4). The ratio $n_0 : n_p$ is ~2 : 1 throughout.

Seasonal variations

Each period of observation is limited to about 14 days and hence only about 12 hr of the day are covered. This 12 hr period gets progressively earlier by about 2 hr each month. Thus the periods all cover different parts of the day and it is not easy to draw firm conclusions with regard to the seasonal variations. Figs. 6–13 indicate that there is a systematic increase in the midday values of n_0 from winter to summer. However the variation of the noon value of n_0 is by no means as large as would be expected on the basis of Chapman's theory, and hence it appears that the *F2* region winter anomaly is not completely removed by considering the total electron content of the region instead of the critical frequency.

VOL. 11 1957

6. Discussion

(*i*) *Ratio between n_0 and n_p*

The parabolic model is based on the critical frequency data for the *F2* region, and the *E* and *F1* regions have been neglected as their contributions to n_p will be small. In general a ratio $n_0 : n_p$ of 2 : 1 has been observed, indicating that there is approximately always 3 times the number of electrons n_a above the level of the maximum to the number below n_b (assuming $n_b = \frac{1}{2} n_p$). For a Chapman region a ratio of 2 : 1 would be expected. Gledhill and Szendrei (1950) have extended Chapman's work to the case of a non-isothermal ionosphere, and shown that the shape of the layer depends upon the lapse rate γ, and a 3 : 1 ratio would be expected where γ was $\sim +2°$/km. Recent work (Ratcliffe *et al.*, 1956) suggests that electrons are removed from the *F* region by an attachment process whose rate decreases rapidly with height, so producing the *F2* region maximum as a subsidiary of the *F1* layer. Hence the work of Gledhill and Szendrei, who have assumed a constant recombination coefficient, is not directly applicable. If ionization is removed from the ionosphere by either an attachment or recombination process whose coefficient decreases with height then it is possible that this will increase the ratio $n_a : n_b$

above that predicted by Chapman, and it may be that the observed ratio represents a balance between this effect and the diffusion of electrons from high to low regions.

Many workers (Ratcliffe, 1951; Osborne, 1952; Chatterjee, 1953; Skinner and Wright, 1954; Sheriff, 1956) have shown that the integrated electron content up to the level of the maximum of the *F2* region (n_b) has a more regular diurnal variation than the maximum electron density N_m deduced from the critical frequency. Thus it is of interest to find that the results presented here indicate that there is generally a constant relationship between the number of electrons below the level of the maximum n_b and the total electron content n_0.

(ii) *Tidal effects*

In the winter months there appears to be an irregularity at night because though the total electron content n_0 is observed to be decreasing the number of electrons n_p in the parabolic model is almost constant. It is suggested that this arises as a result of the Slough method of measuring y_m which does not take into account the effect of the earth's magnetic field. This causes y_m to be overestimated particularly when the critical frequency is low (Whale and Shinn, 1952). As a result n_p is overestimated during the winter night by an amount which becomes progressively larger as the *F* region critical frequency decreases.

One other anomaly remains. This is the decrease in n_0 observed between 1100 and 1200 U.T. in summer, which coincides with a slight decrease in n_p. It must be emphasized that though the actual value of n_0 may be uncertain it can be seen from the fading whether n_0 is increasing or decreasing without ambiguity. Ratcliffe (1951) has suggested that the midday "bite out" in the *F2* region critical frequency is not reflected in the variation of the total electron content. Also Chatterjee (1953) found a peak in the value of n_p at noon. However Chatterjee assumed a value for the height of the maximum of the *F1* layer h_mF1 of 220 km and a semi-thickness of this layer of 100 km. Recent work at Cambridge indicates that h_mF1 is more nearly 180 km (Miss A. R. Robins, privately communicated) and hence y_mF1 should be less than 100 km. Thus the ionization in the *F1* layer appears to have been overestimated and this probably accounts for the noon peaks observed by Chatterjee. Thomas *et al.* (1957) also find that there is a midday "bite out" in the value of n_p during the summer months near sunspot maximum. Thus it seems that at this time some mechanism (presumably tidal) operates in such a manner that the total electron content of the ionosphere is reduced.

7. Conclusion

There appears to be an almost constant ratio between the observed electron content and that expected in a parabolic layer, and thus the variation of the electron content up to the level of the maximum may be taken as representing the variation of the whole region. There is some evidence for tidal effects.

Acknowledgements—I am indebted to Prof. A. C. B. Lovell for his encouragement and the use of the facilities at Jodrell Bank. I should like to thank the Director of the Radio Research Station, Slough, for providing pre-publication ionosphere

records, and the Department of Scientific and Industrial Research for a grant for the period in which this work was done.

References

Browne I. C., Evans J. V., Hargreaves J. K., and Murray W. A. S.	1956	*Proc. Phys. Soc.* B **69,** 901.
Browne I. C. and Evans J. V.	1957	*Jodrell Bank Annals* In press.
Chatterjee B.	1953	*J. Geophys. Res.* **58,** 353.
Evans J. V.	1956	*Proc. Phys. Soc.* B **69,** 953.
Gledhill J. A. and Szendrei M. E.	1950	*Proc. Phys. Soc.* B **63,** 427.
Kerr F. J. and Shain C. A.	1951	*Proc. Inst. Radio. Eng. N.Y.* **39,** 230.
Murray W. A. S. and Hargreaves J. K.	1954	*Nature, Lond.* **173,** 944.
Osborne B. W.	1952	*J. Atmosph. Terr. Phys.* **3,** 58.
Ratcliffe J. A.	1951	*J. Geophys. Res.* **56,** 487.
Ratcliffe J. A. *et al.*	1956	*Phil. Trans. Roy. Soc.* A **248,** 621.
Sheriff R. M.	1956	*J. Atmosph. Terr. Phys.* **8,** 91.
Siedentopf H. *et al.*	1953	*Nature, Lond.* **171,** 1066.
Skinner N. J. and Wright R. W.	1954	*J. Atmosph. Terr. Phys.* **5,** 290.
Storey L. R. O.	1953	*Phil. Trans. Roy. Soc.* A **246,** 113.
Thomas J. O. *et al.*	1957	*J. Atmosph. Terr. Phys.* In press.
Whale H. A. and Shinn D. H.	1952	*J. Atmosph. Terr. Phys.* **2,** 85.

VOL. 11 1957

Journal of Atmospheric and Terrestrial Physics, 1957, Vol. 11, pp. 272 to 283. Pergamon Press Ltd., London

The radon content of the atmosphere in the New York area as measured with an improved technique

H. A. Miranda, Jr.*

(*Received* 30 *July* 1957)

Abstract—A method has been developed for determining the radon concentration of the air, both at the ground, and in the upper atmosphere, employing cocoanut charcoal as a concentrating agent.

Comparison measurements for ground samples were carried out by the conventional method, and show good agreement over more than one order of magnitude.

The method as adapted for upper-air sampling is capable of measuring a radon concentration of $4{\cdot}4 \times 10^{-15}$ c/l. It has the further advantage of being well suited for a synoptic type of investigation, since the sampling procedure utilizes a minimum of flying time, and requires no special training for those actually performing the sampling.

Four determinations of the radon distribution with height up to 10,000 feet were carried out, with a view to testing the feasibility of the method. Large and unexpected variations in radon concentration from one level to another were observed.

Introduction

Among the noble gases to be found in the atmosphere are the radioactive elements radon and thoron. Generated in the ground by the radioactive decay of radium and thorium X, respectively, they enter the lower atmosphere by exhalation through the soil-air interface, and are eventually removed from the atmosphere by radioactive decay and by precipitation.

The vertical transport of these gases in the atmosphere is enhanced by eddy diffusion, radon attaining much greater altitudes than thoron due to its much longer half-life (92 hr, as compared with 54 sec).

Their presence influences the rate of ion production in the atmosphere, and in this regard a knowledge of their concentration is of great interest. Moreover, a study of the vertical distribution of radon would yield additional information concerning atmospheric turbulence.

The early theoretical work of Hess and Schmidt (1918), continued by Schmidt (1925), and elaborated upon by Priebsch (1931), concerning the vertical exchange of radon content in the free atmosphere, has been supported by rather meagre experimental evidence.

Wigand and Wenk (1928) obtained a few measurements up to and above 3000 m (demonstrating that the radon found in the atmosphere did indeed diffuse from the soil). Kosmath (1930) measured the radon content at 0·1 m and 11·5 m. Later, Schmidt (1931) carried out determinations at the 2 m, 30 m and 50 m levels. There is some question as to whether these latter two determinations are indicative of the free-air distribution of radon with height. These measurements were carried out in the valley of Graz, which has a basin-type of topography. It has since become clear that measurements of a synoptic nature up to a height of at least 3 km are required.

* Physics Department, Fordham University, New York 58, N.Y., now with Columbia University–Hudson Laboratories, Dobbs Ferry, N.Y., U.S.A.

More numerous have been measurements of the radioactive decay products of radon in the air, by ALIVERTI (1932), GARRIGUE (1951), HARLEY (1953), WILKENING (1956), and others, especially within the last ten years. On the other hand, these latter methods require the additional assumption that radioactive equilibrium exists at all times between radon and its daughter products, which may not always be justified.

It was felt therefore that further direct measurements of the radon content of the upper air would be desirable, and that a need has for some time been in evidence for a more sensitive (and less cumbersome) measuring technique.

The method described herein is quite straightforward. A measured volume of air suitably dried is passed through a coconut–charcoal trap at a controlled rate of flow. The adsorbed radon is then transferred to an evacuated ionization chamber by heating the charcoal trap to dull red heat (ca. 650°C), and by flushing with nitrogen (previously stored in a tank for at least 30 days). This latter process will subsequently be referred to as the "outgassing process".

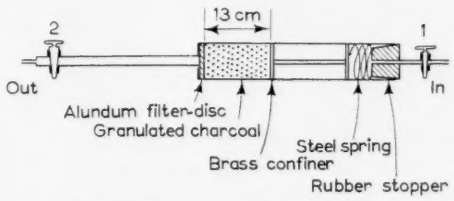

Fig. 1. Diagram of charcoal trap.

The activity of the radon sample thus contained in the chamber is then measured by counting the α-disintegration rate with a pulse counter whose design will be discussed below.

Samples of upper air are brought to the laboratory in plastic bags of polyvinyl-chloride and then are treated as described above. Filling of the bags is achieved by means of a tube projecting about one foot from the fuselage of a moving aircraft.

EXPERIMENTAL PROCEDURE

Sampling with charcoal traps

Each trap consisted of about 35 g of coconut charcoal in granular form confined within a Vycor tube as shown in Fig. 1. The traps fitted snugly in a commercially-available electric furnace.

The collection efficiency of the charcoal trap (i.e. that fraction of the radon contained in a given sample of air which is adsorbed by the trap) was determined for different sampling flow rates by means of sampling ordinary room air with two traps in series.

Of particular interest was the value of the collection efficiency at a flow rate of 1 l/min. The radon concentration of the atmosphere in the vicinity of the ground in this region is such that samples of from 50 to 100 l. are required for rapid determinations. Therefore, sampling flow rates of much less than 1 l/min become time consuming. On the other hand, flow rates of much more than 1 l/min increase

VOL. 11 1957

the difficulty of suitably drying the air sample before passing through the charcoal trap. Therefore, a sampling flow rate of 1 l/min was chosen as a standard procedure.

The results indicate that the collection efficiency does not vary sharply with flow rate; therefore, excessive precautions need not be exercised to keep the flow rate constant during a sampling. This is a fortunate circumstance, especially for field work. The measured collection efficiency was greater than 97 per cent for most of the traps.

Outgassing is achieved as follows: The charcoal having been brought to dull red heat, an evacuated 4 l. ionization chamber is placed in communication with the output end of the trap, and aged nitrogen is flushed through the system until the pressure rises to atmospheric. All stopcocks are opened slowly, no. 1 remaining closed; no. 1 is then used to control the flow of nitrogen so as to complete the process in about 4 min.

With the given arrangement, the outgassing efficiency (i.e. that fraction of the radon in the trap which is transferred in a single outgassing) is for all practical purposes 100 per cent. Of this, 89 per cent is transferred by the first $\frac{1}{2}$ l. of flushing; and 97 per cent of it by the first full litre of flushing.

It was found necessary to incorporate an alundum "filter-disc"* in the trap, as shown in Fig. 1, to keep particles of charcoal dust greater than 0·2 μ radius from entering the chamber during outgassing.

Apparently these particles, while in suspension, act as attachment nuclei for the ions in an α-track. Their mobility is thereupon greatly reduced, resulting in both an increased rise-time of each pulse and also in reduced pulse height due to excessive recombination. This effect was found to persist for as much as 15 hr whenever the filter disc was not in use.

One of the major sources of error in measuring minute concentrations of radon is due to radium contamination of the apparatus. Each part of the apparatus was therefore tested quantitatively for radium content, and corrections for this were applied.

The 35 g of charcoal contained in each trap, for instance, was found to have an inherent radium content of as much as $1{\cdot}5 \times 10^{-12}$ g, amounting to an equilibrium radon activity of about 6 α-disintegrations/min. This was found to vary by not more than a factor of 2 from one batch to another. In order therefore to take into account the generation of radon from this unwanted source, the time between successive outgassings was noted; or preferably (especially when lower counting rates were expected), the trap was outgassed and allowed to cool immediately before use. Since the time required for complete processing of a given sample of radon could easily be kept to less than 3 hr, contamination of the charcoal traps did not present serious difficulty as long as these precautions were taken.

Pulse-counting

Because it was desired to collect the radioactive products of radon on the central electrode, the amplifier was designed to accept positive pulses. Deposition

* Purchased from Fisher Scientific Co., New York.

of these atoms at the central electrode, rather than at the walls of the chamber, would yield a higher counting efficiency, since the electric field at the central electrode is a maximum.

The calculated upper limit of rise time for the pulses resulting from the given geometry and voltage was about 0·08 sec.*

Fig. 2 shows a schematic diagram of the pulse amplifier.

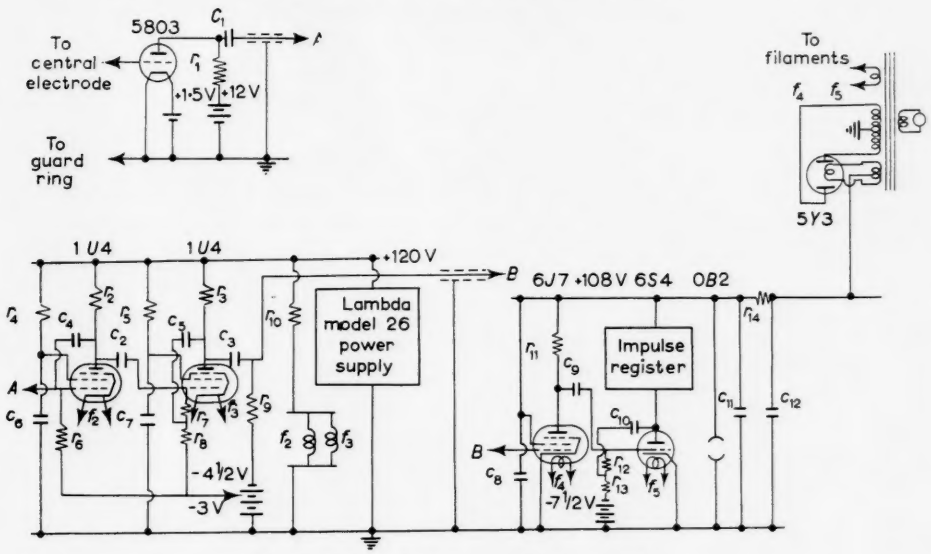

Fig. 2. Schematic diagram of pulse amplifier.

r_1	0·1 mΩ*	r_{10}	1 kΩ†	c_5	0·02 μF
r_2	0·5 mΩ*	r_{11}	0·1 mΩ	c_6	0·5 μF
r_3	0·13 mΩ	r_{12}	0·39 mΩ	c_7	0·5 μF
r_4	0·5 mΩ	r_{13}	22 Ω	c_8	0·5 μF
r_5	0·5 mΩ	r_{14}	7 kΩ	c_9	1 μF
r_6	1 mΩ	c_1	1 μF	c_{10}	4 μF
r_7	1 mΩ	c_2	0·08 μF	c_{11}	20 μF‡
r_8	220 Ω	c_3	1 μF	c_{12}	20 μF‡
r_9	0·47 mΩ	c_4	0·01 μF		

* Wire wound † 25 W ‡ Electrolytic

The preamplifier consists of a single 5803 electrometer tube, manufactured by Victoreen.† Its very low grid current (of the order of 10^{-14} A) permits the use of a grid leak resistor of 10^{-11} Ω without difficulty. This section, which acts as an impedance matching device is attached directly to the guard-ring of the ionization chamber.

The remainder of the pulse amplifier is contained in two physically distinct chassis, each with two stages of amplification. The first section consists of two

* Pulses with rise time of the order of milliseconds result if negative pulse collection is employed. This procedure, however, requires scrupulous removal of all electro-negative gases from the ionization chamber, the most abundant of which is oxygen. It was felt that, for accurate determinations, the extra complications involved with this procedure are greater than the difficulties experienced with the registration of "slow" pulses.

† Purchased from Victoreen Instrument Co., Cleveland, Ohio.

VOL. 11 1957

pentodes (1U4), whose B^+ is provided by a commercial power supply (Lambda Electronics Corp., Model 26), capable of delivering 100 mA of direct current at a voltage of anywhere between 100 V and 200 V with a ripple factor of less than 0·01 per cent. The filaments are wired in parallel, and fed by the same power supply, through a ballast resistor housed in a separate, grounded container.

The second section consists of a 6J7 pentode, followed by a 6S4 power triode, whose plate impedance is provided by an impulse register.* A separate power supply is also included in this section.

All biasing is provided by dry-cell batteries. Negative feedback is employed in the first, second and last stages of the main amplifier, to reduce the gain at higher frequencies.

In addition, the ionization chamber, with all of the associated batteries and leads, together with the preamplifier, was enclosed completely in a grounded aluminium shield, which rested on a heavy iron plate, and in turn on a layer of sponge rubber. With these precautions, spurious pulses arising from electrical transients, microphonics, and 60-cycle pick-up were successfully eliminated.

Spurious pulses due to the flicker effect arose mainly from the first pentode amplifier stage. Some degree of selection had to be employed to overcome this difficulty, about one tube out of three being rejected.

Continuous and satisfactory functioning of the amplifier for as long as three months at a time was thus achieved without special attention.

The time constants of the circuitry are rather large in comparison with conventional pulse-amplifiers. As a result, the response of the pulse-counting system begins to depart from linearity as the counting rate exceeds about 55 counts/min. However, since the actual counting rates found in practice rarely exceeded 20 counts/min, no difficulty was experienced on this account.

Comparison with direct-filling method

The method of radon measurement described above was compared with the more conventional method of direct filling of an ionization chamber. This was carried out by measuring the radon content of the air outside the Physics Building at Fordham University simultaneously with both techniques. Both pieces of apparatus were located inside, and the samples were introduced into each by means of glass tubing which protruded outside. Both samples were dried by passing through sodium-metal traps for water-vapour.

The ionization chamber used was of 44 l. capacity, and a Lindemann electrometer was used to measure its ionization current. In order to lower the background ionization current due to local γ-radiation and soft cosmic radiation, the chamber and electrometer were housed entirely within an "iron house" having walls, ceiling and floor 10 cm thick.

Fig. 3 shows the results of eleven such comparison measurements, taken over a period of two months during the summer of 1955. Each point has as ordinate the radon content as determined by the charcoal-trap-pulse-counting method,

* The impulse register, manufactured by Cyclotron Specialties Corporation, Morage 4, California, requires a minimum current of about 10 mA at about 22 V, and is capable of recording 60 impulses per second.

and as abscissa the radon content as determined by the direct-filling method. Good agreement between both methods is indicated in Fig. 3 over a range of more than one order of magnitude.

Calibration

Direct calibration of the charcoal-trap method was made using a radium standard solution certified by the National Bureau of Standards.

Transfer of the radon from the standard solution to the apparatus was carried out by bubbling about 50 l. of aged nitrogen through the solution, a drying trap, and finally the charcoal trap, at a flow rate of one l/min. No attempt was made to boil the solution, or to operate at reduced pressure, as it has been shown that de-emanation in the manner described is complete for all practical purposes.*

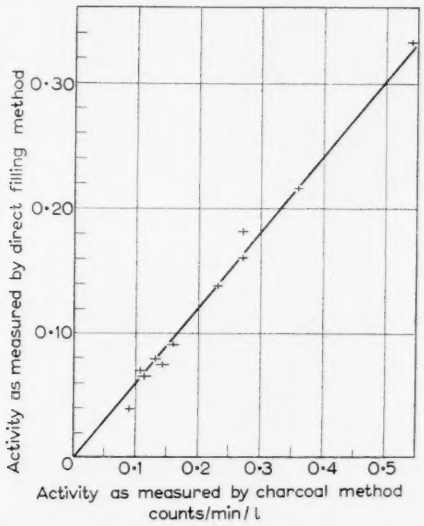

Fig. 3. Comparative measurements with charcoal method and conventional method.

A total of five calibrations were carried out using five different build-up times. In each case, measurements of the counting rate were made over a period of a day or two, and were extrapolated to zero time (the mean time of de-emanation).

If (t) be the build-up time, and C_t be the counting rate extrapolated to the mean time of de-emanation (exclusive of background), then we can write

$$C_t = C_o(1 - e^{-\lambda t}),$$

where C_o is the measured counting rate extrapolated to an infinite build-up time, and λ is the decay constant of radon.

These points were plotted with C_t as ordinate, and $(1 - e^{-\lambda t})$ as abscissa, as shown in Fig 4. The line, drawn in by sight, yields an extrapolated value for C_o of 37·5 $\pm$ 0·5 counts per minute. A least-squares fit computation of the data yielded a value for C_o of 37·53 and an intercept of 0·24. This warrants drawing

* This was first established by Hess (1943). A full discussion of this point will appear elsewhere in the literature.

VOL. 11 1957

the line through the point (o,o), inasmuch as the error quoted for each point is greater than this.

If we consider that the maximum possible counting rate one could obtain from a charge of radon equal to $1{\cdot}03 \times 10^{-11}$ c $\pm$ 0·9 per cent, in equilibrium with its products, is $45{\cdot}7 \pm 0{\cdot}4$ counts/min,* then the counting efficiency of the apparatus (i.e. that fraction of the total counts actually registered) is given by $37{\cdot}5 \pm 0{\cdot}5$ divided by $(45{\cdot}7 \pm 0{\cdot}4)$, or $82{\cdot}1 \pm 1{\cdot}3$ per cent. In other words, 1 count/min as measured by the counting apparatus indicates the presence of $(2{\cdot}74 \pm 0{\cdot}04) \times 10^{-13}$ of radon.

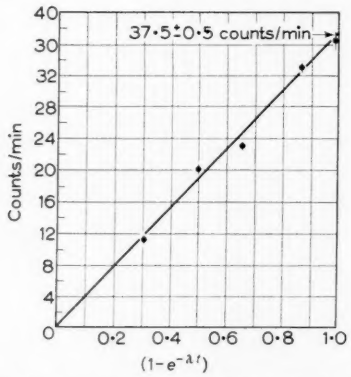

Fig. 4. Measured activity of radon de-emanated from standard radium solution, for different build-up times.

All errors quoted, unless otherwise specified, are 90 per cent confidence limit.†

Sampling with plastic balloons

If one assumes an atmospheric radon content of 10^{-14} c/l. then for every litre of sample, one will obtain on the average about 160 atoms of radon. (A good conversion factor to keep in mind is that a measured counting rate of 1 count/min indicates the presence of about 4300 atoms of radon in the apparatus.)

Since concentrations of not much more than 10^{-14} c/l. were to be expected, it was necessary to take samples of about 100 l. in the upper air, in order to assure good counting statistics.

Samples of air were introduced into plastic beach balloons made of polyvinyl-chloride, and brought to the laboratory for processing in the usual manner. Balloons available commercially were only of 55 l. capacity. They were easily stretched, however, by first filling with air to a pressure of a few pounds per square inch above atmospheric pressure, and then rotating slowly over an electric heater. Repetition of this process four or five times resulted in a capacity of about 120 l.: subsequent shrinkage was prevented by simply filling the balloons every two or three days or so.

* This figure was attained neglecting the presence of radium-*F*, and also considering that the radioactive products, Ra A and Ra C′, which are collected on the central electrode of the ionization chamber, send off half of their α-particles into the metal of the electrode.

† The term "90 per cent confidence limit" indicates that for a set having an indefinitely large number of elements, 90 per cent of these would fall within the specified limits.

Of the utmost importance in selection of the type of balloons was: (1) adsorption of radon during the storage period,* (2) radium contamination, and (3) diffusion through the material. (Mylar, for instance, was found unacceptable on the basis of contamination and diffusion.) Polyvinylchloride was tested for these three properties. No evidence of radon adsorption or diffusion was found.

Tests for undesirable properties

Tests for adsorption were performed on four different occasions in the following manner. A sample of room air was taken into a balloon (by holding the nozzle of the balloon directly in the air stream of an electric fan which had been previously well-cleaned), and simultaneously the same room air was sampled directly with a charcoal trap. The balloon sample was stored for periods of 2·3 hr, 4·6 hr, 5·2 hr, and 6·1 hr respectively before processing. In every case, the radon concentration of room air as measured with both methods agreed within experimental error.

There was, however, evidence of radium contamination of the balloon material, as might have been expected, since one of the constituents is carbon. This was tolerable, since the period of storage was never more than 8 hr. To obtain this correction, a series of "blank runs" was carried out, wherein aged air was introduced in each balloon and stored for various periods of time.

The contamination counting rate for each balloon was plotted as a function of $(1 - e^{-\lambda t})$, where t was the period of storage, and a mean slope was found for each balloon. Also, a standard distribution was then computed from all of the observed deviations. The estimated uncertainty in counting rates for all the balloon contamination values obtained in this manner was $\pm 0{\cdot}6$ counts/min.

The contamination counting rates for each sampling were then interpolated from these graphs, according to the length of storage for each sample.

Upper air sampling

The upper air was sampled from a moving aircraft. A well-cleaned one-inch brass pipe was inserted through the "Verey pistol port" of a C-47 airplane, and secured by rope. It protruded more than one foot from the fuselage, at an angle of about 50° from the horizontal, just behind the pilot's seat. Its outer end was sealed, and a V-notch was cut into the walls of the pipe about one inch from the end, to as to face the airstream. An ordinary plastic garden hose was attached to the other end of the pipe, and led to a more spacious part of the plane, where the actual filling of the balloons could take place.

The balloons having been previously well rinsed with aged air in the laboratory, a final rinsing was carried out just before sampling began. After each rinsing, the air was driven out of the ballooons by simply squeezing, and finally wringing them. The final rinsing air was taken from the garden hose, and not from within the cabin.

The actual sampling was a simple matter. The nozzle of the balloon was inserted into the garden hose, and the hose pressed lightly against the surface of the balloon. At air speeds of the order of 160 m.p.h., the balloons were filled within $2\frac{1}{2}$ min to firmness. They were then sealed by inserting a tapered glass

* Davis (1947), for example, showed that balloons made of neoprene rubber adsorbed as much as 40 per cent of the radon during the first 2 hr of storage.

VOL. 11 1957

plug (made by drawing a glass rod over a flame) into the nozzle. The balloons were then brought back to the laboratory for processing.

Experience showed that handling of the glass plugs with one's hands had to be strictly avoided, as this often resulted in contamination of the sample. As a precaution, only that portion of the plug which protruded from the nozzle of the balloon was touched, and in between use, the plug was placed on a clean Kleenex tissue. After each use, it was washed with an alcohol solution.

Sampling in this manner has the unique advantage of utilizing a minimum of flying time. (Three samples, one at each of three levels up to ten thousand feet altitude, could be obtained in less than 25 min.) Also, the procedure is simple enough so that very little training is required for personnel assigned to the task.

Since the balloons are collapsible, the volume of air contained therein when processed at the laboratory is automatically corrected for pressure and temperature differences. With this in mind, it is more convenient to consider altitude in terms of a constant-density atmosphere.

The above sampling technique is capable of detecting a concentration of $(4{\cdot}4 \pm 1{\cdot}1) \times 10^{-15}$ c of radon per litre from a sampling of 150 l. This is based upon the criterion that an activity of 2/3 background constitutes a lower limit of detection.

Results

A total of four measurements of the distribution of radon concentration with height were carried out during a one-month period beginning in the latter part of April 1956. In each case, the radon content at the ground, and that at each of three other levels was obtained. The ground measurement was obtained either by direct sampling with a charcoal trap, or by filling a balloon.

The aircraft and pilots were graciously placed at our disposal by Major Geyer, Director of Operations, 2500th Air Base Wing, Mitchell Air Force Base, Hempstead, Long Island. Weather data were obtained from the Meteorological Section, Mitchell Air Force Base.

The results of these measurements are shown in Fig. 5. In each graph, the activity is plotted as ordinate, and the altitude (in a corresponding constant-density atmosphere) is plotted as abscissa.

Flight *A* was made on 24 April 1956. The measurements extended from 9.20 a.m. until 9.35 a.m. The weather data, taken at Mitchell Field at 10.00 a.m., indicate a wind shift of about 30° between 4500 ft, and 5500 ft. The ground observer noted that the sky was partially overcast at the beginning of the sampling period, and that it became completely overcast by the end of the sampling period. The ceiling was over 6200 ft. In addition, a bright haze within the lower 1000 ft began to clear during the sampling period. The radon concentration fell very slightly from ground up to 3600 ft, but there was a fivefold increase between this level and 6200 ft. These facts suggest that the uppermost sampling was taken from a different air mass than the other three.

Flight *B* was made on 15 May 1956, between 2.20 p.m. and 2.35 p.m. The weather was fair, with no indication of the existence of different air masses.

Excessive turbulence was noted in flight, however, at the 1000 ft level. The radon concentration indicates a rapid falling off to about 35 per cent of the ground value, up to about 1000 ft, with hardly any change thereafter.

Flight *C* was made on 22 May 1956, between 10.40 a.m. and 10.55 a.m. The weather appeared fair, with a slight haze in the lower 1000 ft. The radiosonde data, however, indicated rather unsettled conditions. The air was classified as Maritime Polar in the first 1000 ft, and as Maritime Tropical in the remainder. A frontal inversion was indicated between the 4500 ft and 5500 ft levels. The radon content showed about a 20 per cent falling off between ground and 3600 ft, then a 75 per cent drop at 6200 ft, followed by a threefold increase at 8400 ft.

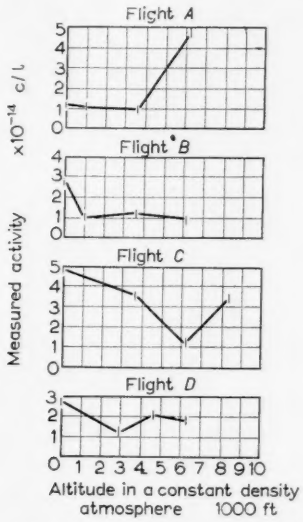

Fig. 5. Distribution of radon content with height as measured on four different flights.

Flight *D* took place on 26 May 1956, between 12.40 p.m. and 12.55 p.m. The sky was overcast, with ceiling at 6200 ft. The weather data (taken, unfortunately, four hours later), indicated a sharp wind shift at 4600 ft, a frontal inversion between the 5400 ft and 6200 ft levels, and severe turbulence between the 4500 ft and 5500 ft levels (although none was observed in flight). The radon content showed a drop of more than 50 per cent between ground and 2800 ft, followed by an 80 per cent increase at 4600 ft, and a slight decrease at 6200 ft.

The most striking feature of the results, as shown graphically in Fig. 5, is the rather wide variation found with altitude, especially in the case of Flights *A*, *C* and *D*. The meteorological data available do not show conclusively that the samplings in these flights were made in different air masses, although the suggestions are rather strong in the case of Flight *A*, and perhaps as well in Flight *C*.

On theoretical grounds, one would not except such large variations of radon concentration at different levels within a given air mass. Whether these are the rule or the exception can only be decided by further measurements. The very

VOL. 11 1957

definite indications are that further work along these lines will be rather fruitless unless carried out on a synoptic basis, and in conjunction with simultaneous meteorological observations.

It is therefore difficult to draw any immediate conclusions from the results of the present investigation, other than that the technique is feasible.

Summary

A method has been developed for measuring the radon concentration of the air, and is described in detail. The method employs coconut charcoal as a concentrating agent, and a specially-designed pulse counter for measuring the activity of the sample after it has been transferred into an ionization chamber.

A series of measurements were carried out in order to compare this method with the conventional method (ionization-current measurements of a sample of air introduced directly into a large ionization chamber). Simultaneous samplings of the air near the ground were made outside the Physics Building at Fordham University, using both techniques. The results show good agreement over more than one order of magnitude.

It is also shown that the new method is easily adapted for upper-air measurements with the aid of plastic balloons of polyvinylchloride. Upper-air samples are taken into the balloons through a tube which protrudes from the fuselage of a moving aircraft, into the airstream. The samples are then brought back to the laboratory in the balloons, for processing in the usual manner.

The method as adapted for upper-air sampling is capable of measuring radon concentrations as low as $4{\cdot}4 \times 10^{-15}$ c/l. It has the further advantages of (*a*) utilizing a minimum of flying time (about $2\frac{1}{2}$ min per sampling), and (*b*) requiring no special training for personnel assigned to the task of obtaining upper-air samples. It is thus well suited for a synoptic type of investigation.

In order to test the feasibility of the method, four flights were made. Each flight included measurements at the ground, and at each of three other levels up to a maximum of 10,000 feet.

The results of these flights are somewhat unexpected. Large variations in radon concentration were found from one level to another, although in all but one case, meteorological data gave little indication that the samples were taken from different air masses.

Acknowledgements—I take great pleasure in expressing my sincere gratitude to Prof. V. F. Hess, who suggested the investigation initially, for his guidance and criticism throughout this investigation.

I am also indebted to Dr. W. Dudley Parkinson for his interest and co-operation during the early part of the work, and to Dr. C. Kanavy for his assistance during the upper-air sampling.

Special thanks are due to Mr. V. J. Kisselback, who helped with many of the measurements, and to the personnel of the 2500th Air Base Wing, Mitchell Air Force Base, Hempstead, Long Island, through whose co-operation was made possible the measurements of the radon concentration of the upper atmosphere.

The research reported herein was supported in full by the Geophysics Research Directorate, Air Force Cambridge Research Center, Air Research and Development Command, under Contract No. AF–19(122)–409.

References

Aliverti G.	1932	*Nuovo Cim.* **9,** 313.
Davis F. J.	1947	*J. Res. Nat. Bur. Stand.* **39,** 545
Garrigue H.	1951	*C. R. Acad. Sci., Paris* **232,** 722.
Harley J. H.	1953	*Nucleonics* **11,** 12.
Hess V. F.	1943	*Trans Amer. Geophys. Union* **24,** 587.
Hess V. F. and Schmidt W.	1918	*Phys. Z.* **19,** 109.
Kosmath W.	1930	*Beitr. Geophys.* **25,** 95.
Priebsch J.	1931	*Phys. Z.* **32,** 622.
Schmid E.	1931	*Wien. Sitzber. IIa* **140,** 27.
Schmidt W.	1925	Der Massenautstauch in freier Luft und verwandte Erscheinungen. Hamburg.
Wigand A. and Wenk F.	1928	*Ann. Lpz. Phys.* **86,** 657.
Wilkening M. H.	1956	*Trans. Amer. Geophys. Union* **37,** 177.

VOL. 11 1957

Journal of Atmospheric and Terrestrial Physics, 1957, Vol. 11, pp. 284 to 288. Pergamon Press Ltd., London

Determination of impact point of a vertically-falling body by acoustical observations

G. V. Groves
Department of Physics, University College, London

(*Received* 20 *September* 1957)

Abstract—Simple formulae are obtained for calculating the co-ordinates of the impact point of a vertically-falling body from the arrival times of its shock wave at a number of microphones on the ground. The effects of wind and variations in the speed of sound are taken into account. When the microphones are closely spaced, the direction of the impact point can be found.

1. Introduction

In upper atmosphere experiments with rockets, the recovery of instrumentation after flight is an essential feature of many firings. The velocity of impact is usually reduced by separating the nose section from the remainder of the vehicle and then deploying a parachute. No less important than ensuring that the instrumentation survives impact is the problem of locating it on the ground, and a reasonably accurate estimate of the point of fall is required, if a tedious and possibly futile search is to be avoided.

On travelling through the atmosphere, a supersonic body, such as a high-altitude rocket, generates a shock wave. If the speed remains supersonic until impact, the point on the ground which receives the shock wave first is clearly the impact point itself. If, on the other hand, the speed becomes subsonic before impact, this result is still very nearly true, because the shock wave produced at Mach number unity is propagated ahead of the body in its direction of travel. In principle, then, the point of impact can be estimated from the arrival times of the shock wave at microphones set out over the area of fall.

In a paper to be published (Groves, 1958), the writer gives a theory by which the co-ordinates of a point on the trajectory of a supersonic body can be found from shock-wave arrival times. For the case of a vertically-falling body, the horizontal co-ordinates of this point are also the co-ordinates of the point of impact. A solution to the problem of determining the impact point is therefore already at hand, and the present paper is concerned with its presentation.

2. Solution for a Point of the Trajectory

Use will be made of the solution already obtained (Groves 1958, Section 5) for the co-ordinates (ξ, η, ζ) of a point on the trajectory of a supersonic body and the time τ when the body was at this point. The determination is based on observations of the arrival time of the shock wave at, at least, four microphones. With more than four, a least-squares determination could be undertaken.

In general, the shock waves received at several microphones will not have originated at the same point of the trajectory. The solution referred to above is based on the assumption that the time intervals between the generation of these shock waves are small and negligible to the second order.

Variations with height z of the horizontal wind-velocity components $u(z)$, $v(z)$ and the speed of sound $c(z)$ are taken into account to the first order in this solution in terms of the mean values u_0, v_0 and c_0 of these functions between ground level and height ζ. This procedure is satisfactory provided the shock wave does not come too near to being totally reflected, when the higher-order variations become more important. It is seen that an initial guess at ζ needs to be made in order to calculate u_0, v_0, c_0. If this value is later found to be in serious error, the process can be repeated with an improved value of ζ. In practice, u_0, v_0, c_0 would be expected to vary only slowly with ζ, so that a very rough value should be adequate.

The effect of (i) differences in microphone heights and (ii) the presence of vertical air motion can be included in the above-mentioned solution by carrying out a second approximation. In the present paper only the first approximation will be used, but the contribution from the second approximation due to the differences in microphone heights will be included (equation (4) below) in terms of the approximate value for ζ.

VOL. 11 1957

If (x_i, y_i, z_i) are the co-ordinates of the ith microphone and t_i the arrival of the shock wave at it, and if

$$\theta_1 = (\xi - u_0\tau)/d_0 \qquad \theta_2 = (\eta - v_0\tau)/d_0$$
$$\theta_3 = c_0\tau/d_0 \qquad \theta_4 = \tfrac{1}{2}(\zeta^2 + \theta_1^2 + \theta_2^2 - \theta_3^2) \tag{1}$$

then it can be shown (Groves, 1958, section 5) that θ_1, θ_2, θ_3, θ_4 satisfy

$$\alpha_i\theta_1 + \beta_i\theta_2 + \gamma_i\theta_3 + \theta_4 = \delta_i', \tag{2}$$

where

$$\alpha_i = (u_0t_i - x_i)/d_0 \qquad \beta_i = (v_0t_i - y_i)/d_0 \qquad \gamma_i = c_0t_i/d_0 \tag{3}$$

$$\delta_i' = \tfrac{1}{2}(\gamma_i^2 - \beta_i^2 - \alpha_i^2) + z_i\zeta/d_0^2 \tag{4}$$

and d_0 is an arbitrary scaling factor with the dimensions of length. Observations with four or more microphones permit a determination of θ_1, θ_2, θ_3, θ_4 from (2) and hence of ξ, η, ζ, τ from (1).

3. Determination of Impact Point using Four Microphones

From (2), with $i = 1, 2, 3, 4$, θ_4 may be eliminated giving

$$\alpha_{i1}\theta_1 + \beta_{i1}\theta_2 + \gamma_{i1}\theta_3 = \delta_i' - \delta_1' \quad , (i = 2, 3, 4),$$

where

$$\alpha_{i1} = \alpha_i - \alpha_1 \qquad \beta_{i1} = \beta_i - \beta_1 \qquad \gamma_{i1} = \gamma_i - \gamma_1 \tag{5}$$

From (1), this becomes

$$\alpha_{i1}(\xi/d_0) + \beta_{i1}(\eta/d_0) + [\gamma_{i1} - (u_0/c_0)\alpha_{i1} - (v_0/c_0)\beta_{i1}]c_0\tau/d_0 = \delta_i' - \delta_1'$$

On taking measurements with respect to microphone 1, this becomes

$$\alpha_{i1}(\xi - x_1)/d_0 + \beta_{i1}(\eta - y_1)/d_0 + [\gamma_{i1} - (u_0/c_0)\alpha_{i1} - (v_0/c_0)\beta_{i1}]c_0(\tau - t_1)/d_0 = \delta_{i1} \quad (6)$$

where

$$\delta_{i1} = \tfrac{1}{2}(\gamma_{i1}^2 - \beta_{i1}^2 - \alpha_{i1}^2) + (z_i - z_1)\zeta/d_0^2 \quad (7)$$

The solution of these equations can be written

$$(\xi - x_1)/d_0 = \frac{1}{\Delta}\begin{vmatrix} \gamma_{21} - (u_0/c_0)\alpha_{21} & \gamma_{31} - (u_0/c_0)\alpha_{31} & \gamma_{41} - (u_0/c_0)\alpha_{41} \\ \beta_{21} & \beta_{31} & \beta_{41} \\ \delta_{21} & \delta_{31} & \delta_{41} \end{vmatrix} \quad (8)$$

$$(\eta - y_1)/d_0 = \frac{1}{\Delta}\begin{vmatrix} \alpha_{21} & \alpha_{31} & \alpha_{41} \\ \gamma_{21} - (v_0/c_0)\beta_{21} & \gamma_{31} - (v_0/c_0)\beta_{31} & \gamma_{41} - (v_0/c_0)\beta_{41} \\ \delta_{21} & \delta_{31} & \delta_{41} \end{vmatrix} \quad (9)$$

$$c_0(\tau - t_1)/d_0 = \frac{1}{\Delta}\begin{vmatrix} \alpha_{21} & \alpha_{31} & \alpha_{41} \\ \beta_{21} & \beta_{31} & \beta_{41} \\ \delta_{21} & \delta_{31} & \delta_{41} \end{vmatrix} \quad (10)$$

where

$$\Delta = \begin{vmatrix} \alpha_{21} & \alpha_{31} & \alpha_{41} \\ \beta_{21} & \beta_{31} & \beta_{41} \\ \gamma_{21} & \gamma_{31} & \gamma_{41} \end{vmatrix} \quad (11)$$

For a vertical trajectory (8) and (9) give the impact point.

4. Determination of Direction of Impact Point using an Array of Closely-spaced Microphones.

An array of closely-spaced microphones is often used to determine the trace velocities a and b with which a shock wave travels past a certain point on the ground, in the Ox- and Oy-directions respectively. The procedure is to lay out a line of microphones in each of the Ox- and Oy-directions, usually in the form of a cross with one microphone in common to both arms. The derivatives of the distance v time curves for the wave to travel in these two directions evaluated at the common microphone are a and b.

The minimum number of microphones required to obtain a and b is clearly three. In practice arrays of five, seven or nine microphones have been used in order to improve accuracy. On account of the curvature of the wave, little improvement in accuracy would be expected by extending the microphones over an area greater than that over which the wave front is sensibly plane. Hence, with

a closely-spaced array, only the *direction* of the impact point would be expected to be determinable.

Take microphones 2 and 3 to be close to microphone 1 in the Ox- and Oy-directions respectively, then

$$y_2 - y_1 = x_3 - x_1 = z_2 - z_1 = z_3 - z_1 = 0 \tag{12}$$

$$\underset{2\to 1}{\text{Lt}}\ (x_2 - x_1)/(t_2 - t_1) = a \qquad \underset{3\to 1}{\text{Lt}}\ (y_3 - y_1)/(t_3 - t_1) = b \tag{13}$$

From (7), by (3) and (5)

$$\underset{2\to 1}{\text{Lt}}\ \delta_{21}/(t_2 - t_1) = \underset{3\to 1}{\text{Lt}}\ \delta_{31}(t_3 - t_1) = 0; \tag{14}$$

and from (6) with $i = 2$ and 3 and (3), (5), (12), (13) and (14)

$$(u_0 - a)(\xi - x_1) + v_0(\eta - y_1) + [c_0 - (u_0/c_0)(u_0 - a) - (v_0/c_0)v_0]c_0(\tau - t_1) = 0$$

$$u_0(\xi - x_1) + (v_0 - b)(\eta - y_1) + [c_0 - (u_0/c_0)u_0 - (v_0/c_0)(v_0 - b)]c_0(\tau - t_1) = 0$$

Hence

$$\xi - x_1 = \frac{(c_0^2 - u_0^2)b + u_0(b - v_0)a}{ab - av_0 - bu_0}(\tau - t_1) \tag{15}$$

$$\eta - y_1 = \frac{(c_0^2 - v_0^2)a + v_0(a - u_0)b}{ab - av_0 - bu_0}(\tau - t_1). \tag{16}$$

The direction of impact is therefore obtained as

$$\frac{\xi - x_1}{\eta - y_1} = \frac{(c_0^2 - u_0^2)b + u_0(b - v_0)a}{(c_0^2 - v_0^2)a + v_0(a - u_0)b}. \tag{17}$$

When $u_0 = v_0 = 0$, (17) reduces to

$$(\xi - x_1)/(\eta - y_1) = b/a. \tag{18}$$

5. Discussion

A simple determination has been obtained for the impact point of a vertically-falling body from the arrival times of its shock wave at a number of microphones. The conditions under which the solution is obtained are mentioned in Section (2), the general theory being presented in a later paper. The effect of these conditions will now be discussed.

Wind and variations in the speed of sound with height have been taken into account by working in terms of the mean values of these quantities over the height range concerned. This approximation becomes less accurate for ray paths whose inclination to the horizontal is small. Such rays are more seriously refracted by vertical variations in the atmospheric structure and should be excluded, even if a more elaborate theory were used.

On account of the particular nature of the temperature structure of the atmosphere, the shock wave from a vertically-falling body will reach the ground only

VOL. 11 1957

within a certain radius of the impact point. Points on the boundary of this region receive extreme (totally-reflected) rays. The radius of the boundary depends on the drag characteristics of the body and the height from which it has fallen and has been shown previously (Groves, 1957) to be about 25 km for a streamlined body (remaining supersonic until impact) and about 45 km for a blunt body (becoming subsonic before impact) falling from heights of a few hundred kilometres. Hence only microphones within these distances of the impact point can be counted for the purpose of determining the impact point. As the impact point is unknown in advance, microphone spacings appear to need to be not more than about 15 and 30 km respectively to give adequate coverage, i.e. receptions at, at least, four microphones in the two cases considered. If the array consists of a number of close clusters of microphones, the distances between neighbouring clusters cannot be much greater than these values without the possibility arising of only one cluster receiving the shock wave.

The solution that has been given is based on the assumption that the points of the trajectory where the shock waves originated are sufficiently close together. Consequently the solution obtained for a close array in Section 4 may be more satisfactory in general than that for a general distribution given in Section 3.

The heights from which shock waves can be received at the ground from a vertically-falling body have been shown theoretically to be in the lower atmosphere* (Groves, 1957): if the velocity becomes subsonic before impact, the shock wave would be received from a short section of the trajectory in a certain height range at about 10 km altitude: if the body has supersonic velocity at impact, it is only from the last 7 or 8 km of the trajectory that the shock wave will reach the ground.

It has been assumed throughout this paper that the body considered falls vertically. This is normally very nearly true for a high-altitude vehicle particularly if its drag is deliberately increased on re-entering the atmosphere. In other cases, a simple correction could possibly be made by estimating the angle of descent from the position of the impact point in relation to the launcher.

References

Groves G. V. 1957 *J. Atmosph. Terr. Phys.* **10,** 73.

Groves G. V. 1958 To be published.

* For bodies falling from heights below 120 km, receptions are also possible from portions of the trajectory in the upper atmosphere.

Journal of Atmospheric and Terrestrial Physics, 1957, Vol. 11, pp. 289 to 290. Pergamon Press Ltd., London

Radar observations of lightning on 1·5 metres

J. L. PAWSEY
C.S.I.R.O., Radiophysics Division, Sydney, Australia

(*Received* 2 *July* 1957)

Abstract—Very early observations on 1·5 m of echoes from lightning flashes are described. Approximate values for the echo cross-section, ($\approx$40 m^2), duration ($\approx\frac{1}{4}$ sec) and horizontal extent (several miles) are given. The associated atmospherics are also described.

IN A RECENT paper LIGDA (1956) has given an interesting account of the general features of the radar echoes and the emitted atmospherics due to lightning and has made suggestions for further work. The observations described are restricted to wavelengths less than 50 cm. Several points made by LIGDA are modified if longer wavelength results are considered. For this reason it seems worth while to give details of some early observations of these effects on a wavelength of 1·5 m. These observations were noted very briefly in *Nature* (1952) where they are stated to be the earliest observations of this type. They were made on the 11 September, 1943, and were originally described in a restricted wartime report (PAWSEY, 1944). The note in *Nature* also mentions early Japanese observations on a wavelength of 4 m.

The radar equipment used by the author was sited on a precipitous hill, 375 feet high, overlooking the sea about 10 miles north of Sydney. The nominal characteristics were: wavelength, 1·5 m; peak power, 35 kW; pulse length, 35 μsec; recurrence frequency, 50 c/s; time base extent, 200 miles; display, Class A; receiver noise factor, 12 dB; aerial gain (spherical), about 100; polarization, horizontal.

The effects observed appeared to originate in an area over the sea distant 110–170 miles and bearing about 110° from the site. At intervals of the order of a minute, echoes and interference appeared simultaneously on the cathode ray tube screen. The echoes produced a distinct break in the base line and endured typically for a time estimated visually as about $\frac{1}{4}$ sec. They typically extended over a distance on the time base of about six miles of which about half was attributed to the pulse length and the remainder to a finite radial extent of the source. The magnitude of the echo was about ten times noise and about twice that from a Beaufighter aircraft, a large type of fighter, at a distance of 120 miles and at the height for maximum echo. A conservative figure for the echo cross-section of a Beaufighter is 10 m^2. In confirmation that the effects were due to real echoes it was noted that they disappeared when the transmitter was switched off.

The interference took the form of a complex pattern of faint traces across the screen of about the same amplitude as the echoes. They seemed to be a series of single traces due to successive impulsive excitation of the receiver by the lightning flash. An interesting point is that they were noted as occurring with each observed echo. With the time base in use, duration of sweep 2000 μsec and

VOL. 11 1957

recurrence interval 20,000 μsec, nine tenths of the time is dead time and the observation implies that this series of impulses endures for at least 1/50 sec. This implication was not realized at the time and it would be desirable to confirm the observation. The field strength of a signal which would yield a deflection of the oscillograph spot equal to the peak amplitude of the impulses was estimated at 4×10^{-6} V/m. (Bandwidth $\approx 10^5$ c/s; distance ≈ 130 miles; height and orientation of flashes unknown.) In contrast to the echoes the interference appeared with or without the transmitter being on.

These results are very much exploratory observations but they establish that lightning echoes can be observed at considerable distances with relatively low power equipment if longer wavelengths are employed. A considerable extension of the range of wavelengths is desirable in order to establish the nature of the echoing process and the form of the echoing regions. For example the suggestion by LIGDA that the echo cross-section may simply be equated approximately to the actual cross-section of the thin column of ionization in the lightning column is one which must have interesting implications about the nature of the discharge channel, particularly at wavelengths where the column is believed to be a tiny fraction of a wavelength. At 1·5 m LIGDA's relation gives the observed order of magnitude.

A second feature of the long wavelengths is the relative freedom from obscuration by precipitation echoes. On a radar such as that described only extremely heavy tropical downpours give visible echoes. On the other hand centimetre wavelengths have other important advantages e.g. high resolution. It seems desirable that those who use radar to study lightning should use both long and short wavelengths and so obtain more complete information.

REFERENCES

LIGDA M. G. H. 1956 The radar observation of lightning. *J. Atmosph. Terr. Phys.* **9,** 329.

(Nature) 1952 Radar echoes from lightning discharges. *Nature, Lond.* **169,** 650.

PAWSEY J. L. 1944 *Note on echoes and atmospherics from lightning flashes. C.S.I.R. Radiophysics Lab. Rep. RP* 49/2.

RESEARCH NOTES

Time variations of cosmic rays at Wellington, New Zealand

(*Received* 13 *June* 1957)

OBSERVATIONS of extensive cosmic ray showers have been in progress in this laboratory (geographic latitude 41° south) for a period of some two years. The purpose of this note is to present the preliminary results obtained by analysis of the data from the period August 1955 to August 1956 inclusive.

The shower detector consisted of three unshielded counter trays, each of 1500 cm^2 sensitive area, situated at the corners of a roughly equilateral triangle of 40 m side. A fourth tray was situated at the centre of the array. The shower rate was about 6/hr and it was estimated that these showers were produced by primary particles of minimum energy about 10^{15} eV.

The shower rate when studied for time variations was found to have no large diurnal variation in either solar or sidereal time. In solar time there was a diurnal variation with a first harmonic of amplitude $1{\cdot}77 \pm 0{\cdot}65$ per cent, the maximum occurring at 0830 hr local solar time. The uncertainty quoted here, and in subsequent results, is the statistical standard deviation. Since no corrections were made for atmospheric effects this solar variation might well be of atmospheric origin.

Sidereal time analysis of the shower data gave a diurnal variation with a first harmonic of amplitude $0{\cdot}88 \pm 0{\cdot}65$ per cent with a maximum at 1700 hr L.S.T. (Local Sidereal Time). It must be concluded that this variation is not significant and that primary cosmic rays of energy about 10^{15} eV are isotropic within 1–2 per cent. However, it may be of interest to note that the time of maximum of the first harmonic (1700 hr L.S.T.) is close to the time (1736 hr L.S.T.) at which the centre of the galaxy crosses the meridian at Wellington, subtending a zenith angle of 15° to the vertical.

During the same period two inclined meson telescopes were operated at the centre of the extensive shower array. The telescopes consisted of three trays similar to those in the shower experiment with 15 cm of lead between the centre and lower trays, and one anticoincidence tray over the centre tray. The telescopes were inclined at an angle of 48° to the vertical and had a half angle of 15° in the E–W plane. At these inclinations the telescopes were directed towards the centre of the galaxy at 1400 hr L.S.T. for the east telescope and 2120 hr L.S.T. for the west telescope. The count rate of each telescope was about 10/min.

The individual telescope rates and the west-minus-east rates were analysed for time variations, but there was no significant evidence for a diurnal variation of amplitude greater than 1 per cent in either solar or sidereal time.

As a further experiment, coincidences between the extensive showers and the individual inclined telescopes were recorded separately. The coincidence rates were about 2/day for each telescope. Ostensibly these rates represent the rates of extensive showers incident from the east and west directions respectively at the inclinations given by the telescopes. Preliminary tests have not revealed the presence of any spurious effects, but in view of the low count rate it is necessary to await the outcome of further tests that are in progress in

VOL. 11 1957

order to establish the validity of the results. The estimate of primary ray energy is rather uncertain but it is considered to be at least 2×10^{16} eV.

From the first analysis of the angular shower data, the most interesting result is that east showers show a diurnal variation with a first harmonic of amplitude $12{\cdot}5 \pm 5{\cdot}4$ per cent with the maximum at 1520 hr L.S.T., and the west showers an amplitude of $9{\cdot}1 \pm 5{\cdot}4$ per cent with maximum at 2040 hr. Since the telescopes had a rather narrow polar diagram the peak shower rates are perhaps of greater interest. The east showers showed a peak of $28{\cdot}8 \pm 19{\cdot}8$ per cent at about 15 hr L.S.T. and the west showers $19{\cdot}9 \pm 18{\cdot}3$ per cent at about 21 hr L.S.T. While no claims can be made for the significance of these peaks, the times of maxima do agree with the calculated times at which the centre of the galaxy bears due east and west of Wellington.

At the present stage of the experiments the results are therefore consistent with the conclusion which may be reached from the review by Elliot (1952) that any diurnal variation of the low energy primary cosmic radiation is certainly much less than 1 per cent. They are not consistent with the earlier observation by Farley and Storey (1954) of a significant sidereal diurnal variation for primary particle energies of about 10^{14} eV.

Victoria University College
Wellington, New Zealand

N. G. Chapman
N. V. Ryder

References

Elliot H. 1952 *Progress in Cosmic Ray Physics* Vol. 1. North Holland Publishing Co.

Farley F. J. M. and Storey J. 1954 *Proc. Phys. Soc.* A **67**, 696.

Drift motions of auroral ionization

(*Received* 15 *June* 1957)

Recent measurements of the frequency spectra of VHF echoes from auroral ionization give approximate values and directions of the electron drift velocities in the region 400–900 km geomagnetically north of College, Alaska. (Hereinafter all directions mentioned refer to geomagnetic co-ordinates.) Records taken during January, February and March 1957 show that the general pattern of the electron drift was horizontally east or west at speeds of 0·5–3·0 km/sec. A brief description of the experiment follows.

Continuous wave transmitters at 106·0 and 41·15 Mc/s, using simple horizontal dipole antennas, were located 40 km east of College. The receiving systems at College were similar on each frequency. Two identical Yagi antennas with 3 dB beamwidths of 60 degrees in azimuth were oriented with their maximum gains at angles of 30 degrees east and west of north respectively. The signals received were separately amplified and converted in frequency to bring them into the audio frequency range. They were then simultaneously recorded on a multichannel magnetic tape recorder. The frequency spectra of the recorded signals were analysed at a later time with an audio frequency spectrum analyser.

Since a small ground-wave signal was always received directly from the transmitter, the frequency spectrum on each channel, in the absence of auroral or airplane echoes, consisted only of a single line whose width was determined by the resolution of the analyser.

Echoes from auroral ionization were spread in frequency and usually showed a mean frequency shift with respect to the direct signal. By interpreting these changes in frequency

VOL.
11
1957

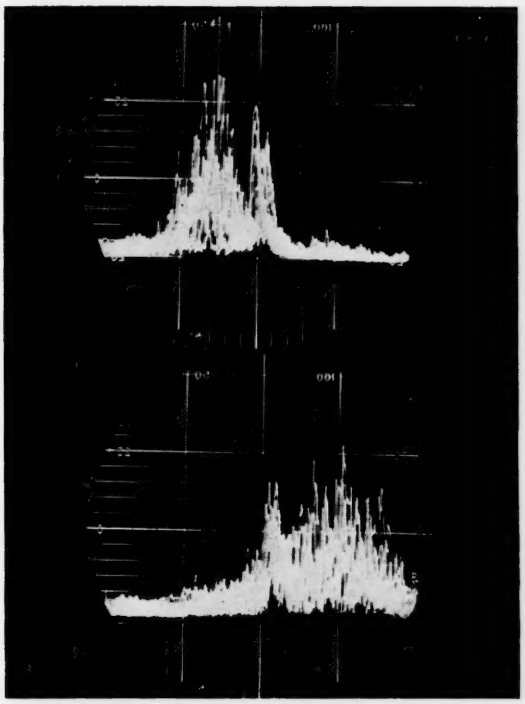

Fig. 1. 23 March 1957, 0051 AST. Frequency spectra of 30 sec section of record taken simultaneously from west of north (upper trace) and east of north (lower trace) at 41·15 Mc/s. The transmitted frequency can be seen very close to the centre line of each picture. Upward and downward shifts in frequency are shown as components to the left and right respectively, of the centre line. The separation between the heavy vertical scale lines is 125 c/s

as Doppler shifts, it was possible to deduce the magnitude and sense of the radial component of the velocity of the electrons responsible for the echo. The fact that the frequency shifts at 106·0 Mc/s were, on the average, two to three times those at 41·15 Mc/s is consistent with this interpretation. The actual direction of the drift motions was determined by considering the simultaneous echoes from east and west of north. The shifts in the two directions were generally in the opposite sense, clearly indicating that the major component was in the east-west direction. A more detailed analysis shows that the motions were typically inclined to the latitude line by about 10 degrees. An example is shown in Fig. 1.

Previous measurements of the amplitudes of the drift motions in auroral ionization were made by BOWLES (1954), who measured radial components of the same magnitude as those found in this experiment. The results described above, however, tend to disprove his conjecture that the motions are mainly directed along the magnetic lines of force.

The ionization responsible for the echoes is undoubtedly in the *E* region. The speeds measured appear to preclude any interpretation in terms of "winds," but are more likely the speeds of the electrons in the disturbance current system. If, following CHAPMAN and LITTLE (1957), we assume an average ionization density of $3 \times 10^5/\text{cm}^3$ in the aurora, the current density associated with a drift motion of 10^3 m/s is 5×10^{-9} A/cm^2. For an east-west current flowing over a 20 km height range this current density would produce a total current of 10^5 A/100 km of latitude. Disturbance currents of this order near the auroral zone have been deduced from magnetic observations by SILSBEE and VESTINE (1942) and other workers.

Radar echoes from auroral ionization are frequently spread in range by more than 100 km. The radar results, together with the measured drift velocities and the suggested electron density, are therefore consistent with the magnetic observations.

The work described above was supported by a contract with the U.S. Air Force Cambridge Research Center, and will be described more fully in a paper currently in preparation.

BENJAMIN NICHOLS

Geophysical Institute
University of Alaska
College, Alaska

VOL. 11 1957

REFERENCES

BOWLES K. L. 1954 *J. Geophys. Res.* **59,** 553.
CHAPMAN S. and LITTLE C. G. 1957 *J. Atmosph. Terr. Phys.* **10,** 20.
SILSBEE H. C. and VESTINE E. H. 1942 *Terr. Mag.* **47,** 195.

Einfluss der erdmagnetischen Unruhe auf die Durchschnittsabweichungen der *F1*-Schicht-Tagesgrenzfrequenzen

(*Received* 26 *June* 1957)

ÜBER die Durchschnittsabweichungen der *F2*-Schicht-Tages- und Nachtgrenzfrequenzen in Abhängigkeit von dem Grade der erdmagnetischen Unruhe wurde vom Verfasser (1954 und 1956) berichtet. Der Einfluss der geomagnetischen Breite auf diese Abhängigkeit wurde vom Verfasser (1955) untersucht. Alle vorstehend genannten Arbeiten stellen eine Fortsetzung der von BERKNER und SEATON (1940) eingeschlagenen Arbeitsrichtung dar.

In Ergänzung hierzu sollen die in Fig. 1 dargestellten Ergebnisse zeigen, wie stark der korpuskulare Einfluss auf die Durchschnittsabweichungen der *F1*-Grenzfrequenzen ist im

Vergleich zu demjenigen auf die Durchschnittsabweichungen der *F2*-Grenzfrequenzen. Die Ergebnisse wurden aus den *F1*- und *F2*-Grenzfrequenzwerten der Ionosphärenstation Lindau ($\phi = 51{,}65°$ N, $\lambda = 10{,}13°$ E) gewonnen und zwar aus den Sommerwerten (22.4.–20.8.) von 1948–1954. Diese Zeit erstreckt sich ungefähr vom Sonnenflecken-Maximum bis zum Minimum. In der Abbildung bedeutet $\Delta(1\text{–}27) f^0F2$ = Mittagsmittelwert (10–14 hr) f^0F2 minus 27 tägiger Medianwert, $\Delta(1\text{–}27)\ f^0F1$ das entsprechende für f^0F1.

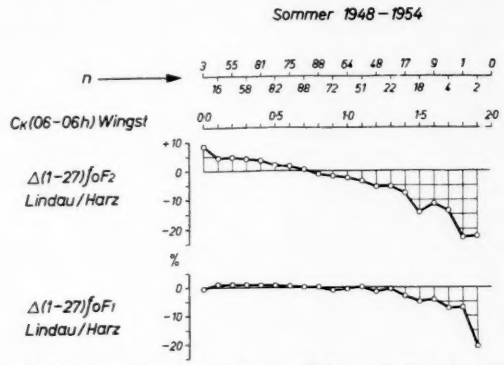

Fig. 1. Die Durchschnittsabweichungen $\Delta(1\text{–}27)\ f^0F1$ und $\Delta(1\text{–}27)\ f^0F2$ verglichen in Bezug auf ihre Abhängigkeit von dem Grade der erdmagnetischen Unruhe [Ck (06..06 h) Wingst].

Als Mass für die erdmagnetische Unruhe wird Ck von Wingst ($\phi = 53{,}7°$ N, $\lambda = 9{,}7°$ E) benutzt für das vorangehende Zeitintervall von 06..06 GMT. Wingst ist das der Station Lindau nächstgelegene Observatorium. In der Abbildung bedeutet $n =$ die für jede Durchschnittsabweichung $\Delta(1\text{–}27)$ benutzte Anzahl Werte. Die Untersuchungsmethode zur Gewinnung der dargestellten Ergebnisse ist in der Veröffentlichung des Verfassers (1955) näher bischrieben.

Wie aus der Abbildung zu erkennen ist, nehmen die $\Delta(1\text{–}27)\ f^0F2$-Werte mit zunehmender erdmagnetischen Unruhe nahezu stetig ab. Bei den $\Delta(1\text{–}27) f^0F1$-Werten macht sich dagegen eine derartige Abnahme erst bei relativ hohen C_k-Werten (1,3–1,4) bemerkbar. Ähnliche Untersuchungen wie die vorstehenden sind in letzter Zeit auch von Eyfrig (1956) durchgeführt.

G. Lange-Hesse

Max-Planck-Institut für
Physik der Ionosphäre
Lindau über Northeim (Hann.), Germany

Literatur

Berkner L. V. and Seaton S. L.	1940	*Terr. Mag.* **45,** 419–424.
Lange-Hesse G.	1954	*Arch. Elektr. Übertr.* **8,** 143–154.
Lange-Hesse G.	1955	*J. Atmosph. Terr. Phys.* **7,** 49–60.
Lange-Hesse G.	1956	*Arch. Elektr. Übertr.* **10,** 139–144.
Eyfrig R.	1956	Vortrag gehalten auf der Tagung der Arbeitsgemeinschaft Ionosphäre, des Deutschen URSI-Landesausschusses und der Fachgruppe Wellenausbreitung der NTG vom 11.–13. Oktober 1956 in Kleinheubach Main. Bisher unveröffentlicht.

On the possibility of observing aurorae in the daytime

(*Received* 29 *July* 1957)

THE importance of auroral observations during the I.G.Y. makes highly desirable a consideration of suitable conditions for detecting activity during hours of daylight, especially since radar echoes have been obtained from the auroral regions. A lead in this direction is given by stellar sightings from high flying aircraft. At an altitude of 40,000–50,000 ft, stars of first magnitude are visible for approximately 2 hr after dawn and 2 hr before dusk. From St. Andrews during the night of 18–19 April 1957, streamers from an aurora were seen against a dawn sky about 2 hr before sunrise when stars fainter than second or third magnitude were not visible.

A special aircraft flight was made during the solar eclipse of 30 June 1954, to detect auroral activity during the total phase. This was done on the suggestion of Prof. S. CHAPMAN. However, no display was seen on this occasion.

Scattering of light from the sky is the decisive factor when considering the question of auroral visibility during the daytime; the only feasible method would seem to be the detection of the auroral green line at 5577 Å.

Assuming isotropic scattering and no polarization we have, if I is the intensity of sunlight and ω the angular area of the sun, then I', the zenith sky intensity, is given by:

$$4\pi I' = \sigma\omega I$$

where σ is the scattering coefficient. Substitution of the appropriate quantities (ALLEN, 1955) gives $I' = 1{\cdot}5$ ergs sterad^{-1} sec^{-1} cm^{-2} Å^{-1} at 5500 Å.

At an altitude of 80,000 ft (approximately 25 km) we see that the scattering per atmosphere is equal to the product of the scattering coefficient for unit volume and the scale height. The variation of refractive index n with density ρ is represented by the Lorentz–Lorenz formula:

$$\frac{n^2 - 1}{(n^2 + 2)\rho} = \text{Constant}.$$

For a height of 25 km we find that $n = 1{\cdot}0000123$. Now the Rayleigh scattering coefficient, σ, is given by:

$$\sigma = \frac{32\pi^3(n-1)^2}{3N\lambda^4}$$

where N is the number of particles per unit volume; hence for a wavelength of 5500 Å, $\sigma = 4{\cdot}87 \times 10^{-9}$. Therefore the scattering per atmosphere is $3{\cdot}17 \times 10^{-3}$, since the scale height is $6{\cdot}5 \times 10^5$ cm. Hence:

$$I'_{25\text{km}} = 4{\cdot}96 \times 10^{-2} \text{ ergs sterad}^{-1} \text{ sec}^{-1} \text{ cm}^{-2} \text{ Å}^{-1}.$$

In this simple treatment secondary scattering has been ignored and at this altitude dust and water vapour will be absent.

The intensity of the 5577 line (HUNTEN, 1955) in a class II to III display is approximately 5×10^9 quanta sterad^{-1} sec^{-1} cm^{-2}, i.e. $1{\cdot}8 \times 10^{-2}$ ergs sterad^{-1} sec^{-1} cm^{-2} per equivalent width. The equivalent width corresponding to a Doppler broadening at about 220°K (the temperature in the lower auroral region) is 0·2 Å.

The fact that the values for I' and $I'_{25\text{km}}$ were calculated for a bandwidth of 1 Å and that the intensity of the auroral line is less than $I'_{25\text{km}}$ means that under these conditions the aurora will be invisible.

VOL. 11 1957

However, if the polarization of the sky is taken into account, then observations made at 90° to the direction of the sun would benefit by a reduction in sky brightness of perhaps ten times (VAN DE HULST, 1952). Unfortunately the auroral light would suffer a depletion of 50 per cent, giving a net gain of five.

A very serious obstacle is the scattering from the ozone layer. At 25 km this amounts to roughly half the ozone scattering at sea level. This implies an increase in scattering from the sky by a factor of 6 at 25 km. A particularly intense aurora might be ten times as bright as the one we have considered. Even so, there seems to be little chance of detecting it unless observations can be made from an even greater altitude.

A. H. JARRETT
P. L. BYARD

University Observatory
St. Andrews, Scotland

REFERENCES

ALLEN C. W. 1955 *Astrophysical Quantities.* University of London.
VAN DE HULST H. C. 1952 *The Atmospheres of the Earth and Planets* p. 79. University of Chicago Press.
HUNTEN D. M. 1955 *J. Atmosph. Terr. Phys.* **7**, 141.

The coefficient of diffusion of ions in the *F2* regions

(*Received* 2 *September* 1957)

THE writer (FERRARO, 1945) derived an expression for the coefficient of diffusion, D_{12}, of ions in the ionosphere based on Sutherland's molecular model. In this the molecules of a gas are treated as smooth rigid elastic spheres surrounded by a weak attractive field of force which for diffusion of ions in an otherwise neutral gas, is due to the attraction between the ion and the charge induced by it on a neutral molecule. Treating this as a conducting sphere the law of force is that of the inverse fifth power of the distance.

The value of D_{12} derived by using Sutherland's model was found to be b/n, where n is the molecular density of the neutral gas and b is a function of the temperature T and of the molecular weight of the gas which is equal to

$$b = 3{\cdot}9 \times 10^{17} T^{3/2}/(T + 187) \qquad (1)$$

for a mean molecular weight of 25.

At a temperature of about 1000°, such as obtains in the *F2* region, b is of the order of 10^{19}, and for this value of the coefficient of diffusion it appears difficult for a stable bank of ionization to persist for long at the level of the *F2* region unless the molecular density there is of the order of 10^{10} mol/cm^3 at least. This conclusion is difficult to reconcile with recent rocket estimates of the molecular density in the *F2* layer, which range between 5×10^9 and 5×10^8 mol/cm^3.

Because of this discrepancy the writer has reconsidered the assumptions made in deriving equation (1) and finds that the Sutherland model, though not suitable in this case

since the attraction between an ion and neutral molecule cannot be regarded as small, nevertheless is not greatly in error at the temperatures obtaining in the *F2* layer.

The case where the attraction between the molecules is not small was first considered by LANGEVIN (1905), who gave a formula for the mobility of ions in a neutral gas. This formula appears to be in fair agreement with the experimental results, even though no account is taken of the effect of electron transfer. LANGEVIN's formula for D_{12} is given by

$$D_{12} = (kT/e)\frac{A}{\sqrt{(\rho(\epsilon - 1)}}\left(1 + \frac{m_1}{m_2}\right)^{\frac{1}{2}} \tag{2}$$

where ρ is the density of the gas, m_1 and m_2 the masses of the neutral molecules and ion respectively, k is Boltzmann's constant, e the electronic charge and ϵ the dielectric constant, The non-dimensional parameter A occurring in equation (2) is a function of λ, where

$$\lambda^2 = \frac{8\pi p\sigma^4}{(\epsilon - 1)e^2} \tag{3}$$

p being the pressure of the gas and σ the sum of the radii of an ion and molecule. The function A has been computed by LANGEVIN and a graph of it is given by TYNDALL (1935, p. 39). It has a maximum value of about 0·6 at $\lambda = 0{\cdot}6$ and as $\lambda \to 0$ the limiting value of A is 0·505. When λ is large, $\lambda A \to \frac{3}{4}$ and equation (2) then reduces to the expression for D_{12} for rigid elastic spheres, namely,

$$D_{12} = \frac{3}{8no^2}\left\{\frac{kT(m_1 + m_2)}{2\pi m_1 m_2}\right\}^{\frac{1}{2}} \tag{4}$$

This is because when λ is large, the attractive forces become negligible. In the *F2* regions both oxygen and nitrogen are largely dissociated into atoms and it becomes difficult to estimate the value of $(\epsilon - 1)$ occurring in equations (2) and (3) appropriate to these atoms. However, $\epsilon - 1$ can scarcely exceed its value for the molecules and accordingly we take $\epsilon - 1 = 5{\cdot}8 \times 10^{-14}$, as was done by the author (1945), which corresponds to the value of ϵ for O_2. Taking also $\sigma \sim 3 \times 10^{-8}$ cm, and inserting numerical values for the constants, we find

$$\lambda^2 \sim 5{\cdot}64 \times 10^{-4}T \tag{5}$$

Thus unless T greatly exceeds 1000°, λ^2 is of order unity. For such values of λ^2, the value of A is about $\frac{1}{2}$ and so may be treated as a constant. As was mentioned by the author (1945) $(\epsilon - 1)/n$ is a constant, whence it follows from equation (2) that $D_{12} \propto n^{-1}$. Adopting the value of $(\epsilon - 1)$ to be that corresponding to O_2 as was done (1945), namely, $5{\cdot}8 \times 10^{-4}$, taking $A = \frac{1}{2}$ and assuming that the mass of the gas particles is that of an oxygen atom, we find from equation (2) that

$$D_{12} = 8{\cdot}69 \times 10^{15}T/n \tag{6}$$

The values of nD_{12} for various values of T are illustrated in the following table; the corresponding earlier values derived by the author (1945) are shown in parentheses.

T	300°	400°	500°	700°	1000°K
$nD_{12} \times 10^{-18}$	2·61 (4·2)	3·48 (5·3)	4·34 (6·4)	6·1 (8·1)	8·69 (10·1)

It will be seen therefore that the values of nD_{12} calculated by the author are about double those calculated from LANGEVIN's formula at ordinary temperatures and not very different at temperatures of the order obtaining in the *F2* region. If the value of $\epsilon - 1$ is much smaller than that corresponding to molecular nitrogen or oxygen, the value of D_{12} to be

VOL. 11 1957

considered is that corresponding to the case when the molecules are treated as rigid elastic spheres. Taking the masses of the ions and atoms to be the mass of an oxygen atom, and inserting numerical values for the various constants, we find that

$$D_{12} = \frac{7{\cdot}24 \times 10^{17}}{n} T^{\frac{1}{2}} \tag{7}$$

For $T = 400°$ and $900°$ the values of nD_{12} are $1{\cdot}47 \times 10^{19}$ and $2{\cdot}17 \times 10^{19}$ respectively that is, a little over three times as large as the values computed from LANGEVIN's formula.

If the number density of the atmosphere in the *F2* region is as low as rocket measurements indicate, and if, as observations appear to suggest, diffusion in the *F2* region is inappreciable, it follows that the calculated values of D_{12} may be too large by a factor of 10, unless diffusion is offset by other factors, such as movements of ions vertically upwards.

Alternatively, the level of maximum electron density is below that of maximum ion-production. One way of reducing the value of D_{12} to the required value would be to suppose that a stable neutral region of positive and negative ions is present below the *F2* layer. When additional ionization is produced in this layer the electrostatic forces between the ions will be according to the inverse square law of the distance, provided there are at least 10^6 ions/cm^3. Taking the temperature of the *F2* layer as 900°, the coefficient of diffusion would then be reduced to one-tenth of the value calculated above. However, the abundance of negative ions in the ionosphere has been investigated by several authors and it would seem that the ratio of the number of ions to electrons per unit volume is not greatly different from unity in the *E* layer and about 10^{-2} or less in the *F* layer. Thus the suggestion that the coefficient of diffusion may be reduced in this way is not attractive.

If the density of the neutral gas is as low as the rocket measurements indicate, there can be little diffusion across the lines of force of the earth's magnetic field. The effect is to reduce the coefficient of diffusion in the ratio of $1 : \sin^2 I$, where I is the magnetic inclination of the locality. However, this reduction is inappreciable except in the magnetic equatorial belt.

V. C. A. FERRARO

Queen Mary College
University of London

REFERENCES

FERRARO V. C. A. 1945 *Terr. Mag.* **50,** 215.
LANGEVIN P. 1905 *Ann. Chim. Phys.* **5,** No. 8, 245.
TYNDALL A. M. 1938 *The Mobility of Positive Ions in Gases.* Cambridge.

Timing errors in an equilateral array of receivers

(*Received* 20 *June* 1957)

IF RECEIVERS are set in an equilateral array, as described by BIBL, HARNISCHMACHER and RAWER (1955), a graphical analysis of drift speed may be convenient. The following construction applies to any form of triangle.

Let the receivers be set at positions A, B and C as in Fig. 1(a). Times are noted at which corresponding signal maxima occur at the three receivers. In the construction of Fig. 1(b), three axes are drawn parallel to the sides of the triangle and their positive directions are the directions of these sides taken in cyclic order. Along these axes are plotted lengths OD, OE, and OF equal to the appropriate time differences divided by the separation of the receivers

$$OD = T_{AB}/AB \qquad OE = T_{BC}/BC \qquad OF = T_{CA}/CA$$

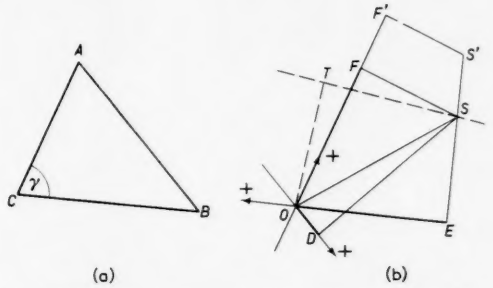

Fig. 1. The triangle of receivers (a) and the vector construction (b). A timing error δ at receiver A shifts point S to S', where
$SS' = FF'/\sin\gamma = \delta/AC \sin\gamma = BC \,.\, \delta/2\Delta$.

Here T_{AB} is the time interval by which an event on receiver A precedes the event on receiver B. Due regard must be paid to sign. These quantities are reciprocal velocities.

Normals are erected at D, E and F, and will be found to be concurrent at some point S. In fact, only two normals are necessary to define this point.

An event (usually a signal maximum) which appears successively at the receivers can be interpreted as being due to a "straight line of maxima" which has drifted across the receivers (RATCLIFFE, 1955). In the present construction it can readily be shown that the line OS is normal to the line of maxima and that the component of drift velocity of this line along its normal is equal to $1/OS$. If a number of lines of maxima with different orientations drift across the receivers in the same direction at the same speed they will give rise to different plotted points S. The locus of the points S is the straight line ST. The true drift direction is the direction of the normal OT and the true drift velocity is given by $1/OT$. This result is analogous to that found by PÜTTER (1955) for a right-angled array.

If an error of magnitude δ is made in reading one of the times, say the time at which a signal maximum occurs at receiver A, the intervals T_{AB} and T_{CA} are affected, but T_{BC} is not. This error therefore displaces the point S along the line ES, normal to the side BC of the array. The amount of displacement is

$$BC \,.\, \delta/2\Delta$$

where BC is the length of the side of the receiver triangle and Δ is the area of the receiver triangle.

Errors can occur in observing events at all three receivers. It is plausible to assume that these errors are independent and have equal variances. In this case the point S is subject to three independent displacements, directed normally to the sides of the receiver array and having standard deviations proportional to the lengths of those sides.

VOL. 11 1957

Thus any point S is subject to a scattering. The scatter pattern will not in general be circular. It can be shown* that the standard deviation of scatter in any direction is proportional to the radius of gyration of the three receivers about an axis drawn in that direction through their centroid. Only an equilateral set of three points has equal radii of gyration about all co-planar axes through its centroid. Thus the scatter pattern is circular, if, and only if the triangle is equilateral. The importance of this scatter pattern has been pointed out by CHAPPELL and HENDERSON (1956). Reading errors are relatively large, and if the scatter pattern they produce is not circular, very misleading estimates can be made of the alignment of the locus ST and hence of the normal OT that indicates the drift. An equilateral array is unique in being free from this distortion.

N. BARBER

Department of Scientific and Industrial Research
Wellington N.Z.

REFERENCES

BIBL K., HARNISCHMACHER E. and RAWER K. 1955 Some observations of ionospheric movements. *The Physics of the Ionosphere* pp. 113–18. Physical Society, London.

CHAPPELL D. G. and HENDERSON C. L. 1956 *J. Atmosph. Terr. Phys.* **8,** 163–68.

PÜTTER P. S. 1955 Measurement of the ionospheric wind. *The Physics of the Ionosphere* pp. 191–201. Physical Society, London.

RATCLIFFE J. A. 1954 *J. Atmosph. Terr. Phys.* **5,** 173–81.

* This may be seen as follows. Consider a set of points whose centroid is at the origin. Then

$$\sum_{1}^{n=N} x_n = 0 = \sum_{1}^{n=N} y_n \tag{1}$$

About an axis through the centroid, whose normal has direction cosines l, m, these points (each weighted unity) have a moment of inertia

$$\sum_{1}^{n=N} (lx_n + my_n)^2 \tag{2}$$

Consider independent gaussian vectors directed along the lines joining every pair of points and having standard deviations equal to the distance between the points. Because they are independent, their mean square components are additive, and in a direction l, m normal to the previous axis, the mean square component of their total vector is

$$\sum_{1}^{n=N} \sum_{1}^{m=N} [l(x_n - x_m) + m(y_n - y_m)]^2 \tag{3}$$

The same expression would apply to the mean square component along the previous axis if the individual vectors were directed at right angles to the lines joining the points.

From equations (1) it follows that the double sums of the products $x_n x_m$, $y_n y_m$, $x_n y_m$ are all zero. Expression (3) therefore reduces to

$$2 \sum_{1}^{n=N} (lx_n + my_n)^2$$

and this is just twice expression (2) for the moment of inertia.

LETTER TO THE EDITOR

Point-discharge current, potentential gradient and wind-speed

(*Received* 15 *July* 1957)

CHAPMAN (1956) has suggested, on theoretical grounds, that the relation between point-discharge current, potential gradient and wind-speed should be of the form:

$$I = A(V - V_0)v \tag{1}$$

where I is the current, V the potential of the point relative to its surroundings and v the velocity with which the ions are removed from the neighbourhood of the point, A and V_0 being constants. He verified this result by laboratory experiments in high winds when $v = W$, the wind-speed, and in still air, when v is proportional to V.

LARGE and PIERCE (1957) put an artificial potential on a point in the free air and found agreement with (1) put into the form:

$$I = A(V - V_0)(W^2 + c^2V^2)^{1/2} \tag{2}$$

where v is now considered as the vector sum of the wind-speed and the ionic mobility speed.

For the potential gradients naturally existing in the atmosphere, point-discharge currents through a point attached to a captive balloon have been measured by CHALMERS and MAPLESON (1955), giving the empirical formula:

$$I = K(Fh)^{7/4}W^{1/4} \tag{3}$$

where F is the potential gradient at the ground nearby and h is the height of the point; if the potential gradient does not alter with height, then $Fh = V$.

KIRKMAN and CHALMERS (1957) have also used the natural potential gradients in the atmosphere, and have measured point-discharge currents through a point at the top of a high mast; their results were expressed by the empirical formula:

$$I = k(F - M)(W + C) \tag{4}$$

There thus appears to be a discrepancy between the results for natural atmospheric potential gradients and those for artificially applied fields, and even between the different results for natural gradients. It therefore seemed worth while to enquire whether the results expressed by (3) and (4) could be equally well expressed by a formula of the form of (2). For example, for large values of W, (4) and (2) agree in giving proportionality to W, but for smaller values, the divergence is of a different form.

It is clear, from a first survey, that the use of (2) with the same constants as used by LARGE and PIERCE (1957) to fit their own results, will not fit the results of CHALMERS and MAPLESON (1955) or KIRKMAN and CHALMERS (1957). But if the constants A, V_0 and c are suitably chosen, then it is found that (2) gives as good a fit as (3) to the results of CHALMERS and MAPLESON (1955) and, with other constants, as good a fit as (4) to the results of KIRKMAN and CHALMERS (1957).

Thus the discrepancies are removed and it seems that point-discharge currents can all be represented by the formula (2).

VOL. 11 1957

Expressing the units in m.k.s., the best fits to the experimental results are given by the following table.

	A	C^2	V_0
Large and Pierce (1957)	$1{\cdot}6 \times 10^{-11}$	8×10^{-9}	7×10^{3}
Chalmers and Mapleson (1955)	$6{\cdot}5 \times 10^{-11}$	8×10^{-8}	$2{\cdot}5 \times 10^{3}$
Kirkman and Chalmers (1957)	6×10^{-12}	2×10^{-9}	8×10^{3}
Chapman (1956)	$1{\cdot}4 \times 10^{-11}$		

It is by no means clear on what the values of the constants depend, though obviously the exact nature of the point, and perhaps its surrounding supports, will be important. While the term cV represents the ionic velocity, it is not easy to see where this velocity must be measured when there is a rapid variation of field with distance from the point, and so it is difficult to give any theoretical significance to the values of c obtained. It may be noted that larger values of A appear to be associated with larger values of c and smaller values of V_0.

In the present analysis, no account has been taken of measurements of point-discharge currents through points at about tree-top height (e.g. those of Whipple and Scrase (1936)), since the wind-speed was not measured.

J. Alan Chalmers

Physics Department
Durham Colleges in the University of Durham

References

Chalmers J. A. and Mapleson W. W. 1955 Point-discharge currents from a captive balloon. *J. Atmosph. Terr. Phys.* **6,** 149–159.

Chapman S. 1956 *Electrostatic field measurements, corona discharge and thunderclouds. Report C.A.L. No.* 68 Cornell Aeronautical Laboratory, Buffalo, N.Y.

Kirkman J. R. and Chalmers J. A. 1957 Point discharge from an isolated point. *J. Atmosph. Terr. Phys.* **10,** 258–265.

Large M. I. and Pierce E. T. 1957 The dependence of point-discharge currents on wind as examined by a new experimental approach. *J. Atmosph. Terr. Phys.* **10,** 251–257.

Whipple F. J. W. and Scrase F. J. 1936 Point discharge in the electric field of the earth. *Geophys. Mem., Lond.* **68,** 1–20.

Journal of Atmospheric and Terrestrial Physics, 1957, Vol. 11, pp. 303 to 304. Pergamon Press Ltd., London

Indices of geomagnetic activity

of the Observatories HARTLAND (*Ha*), ESKDALEMUIR (*Es*), and LERWICK (*Le*), July and August 1957

The figures given on pages 303 to 304 represent the K-indices for three-hour intervals, beginning with 00–03 hrs for the first and ending with 21–24 hrs for the eighth figure.

July 1957

Day	*Ha* Range for $K = 9 : 500\gamma$		*Sum*	*Es* Range for $K = 9 : 750\gamma$		*Sum*	*Le* Range for $K = 9 : 1000\gamma$		*Sum*	*Day*
	K-Indices			*K-Indices*			*K-Indices*			
1	6653	2564	37	9753	2565	42	8863	2453	39	1
2	0134	6542	25	2124	7552	28	1123	7652	27	2
3	–434	4233		5443	4233	28	6534	5233	31	3
4	1112	3344	19	1112	2434	18	1012	2236	17	4
5	4554	2335	31	3654	3236	32	5865	4346	41	5
6	2333	3344	25	2233	3344	24	3332	3335	25	6
7	2222	2332	18	2322	3232	19	3321	2232	18	7
8	3232	2312	18	3322	3322	20	3322	3322	20	8
9	2012	2321	13	2121	2222	14	3121	2322	16	9
10	2210	2210	10	2211	1211	11	2212	1211	12	10
11	1001	3122	10	1111	3122	12	1112	3112	12	11
12	3231	3232	19	3222	3332	20	2221	3331	17	12
13	1112	1210	09	1121	2110	9	1122	1210	10	13
14	0001	3222	10	0112	3222	13	0111	3223	13	14
15	2112	2111	11	2111	2221	11	2121	2100	9	15
16	1033	3443	21	0033	4442	20	1023	3553	22	16
17	2103	2233	16	2102	2233	15	3122	3223	18	17
18	1224	3432	21	2223	3442	22	1223	3443	22	18
19	4332	4444	28	4232	4444	27	3332	4555	30	19
20	3322	3424	23	3322	3334	23	3321	2434	22	20
21	2212	2222	15	2111	2232	14	4112	1222	15	21
22	1344	3454	28	1234	3453	25	1233	4453	25	22
23	4411	1113	16	3312	1113	15	4321	1112	15	23
24	3222	3332	20	3222	3332	20	3122	2442	20	24
25	2231	2322	17	3111	2322	15	3121	2321	15	25
26	0011	1210	6	1101	2211	9	1121	3201	11	26
27	0001	1342	11	0001	2342	12	0112	2232	13	27
28	3222	2221	16	3121	2121	13	2122	1111	11	28
29	2323	3222	19	2323	3222	19	2323	4212	19	29
30	1221	2123	14	1221	2222	14	1221	2222	14	30
31	2122	2323	17	1122	2323	16	2222	2213	16	31

VOL. 11 1957

August 1957

Day	*Ha* Range for $K = 9 : 500\gamma$		*Es* Range for $K = 9 : 750\gamma$		*Le* Range for $K = 9 : 1000\gamma$		Day
	K-Indices	*Sum*	*K-Indices*	*Sum*	*K-Indices*	*Sum*	
1	1322 2221	15	1221 3221	14	1211 2121	11	1
2	3313 3223	20	1211 3222	18	3222 3223	19	2
3	3222 3653	26	3121 3653	24	3122 2665	27	3
4	6221 2321	19	5221 2322	19	6221 1221	17	4
5	2122 2334	19	2110 2334	16	1111 1346	18	5
6	3442 4444	29	3442 4444	29	3443 3444	29	6
7	3222 2211	15	3221 2221	15	3112 3211	14	7
8	1222 3233	18	1222 3133	17	1212 2132	14	8
9	4322 4324	24	4322 5323	24	4422 4324	25	9
10	4322 1122	17	4311 0122	14	4411 2112	16	10
11	2112 2221	13	2001 1221	9	1111 2211	10	11
12	3333 4432	25	2333 4442	25	3332 4432	24	12
13	4443 3443	29	3433 3434	27	4443 4343	29	13
14	1212 3333	18	1212 3333	18	1112 3323	16	14
15	4322 2233	21	3212 2233	18	4311 2133	18	15
16	3212 2221	15	2212 2221	14	3211 1211	12	16
17	1112 3301	12	1111 2311	11	1012 2210	9	17
18	2113 3122	15	2102 3223	15	2112 3212	14	18
19	3433 3212	21	3332 2211	17	4332 2102	17	19
20	0112 3333	16	1112 4323	17	1111 3333	16	20
21	3432 3411	21	3422 3421	21	4442 3431	25	21
22	0112 2211	10	0112 2221	11	0112 1221	10	22
23	0012 2110	7	0012 1110	6	0002 2010	5	23
24	0112 2111	9	0001 2111	6	0011 1111	6	24
25	0223 3333	19	0112 3333	16	0012 2223	12	25
26	2012 2323	15	1112 2322	14	2111 3321	14	26
27	3333 3343	25	3333 3333	24	3333 3333	24	27
28	2233 3333	22	1133 3323	19	1233 4323	21	28
29	2222 2264	22	2111 2254	18	2112 2155	19	29
30	5443 2431	26	5433 3531	27	6533 2321	25	30
31	2221 4464	25	2222 4564	27	3222 4555	28	31

VOL.
11
1957